Coordination Chemistry Reviews 468 (2022) 214644

Contents lists available at ScienceDirect

Coordination Chemistry Reviews

journal homepage: www.elsevier.com/locate/ccr

Review

The chemistry of metal–organic frameworks with face-centered cubic topology

Ayalew H. Assen [a,b], Karim Adil [c], Kyle E. Cordova [d,e,*], Youssef Belmabkhout [a,f,*]

[a] Technology Development Cell (TechCell), Technology Transfer Office (TTO), Mohamed VI Polytechnic University (UM6P), Lot 660 - Hay Moulay Rachid, 43150 Ben Guerir, Morocco
[b] Department of Chemistry, College of Natural Science, Wollo University, Dessie, Ethiopia
[c] Le Mans Université, Institut des Molécules et des Matériaux du Mans (UMR 6283), Avenue Olivier Messiaen, 72085 Le Mans Cedex, France
[d] Materials Discovery Research Unit, Advanced Research Centre (ARC), Royal Scientific Society, 11941 Amman, Jordan
[e] Foundry of Reticular Materials for Sustainability (FORMS), Universiti Putra Malaysia, 43400 UPM Serdang, Selangor, Malaysia
[f] Applied Chemistry and Engineering Research Centre of Excellence (ACER CoE), Mohammed VI Polytechnic University (UM6P), Lot 660 - Hay Moulay Rachid, 43150 Ben Guerir, Morocco

ARTICLE INFO

Article history:
Received 26 December 2021
Accepted 25 May 2022

Keywords:
Reticular chemistry
Solid-state materials
UiO-66
Metal–organic frameworks
fcu-MOFs
Porous materials
Structure–property relationships

ABSTRACT

The precise control of molecular building blocks (MBBs) permits access to various types of tailor-made functional materials. The best example of this is in the assembly of metal–organic frameworks (MOFs) comprising many types and arrangements of pre-designed organic and inorganic MBBs. A MOF platform that has garnered particular attention, given its utility and fidelity in many different environments, is the **fcu**-MOF – a three-dimensional structure that is constructed from linking 12-coordinated face-centered cubic MBBs together. Since the discovery of the first Zr_6 oxocluster-based **fcu**-MOF, known as UiO-66, there has been substantial progress in the synthesis of structures with varying metrics, but with the same underlying **fcu** topology. This family of **fcu**-MOFs has later evolved to incorporate isostructural, hexanuclear non-zirconium metal clusters, including rare earth, actinide and other transition metals as inorganic MBBs. Additionally, the versatility of the **fcu**-MOF platform for design has also attracted researchers to go beyond *in situ* generated hexanuclear metal clusters to transition metal-based non-hexanuclear metal oxocluster MBBs and metal–organic polyhedra (MOP) supermolecular building blocks (SBBs). All in all, reported **fcu**-MOFs are endowed with a wide range of porosity and framework chemistry, which has led to their applicability across energy and environmental sustainability issues of societal importance. In this review, a comprehensive assessment will be directed toward the synthesis and applications of **fcu**-MOFs with particular focus on the chemistry of the MBBs/SBBs and their resulting structure–property relationships. The synthetic and structural characterization challenges will be detailed with future opportunities becoming clear in the process.

© 2022 Elsevier B.V. All rights reserved.

Contents

1. The fcu topology . . . 2
2. Zr_6 oxocluster-based fcu-MOFs: Synthetic and structure–property relationships . . . 4
   2.1. The prototypical Zr-fcu-MOF, UiO-66 . . . 5
   2.2. Impact of synthesis parameters on the assembly of Zr-fcu-MOFs . . . 6
      2.2.1. Zr(IV) salt precursors . . . 6
      2.2.2. Temperature and synthetic routes . . . 6
      2.2.3. Modulating agents . . . 7
      2.2.4. Precursor concentration . . . 9
   2.3. Isoreticular functionalization of Zr-fcu-MOFs . . . 9

* Corresponding authors.
E-mail addresses: kyle.cordova@rss.jo (K.E. Cordova), youssef.belmabkhout@um6p.ma (Y. Belmabkhout).

https://doi.org/10.1016/j.ccr.2022.214644
0010-8545/© 2022 Elsevier B.V. All rights reserved.

2.4. Isoreticular expansion and contraction of Zr-fcu-MOFs . . . 14
2.4.1. Isoreticular Zr-fcu-MOFs from expanded linkers . . . 14
2.4.2. Isoreticular Zr-fcu-MOFs from shorter linkers . . . 18
2.4.3. Isoreticular Zr-fcu-MOFs from flexible aliphatic linkers . . . 18
2.5. Defects in Zr-fcu-MOFs . . . 19
2.6. Interpenetrated Zr-fcu-MOFs . . . 22
2.7. Multivariate (MTV) Zr-fcu-MOFs . . . 23
2.7.1. Post-synthetic modifications of Zr-fcu-MOFs . . . 23
2.7.2. Mixed-linker Zr-fcu-MOFs . . . 24
2.7.3. Mixed-metal $Zr_{6-x}M_x$ or Zr_6M_x oxocluster-based fcu-MOFs . . . 33
3. Non-zirconium oxocluster-based fcu-MOFs . . . 37
3.1. Transition metal cluster-based fcu-MOFs . . . 37
3.1.1. Group IV (Ti and Hf) hexanuclear and non-hexanuclear oxocluster-based fcu-MOFs . . . 37
3.1.2. Divalent transition metal-based fcu-MOFs . . . 38
3.2. Rare earth (RE) oxocluster-based fcu-MOFs . . . 41
3.3. M_6 (M = Actinides or An) oxocluster-based fcu-MOFs . . . 44
4. Conclusions and perspective . . . 46
Declaration of competing interest . . . 47
Acknowledgement . . . 47
References . . . 47

1. The fcu topology

Metal-organic frameworks (MOFs), a burgeoning class of porous solid-state materials, are constructed via the self-assembly of inorganic and organic building blocks. As compared to other conventional porous solids, such as zeolites and porous carbon, MOFs have attracted immense research interest from the viewpoint of design, synthesis, properties and application [1]. This is highlighted by the fact that, according to information available in the Cambridge Structural Database, over 100,000 MOF structures have been synthesized, structurally characterized and reported to date [2].

The amenability of MOFs for topology-directed design from preselected inorganic and organic molecular building blocks (MBBs) has fueled research in the field. MBBs are the basis for one of the most commonly employed conceptual approaches for the rational design and assembly of functional MOFs. In this approach, metal clusters and polyatomic organic linkers of a particular geometry and directionality are selected prior to the assembly process. MOFs with highly connected MBBs are usually suitable targets since highly connected MBBs limit the number of possible topological outcomes leading to a greater degree of predictability in the end MOF structure. A vast library of MBBs that can serve as potential targets to construct highly connected MOFs does exist [3]. Indeed, there are many examples of MOFs that have been rationally designed and assembled by employing this concept [4,5].

One of the most common structures found in reticular chemistry is one based on an underlying **fcu** net (termed hereafter as a '**fcu**-MOF'). The **fcu**-MOF contains the face-centered cubic close-packing of 12-connected (12-c) metal oxocluster MBBs (cuboctahedron secondary building unit; SBU) linked together by linear linkers [6] (Fig. 1A). This structure is the only edge transitive net (nets with one kind of edge) for the assembly of cuboctahedron SBUs. A given structure's transitivity is used by researchers to categorize the networks that comprise them [7]. Transitivity of a structure is represented by *pqrs* where there are *p* types of vertices, *q* types of edges (links), *r* types of tile faces, and *s* types of tiles. Structures with transitivity of 11*rs* (unimodal, edge transitive) are most likely to form when one kind of SBU is joined by one kind of link. The most realistic targets for designed reticular synthesis are structures with just one type of edge and, therefore, the most significant from a design perspective [6–8]. A structure that adopts a **fcu** net has a transitivity of 1112, whereby the two types of tiles defined correspond to two types of empty space (tetrahedra and octahedra shapes sharing triangular faces) found in the structure and occurring in a 2:1 ratio (Fig. 1A) [6].

Being the only 'quasiregular' net (a net whose vertex figure is a quasiregular polyhedron) [9] and the fact of the net's high symmetrical nature with all the links between SBUs being the same, the **fcu** net is the default net formed when cuboctahedron SBUs are joined by linear links. When suitable metal ions and linear organic linkers with the potential to generate cuboctahedron SBUs are mixed under appropriate reaction conditions, the probability of the metal ions to organize themselves into highly symmetrical SBUs is very likely and the assembly of **fcu**-MOFs is chemically reasonable. According to the **fcu** tiling, which contains two polygons constructed exclusively from triangles, **fcu**-MOFs contain distinct, yet interconnected octahedral and tetrahedral cages in a 2:1 ratio, to which a triangular window (aperture) provides sole access to the internal pore environment (Fig. 1A). Controlling the size and accessibility of this triangle window by the length and functionality of the linker would therefore allow for execution of desired applications. Because every tiling has a dual, a second net (dual net) can be found that is the net of the natural tiling's dual with a transitivity of *srqp* [9]. The dual of the **fcu** net is the **flu** net (the net of the fluorite or CaF_2 structure) and has transitivity of 2111. The concept of duality is used to explain why certain nets tend to create interpenetrating pairs [9], with self-dual nets having the highest probability of forming interpenetrated structures.

fcu-MOFs were developed for the first time in 2008 at the University of Oslo (UiO). The first such structure, termed UiO-66, remains one of the most popular examples of a **fcu**-MOF [10] obtained by the MBB approach. The structure of UiO-66 is comprised of *in situ* generated $Zr_6O_4(OH)_4$ cuboctahedra building units that are 12-c to adjacent cuboctahedra through a 1,4-benzenedicarboxylate (BDC) linker, resulting in a highly packed face-centered cubic arrangement of metal cluster MBBs. The archetypal structure of UiO-66 is featured by two types of cages, one with octahedral and the other with tetrahedral shape displaying pore diameters of approximately 11 and 7.5 Å, respectively. Since this first report, the assembly of MOFs based on the edge transitive **fcu** net from *in situ* generated 12-c metal oxoclusters displaying cuboctahedron SBUs (generated from one type of metal

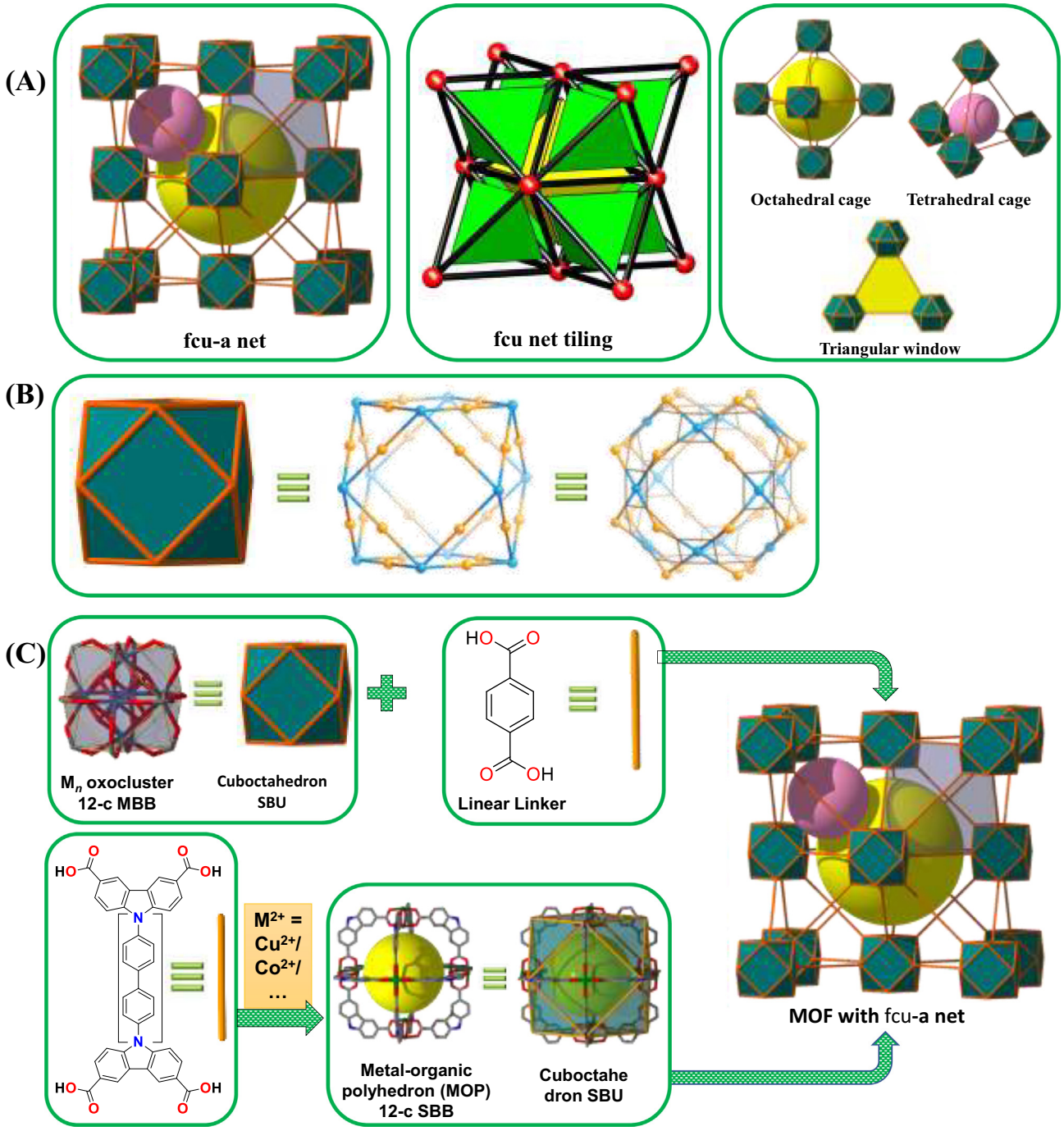

Fig. 1. (A) Representation of augmented **fcu** net and its tiling that exhibits interconnected tetrahedral and octahedral cages in a 2:1 ratio sharing triangular faces; (B) Configuration of a cuboctahedron SBU which has 12 tetravalent SBUs joined by linear links; and (C) Representative examples of the MBB and SBB approaches to assemble **fcu**-MOFs.

cation or mixed-metal ions) and linear linkers (single linker or mixed-linker) has attracted immense attention. This is due to the various features of the MOF platform that will be highlighted in the review. The relatively higher thermal, chemical, and mechanical stability of most Zr-based **fcu**-MOFs, especially in comparison with other MOFs, are usually reflected in the retention of crystallinity and porosity even after immersing the **fcu**-MOF in boiling water, after conducting water vapor sorption isotherms for many cycles [11], heating in air to ca. 300 °C, soaking the materials in harsh chemicals (solvents, acids, and bases), and exposing the material to 10,000 kg/cm^2 of external pressure [10]. Such properties of **fcu**-MOFs have opened many opportunities for exploration of these specific materials in different applications. Zr-**fcu**-MOF in general, and UiO-66 in particular, is the progenitor for a large family of zirconium and non-zirconium multinuclear cluster-based MOFs synthesized by employing linkers having specific geometrical and symmetrical features (*i.e.*, the same $M_6O_4(OH)_4$ clusters found in **fcu**-MOFs serve as MBBs for a wide range of MOF materials displaying different topologies) [12]. Following the discussions in this review, readers will realize that the 12-c **fcu**-MOFs are among the most explored frameworks due to their ease of design and assembly for a particular end function.

Table 1
Some representative isoreticular Zr-**fcu**-MOFs and their pore dimensions.

MOF Name	Linker	Cage/Aperture size (Å)			Ref.
		Octahedral cage	Tetrahedral cage	Pore aperture	
Zr-Squa-**fcu**-MOF	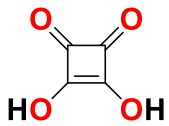	5.6	4.7	2.4	[20]
Zr-fum-**fcu**-MOF (MOF-801)	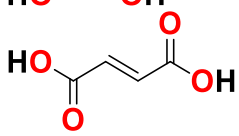	7.4	5.6	4.7	[21]
UiO-66	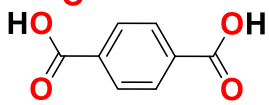	11	7.5	6	[22]
UiO-67	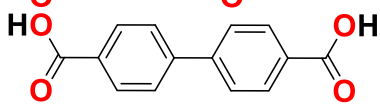	16	11.5	8	[10,23]
UiO-68	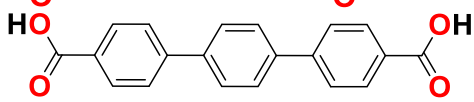	25.6	–	10	[24]

Aside from the MBB strategy, **fcu**-MOFs can be assembled via a supermolecular building block (SBB) approach through metal–organic polyhedra (MOP) building units that resemble augmented cuboctahedron SBU (Fig. 1C). In an augmented cuboctahedron SBU, twelve 4-c nodes are joined by linear, ditopic linkers (Fig. 1B). As represented in Fig. 1B (right), the linear connections that join the vertices of a cuboctahedron are not straight linkers, which is particularly important in the design and construction of MOP-based **fcu**-MOFs. There are then two types of angles that characterize the augmented cuboctahedron SBU: (i) the angle between the links to the center of the tetravalent node (η); and (ii) the angle between the links of a ditopic linker (θ). If a metal ion that can generate a 4-c square SBU (η = 90° between the links to the center of the SBU as in a Cu paddle-wheel SBU) is used, the ditopic linker must be bent at an angle close to 120° as in the case of 1,3-benzenedicarboxylate linker [13]. One example of this strategy is shown in Fig. 1C. It is noted that many different examples of MOP-based **fcu**-MOFs will be discussed in the review.

Even though Zr_6 oxocluster-based MOFs represent by far the largest proportion of **fcu**-MOFs, 12-c building units of other elements do exist. One of the great achievements in the family of **fcu**-MOFs is the discovery of the experimental conditions that allow for the *in-situ* formation of hexanuclear actinide (An) and rare earth (RE) metal oxoclusters to assemble M–**fcu**–MOFs, which are isostructural to UiO-66(Zr). In this review, discussion will cover the assembly of various isostructural and isoreticular M–**fcu**–MOFs. The chemistry behind the linker size/functionality and the effects of the variations in the metal ions on the structures and properties of the respective **fcu**-MOFs will also be assessed and explained. We note that in the literature, the terms 'isostructural' and 'isoreticular' are used interchangeably in an arbitrary way. For this review, isostructural MOFs refer to MOFs with the same topology obtained from the same linker but by substitution of one metal ion with another, whereas isoreticular series refers to MOFs of the same underlying topology assembled from different linkers but possessing similar metal clusters. As will be illustrated, the architectural stability, diversity and amenability of **fcu**-MOFs for structural tunability either by pre-targeted design or by post-synthetic modification and synthetic flexibility, with respect to both the organic and inorganic components, make them materials of great potential interest and importance for many applications relevant to energy and environmental sustainability. One of the important structural features of **fcu**-MOFs is the presence of triangular window apertures that serve as the only path in and out of the interconnected tetrahedral and octahedral cages. This feature, in turn, allows for the deployment of the MOF platform for size- and/or shape-selective separation of different molecules [14–18]. The review generally highlights the significant amounts of research work that have been reported in order to understand the overarching trends in the chemistry and application of **fcu**-MOFs.

2. Zr_6 oxocluster-based fcu-MOFs: Synthetic and structure–property relationships

Since the synthesis of UiO-66, tremendous progress has been made in the assembly of isoreticular Zr-**fcu**-MOFs that exhibit wide ranges of porosity and chemistry. One of the most useful and powerful concepts in MOF chemistry, isoreticular chemistry, enables the expansion, contraction, decoration, and functionalization of a set porous material without disrupting the original topology. After being proven by the successful assembly of a series of IRMOFs having the same network topology to that of MOF-5 (IRMOF-1), with a wide range of pore volumes and chemistry [19], the isoreticular concept was later expanded to different MOF platforms. The pore expansion of UiO-6*x*, from its original link of one phenylene ring (UiO-66) to 4 rings (UiO-69), and even to linkers shorter due to a core unit smaller than a phenylene moiety, has resulted in isoreticular Zr-**fcu**-MOFs structures displaying wide ranges of pore dimensions (Table 1). The possibility to introduce functional groups tethered to the backbone of the linkers as well as on the metal cluster SBUs also expanded the family of Zr-**fcu**-MOFs, creating many opportunities for their deployment in different areas. In this section, a detailed discussion on the design, synthesis, characterization, crystal structure description, and representative applications of various isoreticular Zr-**fcu**-MOFs will be made.

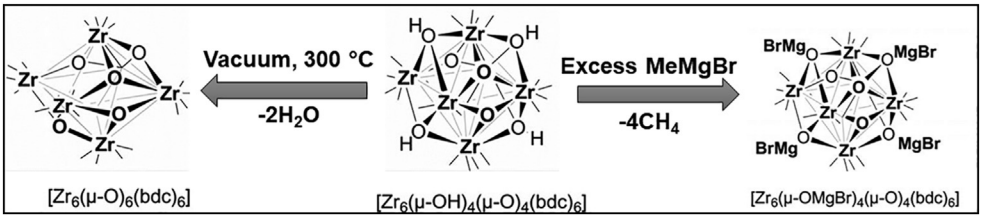

Fig. 2. Schematic showing dehydroxylation of μ_3–OH upon heating and reaction with Grignard reagent.

2.1. The prototypical Zr-fcu-MOF, UiO-66

The breakthrough discovery in the assembly of zirconium hexanuclear cluster-based MOFs with underlying **fcu** topology (named as UiO-66), $Zr_6(\mu_3\text{–}O_4)(\mu_3\text{–}OH)_4(BDC)_6$, was made in 2008 by Cavka and co-workers who synthesized the MOF by solvothermal reaction between $ZrCl_4$ and H_2BDC in *N,N'*-dimethylformamide (DMF) [10]. The detailed structure of UiO-66 was validated by a combination of experimental and theoretical characterizations including X-ray diffraction (XRD), extended X-ray absorption fine structure spectroscopy (EXAFS), calorimetry, Fourier-transform infrared spectroscopy (FT–IR) and/or diffuse reflectance infrared Fourier–transform (DRIFT) spectroscopy, and *ab initio* combined structure refinement [22,25,26]. The $Zr_6(\mu_3\text{–}O_4)(\mu_3\text{–}OH)_4(CO_2)_{12}$ building units consist of Zr_6 octahedra, the edges of which are bridged by organic linkers and the eight triangular faces of which are capped alternately by four μ_3–O and four μ_3–OH ligands. The identity of the μ_3–OH/μ_3–O groups in $Zr_6(\mu_3\text{–}O_4)(\mu_3\text{–}OH)_4(CO_2)_{12}$ cluster was validated by quantitative determination of the chemically accessible μ_3–OH groups using FT–IR spectroscopy, thermogravimetric analysis (TGA), and chemical titration with CH_3MgBr [26,27]. The FT–IR spectroscopically measured OH content, 2.2 mmol/g (37 mgOH/g), was in good agreement to the calculated value (1.9 mmolOH/g or 32 mgOH/g) obtained from the expected molecular formula, $Zr_6O_4(OH)_4(linker)_6$. The information obtained by FT–IR spectroscopic studies shows the complete transformation of the hydrated forms of UiO-6*x*, $[Zr_6(\mu_3\text{–}O)_4(\mu_3\text{–}OH)_4(linker)_6]$, into the dehydroxylated form, $[Zr_6(\mu_3\text{–}O)_6(linker)_6]$, at ~ 250 °C (Fig. 2). The stability of the dehydroxylated phase, up to 450 °C, then allowed for the estimation of the μ_3–OH content by TGA [10,22,27]. The bulk OH content, 1.6 mmol OH/g (27 mg OH/g), estimated from TGA traces by extrapolation of the measured weight loss between 250 and 400 °C, is in close agreement with the calculated value (1.9 mmolOH/g or 32 mgOH/g). The bulk OH content in the Zr_6 oxocluster of Zr-**fcu**-MOFs was further confirmed by chemical titration with excess methyl magnesium bromide (CH_3MgBr) in dry diethyl ether that reacts quantitatively with the surface hydroxyl groups of the MOF to yield methane (CH_4) (Fig. 2). The gas chromatography (GC) determination of the methane evolved during the Grignard reaction corresponded to 1.8 mmol OH/g (31 mgOH/g), which was in good agreement with the theoretically estimated value (1.9 mmolOH/g or 32 mgOH/g).

Aside from the permanent porosity observed for UiO-66, the material was reported to possess remarkable chemical and hydrolytic stability as confirmed by the maintenance of powder XRD (PXRD) peaks after soaking the MOF in water and different organic solvents [10]. The high stability of the framework with respect to water and, thus, the complete reversibility of the dehydration/hydration phenomenon was further confirmed by FT–IR data [22]. Moreover, temperature-dependent PXRD, TGA and TGA/mass spectrometry (MS) measurements provided evidence for the thermal stability of the MOF with a decomposition temperature reaching above 500 °C [22]. The high chemical and thermal stability of the MOF has been attributed to the highly connected nature of the individual Zr ions as well as the resultant inorganic MBBs. The strong Zr–O coordination bonds between the high valence, oxophilic Zr(IV) ions and the carboxylate functional groups (Zr–O bond dissociation energy is ~ 766 kJ/mol)[28] and the inner Zr_6 oxocluster allows for reversible dehydroxylation or rehydration of μ_3–OH groups without compromising the dicarboxylate bridges' stabilities [22]. In recent years, the notable stability of the MOF sparked research focused on deploying the material for the adsorption of different molecules under harsh aqueous phases with the adsorption of dyes from aqueous solutions being an example [29].

The chemical and thermal stability of UiO-66 also extends to mechanical stability. The MOF was found to retain its PXRD patterns upon applying high pressures (up to 10,000 kg/cm^2) on powder samples [10]. This property is an important factor for deployment of MOFs in industrial applications since materials often need to be mechanically stable to avoid structural distortion or framework collapse under hydrostatic compression during the shaping steps. Gas storage and separation are among the applications of porous MOFs that require dense packing of the powders without collapse of the pores under mechanical compression. In UiO-66, the highly connected nature of the Zr_6 cluster and the high Zr–O coordination were suggested to be major contributors to the enhanced shear resistance of the MOF under mechanical stress by effectively restricting the freedom of the coordination bond stretching and/or compression [30].

Though, in a more general sense, UiO-66 has been claimed to be chemically stable, the chemical stability in aqueous media of different pH is a relative term that requires very sensitive analytical techniques to detect MOF degradations at very small levels. For example, high performance liquid chromatography (HPLC) and inductively coupled plasma mass spectrometry (ICP–MS) data demonstrated the release of terephthalate linkers from UiO-66 to different degrees at 25 °C when the material was immersed in aqueous solutions containing 2-amino-2-(hydroxymethyl)-1,3-propanediol, 4-(2-hydroxyethyl)piperazine-1-ethane sulfonic acid, *N*-ethyl morpholine and phosphate buffers [31]. However, PXRD measurements performed after immersion of the UiO-66 samples in the buffers were unable to detect any level of MOF degradation. No noticeable changes were also detected in the scanning electron microscopy (SEM) images of the post-exposed samples when compared with the parent UiO-66. Even though the N_2 adsorption isotherm measurements were more sensitive than the PXRD to detect the degradations of the post-exposed samples by showing a decrease in specific surface areas, the measurements could not reflect the degree of degradation given that the decreases in specific surface area could not be correlated with a percentage of released linker [31].

The pH of the aqueous media also has a significant influence on the chemical robustness of the UiO-66 framework and its deployment for a particular end function. For example, Zhao *et al.* [32] investigated the stability and defluorination performance of UiO-66 in aqueous solutions of differing pH values. As evidenced by PXRD analysis, the MOF was observed to retain its crystallinity in acidic solutions with pH = 2.0 – 6.0 without F^- ions present (pH

values adjusted by HCl). However, structure collapse was seen for those pH values when the solution contained F^- ions, which was attributed to the rupture of Zr—O—C bonds as a result of strong H–bonding interactions between HF formed in the acidic conditions and the carboxylate groups of the linkers. The UiO-66 structure remained intact in neutral and basic solutions (pH = 6.0 and 9.0) even in the presence of F^-, suggesting no HF formation in such conditions. However, UiO-66 was observed to be less crystalline when pH = 10.4 and to decompose completely at a slightly higher pH of 11.0, which was attributed to the competitive interaction of OH^- with the linker to form Zr–OH bonds. Owing to its chemical stability at neutral and slightly basic conditions, UiO-66 has high efficiency for removal of F^- ions from aqueous solutions (41.36 mg/g), with FT–IR spectroscopy measurements revealing the μ_3–OH groups of the Zr_6 oxocluster as the adsorption sites for F^-.

2.2. Impact of synthesis parameters on the assembly of Zr-fcu-MOFs

As for most other MOFs, Zr-**fcu**-MOFs are mainly assembled solvothermally by mixing Zr(IV) salts and organic linkers in appropriate solvents with and without modulating agents at higher temperatures for a certain duration of time. Therefore, the isolation of the targeted **fcu** framework can be dictated by any of these synthetic parameters.

2.2.1. Zr(IV) salt precursors

Zirconium chloride ($ZrCl_4$) and zirconyl oxychloride ($ZrOCl_2$) are the two commonly employed Zr(IV) salts for the assembly of Zr-**fcu**-MOFs. Experiments conducted on the role of zirconium metal salt precursors demonstrated the suitability of the less acidic $ZrOCl_2{\cdot}8H_2O$ source than $ZrCl_4$ to avoid possible reproducibility issues [33]. Due to the high hygroscopic character of $ZrCl_4$, this salt tends to form mixtures of unknown proportions of $ZrCl_4$ and $ZrOCl_2{\cdot}8H_2O$ upon exposure to air moisture, which creates issues in handling and concerns about synthetic reproducibility.

The use of chloride salt precursors generates HCl during the solvothermal assembly of UiO-6*x* MOFs. The generation of HCl is hypothesized to be undesirable in some HCl-sensitive reactions, as in the controlled synthesis of Zr-**fcu**-MOF@metal nanoparticle composites [34]. In the search for reactions with no generation of HCl, the use of other zirconium precursors such as zirconium propoxide ($Zr(O\text{-}nPr)_4$) in place of $ZrCl_4$ were reported to be appropriate for the solvothermal assembly of UiO-66 with simultaneous encapsulation of gold nanoparticles within the framework [34]. Other Zr(IV) salts were reported to be effective precursors for the *in situ* generation of the desired Zr_6 oxoclusters [35–37]. For example, $Zr(NO_3)_4$, $Zr(NO_3)_4{\cdot}5H_2O$, $ZrO(NO_3)_2{\cdot}4H_2O$, $Zr(SO_4)_2$, and Zr (acetyl acetonate)$_2$ have all been successfully employed in the synthesis of UiO-66 and various isoreticular Zr-**fcu**-MOFs, including MOF-801, UiO-66-NH_2, UiO-66-NO_2, UiO-66-Br, UiO-66–2,5-$(OH)_2$, UiO-66–2,5-F_4, UiO-66-COOH and UiO-66–2,5-$(COOH)_2$ [35,36,38–42].

In addition to commercially-available zirconium salts, pre-synthesized hexanuclear zirconium-methacrylate oxocluster, $[Zr_6O_4(OH)_4(CH_2C(CH_3)COO)_{12}]$, and dodecanuclear zirconium acetate cluster, $[Zr_6O_4(OH)_4(CH_3COO)_{12}]_2$, were also reported to be suitable for preparing several UiO-6*x* MOFs, such as UiO-66 and UiO-67 [41,43]. Regardless of the different Zr(IV) salt precursors, **fcu**-MOFs prepared from the different precursors were all claimed to have similar textural, morphological and stability characteristics with only slight differences in their surface areas, pore volumes, and gas adsorption properties due to the presence of missing-linker defects [38,40,42]. It is noted though that an accurate comparison of the properties for the MOFs assembled from the same linker but using different Zr(IV) salt precursors is not possible. This is because different researchers have reported similar MOFs by varying not only the metal salt precursors, but also other synthetic parameters such as solvent type, temperature, time, amount and type of monocarboxylic acid modulators.

2.2.2. Temperature and synthetic routes

In terms of the temperature used for the solvothermal assembly of the **fcu**-MOFs, heating in a pre-heated oven at 120–130 °C in DMF or DMF/H_2O solvent is the typical reaction conditions employed, however, researchers have reported the assembly of Zr-**fcu**-MOFs at different temperatures (from room temperature up to 220 °C) in different solvents that range from pure DMF, *N*, *N*′-diethylformamide (DEF), *N*,*N*′-dimethylacetamide (DMA), and water, among other more exotic solvents [17,35,36,38–40,44–49]. Nevertheless, it must be emphasized that the synthetic conditions employed to assemble the MOFs should lower the activation energy down to an appropriate value (~71 kJ/mol for UiO-type MOFs [50]) without any detrimental impacts on the kinetics of nucleation. Various parameters are usually adjusted to achieve the desired activation energy and kinetics of nucleation for the synthesis of Zr-**fcu**-MOFs, which include the use of more soluble linkers and/or appropriate solvent(s) to enhance the solubility and the addition of HCl [33,50,51]. The use of appropriate Zr(IV) salt precursor and solvent mixtures that favor the hydrolysis of Zr(IV) and hence the easier formation of Zr_6 oxoclusters were also reported to be successful routes to achieve UiO-6*x*(Zr) MOFs and other isostructural analogs, such as UiO-6*x*(Hf) and UiO-6*x*(Ce) [46]. This was proven using a low concentration of $ZrCl_4$ or $ZrOCl_2$ and pure H_2O with ~300 equivalent H_2O/Zr that affords relatively lower pH values (~0.24) than the conventional $ZrCl_4/ZrOCl_2$ and DMF mixtures. The excess water then favors the hydrolysis of Zr (IV) species to yield the successful room temperature assembly of Zr-**fcu**-MOFs (*e.g.*, MOF-801, UiO-66-NH_2, and UiO-66-COOH) as well as their Ce and Hf isostructures [46,52]. For this example, the higher pH values that are often required to accelerate the nucleation/growth process by facilitating the facile deprotonation of linkers and the ease of formation of Zr oxoclusters [33,53] was compensated by the low concentration of the Zr(IV) salt precursors. The use of ambient conditions for the assembly of Zr-**fcu**-MOFs is, however, demonstrated to be associated with the formation of more missing-linker defects within the frameworks than the synthesis at higher temperatures [46,49,54,55]. For example, MOF-801, UiO-66-NH_2, and UiO-66-COOH synthesized at room temperature were reported to have coordination numbers (per Zr_6 cluster) of 4.1, 4.7, and 3.8, respectively [46]. The presence of defects in the MOFs were also substantiated by their higher Brunauer–Emmett–Teller (BET) surface areas, pore volumes, and pore sizes than the respective MOFs prepared at the conventional temperature conditions.

The assembly of Zr-**fcu**-MOFs have also been reported to be adaptable to different types of synthetic routes. In this aspect, microwave-assisted synthesis, spray-drying, sol–gel process, and the environmentally benign mechanochemical techniques were shown to be effective in preparing various isoreticular Zr-**fcu**-MOFs [36,41,56–64]. Among the different synthetic routes, microwave-aided synthesis has been widely applied as an alternative to the conventional solvothermal approach. For example, synthesis of MOF-801, UiO-66-NH_2, and UiO-66 was reported as successful by microwave irradiation, with no significant effects on morphology, crystal size, or defects of the synthesized MOFs compared to the results obtained by the conventional solvothermal heating [58,63,65,66]. Moreover, UiO-66 and UiO-66-NH_2 were reported to be accessible via the greener mechanochemical synthesis without requiring strong acids, high temperature and excess reactants [62]. In a typical mechanochemical synthesis, either liquid (methanol or DMF) assisted grinding (LAG) or

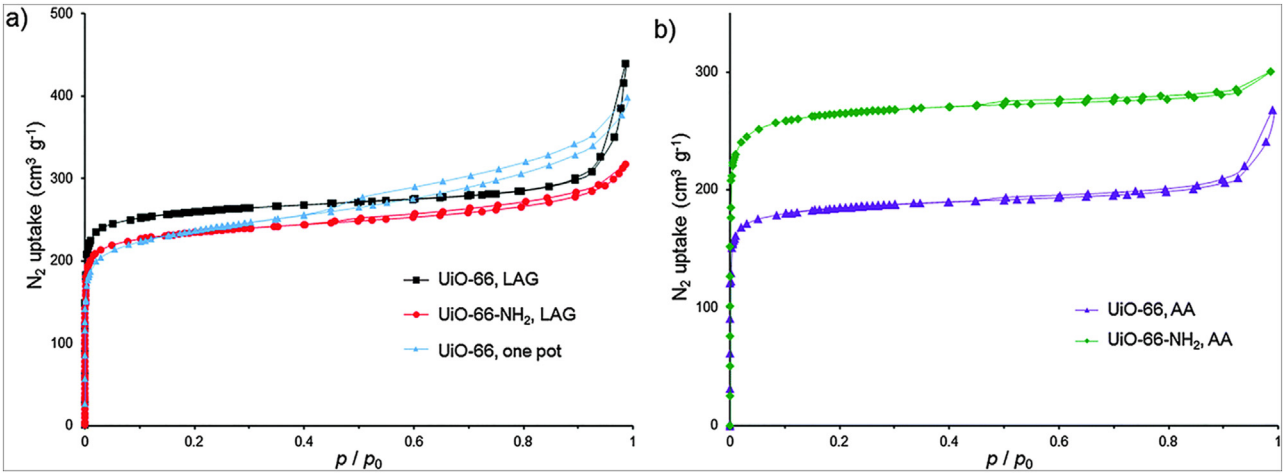

Fig. 3. N_2 sorption isotherms at 77 K for UiO-66 and UiO-66-NH_2 synthesized via: (a) LAG in MeOH, and solvothermal route from $Zr(OPr)_4$ for UiO-66; (b) AA in MeOH vapor at 45 °C. Reproduced with permission from ref. [62].

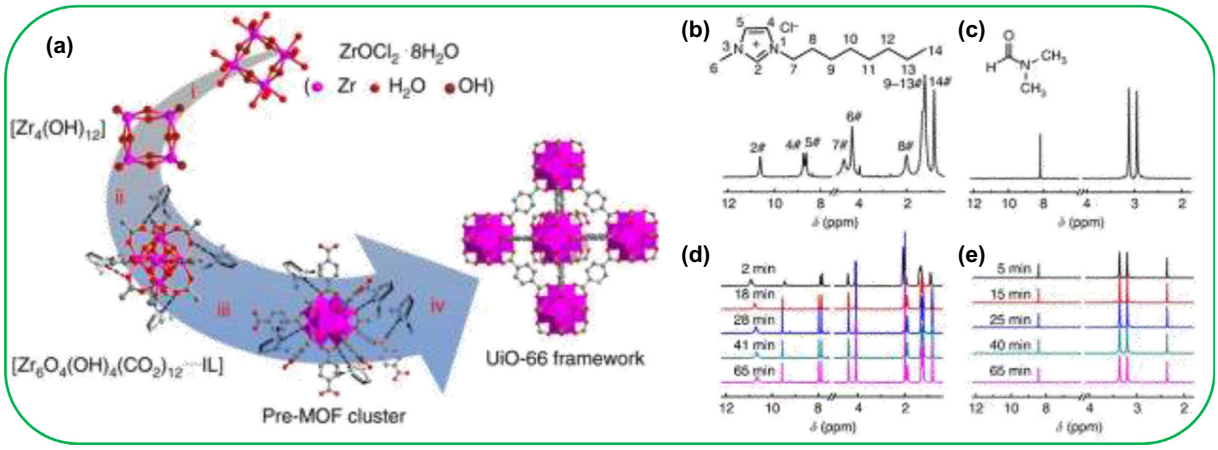

Fig. 4. Schematic showing the plausible mechanism for the acetic acid modulated assembly of UiO-66 in IL (a). Molecular structures and ^1H NMR spectra of [Omim]Cl and DMF (b & c) and *in situ* ^1H NMR spectra of the UiO-66 synthesis in [Omim]Cl (d) and DMF (e) at 298 K. Adapted and reproduced with permission from ref. [67].

solvent-free accelerated aging (AA) of a pre-assembled methacrylate or benzoate Zr_6 oxocluster MBB, $Zr_6O_4(OH)_4(C_2H_3CO_2)_{12}$ or $Zr_6O_4(OH)_4(C_6H_5CO_2)_{12}$, with terephthalic acid or 2-aminoterephthalic acid resulted in UiO-66 or UiO-66-NH_2, respectively, having crystal morphology and porosity (Fig. 3) attributes very similar to their counterparts synthesized via traditional solvothermal routes.

Ionothermal synthesis, using ionic liquids (ILs) as solvents, is another approach that has been employed for the assembly of Zr-**fcu**-MOFs due to the appealing properties of tunable ILs to dissolve both organic and inorganic precursors and the consequential effect in shortening reaction time and reducing temperature. In this regard, Sang *et al.* [67] synthesized UiO-66 in 1-octyl-3-methylimidazolium chloride ([Omim]Cl) and 1-decyl-3-methylimidazolium chloride ([Dmim]Cl) at room temperature in 0.5 h by the reaction of $ZrOCl_2{\cdot}8H_2O$ and terephthalic acid in the presence of acetic acid as a modulator. On the contrary, it was observed to take at least 120 h to assemble the same MOF in DMF at room temperature. The rapid formation of UiO-66 in [Omim]Cl and ([Dmim]Cl was confirmed by PXRD, FT-IR and X-ray photoelectron spectroscopy (XPS). Other ILs, such as 1-hexyl-3-methylimidazolium chloride ([Hmim]Cl), [Omim]Br and [Omim]I, were also employed to assemble UiO-66. However, the rapid ionothermal crystallization led to missing-linker defects that resulted in an overall framework composition of $Zr_6O_4(OH)_4(BDC)_{5.1}$. The presence of defects in the prepared sample was further supported by TGA and N_2 adsorption measurements that gave higher surface area (1519 m^2/g) for the ionothermal assembled UiO-66 than the one produced by the traditional solvothermal process in DMF (1187 m^2/g) [10]. Mechanistically, as supported by *in situ* ^1H nuclear magnetic resonance (NMR) spectroscopy studies, the IL played a significant role in accelerating linker exchange between the modulators and the linkers at the coordination sites of Zr complexation (*i.e.*, in facilitating Zr–linker coordination), which is due to the strong H–bonding interactions between the modulators and the aprotic alkyl-3-methylimidazolium halide IL, [$C_n$mim]X, (X = Cl^-, Br^-, and I^-) (Fig. 4). The successful crystallization of Zr-**fcu**-MOFs in [Omim]Cl at room temperature was also extended to other isoreticular MOFs, including UiO-66-NO_2, UiO-66-NH_2, UiO-66-OH, UiO-67, and UiO-67-BPyDC, demonstrating the adaptability of the MOF platform to different synthetic approaches.

2.2.3. Modulating agents

One key point that has enabled the consistent and reproducible *in situ* generation of the Zr_6 oxocluster MBBs and the consequential

MOF nucleation into high quality, large single crystals is the development of the modulated synthesis approach, which entails the use of ligands with just one coordination site to compete with linkers for coordination to metal cations. [68]. The modulating agent acts as a regulator for the reaction rate and the crystal morphology. The monofunctional modulators are usually applied in large concentrations and are speculated to form intermediate complexes with the metal cations. The growth of MOF crystals then proceeds through an exchange between the linker and modulator. With respect to the Zr-**fcu**-MOFs, Schaate *et al.* [24] investigated the impact of monocarboxylic acid-based modulators (*e.g.*, benzoic acid and acetic acid) and their concentration effect on the assembly of UiO-66, UiO-66-NH_2, UiO-67, and UiO-68-NH_2 in terms of crystallization and nucleation rate, particle size and morphology. Depending on the concentration of the monocarboxylic acid modulator, development from a disordered phase and/or intergrown aggregates of extremely tiny crystals as well as larger size individual octahedral-shaped nanocrystals were observed during assembly of isoreticular Zr-**fcu**-MOFs as evidenced by SEM images, PXRD peak broadening effects and dynamic light scattering (DLS) analyses. The preferential *in situ* formation of complexes between Zr(IV) cations and the monocarboxylic acid modulators and the later slow substitution of the monocarboxylate modulators by the dicarboxylate linkers is due to the formation of large crystals upon using large equivalents of modulators. However, the possibility to get large size single crystals by increasing modulator concentration depends on the solubility of the linker in the solvent(s) employed for the reaction. This is exemplified by the impact of modulator amount in the solvothermal assembly of UiO-66 and UiO-67. Due to the much lower solubility of the H_2BPDC linker as compared to the H_2BDC, the concentration of monocarboxylic acid modulator does not control the size of the UiO-67 particles [24,69]. As described in literature [69], the competitive reaction equilibria between the carboxylates of either the linker or the modulator with $[Zr_6O_4(OH)_4]^{12+}$ MBBs dictates the particle size of the resultant MOF. The high solubility of both the modulator and the linker, as in H_2BDC of UiO-66, leads to efficient participation of both components in the reaction equilibria, so that the concentration of the modulator can influence the result. However, the poor solubility of the linker, as in the H_2BPDC of UiO-67, decreases the influence of the modulator on the particle size of the resultant product due to a strong tendency of the linker to stay coordinated to the growing crystallites. The effect of increasing benzoic acid modulator on the textural properties of Zr-**fcu**-MOFs to change the morphology from intergrown aggregates of very small crystals at zero concentration to well-defined octahedral single crystals at higher amounts was also evidenced in UiO-66–1,4-NDC [70]. In addition to the crystal size and shape, the modulator was also observed to increase the surface area and reduce its thermal stability due to the formation of defects either as missing linkers or missing $Zr_6(OH)_4O_4$ clusters, with the defect density increasing up to 50% as a function of increasing amounts of benzoic acid used.

Apart from the commonly used benzoic, formic and acetic acids, other monocarboxylic acids have also been explored as modulators for consistent *in situ* generation of Zr_6 oxocluster MBBs. Among the range of potential modulators that have been investigated, amino acids, such as *l*-proline, glycine, and *l*-phenylalanine, were found to be efficient in controlling the particle size allowing for the isolation of large, X-ray diffraction quality single crystals of Zr-**fcu**-MOFs, such as Zr-muconate, UiO-66, UiO-67-Cl, UiO-67-*m*-CH_3, and PCN-56 [71,72]. The possibility to modify synthetic conditions to permit the synthesis of defective **fcu**-MOFs by incorporating amino acid modulators at defect sites was also demonstrated [71]. The amino acid pendant groups are then asserted to create further opportunities for the preparation of suitable MOFs for CO_2 capture, catalysis, and the installation of bigger peptide molecules.

The influence of other additives on the structure and properties of Zr-**fcu**-MOFs have also been investigated. According to a study by Ragon *et al.* [33], the addition of water was found to induce a faster crystallization rate of UiO-66 by favoring the formation of the Zr_6 oxocluster. This agrees with the previous study by Schaate *et al.* [24] who explored the impact of water on the crystallinity of UiO-66 and UiO-66-NH_2. Though the addition of a large amount of water was demonstrated to reduce the particle size of UiO-66 as confirmed by very broad reflections in the PXRD patterns and intergrown crystallites in the SEM images, it had minimal influence on the crystallization of UiO-66-NH_2. In a later study, water was also reported to play a significant role as a structure-directing agent in the nucleation process of UiO-66 [73]. Indeed, the solvothermal synthesis reaction between Zr(IV) salt and H_2BDC could result in the assembly of either UiO-66 ($Zr_6O_6(OH)_4(BDC)_6$) or MIL-140A (ZrO(BDC)) polymorphs. The addition of a controlled amount of water at a particular reaction temperature is then important for directing the selective formation of UiO-66 with symmetrical $Zr_6(OH)_4O_4$ octahedra SBUs through producing, at the nucleation stage, tetragonal ZrO_2 (T–ZrO_2) nanoparticles (NPs) via the interaction of $ZrCl_4$ with water. The local arrangement of Zr and O atoms in T–ZrO_2 is very similar to Zr oxocluster (Zr_6O_6) MBBs in UiO-66 (Fig. 5). Among the different forms of ZrO_2, the formation of T–ZrO_2 is kinetically favored and its successive transformation to the thermodynamically more stable monoclinic (M−ZrO_2) phase is hypothesized to be prevented by the presence of BDC linkers, which direct the growth into UiO-66.

Other additives were also shown to have impact on the structure and properties of Zr-**fcu**-MOFs. Abid *et al.* [74] investigated the role of adding ammonium hydroxide (NH_4OH) during the solvothermal synthesis of UiO-66 on the particle size, structure and adsorption properties of the MOF. Successive N_2 adsorption isotherms, XRD, SEM, FT–IR, and TGA characterizations of the

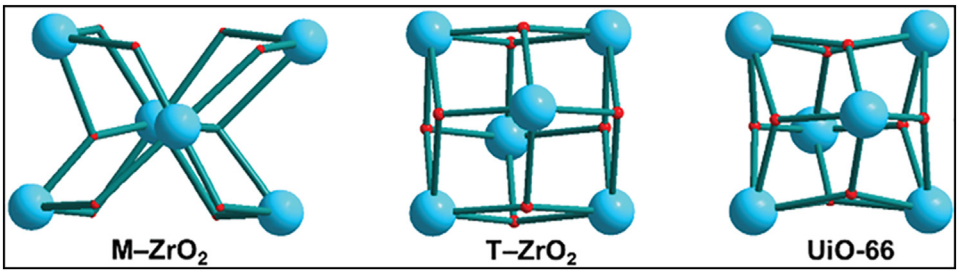

Fig. 5. Representation of Zr–O clusters (Zr blue and O red) in the monoclinic and tetragonal forms of ZrO_2 and in the UiO-66 based Zr oxocluster MBB. Reproduced with permission from ref. [73]. (For interpretation of the references to color in this figure legend, the reader is referred to the web version of this article.)

physicochemical properties of the UiO-66 samples displayed decreases in the BET surface areas, an increase in the pore size and volume, and a reduction in particle sizes upon addition of NH_4-OH. The increase in pH of the solution upon adding NH_4OH enhances the solubility of the solute and the rate of the reaction impacts the crystal size of the final product. The formation of zirconium hydroxide or zirconium oxide induced by the added NH_4-OH and possible coordination of OH^- groups on the metal cluster could also exert influence on the specific surface areas and pore volumes of the product.

Introducing inorganic acids as additives during the solvothermal assembly of Zr-**fcu**-MOFs is another approach that has been implemented to modulate crystal size and morphologies of this MOF platform. For example, Han *et al.* [75] studied the influence of HF additive on the crystal size and morphology of UiO-66. Increasing the concentration of HF resulted in a change to crystal size and morphology of UiO-66 from irregular cubes of size equal to 150 nm to large cuboctahedron with sizes of around 7 μm. According to the energy dispersive spectrometry (EDS) and ^{19}F magic angle spinning (MAS) NMR studies, fluorine ions were directly bonded to Zr(IV) in the MBBs of the MOF. The competitive interactions between F^- and the linker to coordinate with Zr(IV) ions is the plausible mechanism for controlling nucleation and, therefore, the size of UiO-66 crystals.

The other inorganic acid that has been widely employed as an additive during solvothermal synthesis of Zr-**fcu**-MOFs is HCl [23]. In order to gleam mechanistic insight about the role of HCl in the assembly of Zr-**fcu**-MOFs, solvothermal syntheses of UiO-66, functionalized UiO-66-X derivatives from BDC-X linkers (X = OH, NH_2, NO_2, $(OH)_2$, $(NH_2)_2$), UiO-67, and UiO-67-X (X = NO_2, NH_2) were conducted with and without HCl additive. Though it was expected that the acid would slow down the reaction, for all solvothermal syntheses of the MOFs, the formation of MOF crystals was observed to be sped up by increasing the concentration of the acid with simultaneous increase in surface area of the resultant MOF structures. Ragon *et al.* [33] also observed a similar effect for the HCl additive on the solvothermal crystallization of UiO-66, with *in situ* EDX studies demonstrating a faster MOF crystallization upon the addition of different amounts of 37% HCl solution and with increasing HCl/Zr ratio. Owing to the enhancement in the solubility of $ZrCl_4$ and H_2BDC upon adding HCl, the modulation mechanism of the acid is postulated to originate from the role that the acid plays in dissociating linkers concentrated around the Zr nodes blocking the connection of nodes to one another and eventually creating reaction mixtures that facilitate joining of nodes [23]. Moreover, the presence of water in the HCl is responsible for the faster crystallization rate by facilitating the *in situ* formation of the Zr_6 oxocluster MBBs [33]. The observed increase in the surface areas of the resultant MOFs as compared to those obtained by acid-free synthesis is due to missing-linker defects. FT–IR, TGA, and elemental analysis (EA) studies also confirmed the presence of more missing linkers in UiO-66 made via the HCl route than the conventionally prepared material. Pore size distribution analysis demonstrated a noticeable shift in the size of the tetrahedral pore from ca. 8.5 to 11.5 Å and PXRD measurements indicated a more intense [200] reflection, which is expected when linkers are missing [33].

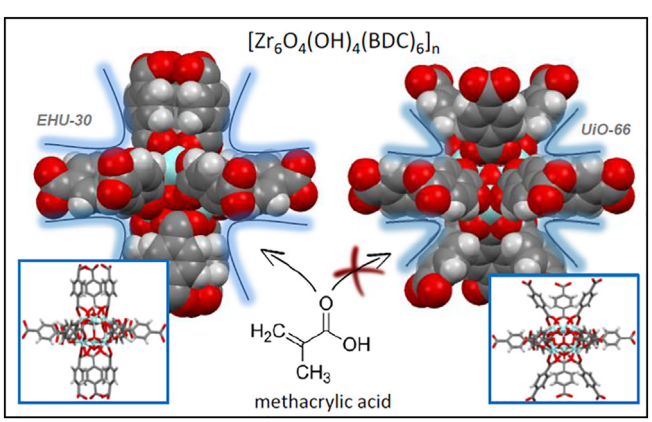

Fig. 6. The structural differences around the Zr-oxocluster of EHU-30 and UiO-66. Reproduced with permission from ref. [76].

2.2.4. Precursor concentration

The overall concentration of precursors present in the synthesis is also important for the assembly of UiO-66. The impact of this parameter was clearly evidenced in the work of Perfecto-Irigaray *et al.* [76] who isolated a polymorph of UiO-66, $[Zr_6(\mu_3\text{–}O)_4(\mu_3\text{–}OH)_4(\mu_4\text{–}BDC)_6]_n$ and named as EHU-30, from mixtures of Zr(IV) isopropoxide, methacrylic acid and H_2BDC under solvothermal conditions at 140 °C for 90 min. The two polymorphs (Fig. 6) have different network topologies with EHU-30 adopting an 8-c **hex** underlying net. The use of relatively dilute precursor concentrations was reported to be critical for the exclusive formation of the thermodynamically favored UiO-66 and with concentrated conditions leading to the kinetic **hex**-MOF. EHU-30, as the kinetically favored product, was further evidenced by periodic density functional theory (DFT) calculations that demonstrated a higher thermodynamic stability for the more dense-packed UiO-66 (BET surface area of 1283 m^2/g) than the slightly more porous EHU-30 (BET surface area of 1399 m^2/g) by 30 kJ/mol. The correlation of precursor concentration to the final MOF products was also studied in four MOFs isostructural or isoreticular to EHU-30, namely EHU-30-NH_2(Zr), EHU-30-NH_2(Hf), EHU-30-NHR(Zr) and EHU-30-NHR (Hf) (R = 2-carboxypropyl), and their M–**fcu**–MOF polymorphs [77]. However, the generality of the concentration effect on the assembly of other Zr-**fcu**-MOFs remains largely underdeveloped.

Aside from exploring the different factors that potentially dictate the assembly of Zr-**fcu**-MOFs, the will to attain efficient, faster and more scalable synthesis of the MOFs is highly sought after. So far, the preparation of Zr-**fcu**-MOFs has been realized by the conventional batch synthesis approach. Although not well-investigated due to challenges in the precise control of mixing the reagents, the possibility to synthesize materials within this MOF platform in continuous flow reactors was demonstrated by Rubio-Martinez *et al.* [78] who reported a continuous production of UiO-66 with a rate of 60 g/h. The preparation of UiO-66 and derivatives in continuous flow nanoreactors was also later demonstrated by other researchers [79–81]. However, this strategy, which is very promising for large-scale synthesis of MOFs, needs further study and optimization before being employed as a general approach.

2.3. Isoreticular functionalization of Zr-fcu-MOFs

The chemical stability of UiO-66 has added fuel to the research community for further design and assembly of isoreticular Zr-**fcu**-MOFs using functionalized BDC linkers (BDC-X). Functionalization is driven by the desire to tune the pore and/or pore aperture metrics and functionality for different applications including gas separation and catalytic transformations. The use of BDC-X linkers (Fig. 7) has led to the synthesis of many isoreticular UiO-66-X MOFs, X = F, Cl, Br, I, CN, NH_2, NO_2, CH_3, $(CH_3)_2$, CF_3, $(CF_3)_2$, CO_2H, $(CO_2H)_2$, $(CO_2H)_4$, F_2, F_4, Cl_2, Br_2, OH, $(OH)_2$, $(SH)_2$, OCH_3, $(OCH_3)_2$, $(OCH_2CH_3)_2$, $(SCH_2CH = CH_2)_2$, SO_3H, O–Ph–NO_2, and C_6H_4 [37,39,40,45,47,51,82–99].

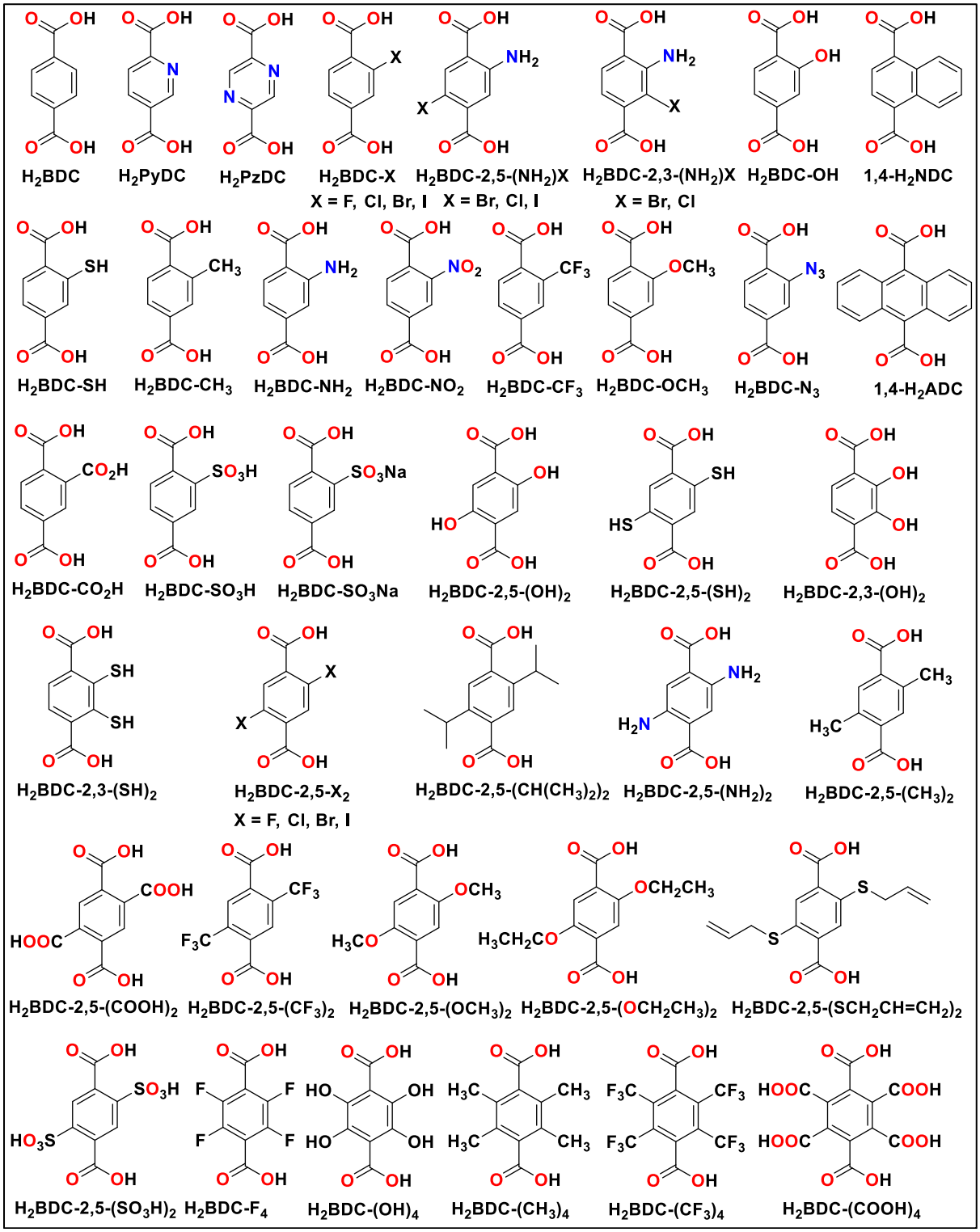

Fig. 7. The diverse BDC-X linkers that have been employed to prepare Zr-**fcu**-MOFs.

Due to the presence of functional groups, UiO-66-X MOFs exhibit different features than the parent UiO-66, which are suitable for different applications through specific MOF-guest interaction. The functional groups also allow for the fine-tuning of the triangular window of the **fcu**-MOF for gas/vapor separations. For example, the window size of UiO-66 (ca. 6 Å) is reduced to ca. 5.3 and 4.8 Å in UiO-66-COOH and UiO-66-$(COOH)_2$, respectively, with the later possessing enhanced ethylene/ethane adsorption selectivity due to its constricted aperture size [100].

UiO-66-NH_2 is among the first and most studied functionalized UiO-66-X MOF. Similar to its parent UiO-66, this amino-

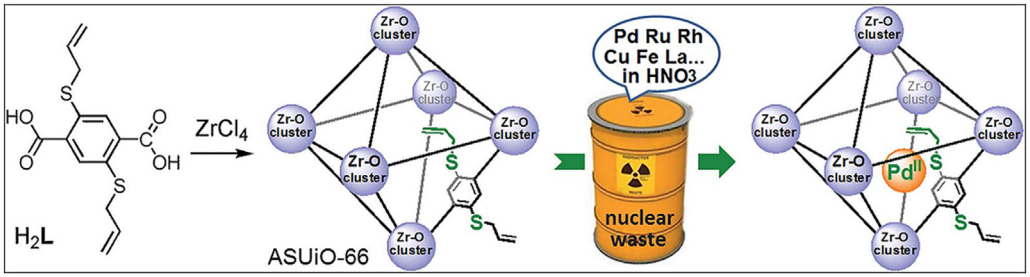

Fig. 8. Schematic showing the application of UiO-66–2,5-($SCH_2CH = CH_2)_2$ for extracting Pd(II) ions from a solution mimicking high-level acidic liquid waste. Reproduced with permission from ref. [95].

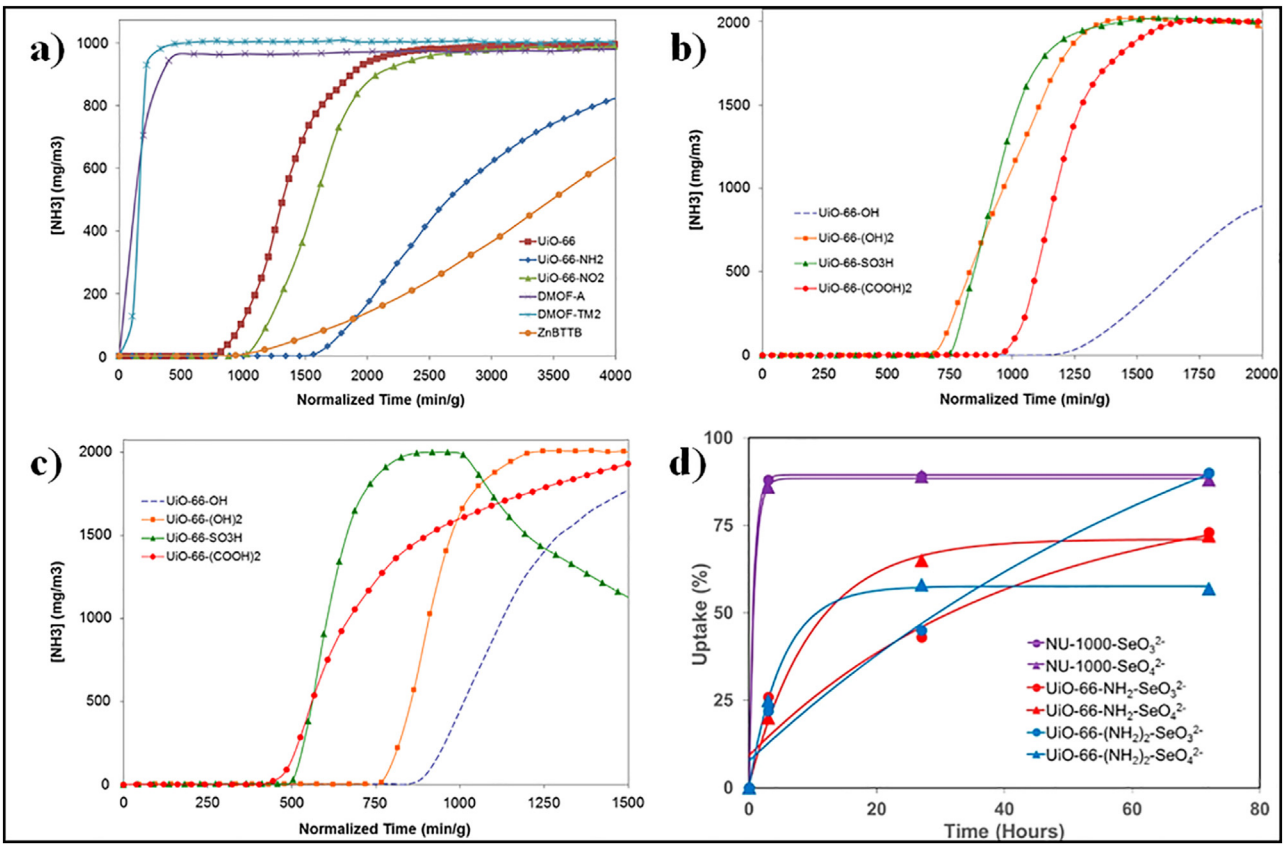

Fig. 9. NH_3 breakthrough curves for UiO-66-X MOFs under dry (a and b) and humid (c) air conditions at a feed concentration of 1000 mg/m^3 (1438 ppm) (a) and 2000 mg/m^3 (2876 ppm) (b and c); kinetics of selenate and selenite uptake in UiO-66-X MOFs (d). Reproduced with permission from references [106,107].

functionalized analogue was shown to maintain its high thermal stability and chemical robustness upon exposure to organic solvents, water, strong acid (HCl, pH = 1) and base (NaOH, pH = 14) media as evidenced by TGA and PXRD measurements [98]. The considerable stability of UiO-66-NH_2 was also evidenced in a different study, which showed reversible ammonia adsorption uptake with no alteration to the structure's crystallinity nor porosity [87]. In addition to its stability, the amino functional group of UiO-66-NH_2 paved the way for the deployment of this MOF for applications such as CO_2 capture with enhanced selectivity, reasonable working capacity and moderate CO_2 adsorption enthalpy due to the availability of free *N*-donor Lewis bases within the framework [101], catalysis in the conversion of toxic agents to non-toxic products [102], and sensing of toxic chemicals [103]. For example, due to its amino functionality, UiO-66-NH_2 was reported to be an useful catalyst for the hydrolysis of phosphate-ester based nerve agents [104]. As compared to the parent UiO-66 and to the other functionalized isoreticular MOFs, UiO-66-NO_2 and UiO-66-$(OH)_2$, the hydrolysis rate of phosphate-ester based nerve agents by UiO-66-NH_2 was reported to be 20-fold faster. Mechanistically, the amino functional group is hypothesized to play a central role in the enhancement of the catalytic activity by acting as a proton-transfer agent during the catalytic cycle (first as a Brønsted base and then as a Brønsted acid). It is noted, however, that the interaction of the amino group with phosphate esters via a H–bond and the generation of a phosphorane-amino intermediate were not considered as plausible pathways in the catalytic mechanism.

For similar mechanistic explanations, UiO-66-NH_2 coated electrodes were also shown to have high sensing capability upon exposure to ppb-level concentrations of nerve agents such as dimethyl methylphosphonate and sarin [103]. This detection capability was ascribed to the presence of the amino functionality that can trans-

fer protons to and from nearby $[Zr_6O_4(OH)_4]^{12+}$ clusters, thereby inducing stronger chemical adsorption of the phosphonates (possibly bidentate linkage to two Zr(IV) ions) and subsequent regeneration of the catalyst [104]. In a different report into the investigation of UiO-66-NH_2 for toxic gas removal, the MOF was proven effective for the removal of the toxic NO_2 with a removal capacity of 1.4 g of NO_2/g of MOF [105]. This property was once again attributed to the presence of the amino functional group together with other active sites within the MOF. The formation of a diazonium ion on the aromatic ring of the MOF, as well as the possible reduction of NO_2 to N_2, were also verified.

The presence of other substituent groups on the terephthalate linker backbone expanded the application of the MOF series to different arenas. One area of study was the exploration of the functionalized MOFs for selective adsorption and sensing of toxic ions and gases. For example, the chemical stability of the MOF and the presence of both sulfur and olefin moieties in UiO-66–2,5-$(SCH_2CH = CH_2)_2$ permitted its deployment for extraction of Pd (II) from nuclear waste-like acidic solutions (Fig. 8) [95]. In another work, UiO-66–2,5-$(SH)_2$ was shown to be efficient in lowering the Hg(II) concentration in water to <0.01 ppm and in adsorbing Hg from the vapor phase as a result of the availability of free-standing, accessible soft thiol (–SH) groups decorating the pores that interact strongly with the soft metal cation [93].

The influence of functionalities on the adsorption of ions and/or molecules has also been demonstrated by adsorption of ammonia by a series of chemically stable functionalized UiO-66-X MOFs (Fig. 9) [106]. The study showed that UiO-66-X MOFs functionalized with polar groups (UiO-66-NH_2, UiO-66-NO_2, UiO-66-OH, UiO-66-$(OH)_2$, UiO-66-SO_3H, and UiO-66-$(COOH)_2$) achieved higher ammonia uptake (3.56, 1.98, 5.69, 2.29, 2.24, 2.83 mmol/g, respectively) than the parent UiO-66 (1.79 mmol/g) under dry conditions. Despite the expectation that acid functional groups would strongly interact with ammonia, UiO-66-SO_3H and UiO-66-$(COOH)_2$ displayed lower ammonia capabilities than UiO-66-OH and UiO-66-NH_2. This was attributed to the substantial decrease in framework porosity (surface area and pore volume) when bulky functional groups like –COOH and –SO_3H were used. Indeed, UiO-66-OH, with the least bulky functional group, showed the highest ammonia uptake. The stronger H–bonding interaction of ammonia with –OH as compared to –NH_2 was also concluded to be a critical factor for achieving the higher ammonia uptake of UiO-66-OH than UiO-66-NH_2. Due to competition between water and ammonia molecules for adsorption at the active sites, the ammonia capacities of functionalized UiO-66 variants decreased under humid environments. This study confirmed that designing UiO-66-X MOFs with an appropriate balance between functionality and porosity can lead to enhanced adsorption properties. In a similar study, a series of related UiO-66-X structures with H–bond donors, UiO-66-NH_2 and UiO-66-$(NH_2)_2$, were shown to exhibit better selenate (SeO_4^{2-}) and selenite (SeO_3^{2-}) removal capacity from aqueous solutions than the unfunctionalized analogue [107]. In this work, the impact of aperture size of the MOFs versus analyte size was also reflected in the relatively faster diffusion of the smaller selenate (diameter of 4.8 Å) than selenite (diameter of 5.2 Å) anions in both MOFs (Fig. 9d).

The possibility to undergo chemical reactions between analytes and functional groups of MOFs enabled the development of UiO-66-X MOF sensors. This was illustrated by the recently reported UiO-66-O-Ph-NO_2 MOF-based fluorescence switch-on sensor that selectively detected H_2S in both liquid water and in the vapor phase [97]. Upon interaction with H_2S at a particular wavelength, the 2-(nitrophenoxy)terephthalate (BDC-O–Ph–NO_2) moiety decomposes into BDC–OH and 4-nitrophenylthiol, enabling the detection of the analyte. Similarly, maleimide-functionalized UiO-66 (UiO-66-Mi) was reported as promising for bioimaging applications due to its sensitive and selective luminescent sensing capability in detecting cysteine (Cys) and glutathione (GSH) in living cells, via a 1, 4-Michael addition of the thiol functional group to the electron deficient alkene group of the maleimide moiety in the linker leading to their thiolated adducts (Fig. 10) [108].

The synergy between optimized pore structures by the functional groups and the intrinsic properties of the groups facilitates the exploration of UiO-66-X MOFs for targeted molecular adsorption processes, such as CO_2 capture from different sources. In spite of the reduced specific surface areas and pore volumes of UiO-66-X MOFs, some of the functionalized analogues afford enhanced properties as exemplified by the increased CO_2 uptake and high CO_2/N_2 selectivity of UiO-66-$(CH_3)_2$ over the unfunctionalized parent UiO-66 structure, which can be attributed to pore constriction effects exerted by the introduced substituents [82,109]. Similarly, enhanced CO_2/CH_4 adsorption selectivity, an important property for natural gas or biogas upgrading, was observed in –SO_3H and –CO_2H functionalized UiO-66-X MOFs compared with the parent UiO-66. This was ascribed to the contribution of the attached polar functional groups and the corresponding pore constriction for the increased CO_2–framework interactions [83,89]. The experimental results were found to be in agreement with the computational work on the CO_2/CH_4 selectivity performance of UiO-66-X MOFs [84]. According to theoretical investigations, the CO_2 adsorption enthalpy in the modified materials generally followed the order of the functional groups' polarity: –SO_3H > –CO_2H > –NH_2 > –OH > –NO_2 > –Br > –CF_3. In addition to the polarity, a high degree of confinement experienced by the adsorbate molecules resulting from a significant decrease in accessible pore space was also predicted to play a substantial role in enhancing the CO_2 adsorption enthalpy. The synergistic contribution of the contracted pores and the introduction of favorable binding sites in UiO-66-X MOFs for selective gas separation was further evidenced in the enhanced CO_2/N_2, CO_2/CH_4, and CH_4/N_2 separations by UiO-66–$(OH)_2$,

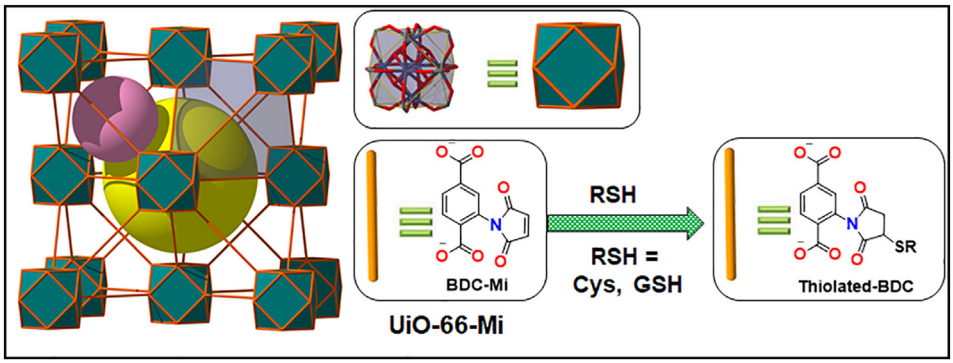

Fig. 10. Representation of UiO-66-Mi and UiO-67-Mi **fcu**-MOFs and the sensing mechanism that leads to their thiolated adducts.

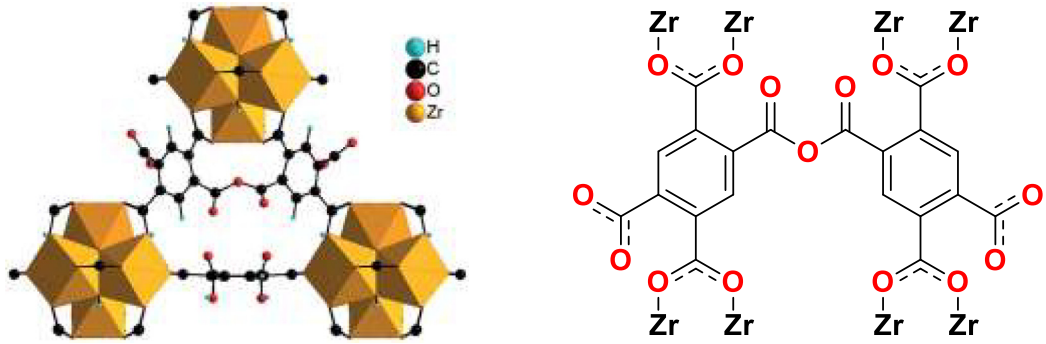

Fig. 11. Representation of the anhydride form, UiO-66(Zr)-Anhydride, obtained from intra-framework cross-linking of UiO-66(Zr)–$(COOH)_2$. Reproduced with permission from ref. [37].

UiO-66–$(OCH_3)_2$, and UiO-66–$(OCH_2CH_3)_2$ MOFs compared to that of UiO-66 [110].

Due to the possibility to introduce suitable functional groups within their pores, UiO-66-X MOFs are emerging as potential candidates for ionic conductivity applications. UiO-66$(SO_3H)_2$ exhibited high proton conductivity and long-term conduction stability due to the presence of covalently attached $-SO_3H$ groups to the backbone of the MOF that facilitate conductivity by donating labile protons to the conduction channels [94]. The reported superprotonic conductivity of 8.4×10^{-2} S/cm at 80 °C and 90% relative humidity for UiO-66-$(SO_3H)_2$ was comparable to the conductivity of the well-known electrolyte, Nafion [94]. Very recently, light responsive, reversible hydroxide ion conduction was accomplished using UiO-66-NH_2, demonstrating a promising potential to create hydroxide ion conductive smart devices that can be controlled remotely [111]. The amino functional group on the organic linker plays a central role in promoting hydroxide ion transport by forming a H–bond network with water molecules that results in a visible light absorption band. The hydroxide ion conductivity was reversibly attenuated or restored by turning the light on and off, respectively.

The successful installation of other functional groups permits access to **fcu**-MOFs with particular structure–property relationships. For example, the photocatalytic activity of functionalized **fcu**-MOFs, UiO-66-X (X = H, Br, NH_2, NO_2), was found to be strongly dependent on the electronic nature of the linker substituents with electron-donating substituents increasing the photoreactivity of UiO-66 [112]. This photocatalytic relationship, together with the water tolerance of the UiO-66-X MOFs, creates avenues to develop suitable **fcu**-MOF photocatalysts that can be utilized for CO_2 reduction [113], water splitting [114], water treatment through the oxidation of As(III) and reduction of Cr(VI) [112], a multitude of photocatalytic oxidations [115], and Lewis acid reactions [116].

The possibility for realizing functionalized UiO-66 analogue has created more synthetic opportunities and applications. Apart from site availability for molecular adsorption, the UiO-66-X MOFs con-

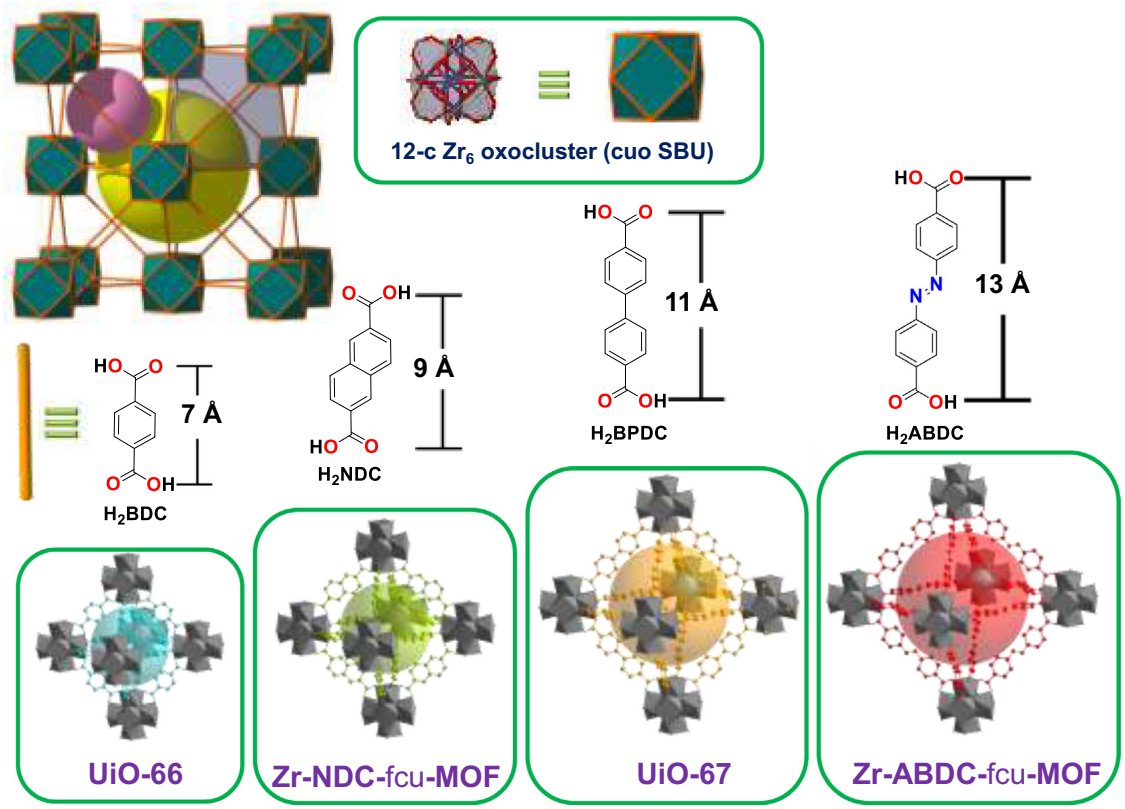

Fig. 12. Isoreticular Zr-**fcu**-MOFs displaying different pore sizes.

structed from trimelitic and pyromellitic linkers, UiO-66-COOH and UiO-66-$(COOH)_2$, were shown to undergo intra-framework cross-linking of the carboxylate groups to form anhydride bonds upon simple thermal heating (Fig. 11) [37]. As confirmed by FT–IR and ^{13}C cross–polarization MAS NMR analyses, the cross-linking process was found to be completely reversible upon re-exposure to water. This reversible storage and release of water within the cross-linked MOFs was then hypothesized to have potential in deploying the MOFs in applications ranging from water storage, thermal batteries, and electric dehumidifiers to fabrication of smart devices [21]. Though exciting, the crosslinking chemistry of MOFs, in general, remains underexplored due to challenges associated with the sensitivity of the process to external stimuli such as chemical exposure, vacuum, and heat. Exploiting the utility of functional groups in UiO-66-X structures for a particular application remains a very important research topic with further exploration and new solutions being developed.

2.4. Isoreticular expansion and contraction of Zr-fcu-MOFs

Many applications, including the storage of large molecules and catalytic reactions that involve larger molecules, require sufficient void space within MOFs. On the other hand, separation of industrially relevant molecules requires better control of the triangular aperture size of **fcu**-MOFs by employing linkers that are shorter in size than H_2BDC. The amenability of Zr-**fcu**-MOFs has led to the design of other functional, isoreticular MOFs with a range of surface areas, pore sizes and chemistry by replacing the H_2BDC of the parent UiO-66 with different linear dicarboxylates longer or shorter in length and decorated with various functional groups. Representative isoreticular UiO-6*x* MOFs are presented in Fig. 12.

2.4.1. Isoreticular Zr-fcu-MOFs from expanded linkers

The implementation of isoreticular chemistry on the Zr-**fcu**-MOF platform using linkers longer than H_2BDC has led to the isoreticular MOFs, denoted as UiO-67, UiO-68, UiO-69, and their functionalized derivatives (UiO-67, H_2BPDC: biphenyl-4,4′-dicarboxylate; UiO-68, H_2TPDC: terphenyl-4,4″-dicarboxylate) [10,23,24]. From a topological point of view, all isoreticular MOFs that are constructed from the Zr_6 oxocluster MBB and corresponding linear organic linkers adopt 12-c **fcu**-a nets but with more expanded pores than UiO-66. The increase in cavity size as a result of isoreticular expansion plays a very important role in different adsorption-based applications. This is exemplified by the recent work on the role of cavity size in the encapsulation of ruthenium (II) tris-(2,2′-bipyridine) (RuBpy) within UiO-66, UiO-67, and UiO-68 and the consequential photophysical properties of RuBpy@UiO-6x MOFs [117].

Other than the H_2BPDC linker, different types of linear dicarboxylate linkers having two phenylene units, with or without decorating functional groups, have been used in the synthesis of UiO-67-X MOFs that exhibit ranges of porosities and chemistry [71,108,118–125]. Representative organic linkers that have been reported for making UiO-67-X MOFs are presented in Fig. 13.

In the same way as UiO-66-X MOFs, the functional groups of UiO-67-X analogues were pursued for different applications. Due to the presence of integrated N atoms, UiO-67-BPyDC exhibited high storage capacities for gases such as CO_2 with stepwise adsorption for liquid CO_2 indicating a sequential pore filling mechanism onto different adsorption sites [119]. One main challenge associated with the practical deployment of UiO-67-BPyDC for CO_2 capture is its limited stability upon exposure to moisture. Among the different strategies being explored, the use of hydrophobic methyl group substituted H_2BPyDC ligand, 6,6′-dimethyl-2,2′-bipyridine-5,5′-dicarboxylic acid, was reported to give the hydrolytically stable **fcu**-MOF (denoted MOF-553) with enhanced CO_2 uptake compared to the unfunctionalized analog [124]. The exploitation of the N functionality for practical applications is also exemplified by the *N*-functionalized 2-phenylpyridine-5,4′-dicarboxylate (PPyDC) based UiO-67@N, which displayed highly selective detection of nitro explosives in aqueous environments [118]. Similarly, fluorenone and dibenzothiophene based UiO-67-X MOFs, denoted BUT-10 $[Zr_6O_4(OH)_4(FDCA)_6]$ and BUT-11 $[Zr_6O_4(OH)_4(DTDAO)_6]$, respectively, were also shown to possess enhanced CO_2 adsorption with reasonable CO_2/N_2 and CO_2/CH_4 selectivities as compared to

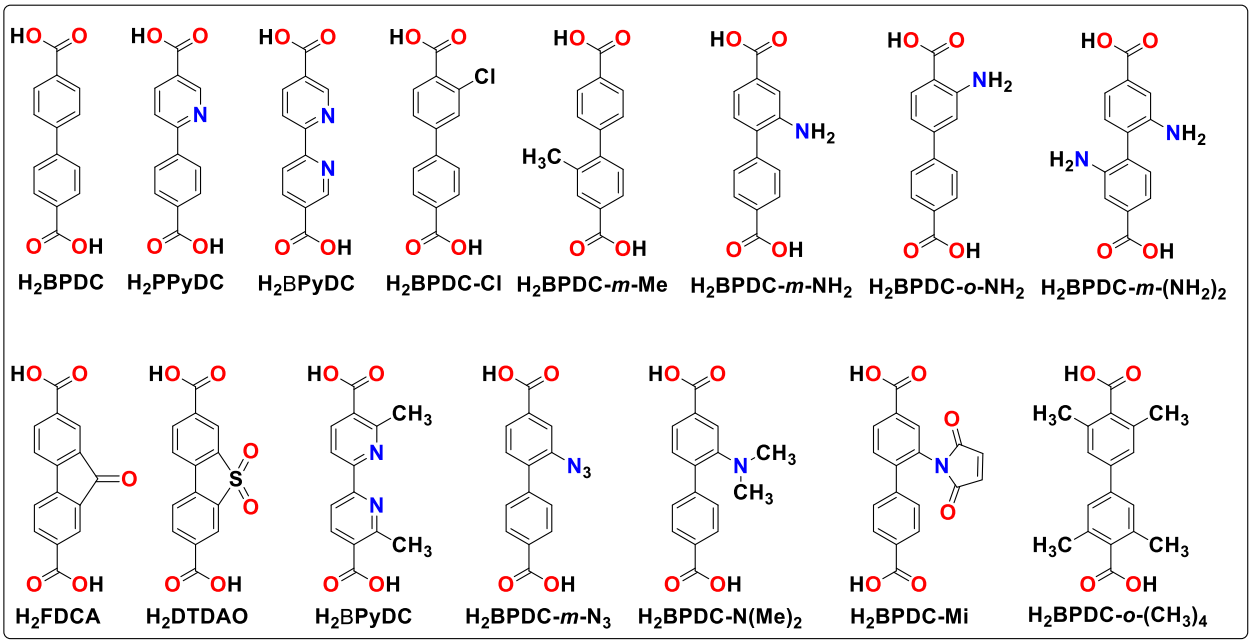

Fig. 13. Representative organic linkers used to synthesize isoreticular UiO-67 MOFs.

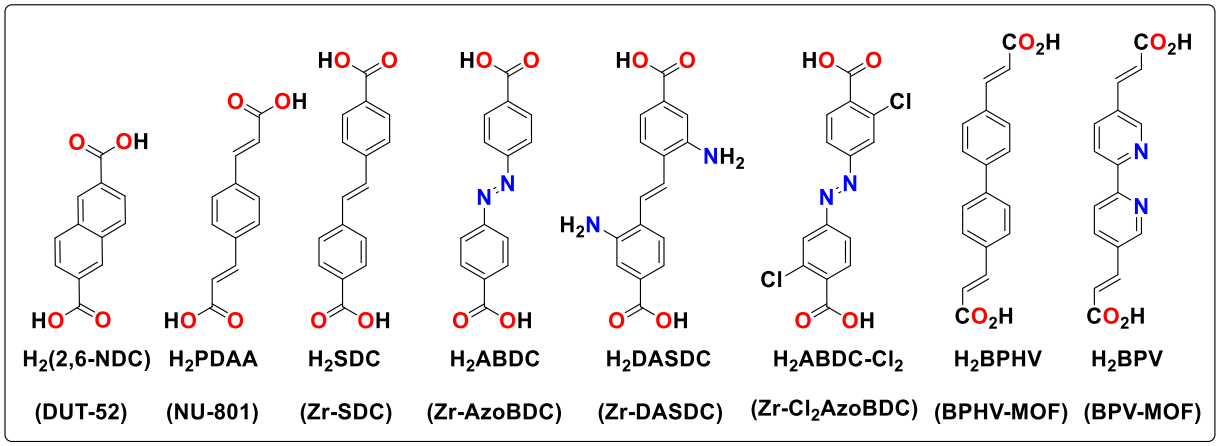

Fig. 14. Organic linkers with lengths shorter than the biphenylene unit used in UiO-67 and between biphenylene and triphenylene units used to assemble various isoreticular Zr-**fcu**-MOFs. The names of the MOFs produced from each linker are shown in brackets.

UiO-67, which is attributed to the incorporated carbonyl and sulfone functional groups [122,123].

Like UiO-66-NH_2, the amino-functionalized UiO-67 MOFs were demonstrated to have catalytic activity for the hydrolysis of organophosphonate-based toxic chemicals. These MOFs demonstrated enhanced performance when compared to UiO-66-NH_2 because of pore expansion and better activity when compared to their non-functionalized UiO-66 and UiO-67 analogues due to the amino functional group. The rate of catalytic activity was observed to be dependent not only on the presence of the amino functional group but also on its proximity to the Zr-based active site. This was proven by the higher activity of UiO-67-*o*-NH_2 than UiO-67-*m*-NH_2, which had the amino functional group closer to the Zr-based SBU providing better control of the microsolvation environment and, thus, increasing the overall catalytic rates.

Following a similar mechanism to that of UiO-66-Mi (Fig. 10), the maleimide-functionalized UiO-67 was proven to have sensitive and selective luminescent sensing of cysteine (Cys) and glutathione (GSH) under simulated physiological conditions, a property useful for bioimaging applications [108]. However, the fluorescence response of UiO-67-Mi for both Cys and GSH was observed to be higher than that of UiO-66-Mi, which was attributed to the larger porosity of the extended MOF that facilitates diffusion of the amino acids into the pores with ease.

Apart from the above-mentioned BPDC-X linkers, the organic linkers with intermediate length between phenylene and biphenylene, 2,6-naphthanedicarboxylic acid (H_2NDC) and 1,4-phenylenediacrylic acid (H_2PDAA), were successfully employed to construct the isoreticular **fcu**-MOFs, Zr-NDC-**fcu**-MOF (DUT-52) and NU-801, respectively [71,126]. Other dicarboxylate linkers of length shorter than H_2TPDC (the organic linker used in the synthesis of UiO-68), but longer than H_2BPDC (the organic linker employed to realize UiO-67) were successfully installed in this MOF platform to assemble expanded pore **fcu**-MOFs.

Zr_6 oxocluster-based **fcu**-MOFs have been synthesized from 4,4′-azobenzenedicarboxylic acid (H_2ABDC), functionalized H_2-ABDC, such as 3,3′-dichloro-4,4′-azobenzenedicarboxylic acid (H_2BDC-Cl_2), 4,4′-(ethene-1,2-diyl)dibenzoic acid (H_2EDDB) or 4,4-stilbenedicarboxylic acid (H_2SDC), diaminostilbenedicarboxylate (H_2DASDC), elongated biphenyl and bipyridyl containing dicarboxylate linkers, 4,4′-bis(carboxyethenyl)-1,1′-biphenyl (H_2-BPHV) and 5,5′-bis(carboxyethenyl)-2,2′-bipyridine (H_2BPV) (Fig. 14) [69,72,127–129]. Even though the linkers have kinks in their structure due to the possibility of *cis*/*trans* isomerization of the groups around the double bonds that make their geometries deviate from ideal UiO type linkers, PXRD, single crystal-XRD (SCXRD), and TGA characterizations confirmed the assembly of Zr_6 oxocluster-based MOF with the expected underlying **fcu** topology. The unit cell sizes of these MOFs all lie between those of UiO-67 and UiO-68. UV–vis spectroscopic experiments also confirmed the *trans* configuration of the azobenzene linker upon its incorporation within the Zr-ABDC-**fcu**-MOF [69]. Although it maintained an overall **fcu** topology, due to the bending nature of the linker, the BPHV-MOF was observed to have structural distortions and to crystallize in a lower tetragonal space group [127].

Linear dicarboxylate linkers having three phenylene units with and without decorating functional groups (Fig. 15) were reported to produce isoreticular Zr-**fcu**-MOFs (UiO-68). Owing to the insolubility of the terphenylenedicarboxylic acid (H_2TPDC) linker in DMF, isolation of unfunctionalized UiO-68 was difficult. To overcome this challenge, researchers mostly employ H_2TPDC-X linkers decorated with suitable functional groups, such as the amino, methyl, and maleimide functionalized H_2TPDC (H_2TPDC-NH_2, H_2-TPDC-CH_3, and H_2TPDC-Mi) to enhance the solubility of the linkers and to isolate the corresponding UiO-68-X MOFs [10,130,131]. The use of H_2TPDC-X linkers was illustrated by a series of isoreticular Zr-**fcu**-MOFs, termed PCN-56, PCN-57, PCN-58 and PCN-59, which were created by using 2′,5′-dimethyl-terphenyl-4,4′′-dicarboxylic acid (TPDC-2CH_3), 2′,3′,5′,6′-tetramethyl-terphenyl-4,4′′-dicar boxylic acid (TPDC-4CH_3), and their corresponding azide derivatives (TPDC-2CH_2N_3 and TPDC-4CH_2N_3), respectively (Fig. 15) [132]. PXRD measurements confirmed the structures with phase purity and their structural robustness in aqueous acidic and basic media. The successful isolation of isoreticular UiO-68-X MOFs was further exemplified by Zr-BTDB-**fcu**-MOF [133,134] obtained using the thiadiazole functionalized H_2BTDB linker, H_2BTDB = 4,4′-(benzoic[*i*1,2,5]thiadiazole-4,7-diyl) dibenzoic acid and Zr-BI-**fcu**-MOF [135] assembled from imidazole functionalized H_2BI linker, H_2BI = 4,4′-(1H-benzo[*d*]imidazole-4,7-diyl)dibenzoic acid (Fig. 15).

The pursuit of functionalized UiO-68-X MOFs is driven by their inherent superior porosities compared to UiO-66 and UiO-67 analogues. This is particularly important in adsorption-based applications involving larger molecules. For instance, the electron-donor and -acceptor characteristics induced by either the thiadiazole or imidazole moieties of Zr-BTDB or Zr-BI **fcu**-MOF, respectively, and the large pore structures facilitate the deployment of these MOFs in electron transfer processes and for sensitive detection of analytes, such as amines and picric acid (2,4,6-trinitrophenol, TNT). The sensitivity is driven by H–bonding interactions between

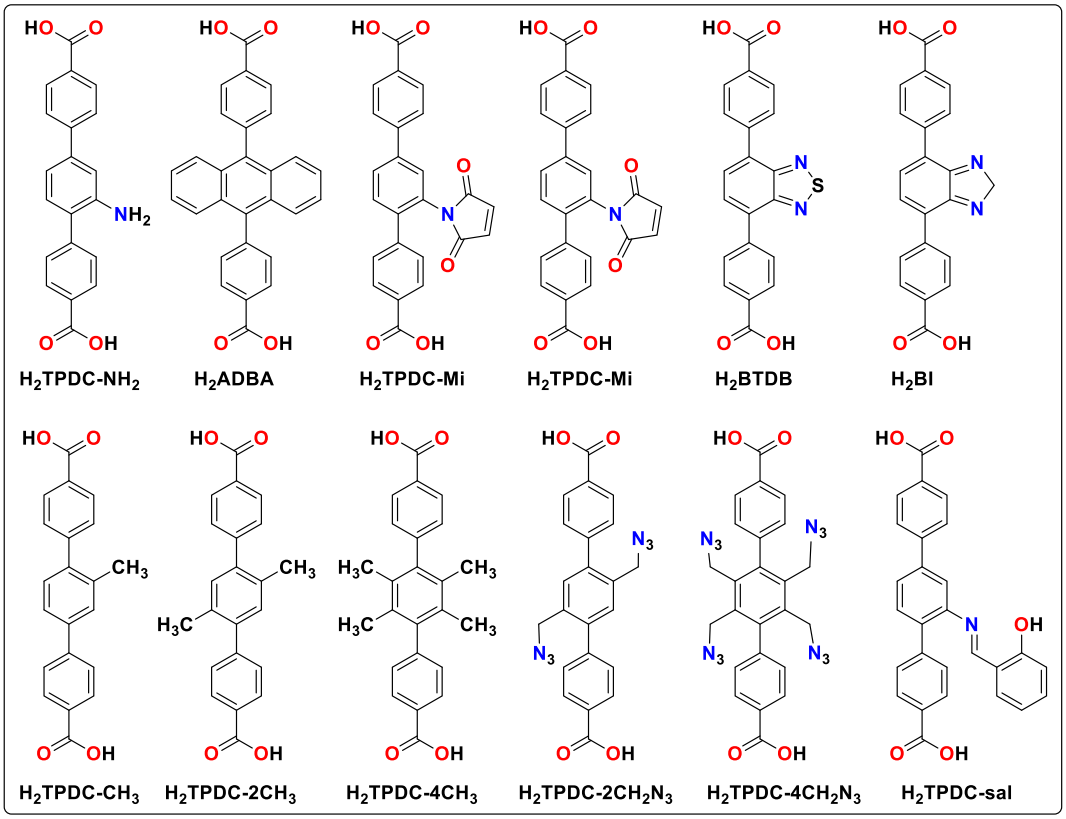

Fig. 15. Representative examples of organic linkers employed to assemble UiO-68 MOFs.

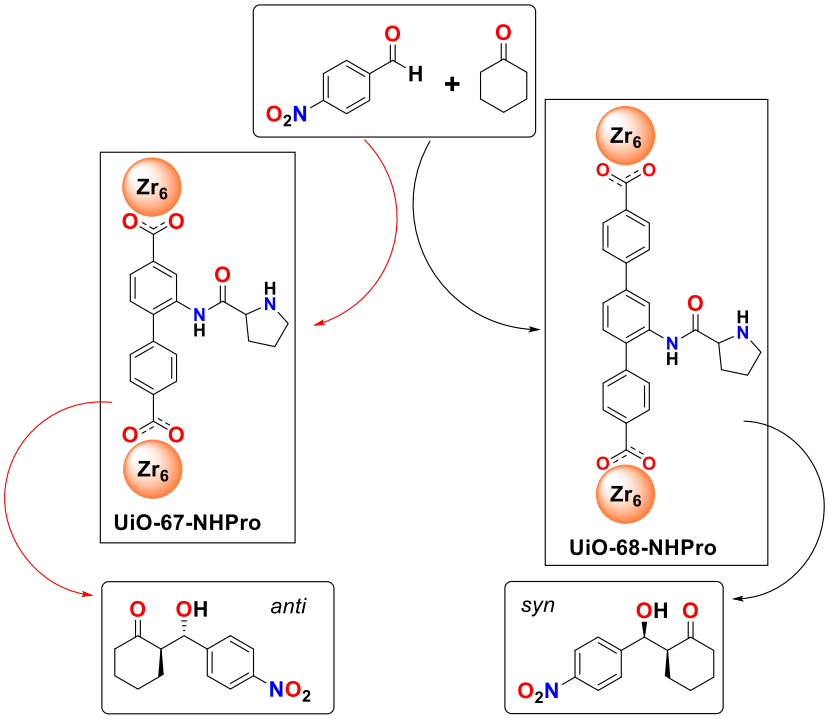

Fig. 16. L-proline-functionalized UiO-67 and UiO-68-type MOFs and their catalytic role in the asymmetric aldol addition of 4-nitrobenzaldehyde and cyclohexanone.[136].

the N atoms of linker and the –OH group of the analytes [133–135]. The expanded pores of UiO-68-X MOFs that are decorated with suitable functional groups are also important in catalytic applications. This was illustrated by the chemically robust L-proline-functionalized chiral UiO-67-NHPro and UiO-68-NHPro MOFs, both of which displayed reverse diastereoselectivity in the asymmetric Aldol addition reaction of 4-nitrobenzaldehyde and cyclohexanone (Fig. 16) [136]. The opposite regioselectivity observed in the two MOFs is imputed to the difference in the location of the catalytic chiral L-proline groups within the confined pore spaces. According to the crystal structures of UiO-67-NHPro, the L-proline groups are oriented toward the octahedral cages. The structure of UiO-68-NHPro, on the other hand, characterized by the different location of the middle phenyl ring where the L-proline is coordinated, contains the side groups within tetrahedral pores or close to triangular pore apertures.

Zr-**fcu**-MOFs with suitable pore metrics and functionality were also shown to be excellent X-ray scintillators [137]. The presence of heavy Zr-oxo clusters with ultrafast energy transfer properties were exploited to interact with the ionizing radiation. Additionally, the possibility to incorporate fluorescent groups in the linkers has made the MOF platform suitable for radiation detection applications. In a representative example, a UiO-68 type MOF synthesized from dicarboxylate-9,10-diphenylanthracene linker, Zr-ADBA-**fcu**-MOF, was embedded in a polymer matrix and then demonstrated to be a promising nanocomposite scintillator.[137] The ordered arrangement of the 9,10-diphenylanthracene emitters with appropriate distance between the clusters and ligands (~12 Å) were critical for sensitizing linker emission through energy transfer. Further information on the deployment of luminescent MOFs for emerging energy-transfer applications can be found in a recently published review article.[138].

Isoreticular expansion of the UiO-6*x* series to achieve a Zr-**fcu**-MOF with much larger pores and channels was successful with the synthesis of TPHN-MOF (*i.e.*, UiO-69-NO_2), from the linear dicarboxylate linker comprised of 4 phenylene units, 4,4′-bis(carboxy phenyl)-2-nitro-1,1′-biphenyl (H_2TPHN) [127]. The synthesis of TPHN-MOF allowed for the incorporation of active sites that facilitate catalytic reactions for different organic transformations [139]. With the successful synthesis of TPHN-MOF, attention turned to incorporating a coordination complex within the internal pore environment. Accordingly, the [Ir(BPP)(PPy)$_2$]Cl-derived 4,4′-(2,2′-bipyridyl-5,5′-diyl)dibenzoic acid (H_2BPP) linker was used in the synthesis of a UiO-69 type MOF and its incorporation proved useful for achieving intriguing phosphorescence properties with the steric bulk of the linker precluding the formation of interpenetrated structure (Fig. 17) [140]. It is noted that preparation of the isoreticular [Ir(BPyDC)(PPy)$_2$]-based UiO-67 analogue is synthetically challenging due to the bulky substituent group. The presence of the [Ir(PPy)$_2$(BPy)] moiety coupled with sufficient porosity permitted the loading of Pt nanoparticles (NPs) inside the expanded cavities via photoreduction of K_2PtCl_4 in a mixed solvent system of tetrahydrofuran (THF)/triethylamine (TEA)/H_2O. The reduced radical [Ir^{III}(PPy)$_2$(BPP•$^-$)] generated by TEA reductive quenching of the photoexcited [Ir^{III}(PPy)$_2$(BPP)]$^{+*}$, was asserted to reduce K_2PtCl_4 to form the corresponding Pt NPs. Due to synergistic photoexcitation of the MOF and electron injection into the Pt NPs, the resulting Pt@MOF assembly acted as an effective photocatalyst for hydrogen evolution with a turnover number of 7000 [140].

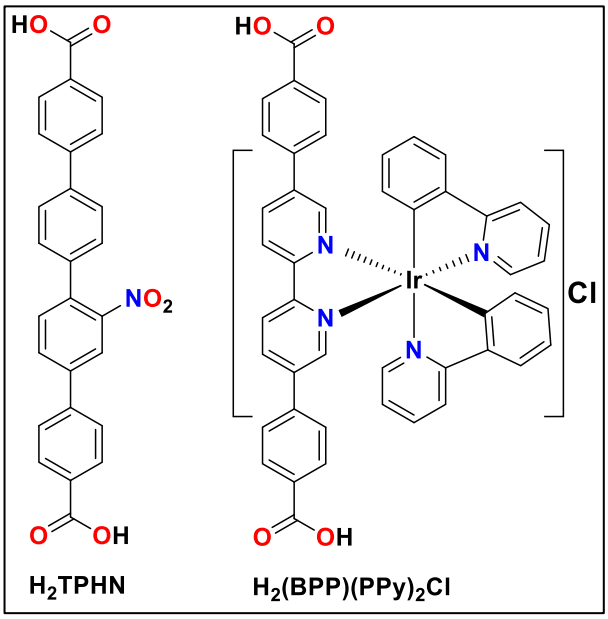

Fig. 17. Linkers reported in the assembly of functionalized UiO-69 type MOFs.

Thus far, the assembly of pore expanded Zr-**fcu**-MOFs has been made possible through the use of linear ditopic linkers comprised of up to 4 phenylene units. Further design of UiO-6*x* MOFs bearing ultrahigh porosity remains possible by targeting linkers comprised of more than 4 phenylene units. These linkers will need to be decorated with bulky substituent groups to ensure solubility and to avoid interpenetration of the resulting MOF. One drawback associated with pore-expanded Zr-**fcu**-MOFs is the susceptibility of the products to framework degradation in the presence of water, acid, and some protic solvents [141,142]. This has been proven by the significant decrease in the chemical and hydrolytic stabilities of UiO-67-X MOFs as compared to that of UiO-66 [141,143]. As explained in various reports [144], the lower stability of isoreticularly expanded **fcu**-MOFs with longer linkers is expected due to the ease at which linker substitution occurs (*i.e.*, lowering activation energy barriers by either dissociative or associative mechanisms rendering the MOFs kinetic lability). In addition to the chemical stability, the mechanical stability of the isoreticularly expanded Zr-**fcu**-MOFs were found to be lower than that of the relatively rigid UiO-66. This is evidenced by the poor crystallinity of UiO-67 and UiO-68 samples after applying high pressures [30,145,146]. The decrease in mechanical stability with increasing porosity is not unusual given that, upon applying mechanical stress, the relatively higher energy porous MOFs can be transformed into less porous dense phases with lower system energies. The amount of such deformation is less for more dense MOFs under equal mechanical compressions and shear forces.

2.4.2. Isoreticular Zr-fcu-MOFs from shorter linkers

Zr-**fcu**-MOFs assembled from organic linkers shorter than H_2BDC (the short distance between coordinating O–atoms = 7.0 Å for H_2BDC) have also attracted interest owing to their enhanced chemical stabilities and their potential prospects for different applications, including small molecule adsorption and separations. The Zr-**fcu**-MOF that adopts the smallest unit cell as result of being constructed from the shortest linker was reported by Bueken and co-workers [20]. This MOF, termed Zr-squ-**fcu**-MOF, was prepared through a solvothermal reaction between squaric acid and $ZrCl_4$ in the presence of either formic acid or acetic acid functioning as a modulator. Zr-squ-**fcu**-MOF was reported to have a unit cell length of 15.784(3) Å with tetrahedral and octahedral cages of 4.7 and 5.6 Å, respectively. The fully coordinated Zr-squ-**fcu**-MOF was initially expected to be nonporous due to its very small triangular aperture (~2.4 Å), which is smaller than the molecular dimensions of adsorbates such as H_2 (kinetic diameter of 2.82 Å) and N_2 (kinetic diameter of 3.64 Å). Surprisingly, the MOF showed adsorption of H_2 (uptake of 50.5 cm^3/g at 1 bar) and N_2 (uptake of 40.4 cm^3/g

at P/P_0 = 0.95) at 77 K for the formic acid modulated MOF. From the theoretical calculation conducted by the authors, the ideal fully coordinated Zr-squ-**fcu**-MOF was nonporous to such probe molecules. The discrepancy between the experimental and theoretical results was attributed to the formation of missing linker defects during the formic acid-modulated syntheses. Evidence for these missing linker defects was found in the composition analyses of the MOF samples by TGA, which led to structural formulae of $Zr_6O_4(OH)_4(squ)_{5.25}(CH_3COO)_{1.5}$ and $Zr_6O_4(OH)_4(squ)_{4.45}(HCOO)_{3.1}$ for the acetic acid and formic acid modulated products, respectively. The presence of acetates and formates in the frameworks was further validated by ^{1}H NMR analyses.

The second prominent example of an isoreticularly contracted Zr-**fcu**-MOF is Zr-fum-**fcu**-MOF (*i.e.*, MOF-801), $Zr_6O_4(OH)_4(O_2C–(CH)_2–CO_2)_6$, which is prepared by the reaction between fumaric acid (fum) and $ZrCl_4$ in DMF/H_2O solvent with and without modulators (*e.g.*, formic acid, acetic acid or propionic acid) [50,147–149]. Even though the bent nature of the fumarate linker creates a slight deviation from the ideal linearity, the prepared MOF-801 exhibits an **fcu** topology like that of UiO-66. BET surface areas of 856 m^2/g (when synthesized in DMF) or 970 m^2/g (when synthesized in water) were achieved and, as expected, octahedral and tetrahedral cages of about 7 and 5 Å, respectively, were verified by pore size distribution analyses. When compared to UiO-66 analogues made with longer ligands, MOF-801 is known for its enhanced chemical stability in aqueous solutions of wide pH range (pH = 1–12) [148]. The chemical stability was further established upon PXRD characterization of MOF-801 revealing that the material was resistant to 0.1 M NaOH for 3 days at room temperature [150]. The high hydrolytic stability is also reflected in the reproducible cyclic water sorption properties of the MOF [11,21].

Further reduction of the pore size in MOF-801 was accomplished by employing methyl functionalized fumaric acid (*i.e.*, mesaconic acid) as the linker to create the isoreticular Zr-mes-**fcu**-MOF [35,151]. Structural characterization by XRD analysis exhibited unit cell constants comparable to that of MOF-801, but with reduced octahedral and tetrahedral pore cages due to the methyl groups protruding into the internal cages. Similar to UiO-66-X, the Zr-mes-**fcu**-MOF demonstrated stability in water and aqueous acidic solutions, but not in strongly basic media. As detailed [144], the relatively poor stability of this MOF system in basic media is attributed to the competitive formation of M−OH bonds that replace the M−linker bonds that are foundational to the structure.

Aside from the improved stability, one major driving force to assemble **fcu**-MOFs with short linkers is to obtain an optimal triangular aperture size for a given gas or vapor separation property. Inspired by the contracted aperture size MOF-801, Zhou *et al.* [152] recently reported a MOF-801-based membrane that is capable of separating propylene from propane with a mixture separation factor reaching ca. 110. Owing to the contracted cages and the corresponding enhanced van der Waals interactions of the pore walls with C_2H_6 and C_3H_8 compared to CH_4, MOF-801 was also reported to be efficient in the adsorptive separation of CH_4 from the longer alkanes [153]. Despite these reports, we note that the design of Zr-**fcu**-MOFs with contracted windows specifically designed to meet the specifications to carry out challenging gas or vapor separations remains under-explored. Although not as diverse as the UiO-6*x* MOFs assembled from BDC-X and its extended analogue linkers, the above-mentioned examples illustrate the possibility to fine-control the porosity of Zr-**fcu**-MOFs. The Zr-**fcu**-MOFs that have been constructed from linear linkers with lengths shorter than one phenylene unit are summarized in Fig. 18.

2.4.3. Isoreticular Zr-fcu-MOFs from flexible aliphatic linkers

The isoreticulation of Zr-**fcu**-MOFs has been extended to linkers that contain flexible aliphatic carbon chains. This is illustrated by the porous Zr-**fcu**-MOF containing *trans*,*trans*-muconic acid, $Zr_6O_4(OH)_4[O_2C–C_4H_4–CO_2]_6$·solv (solv = DMF, H_2O) [43,71,154]. This MOF was prepared by using a post-synthetic exchange strategy to replace a monocarboxylate capping ligand of the zirconium methacrylate oxocluster precursor, $Zr_6O_4(OH)_4(OMc)_{12}$ (OMc = CH_2 = $CH(CH_3)COO$), with the *trans*,*trans*-muconic acid linker in DMF at different temperatures and reaction times [43]. Post-synthetic exchange was achieved by pursuing a conventional solvothermal reaction between $ZrCl_4$ and the linker in the presence of small amounts of H_2O or conc. HCl additives in DMF [154]. Even though the muconate spacer with *trans*,*trans* configuration was used as a precursor, the configuration of the linker incorporated within the MOF structure was disordered in a *cis* conformation (Fig. 19) [43,154], indicating that isomerization had occurred over the course of the reaction. When compared to the terephthalate-based **fcu**-MOFs, Zr-*cis*-muc-**fcu**-MOF possessed relatively less chemical and thermal stability as reflected in the TGA data that shows thermal stability up to 250 °C under air atmosphere (450 °C for UiO-66) and an unexpected lower BET surface area. These properties may result due to the easier thermal degradation of the olefin spacer (muconate) with respect to the aromatic spacer

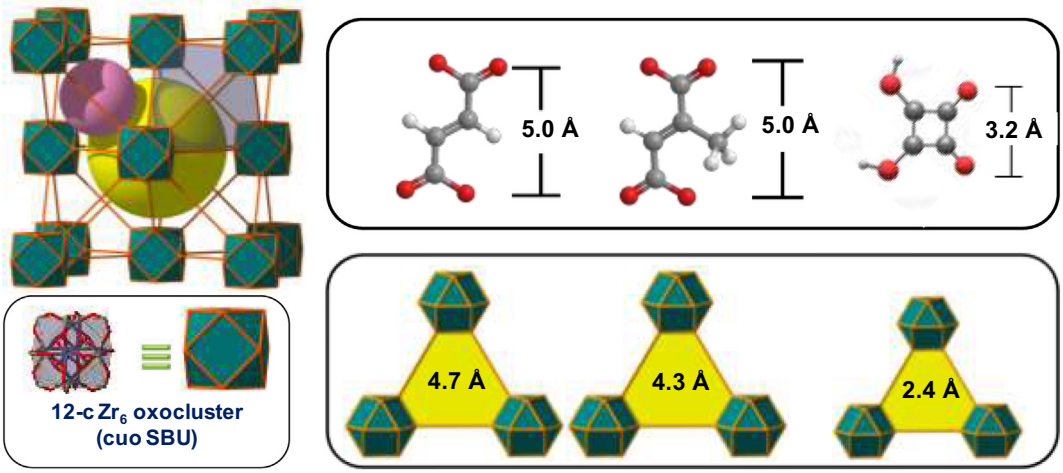

Fig. 18. Isoreticular Zr-**fcu**-MOFs assembled from linear linkers that are shorter in size than BDC.

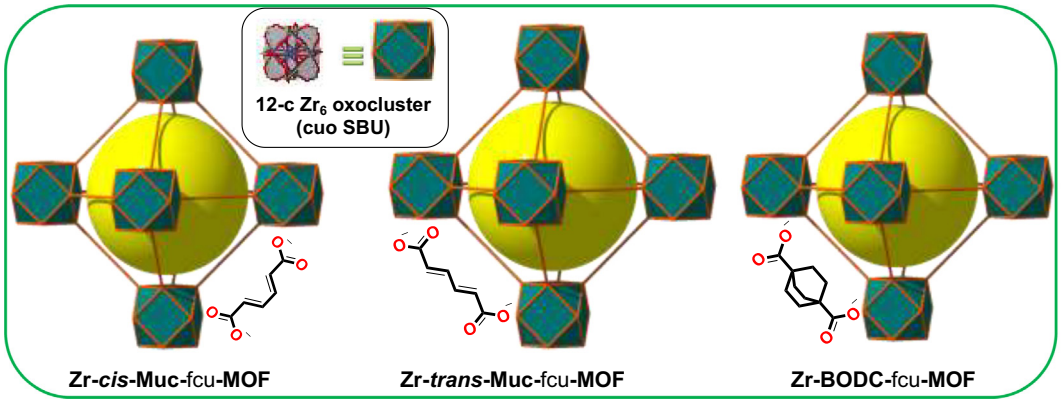

Fig. 19. Octahedral cage representation of the isoreticular Zr-**fcu**-MOFs assembled from aliphatic dicarboxylate linkers.

(terephthalate) and the lower stability of the Zr-muconate solid upon removal of guest molecules occupying the pores. In a separate report, the Zr-muc-**fcu**-MOF containing the muconate linker in the *s*-trans conformation, Zr-*trans*-muc-**fcu**-MOF, without isomerization of the starting *trans*,*trans*-muconic acid, was also obtained upon using amino acid (L-proline) modulator during the solvothermal reaction between the linker and $ZrCl_4$ [71]. The role of the amino acid modulator in preventing the isomerization of the linker is not yet understood.

As a further example to using flexible aliphatic-based linkers to construct Zr-**fcu**-MOFs, the three-dimensional linker, bicyclo[2.2.2]octane-1,4-dicarboxylic acid (H_2BODC), which is slightly smaller in size (ca. 6.8 Å) than H_2BDC (ca. 7 Å), yet bulkier in width (Fig. 19), was effectively installed as a linker to assemble a Zr-BODC-**fcu**-MOF denoted NU-403 [155]. The prepared MOF with linker-dimensionality-induced tailored pore and aperture sizes (octahedral and tetrahedral cage of 10 and 5 Å, respectively, *vs* 11 and 7 Å for UiO-66, respectively) exhibited enhanced Kr/Xe separation capability (IAST selectivity of ca. 9 *vs* ca. 7 for UiO-66).

We have provided in Table 2, various reported Zr-**fcu**-MOFs and their structural and porosity characteristics in order to provide the reader with a better understanding of the porosity attributes upon shortening and extending the organic linkers. We do note that different surface area and pore volume values are reported by different researchers for any given **fcu**-MOF material as a result of variations in synthetic procedures leading to different levels of defects. To gain insights about the defect levels, the geometric surface areas for fully coordinated UiO-66, UiO-66-NH_2, UiO-66-$(NH_2)_2$, UiO-66-OH, UiO-66-$(OH)_2$, UiO-66-NO_2, UiO-67, UiO-67-NO_2, and UiO-67-NH_2 are 800, 700, 450, 600, 400, 500, 2700, 2000, 2150 m^2/g, respectively [23]. Similarly, the geometric surface areas calculated assuming 8 linkers per Zr_6 node for UiO-66, UiO-66-NH_2, UiO-66-OH, UiO-66-NO_2, and UiO-67 are 1550, 1150, 1250, 1100, and 3100 m^2/g, respectively.

The main reason for Zr-**fcu**-MOFs becoming an attractive system to explore is the versatility they exhibits toward different applications. Zr-**fcu**-MOFs have been applied in a multitude of important areas such as adsorption and storage of molecules or ions [164–170], water sorption-based applications [11,21,161], separation of molecules with very similar physical properties [14–17,83,105–107,123,156,169,171–175], heterogeneous catalysis [113,159,162,176–185], drug loading and delivery [130,158,186–188], and chemical sensing [103,108,118,133,189–196].

2.5. Defects in Zr-fcu-MOFs

As shown in Table 2, surface areas and pore volumes differ for the same MOF and vary widely from one report to the next. One peculiar feature that is prevalent in Zr-**fcu**-MOFs and is responsible for such variations is the presence of defects. UiO-6*x* structures have been proven to be prone to defects (without collapse of the framework structures) in the form of missing linkers or missing inorganic building units [197,198]. The defect tolerance of **fcu**-MOF structures [199] is likely due to the highly connected SBU with strong M−O bonds, which makes these structures popular targets and model platforms for defect engineering and defect studies by different characterizations. It is important to note that owing to the dominance in diffraction by the inorganic part of **fcu**-MOFs, routine PXRD characterizations usually cannot detect the presence of defects. The presence of defects was first observed in UiO-66 in 2011 [22] through a TGA experiment. The researchers observed that the experimental TGA weight loss of UiO-66 above 400 °C was smaller than the theoretically expected value calculated from the fully coordinated UiO-66 structure. Since this observation, UiO-66 and its isoreticular analogues were subject to an immense number of studies on defects and the properties resulting thereof [197,198].

Defects in Zr-**fcu**-MOFs are often considered as unwanted structural abnormalities that form during the synthesis of porous materials, which lead to decreased chemical and mechanical stability [200,201] or difficulty in controlling the sizes of the pore apertures for a particular molecular separation application [202,203]. However, for MOFs, defects are widely considered as opportunities to assemble hierarchically porous solids that possess enhanced porosity (surface area and pore volume) and appropriate functionality attributes [196,204–209] with suitable sites for chemical affinity or reactivity [210,211], adsorption [212–217] and/or catalysis [218–227]. Fine control of the defect amounts, and hence the tuning of the properties associated with it, is usually achieved by adjusting specific reaction parameters such as temperature, linker and metal ratio, acid, base, and/or water modulation, and the final workup procedure [228–230]. The use of monocarboxylic acid modulators during the synthesis of Zr-**fcu**-MOFs is usually associated with the formation of missing linker or missing-cluster defects within Zr-**fcu**-MOFs [197,231,232]. Ideally, the formation of missing-linker defects should be related to a transition of network dimensionality from the 12-c **fcu** to 10-c **reo** or 10-c **bct**, and then to 8-c **bcu** topology or even lower cluster connectivity with the remaining coordination sites being compensated by monocarboxylic acid modulators [126]. However, in most cases, defects are formed randomly without homogeneous distribution and are crystallographically described by reduced occupancy of the framework component atoms [197].

Defects are typically elucidated through a combination of experimental and computational techniques [233,234]. Experimentally, TGA, ^{1}H NMR spectroscopy, porosity analysis from N_2

Table 2
Reported isoreticular Zr-**fcu**-MOFs with their unit cell parameters and porosity attributes.

MOF	Linker*	Unit cell length (Å)	Porosity attributes		Ref.
			S_{BET} ($S_{Langmuir}$) (m^2/g)	Pore volume (cm^3/g)	
Zr-squa-**fcu**-MOF	squaric acid	15.784(3)	179		[20]
Zr-mes-**fcu**-MOF	mesaconic acid	17.854(7) 17.7804(2)	662–725	0.32	[35,151]
Zr-fum-**fcu**-MOF	fumaric acid	17.943	690–990 (770–1070)	0.27–0.45	[21,35,156]
NU-403	H_2BODC	20.5606(5)			[155]
UiO-66	H_2BDC	20.7551(5)	950–1290 (1187–1390)	0.49–0.63	[10,21,82,90,157]
UiO-66-PyDC	H_2PyDC	20.6754(12)	1797	0.68	[99]
UiO-66-PzDC	H_2PzDC	20.6656(18)	1539	0.58	[99]
UiO-66-F	H_2BDC-F		(919)	0.26	[45]
UiO-66-Cl	H_2BDC-Cl		430–766	0.23–0.25	[45,158]
UiO-66-Br	H_2BDC-Br		640–851 (654–1004)	0.18–0.30	[45,82,90,158]
UiO-66-I	H_2BDC-I		(799)	0.27	[45]
UiO-66-CH_3	H_2BDC- CH_3		760 (856)	0.27–0.34	[45,158]
UiO-66-$(CH_3)_2$	H_2BDC-2,5-$(CH_3)_2$		680–868 (825–968)	0.30–0.31	[45,82,158]
UiO-66-NO_2	H_2BDC- NO_2		660–869 (893–980)	0.28–0.40	[82,90,92,158]
UiO-66-NH_2	H_2BDC- NH_2		930–1112 (1073–1313)	0.35–0.76	[39,82,90,92,157,158]
UiO-66-$(NH_2)_2$	H_2BDC-2,5-$(NH_2)_2$		540		[23]
UiO-66-SH	H_2BDC-SH		1432	0.57	[159]
UiO-66-$(SH)_2$	H_2BDC- $(SH)_2$		308		[94]
UiO-66-OH	H_2BDC- OH		1000	0.29	[23,45]
UiO-66-$(OH)_2$	2,5-H_2BDC- $(OH)_2$	20.7849(2)	560–1145	0.22–0.37	[23,35,45,158]
UiO-66-CF_3	H_2BDC-CF_3	20.43(5)	(739)	0.27	[45]
UiO-$(CF_3)_2$	H_2BDC-2,5-$(CF_3)_2$		503–540	0.18–0.24	[45,88,158]
UiO-66-OCH_3	H_2BDC-OCH_3		(763)	0.25	[45]
UiO-66-$(OCH_3)_2$	2,5-H_2BDC-$(OCH_3)_2$		868	0.38	[92]
UiO-66-$(OCH_2CH_3)_2$	2,5-H_2BDC-$(OCH_2CH_3)_2$		405 (574)	0.41	[39]
UiO-66-(2,5-$SCH_2CH = CH_2)_2$	2,5-H_2BDC-$(SCH_2CH = CH_2)_2$		566	0.31	[95]
UiO-66-CO_2H	H_2BDC-CO_2H	20.758(1)	658–661 (842)	0.26–0.29	[37,45,160]
UiO-66-$(CO_2H)_2$	2,5-H_2BDC-$(CO_2H)_2$	20.54(6) 20.731(5)	364–527 (608)	0.18–0.29	[37,39,160]
UiO-66-$(CO_2H)_4$	H_2BDC-$(CO_2H)_4$		212 (342)	0.42	[39]
UiO-66-F_2	2,5-H_2BDC-F_2	20.33(5)	836	0.28	[45]
UiO-66-F_4	H_2BDC-F_4		833 (537–1348)	0.39–0.65	[39,57]
UiO-66-Cl_2	2,5-H_2BDC-Cl_2	20.27(13)	609	0.21	[45]
UiO-66-Br_2	2,5-H_2BDC-Br_2	20.23(3)	(339)	0.12	[45]
UiO-66-SO_3H	H_2BDC-SO_3H		975, (769)	0.26, 0.44	[45,159]
UiO-66-$(SO_3H)_2$	H_2BDC-2,5-$(SO_3H)_2$		35		[94]
UiO-66-C_6H_4	H_2BDC-SO_3H		(416)	0.14	[45]
UiO-66–2,3-NH_2Cl	H_2BDC-2,3-NH_2Cl		760		[85]
UiO-66–2,5-NH_2Cl	H_2BDC-2,5-NH_2Cl		876		[85]
UiO-66–2,3-NH_2Br	H_2BDC-2,3-NH_2Br		613		[85]
UiO-66–2,5-NH_2Br	H_2BDC-2,5-NH_2Br		727		[85]
UiO-66–2,5-NH_2BI	H_2BDC-2,5-NH_2BI		899		[85]
UiO-66-O-Ph-NO_2	H_2BDC-O-Ph-NO_2		1040	0.6	[97]
Zr-*cis*-muc-**fcu**-MOF	*trans*,*trans*-muconic acid	20.818(1)	557–705	0.34	[43,154]
Zr-*trans*-muc-**fcu**-MOF	*trans*,*trans*-muconic acid	20.87820(10)			[71]
UiO-66–1,4-NDC	1,4-H_2NDC	20.7786	615–876 (732)	0.42–0.43	[90,92,156,157]
NU-801	H_2PDAA	26.9170(5)			[71]
Zr-2,6-NDC-**fcu**-MOF	2,6-H_2NDC	23.910(3)	1300–1717	0.60–0.74	[72,126,156]
BUT-10	H_2FDCA	26.051(10)	1848 (2185)	0.82	[122]
BUT-11	H_2DTDAO	26.347(10)	1310 (1571)	0.62	[122]
UiO-67	H_2BPDC	26.768(5)	2145–2505 (~3000)	1.05–1.10	[10,23,121,122,141,156]
UiO-67-Cl	H_2BPDC-Cl	26.7863(16)			[71]
UiO-67-NO_2	H_2BPDC-NO_2		2160		[23]
UiO-67-*o*-NH_2	H_2BPDC-*o*-NH_2		2050		[121]
UiO-67-*m*-NH_2	H_2BPDC-NH_2		2020		[121]
UiO-67-*m*-$(NH_2)_2$	H_2BPDC-*m*- $(NH_2)_2$		1360 (1780)	0.64	[161]

Table 2 (*continued*)

MOF	Linker*	Unit cell length (Å)	Porosity attributes		Ref.
			S_{BET} ($S_{Langmuir}$) (m^2/g)	Pore volume (cm^3/g)	
UiO-67-*m*-Me	H_2BPDC- *m*-Me	26.7390(8)			[71]
UiO-67-BPyDC	H_2BPyDC	26.5460(19)	2385–2646 (2965)	1.00–1.06	[119,141,162]
UiO-67–Tz–NH_2	H_2BPDC-Tz-NH_2		404 (554)		[120]
UiO-67–Tz–OH	H_2BPDC-Tz-OH		84 (133)		[120]
UiO-67–Tz–$COOCH_3$	H_2BPDC-Tz-CO_2CH_3		148 (211)		[120]
UiO-67-NHPro	H_2bpdc-NHProBoc	26.8663(1)		0.51	[136]
Zr-ABDC-**fcu**-MOF	H_2ABDC	29.4227(4) 29.3248(8)	2830–3000	1.41	[69,72]
Zr-SDC-**fcu**-MOF	H_2SDC	29.8884(3)	2950		[72]
Zr-ABDC-Cl_2 **fcu**-MOF	H_2ABDC-Cl_2	29.5710	2226	0.94	[128]
BPHV-MOF	H_2BPHV	*a* = 23.239(4) *c* = 32.854(13)			[127]
BPV-MOF	H_2BPV		373		[127]
UiO-68-NH_2	H_2TPDC-NH_2	32.7767(5)	(4170)		[10,24]
UiO-68-Me	H_2TPDC-CH_3		3738		[131]
PCN-56	TPDC-2CH_3	32.6003(11) 32.625(3)	3741		[71,132]
PCN-57	TPDC-4CH_3	32.657(19)	2572		[132]
PCN-58	TPDC-2CH_2N_3	32.6919(14)	2185		[132]
PCN-59	TPDC-4CH_2N_3		1279		[132]
UiO-68-sal	H_2TPDC-sal	32.6205(16)	3311		[163]
UiO-68-NHPro	H_2tpdc-NHProBoc	32.880(4)		0.93	[136]
TPHN-MOF	H_2TPHN	38.678(3)	365		[139]

* For abbreviations of the organic linkers, see Figs. 7, 13, 14 and 15.

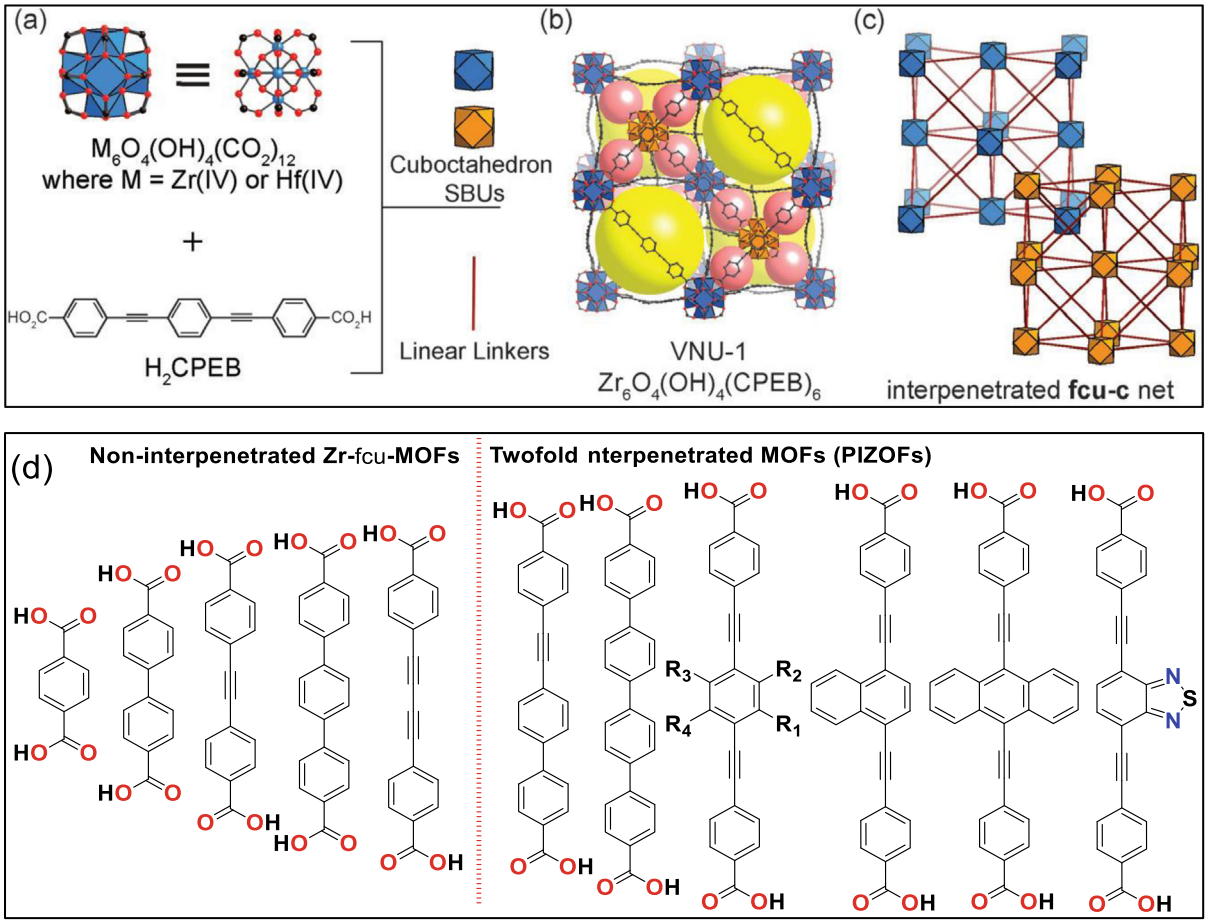

Fig. 20. Crystal structure and topology representation of PIZOF-0 (VNU-1) (a-c) and the linear dicarboxylate linkers employed to assemble interpenetrated or non-interpenetrated **fcu**-MOFs (d). The figures from a-c are reproduced with permission from ref. [247].

Table 3
The functionalized dicarboxylic acid linkers and their corresponding PIZOFs.

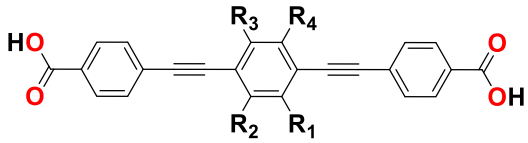

PIZOF	R_1	R_2	R_3	R_4	Ref.
PIZOF-0 (VNU-1)	H	H	H	H	[248–250]
PIZOF-1	NH_2	H	H	H	[76]
PIZOF-2	OCH_3	H	OCH_3	H	[76]
PIZOF-3	OCH_2CCH	H	OCH_3	H	[76]
PIZOF-4	$OCH_2CCTIPS$	H	OCH_3	H	[76]
PIZOF-5	$OCH_2CH_2CH_2CH_2CH_3$ (OPentyl)	H	$OCH_2CH_2CH_2CH_2CH_3$ (OPentyl)	H	[76]
PIZOF-6	dodec	H	dodec	H	[76]
PIZOF-7	$O(CH_2CH_2O)_2CH_3$	H	$O(CH_2CH_2O)_2CH_3$	H	[76]
PIZOF-8	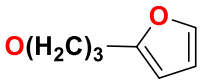	H	OCH_3	H	[76]
	CH_3	H	CH_3	H	[251]
	F	F	H	H	[251]
	F	H	F	H	[251]
	F	F	F	F	[251]

sorption, and vibrational spectroscopy (FT–IR and Raman) are the most common techniques employed to quantify the defect loading [44,235–237]. Recently, ammonia (NH_3) adsorption with subsequent characterizations by temperature programmed desorption mass spectrometry (TPD-MS) and FT–IR spectroscopy has also provided promising results for further exploration in identifying defects in Zr-**fcu**-MOFs [238]. The use of high pressure PXRD measurements to detect the mechanical response and quantitative estimation of missing linkers by potentiometric titrations have been reported to be useful in elucidating defects in Zr-**fcu**-MOFs [239,240]. Lately, scanning electron diffraction [241] and low-dose high-resolution transmission electron microscopy [242] were shown to be efficient tools for the direct observation of individual defects within UiO-6*x* frameworks. We refer the readers to recently reported reviews for more detailed information concerning the presence and characterization of defects in **fcu**-MOFs [243–246].

2.6. Interpenetrated Zr-fcu-MOFs

Employing linkers longer than the UiO-68 linker leads to the assembly of porous interpenetrated zirconium-organic frameworks (PIZOFs) [247]. Upon solvothermal mixing of $ZrCl_4$ and the long, linear dicarboxylic acids, $HO_2C[PE\text{-}P(R_1,R_2,R_3,R_4)\text{-}EP]CO_2H$ that contains alternating phenylene (P) and ethynylene (E) units (PEPEP) and various substituent R groups, a series of isoreticular PIZOFs, PIZOF-0 (also called VNU-1 where VNU = Vietnam National University) to PIZOF-8, were obtained (Fig. 20 and Table 3) [76,248–251]. Other isoreticular PIZOFs assembled using $[Zr_6O_4(OH)_4(O_2C)_{12}]$ nodes and dicarboxylic acid linkers with PPPP and PEPP units, denoted PPPP-PIZOF-1 and PEPP-PIZOF-1, have also been reported [252]. Reduction of the linker length to PEEP units results in non-interpenetrated Zr-**fcu**-MOF (Fig. 20). The possibility for further tuning the pore structure of the isoreticular PIZOFs was demonstrated by using organic linkers containing naphthyl, anthracyl, and benzothiadiazolyl units (Fig. 20) in place of the central benzene group of PIZOF-0 [251,253]. The structure of these PIZOFs, obtained from PXRD and SCXRD analyses, are described as twofold interpenetrated isoreticularly expanded Zr-**fcu**-MOFs.

PIZOFs have two independent interpenetrating networks consisting of convex and concave tetrahedral cages. However, due to interpenetration, the concave tetrahedral cavities contain the SBUs of the second framework, which results in small cavities [248]. Depending on the length and shape of the integrated functional groups, the large cavity diameter can vary from ca. 19 Å in PIZOF-0 to ca. 11 Å in PIZOF-7. Deeper inspection of the framework structures reveals that the integrated functional groups do not protrude into the small cavities and, therefore, the small cavity with a diameter of ca. 5 Å remains identical for the entire PIZOF series. As probed by solid-state photoluminescence spectroscopy studies, the introduction of functional groups such as methyl, fluoro, naphthyl and benzothiadiazolyl units induced subtle structural changes, such as linker rotation, and mediated host–guest interactions without affecting the underlying topology [251]. As a representative example, the MOF prepared from the dimethyl substituted linker exhibited a temperature-dependent phase transition regulated by steric clashes between interpenetrated nets. Moreover, the tetrafluorinated linker led to a PIZOF material with superhydrophobic properties. The dynamics of PIZOF (i.e., guest dependent linker rotation and electronic effects) is also a research topic of current importance that could help to develop synthetic molecular machines [254].

The amenability of the interpenetrated frameworks for functionalization has enabled the exploration of these MOFs for experimental and simulated CO_2 adsorption measurements. Indeed, several PIZOF materials, including PIZOF-7, achieved enhanced CO_2 uptakes and CO_2/N_2 and CO_2/CH_4 selectivities due to reduction in pore size [248]. Owing to its large pores and enhanced chemical stability, PIZOF-0 (VNU-1) was also investigated as an heterogeneous Lewis acid catalyst for the Friedel-Crafts benzoylation of aromatic compounds and was reported to achieve high yields of the aromatic ketones within a few minutes in a recyclable manner [255]. In addition to their mechanical robustness, the water stability of PIZOFs is an attractive feature that has led to increased interest for their deployment in different applications. As a representative example, the water stability of PIZOF-0 allows for aqueous stereoselective halogenation of the C—C unsaturated

bonds, such as reversible bromination and irreversible iodination, which represents an immense opportunity for radioactive iodine sequestration [250,256].

Finally, a PIZOF structure, named NNU-28, exploited a visible light responsive organic linker that contained an anthracene group and was shown to be an efficient photocatalyst for visible-light-driven photoreduction of CO_2 to formate [253]. The PIZOFs with naphthyl and benzothiadiazolyl functionalized linkers were also demonstrated as stable fluorescent water sensors [251]. Generally, the examples mentioned in this section demonstrate the possibility of tuning interpenetrated frameworks that adopt an underlying **fcu** topology by employing a large variety of dicarboxylic acids with widely differing organic functionalities.

2.7. Multivariate (MTV) Zr-fcu-MOFs

The assembly of multivariate (MTV) Zr-**fcu**-MOFs has attracted research interest for many reasons, some of which include the systematic alteration of adsorption or catalytic sites and improving the chemical and thermal stability. MTV-MOFs can be prepared by mixing appropriate ratios of MBB precursors in a one-pot synthesis. However, one-pot pathways sometimes lead to physical mixtures of two or more MOFs rather than mixed MBBs within one framework. In such cases, post-synthetic modification (PSM) [257] has emerged as a powerful tool to realize MTV-MOFs. Herein, progress made in the assembly of mixed-linker and mixed-metal Zr-**fcu**-MOFs will be discussed. Prior to the discussion on MTV-MOFs, a brief overview on PSM will be presented.

2.7.1. Post-synthetic modifications of Zr-fcu-MOFs

Most MOFs discussed so far are assembled by a one-pot solvothermal synthesis approach using a pre-functionalized linker. However, PSM, as a strategy, has been successfully implemented for the construction of functionalized Zr-**fcu**-MOFs that are otherwise difficult or impossible to be accessed by conventional direct synthetic approaches. An early example was one in which a cyano-functionalized MOF (UiO-66-CN) was prepared via cyanation of pre-synthesized UiO-66-Br with CuCN and microwave irradiation [86]. Due to the presence of a reactive and labile functional group, attempts for the direct synthesis of the MOF from H_2BDC-CN and various Zr(IV) salt precursors was reported as unsuccessful. In this sub-section, several examples of isoreticular UiO-6*x* MOFs that have been prepared by PSMs of linker functional groups will be discussed with further examples of PSM on Zr-**fcu**-MOFs provided in the forthcoming sub-sections.

Owing to the reactivity of $-NH_2$ functional group, UiO-66-NH_2 is one of the most explored Zr-**fcu**-MOFs for covalent and metalation chemistry-based PSM. As a representative example, the presence of the $-NH_2$ functionality in UiO-66-NH_2 produced post-synthetically grafted Cu species with mixed-valence-states (*i.e.*, Cu(I)/Cu(II)) on the MOF, thereby making the MOF a suitable photocatalyst for air cleaning [258]. The Cu(I)/Cu(II) active centers, introduced by an *in situ* partial reduction of Cu(II) to Cu(I) during its coordination with the $-NH_2$ group and O-donor of the linker, allowed electron transfer from the organic linkers to the Cu centers on the linker via a linker-to-linker-metal-charge-transfer (LLMCT) route. This resulted in a longer photogenerated charge lifetime by enhancing the rate of electron transfer while inhibiting photogenerated electron-hole pair recombination. Under visible light irradiation, the Cu(I)/Cu(II) grafted UiO-66-NH_2 displayed photocatalytic performance for oxidizing NO to NO_3^-. In related work, the exploitation of the $-NH_2$ group in UiO-66-NH_2 as an anchoring site allowed for the coordination of single-atom Ru(III) (Ru-NH_2-UiO-66) by simple mixing and stirring of UiO-66-NH_2 and $RuCl_3$ [259]. The modified MOF acted as a selective catalyst for the oxidation of NO_x (NO/NO_2) to NO_2^- and NO_3^- by plasma activation. Ru(III) single atoms were coordinated to both the BDC-NH_2 units and the Zr(IV) sites via an oxo-bridged Zr(IV)–O–Ru(III), which sped up electron transfer. Additionally, the $-NH_2$ group of UiO-66-NH_2 has created opportunities for doping metal nanoparticles within the MOF, which were exploited to heterogeneously catalyze several chemical transformations [260–262]. The metalation-based PSM routes for the transformation of $-NH_2$ groups in UiO-6*x*-NH_2 MOFs to other functional groups are summarized in Fig. 21.

Other BDC-X linkers have also been used as a starting point in the preparation of post-synthetically modified Zr-**fcu**-MOFs. This is exemplified by the free carboxylic acid functional groups in UiO-66-COOH and UiO-66-$(COOH)_2$ that provide cation binding sites for PSM to generate UiO-66-COOM and UiO-66-$(COOM)_2$ (M = Cu(I), Li(I), Na(I), K(I)) [160]. The introduced metal cations enabled selective interactions with particular adsorbates and, in some cases, tuned the aperture size of the MOFs to permit their use in different applications. Specifically, copper functionalized Zr-**fcu**-MOFs were found to exhibit high ammonia adsorption capacities under both dry and humid conditions. Ionized UiO-66-$(COOM)_2$ (M = Li(I), Na(I), K(I)) were shown to have optimal features for post-combustion CO_2 capture [171]. Similarly, post-synthetic metalation of the free –COOH groups in UiO-66-$(COOH)_2$ by Eu(III)/Cu(II) permitted the construction of a MOF-based H_2S sensor [263]. In this case, the high affinity of H_2S to Cu(II) ions enhances the fluorescence of Eu(III) and quenches the broad ligand-centered emission. This was hypothesized to contribute for the sensitive and selective turn-on detection of H_2S over other environmentally- and biologically-relevant species under physiological conditions. Cu(I)-chelated UiO-66-COOH and UiO-66-$(COOH)_2$ MOFs were also demonstrated to have impact in boosting the ethylene/ethane adsorption selectivity due to constricted apertures and specific π-complexation (Fig. 22) [100].

PSM is common in pore-expanded Zr-**fcu**-MOFs especially in the metalation of bipyridine moieties for catalytic applications (Fig. 23A). The presence of freely available *N*-donors as anchoring sites for metal ions made the UiO-67-BPyDC MOF a suitable precursor to prepare mixed-linker UiO-67(BPyDC)(BPyDC-M^{n+})-type MOFs (M = Cr, Co, Co, Ir, Pd, Pt, Pt/Ir, Ru) [139,140,264–272]. The open N-donors of the linker's bipyridine backbone create an opportunity to design and assemble **fcu**-MOFs that can be deployed as sensitized solar cells and heterogeneous catalysts in different types of chemical reactions. Apart from the metalation strategy, the implementation of click chemistry on pre-synthesized azido-functionalized pore-expanded Zr-**fcu**-MOFs has resulted in the conversion of the $-N_3$ functional group to 1,2,3-triazole (Tz) (Fig. 23B and C). As described in Section 2.4.1, UiO-67-N_3, PCN-57 and PCN-58 were prepared solvothermally from pre-synthesized azido functionalized BPDC-*m*-N_3, TPDC-2CH_2N_3 and TPDC-4CH_2N_3 linkers, respectively [120,132]. The MOFs were then transformed to their isoreticular Tz-functionalized analogs (UiO-67-Tz-R and UiO-68-Tz-CH_2-R) via the post-synthetic click reactions between the $-N_3$ functional group and different alkyne compounds in the presence of CuI as a catalyst [120,132]. These PSM-MOFs were demonstrated as catalysts for Knoevenagel condensation reactions between benzaldehyde and different methylene compounds.

The presence of the $-NH_2$ functional group together with the high porosity in UiO-68-NH_2 creates opportunities to transform this material into a suitable catalyst. Post-synthetic amine-aldehyde condensation on UiO-68-NH_2 by treating the framework with excess pyridine-2-carboxaldehyde led to the formation of an isoreticular MOF, denoted UiO-68-IP [273]. Subsequent metalation of UiO-68-IP with $Pd(NO_3)_2$ led to the doping of Pd(II) within the framework (Fig. 24 left). A catalyst, denoted Pd(0)@UiO-68-AP, synthesized by the reduction of the Pd(II)-doped MOF with $NaBH_4$ in an aqueous solution, served as an active bifunctional heteroge-

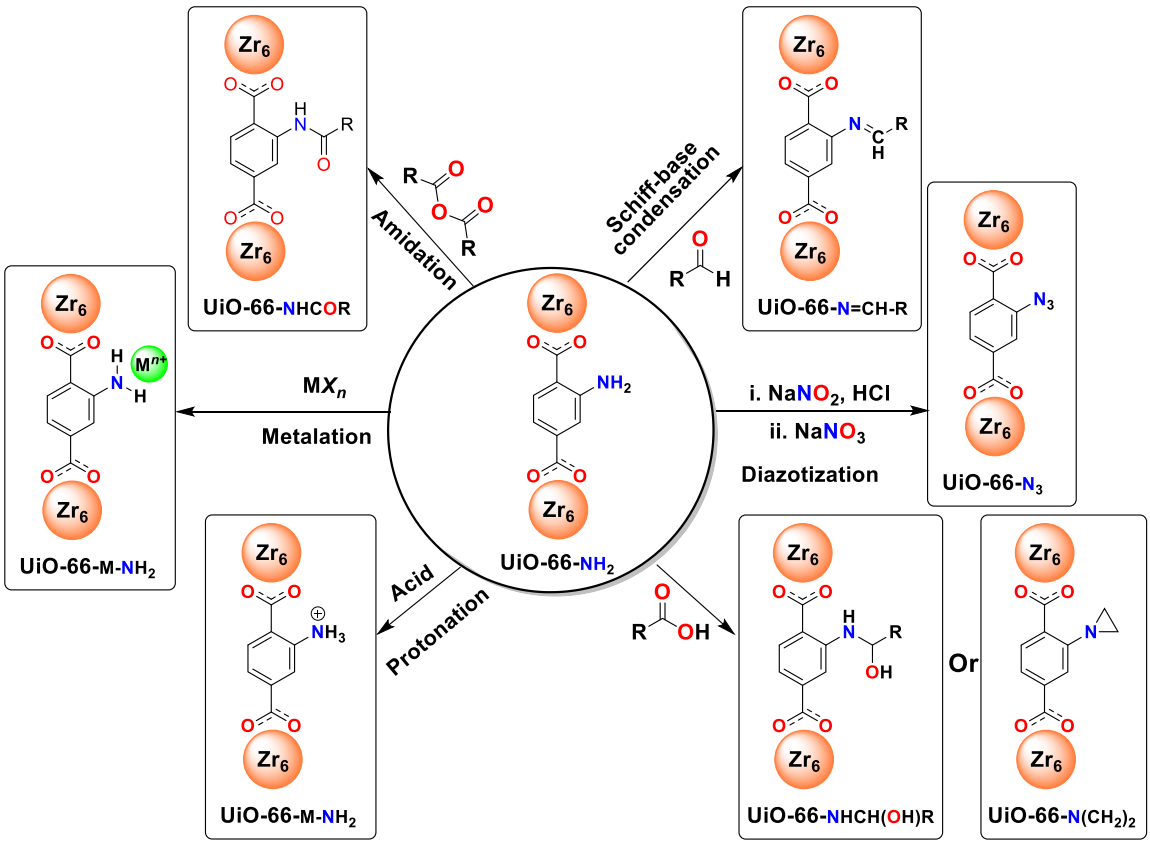

Fig. 21. The commonly employed PSM pathways to convert UiO-6*x*-NH_2 to UiO-6*x*-X and/or UiO-6*x*-(X)(NH_2) MOFs.

neous catalyst for a benzyl alcohol oxidation-condensation reaction under relatively mild conditions. In related work, post-synthetic metalation of salicylaldimine (sal)-functionalized MOF (UiO-68-sal) permitted the assembly of single-site, recyclable heterogeneous MOF catalysts, named sal-M−MOF (M = Fe or Co), for olefin hydrogenation (Fig. 24 right) [163]. The sal-M−MOFs were formed as mixed linker **fcu**-MOFs, UiO-68-(TPDC-sal)(TPDC-M−sal), with ICP-MS and ^{1}H NMR analyses of the digested sal-M−MOFs showing Fe and Co loadings of 66 and 6%, respectively. Owing to mass transport problems and other factors like short-range defects or imperfections in the crystal, it is assumed to be difficult for any system to reach 100% conversion during post-synthetic modifications.

Complete transformations of all the functional groups in UiO-6*x*-X MOFs (*i.e.*, 100% conversion) to UiO-66-Y is not expected, therefore, post-synthetically modified Zr-**fcu**-MOFs are expected to possess multivariate functional groups within the pores. The impact of the untransformed functional groups on the structure–property relationships of the MOFs are rarely studied and explained. For example, post-synthetic diazotization of the –NH_2 functional group was reported to result in an isoreticular **fcu**-MOF, UiO-66-N_3 [118]. In this scenario, the reality is that both BDC-N_3 and BDC-NH_2 could exist within the structure resulting in a mixed-linker UiO-66-(BDC-NH_2)(BDC-N_3) MOF with different linker ratios depending on the degree of the conversion. UiO-66-N_3 was shown to have a selective and rapid fluorescence turn-on response towards H_2S even in the presence of potentially competing biomolecules under physiological conditions. Upon interaction with H_2S, the –N_3 functional groups are reduced to –NH_2 allowing the Zr-**fcu**-MOF to act as selective turn-on probe for H_2S. Undoubtedly, the nature and amount of the co-existing untransformed functional group (*i.e.*, –NH_2 in this case) can have either a positive or negative effect on the properties of the MOF. Future experimental and theoretical studies are required to provide more understanding into whether there is synergy between the different functionalities when applied for a certain end function.

PSM is not limited to the organic component of Zr-**fcu**-MOFs. Several tailor-made MOFs have been synthesized by post-synthetically modifying the inorganic cluster. The possibility of doping metal ions by post-synthetic exchange process has been demonstrated through the formation of mixed-metal $Zr_6M(n)_x$ cluster-based UiO-66 MOFs (M(*n*) = Yb(III), Eu(III), Nd(III), and Ce (IV)) [274]. These MOFs combine the electronic properties of the lanthanide ions, such as luminescence and photocatalysis, and the stability of the Zr-**fcu**-MOFs. A combination of PXRD measurements, ICP-optical emission spectroscopy (ICP-OES) analysis, bright-field scanning transmission electron microscopy (BF-STEM) and energy dispersive X-ray spectroscopy (EDX) mapping characterizations supported the homogeneous distribution of the doped lanthanide ions with no cluster formation (*i.e.*, all dopant ions were included on a Zr(IV) site with no other Ti–O or Ln–O species within the framework). The versatility of the UiO-6*x* frameworks enabled researchers to dope the lanthanide and Ti(IV) ions within UiO-66-BDC-NH_2 and Zr-fum-**fcu**-MOF [274]. As evidenced by solid-state ultraviolet–visible (UV–vis) light measurements, the prepared mixed-metal MOFs exhibited charge transfer properties that cannot be observed in the host Zr-**fcu**-MOFs. More examples will be provided in Section 2.7.3.

2.7.2. Mixed-linker Zr-fcu-MOFs

The adaptability of the Zr-**fcu**-MOF platform towards linker variations enabled the assembly of various MOFs that possess two or more linear dicarboxylate linkers within the same structure

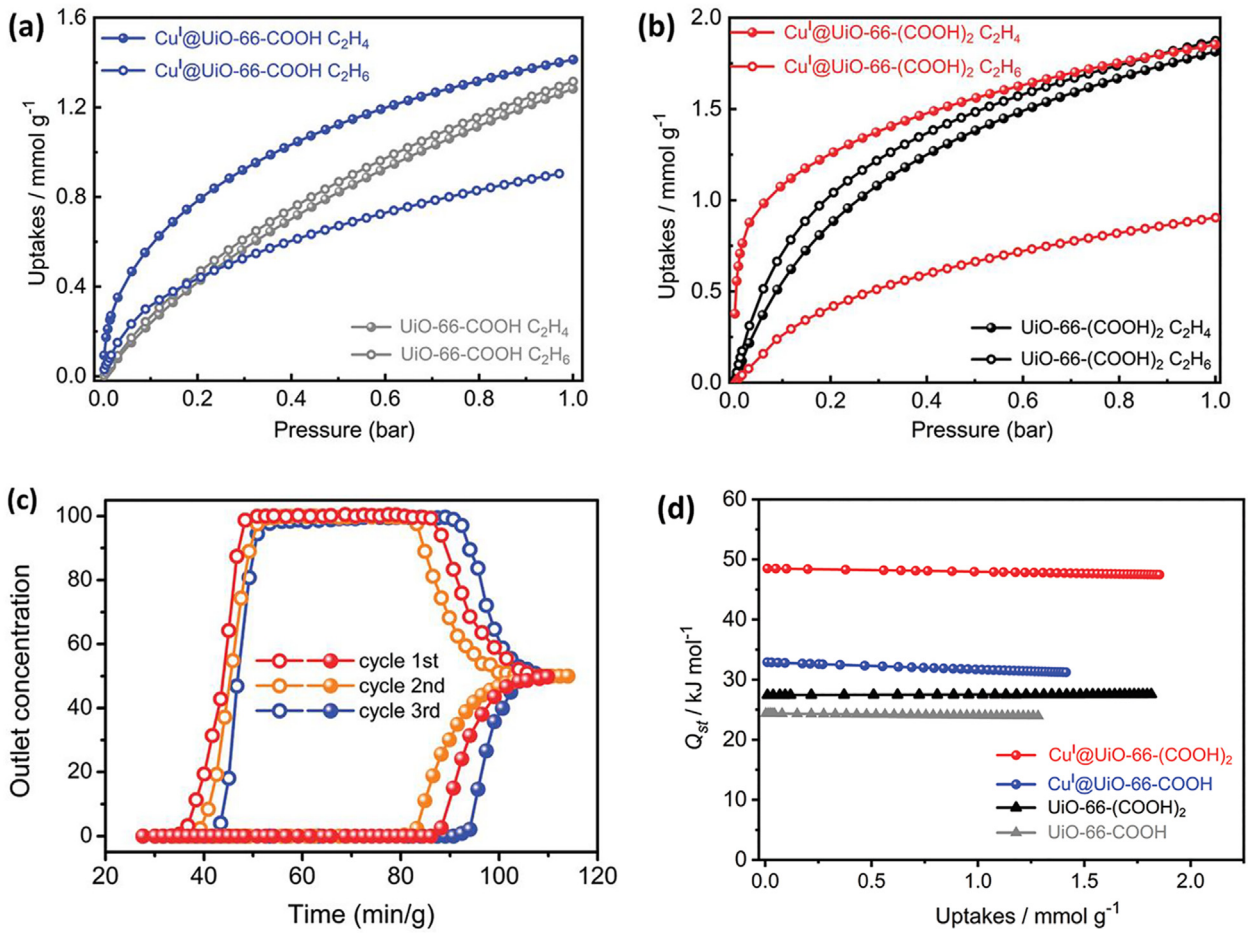

Fig. 22. Single-component C_2H_4 and C_2H_6 adsorption isotherms on UiO-66-COOCu (a) and UiO-66-(COOCu)$_2$ (b) MOFs at 298 K; C_2H_4/C_2H_6 (50/50, *v*/*v*) breakthrough curves of UiO-66-(COOCu)$_2$ (c); and the isosteric heat (Q_{st}) of C_2H_4 adsorption in UiO-66-COOCu and UiO-66-(COOCu)$_2$ (d). . Reproduced with permission from [100]

while keeping the underlying topology intact. Mixed-linker MOFs have been prepared by as follows: (i) one-pot solvothermal assembly using two or more linkers simultaneously in solutions; (ii) partial exchange of the original linkers in pre-assembled MOFs by other linkers of similar length; or (iii) partial post-synthetic reactions or metalations of the functional groups on the linkers being the commonly applied routes.

2.7.2.1. Mixed-linker Zr-fcu-MOFs by one-pot synthesis. Various mixed-linker UiO-66 type MOFs that contain two or more BDC-X have been reported. In 2011, Kim *et al.* [275] prepared a series of bifunctional UiO-66-(NH_2)(Br) MOFs employing one-pot solvothermal reactions of H_2BDC-NH_2 and H_2BDC-Br with $ZrCl_4$. Aside from the confirmation of the resultant framework structures by PXRD and thermal properties by TGA, the existence of both linkers in the structure was confirmed by ^{1}H NMR spectroscopy and electrospray ionization (ESI)-MS. To ensure that both linkers are within one structure as opposed to being incorporated as mechanical, physical mixtures of UiO-66-NH_2 and UiO-66-Br MOFs, aerosol time-of-flight mass spectrometry (ATOFMS) measurements were used. Indeed, both linkers were determined to exist within one structure.

Lee *et al.* [276] prepared a Zr-**fcu**-MOF that was comprised of 86% BDC-NH_2 and 14% 2,5-BDC-(NH_2)$_2$ linkers within the same UiO-66 type framework. Additionally, Goh *et al.* [277] employed an one-pot reaction to assemble a series of mixed-linker Zr-**fcu**-MOFs from BDC-NH_2 as the primary linker and BDC-X (X = –H, –F, –Cl, –Br) as a secondary linker. This work reported the effects of different linkers on the photocatalytic property of the end MOFs while also demonstrating that UiO-66-(BDC-NH_2)(BDC-F) was capable of achieving five times more conversion in the oxidation of benzyl alcohol to benzaldehyde when compared to the single linker-based UiO-66-(BDC-NH_2) or UiO-66-(BDC-F) MOFs. Furthermore, the one-pot solvothermal construction of isoreticular bifunctional UiO-66 type MOFs, containing BDC-NH_2 and BDC-X linkers within one framework, was reported [278]. In this work, the synthesized mixed-linker MOFs, denoted UiO-66-NO_2-X (X = –NH_2, –(OH)$_2$, –(COOH)$_2$), exhibited promising CO_2 capture performance with high CO_2/N_2 selectivity [278].

Butova *et al.* [279,280] reported various mixed-linker UiO-66 type MOFs synthesized solvothermally through an one-pot reaction in the presence of two linkers, BDC and 1,4-NDC. The introduction of different amounts of NDC linker together with BDC was reflected in slight differences of the lattice parameter *a*, which increased with increasing NDC content. The trend in the lattice parameter and the resulting slight leftward shift in the PXRD patterns as a function of increasing NDC content was attributed to the stress created by NDC's extra benzene rings in comparison with the BDC linkers. Indeed, it is a common phenomenon to observe gradual shifts in the reflections in high resolution PXRD pattern for mixed-linker MOFs with varying ratios of linkers [281]. For example, in the mixed linker UiO-66-(BDC)(BDC-NH_2) and UiO-66-(BDC)(BDC-Br) systems with varying ratios of linkers, the structures' adaptability to the presence of linkers with differing characteristics resulted in either shrinkage or expansion of the unit cells and a corresponding shift in their PXRD patterns [282].

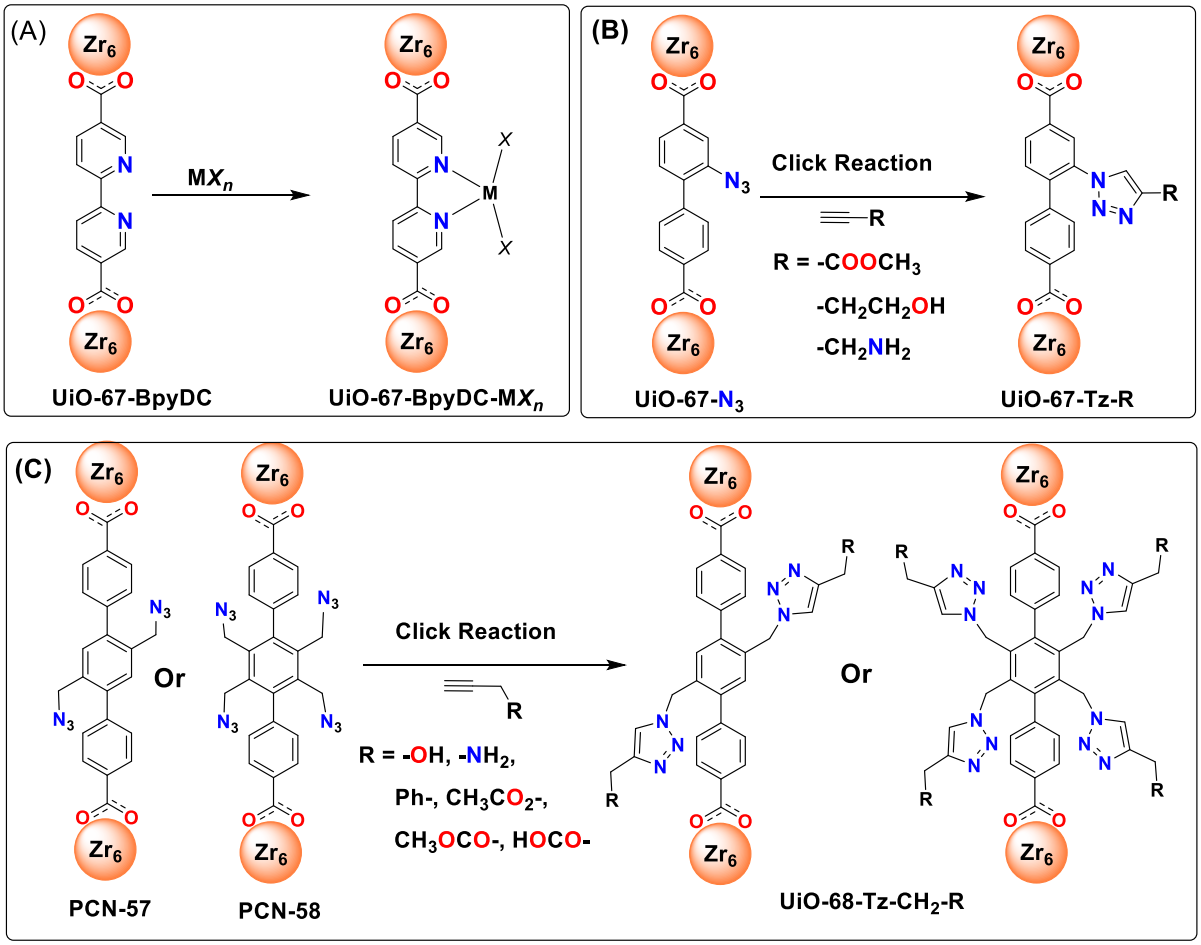

Fig. 23. Schematic showing the PSM of functionalized UiO-67 and UiO-68 MOFs.

In a different example, Hu *et al.* [47] prepared a series of UiO-66-NH_2-F_4-*x* MOFs (*x* represents the incorporated molar fraction of BDC-F_4 linker), denoted UiO-66-NH_2-F_4-0.27, UiO-66-NH_2-F_4-0.53, and UiO-66-NH_2-F_4-0.72, by acetic acid modulated hydrothermal synthesis in the presence of $ZrOCl_2{\cdot}8H_2O$, BDC-NH_2 and BDC-F_4 with different molar feed ratios. Among these mixed-linker MOFs, UiO-66-NH_2-F_4-0.53 achieved high CO_2 uptake capacity (0.76 mmol/g) and CO_2/N_2 selectivity (18.9 for CO_2/N_2 = 15/85) at 298 K under humid conditions with negligible losses at very high relative humidity levels. These performance values were

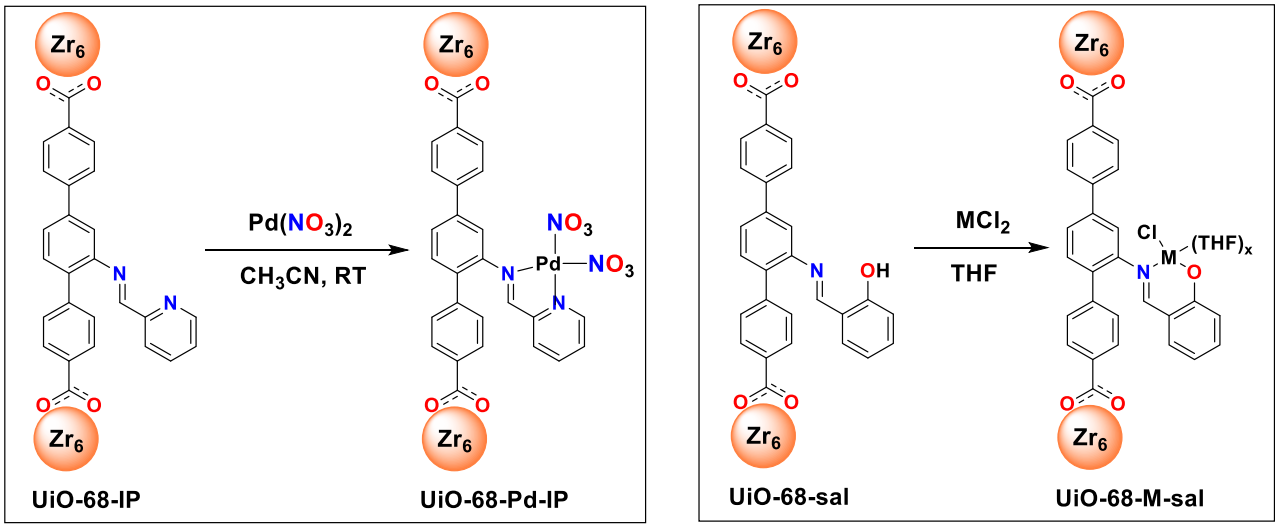

Fig. 24. Schematic showing post-synthetic metalation of UiO-68 type MOFs.[163,273].

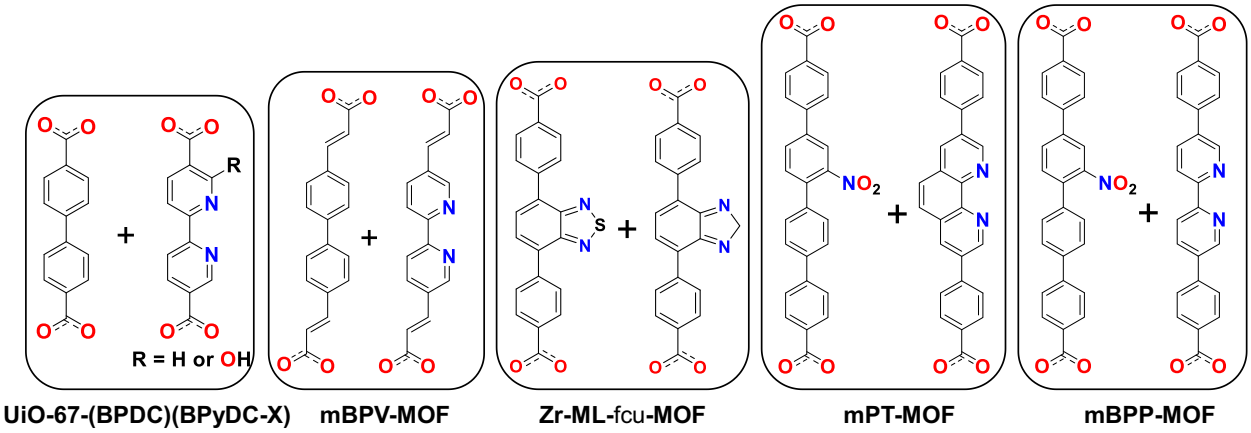

Fig. 25. Representative examples of mixed-linkers that have been used in the one-pot solvothermal synthesis of pore-expanded isoreticular Zr-**fcu**-MOFs.

claimed as amongst the highest for UiO-66-type MOFs due to the presence of optimal CO_2-philic amino groups and hydrophobic fluorine moieties.

One-pot solvothermal synthesis of mixed-linker Zr-**fcu**-MOFs has not been limited to isostructural UiO-66-X MOFs. MTV-UiO-67 or UiO-68 type architectures are also known. For example, Fei *et al.* [283] reported a successful one-pot synthesis of UiO-67-$(BPDC)_x(BPyDC)_{6-x}$ MOFs using different molar ratios of H_2BPDC and H_2BPyDC with $ZrCl_4$. An *et al.* [284] reported MTV UiO-67 MOFs that contain mixed BPDC and BPyDC-X with and without –OH substitution on the 6-position (BPyDC-OH or BPyDC, respectively) (Fig. 25). The synthesis of mixed linker **fcu**-MOFs from expanded biphenyl and bipyridyl containing dicarboxylate linkers has also been reported [127]. This is illustrated by $Zr_6O_4(OH)_4$-$(BPHV)_4(BPV)_2$, known as mBPV-MOF, which is synthesized by the trifluoroacetic acid-modulated solvothermal reaction of $ZrCl_4$ and two linkers, H_2BPV and H_2BPHV (Fig. 25) [127,272].

One-pot solvothermal synthesis of pore-expanded mixed-linker Zr-**fcu**-MOFs was further exemplified by the UiO-68 type MOF, named Zr-ML-**fcu**-MOF, which contains two linear dicarboxylate organic linkers of identical length and symmetry yet with the different functional groups, benzimidazole and thiadiazole (BI and TD, respectively) (Fig. 25) [135]. The presence of both linkers within the framework was confirmed by ^1H NMR and high-resolution XPS analyses. Steady state and time-resolved spectroscopy measurements on the MOF displayed a highly efficient energy transfer (ET; ~90% efficiency) that can mimic natural photosynthetic systems. The close proximity of the two linkers (average distance of 17 Å) and their distribution throughout the structure, as evidenced by elemental mapping scan of N and S using SEM-EDX, led to significant overlap between the emission spectrum of benzimidazole (energy donor) and the absorption spectrum of thiadiazole (energy acceptor). This, in turn, produced rapid (picosecond time scale) ET performance. On the other hand, Zr-BI-**fcu**-MOF [133] and Zr-TD-**fcu**-MOF [134] were not observed to exhibit the rapid ET process exhibited by the mixed-linker MOF. These and other examples demonstrate the importance of designing mixed-linker **fcu**-MOFs for particular end-functions. A final note is that the successful one-pot synthesis of mixed-linker Zr-**fcu**-MOFs was also demonstrated by UiO-69 type MOFs, $Zr_6O_4(OH)_4(TPHN)_4(PT)_2$ (mPT-MOF) and $Zr_6O_4(OH)_4(TPHN)_4(BPP)_2$ (mBPP-MOF) (Fig. 25) [127,272].

In general, many isoreticular mixed-linker Zr-**fcu**-MOFs have been prepared by one-pot solvothermal syntheses. In some cases, preparation of mixed-linker Zr-**fcu**-MOFs by this approach is very challenging, if not impossible, due to the high probability of forming mechanical, physical mixtures of two single-linker containing MOFs. In such cases, PSM permits the development of various made-to-order **fcu**-MOFs.

2.7.2.2. Mixed-linker Zr-fcu-MOFs by post-synthetic linker exchange. Post-synthetic linker exchange (PSE) is an approach that has proven successful in the realization of mixed-linker Zr-**fcu**-MOFs via single crystal-to-single crystal transformation. Though UiO-6*x* materials are stable, they are endowed with enough lability to carry out PSE [285]. This feature has created opportunities for preparing functionalized mixed-linker **fcu**-MOFs that are otherwise difficult to be assembled by direct solvothermal reactions. PSE is accomplished via either solid–solid interactions of two single linker-containing MOFs or solid–liquid (biphasic) systems that involve a MOF synthesized from one linker and a solution of another linker. One of the earliest examples of PSE to achieve a mixed-linker Zr-**fcu**-MOF is the bifunctional UiO-66-(Br)(NH_2) [286]. UiO-66-(Br)(NH_2) was prepared either by particle-to-particle or biphasic (solid–liquid) linker exchange. In the particle–particle linker exchange process, pre-assembled UiO-66-Br and UiO-66-NH_2 MOFs were suspended in a solvent (chloroform, methanol, DMF, and water) at different temperatures. The existence of both linkers in the single particle of the MOF was confirmed by ATOFMS characterization. The exchange rate and hence the ratio of the linkers in the framework was found to be strongly correlated with solvent polarity and temperature, with the highest temperature and the most polar solvent providing the highest exchange rates. In the biphasic (solid–liquid) linker exchange experiments, pre-assembled UiO-66-Br was suspended in an aqueous solution containing NH_2-BDC at different temperatures. Analysis of both the solution phase and the HF digested solid phase after the exchange process by ^1H NMR spectroscopy revealed the existence of both Br-BDC and NH_2-BDC in the aqueous solution and in the solid UiO-66-X MOF. Consistent with the particle-to-particle linker exchange findings, the linker exchange between NH_2-BDC solution and solid UiO-66-Br material was temperature dependent with the exchange rates being higher at higher temperature (9, 63, and 76% at room temperature, 55, and 85 °C, respectively). The biphasic linker exchange experiment conducted using pre-assembled UiO-66-NH_2 and an aqueous solution of Br-BDC led to similar findings but with lower degrees of exchange. In this case, the results were attributed to differences in donor ability, steric effect, and solubility of the NH_2-BDC versus Br-BDC. Similarly, higher exchange rate of NH_2-BDC than Br-BDC was

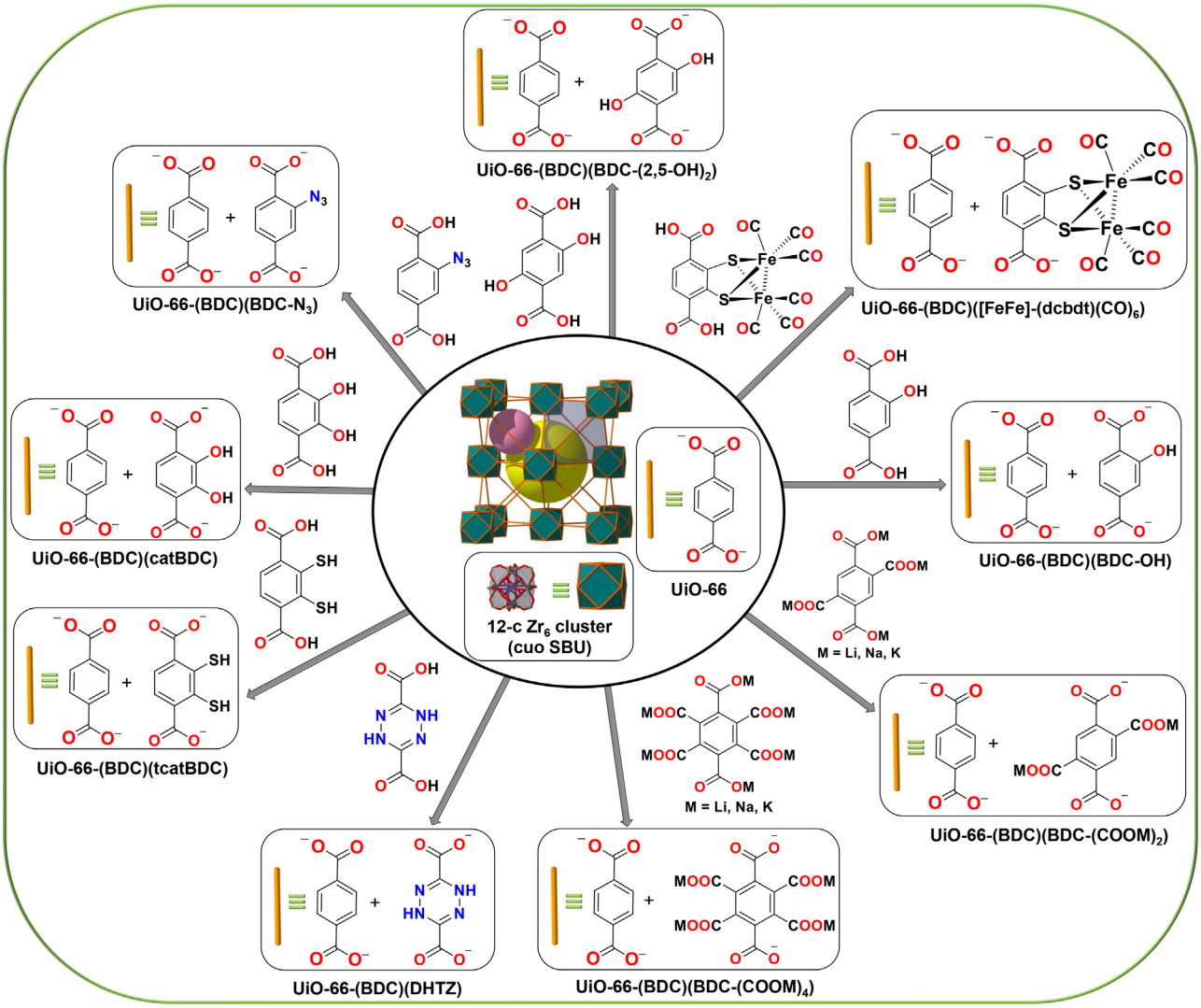

Fig. 26. Examples of UiO-66-(BDC)(BDC-X*n*) MOFs prepared by post-synthetic linker exchange (PSE).

demonstrated upon post-synthetic biphasic linker exchange experiments performed using pre-assembled UiO-66 and aqueous solutions of either the substituted linkers.

The power of PSE to prepare mixed-linker UiO-66-X MOFs was evidenced in the synthesis of the bifunctional UiO-66-(BDC)(BDC-X) MOFs summarized in Fig. 26 [286–291]. The prepared mixed-linker MOFs yielded properties that cannot otherwise be obtained in the parent UiO-66 structure. UiO-66-(BDC)(BDC-COONa)$_2$ and UiO-66-(BDC)(BDC-COOLi)$_4$ exhibited enhanced CO_2/N_2 selectivity when compared to the parent UiO-66 making them suitable candidates for post-combustion CO_2 capture [290]. The enhanced CO_2 separation performance of the resultant mixed-linker MOFs was due to the electrostatic interactions of CO_2 with the introduced polar metal sites and pore sizes that were tuned for optimal van der Waals interactions with CO_2. The other mixed-linker Zr-**fcu**-MOF, UiO-66-(BDC)(DHTZ), was reported as an effective optical sensor for the detection of NO_x due to the reversible oxidation and reduction of the introduced tetrazine unit and the high stability of the framework during the redox reaction (Fig. 27) [291].

Preparation of mixed-linker Zr-**fcu**-MOFs through a linker-exchange process has also been utilized in pore-expanded UiO-67 and UiO-68 MOFs. Fei *et al.* [283] reported the synthesis of UiO-67-(BPDC)$_x$(BPyDC)$_{6-x}$ by PSE of the BPDC linkers in pre-synthesized UiO-67 using a H_2O/DMF solution of H_2BPyDC. More recently, Zhu *et al.* [125] reported various UiO-67 type mixed-linker MOFs, denoted, UiO-67-4Me-R$_2$-*x*%, which contain different ratios of the tetramethyl substituted BPDC linker, BPDC-*o*-(CH$_3$)$_4$, and one of the BPDC-*m*-X linkers (X = NH_2, OH, COOH, 2 NH_2). The MOFs were prepared by partial post-synthetic replacement of BPDC-*o*-(CH$_3$)$_4$ in pre-assembled UiO-67-4Me MOF with the DMF solution of H_2BDC-NH_2, H_2BDC-OH, H_2BDC-COOH, or H_2BDC-2NH_2. The facile tuning of the degree of hydrophilicity/hydrophobicity via mixed-linker strategy allowed for the assembly of hydrolytically stable Zr-**fcu**-MOFs with water sorption isotherm shapes suitable for water-related applications. Among the prepared UiO-67 type MOFs, UiO-67-4Me-NH_2-38% was reported to give reproducible S-shaped water sorption isotherm appropriate for indoor humidity control within the recommended 45–65% relative humidity range. It is worth to note that the pristine UiO-67 MOF is not hydrolytically stable. PSE was further proven a successful strategy to construct expanded Zr-**fcu**-MOFs as demonstrated by the series of metallosalen-based isostructural UiO-68 type MOFs, UiO-68-[M] and UiO-68-[M]-[M'] ([M] = Cu, Fe–OAc, Cr–Cl, Mn–Cl, V = O); [M]-[M'] = Mn-Cr, Mn-V), obtained by a one- or

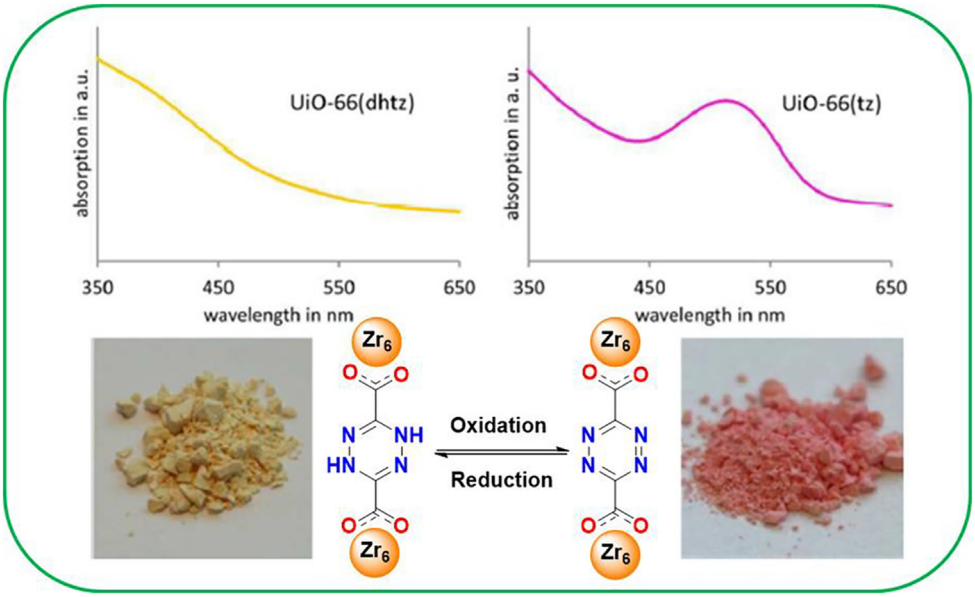

Fig. 27. Reversible oxidation and reduction of the tetrazine unit in UiO-66-(BDC)(DHTZ) and the corresponding change in color. . Reproduced with permission from [291]

two-step PSE of TPDC-Me linker from the pre-assembled UiO-68-Me (Fig. 28 top) [131]. The prepared MTV-MOFs containing one or two types of -M(salen) linkers were reported as efficient, recyclable, enantioselective heterogeneous chiral catalysts for different types of organic transformations such as asymmetric cyanosilylation of aldehydes, oxidative kinetic resolution of secondary alcohols, and sequential asymmetric alkene epoxidation/epoxide ring-opening reactions (Fig. 28 bottom).

2.7.2.3. Mixed-linker Zr-fcu-MOFs by post-synthetic reactions on linker functional groups. The use of PSM to prepare mixed-linker Zr-fcu-MOFs is not solely limited to linker exchanges. Post-synthetic transformations of the linker functional groups through chemical reactions are common. The mixed-linker amide functionalized UiO-66-(BDC-NH_2)(BDC-X) MOF, obtained by PSM of the –NH_2 functional group of UiO-66-NH_2, was among the first examples of mixed-linker Zr-based **fcu**-MOFs [90,292]. In typical covalent PSMs, a series of aliphatic and cyclic anhydrides were reacted with the –NH_2 group of UiO-66-NH_2 in dichloromethane or chloroform at different temperatures and exchange times to produce the amide modified mixed-linker MOF, UiO-66-(BDC-NH_2)(BDC-NHCOR) (Fig. 29) [90,292]. As confirmed by ^{1}H NMR spectroscopy characterization on HF and DMSO d_6 digested samples, different degrees of conversion of the amide were obtained depending on the chain length of the starting alkyl anhydride reagent. Furthermore, the exchange time was shown to impact the conversion rate, which was higher at longer durations [292]. The PXRD patterns of the amide modified materials were consistent with the precursor UiO-66-NH_2 framework topology. Moreover, FT–IR spectroscopy and ESI–MS of the digested modified samples further evidenced the incorporation of the amide substituents within the frameworks. N_2 adsorption isotherms at 77 K verified the progressive decrease in BET surface areas and pore volumes with increasing chain length of the precursor anhydrides.

Solvothermal synthesis of UiO-66-NH_2 using $ZrCl_4$ and ^{15}N-enriched BDC-NH_2 in DMF was reported to produce $Zr_6O_4(OH)_4$(BDC-NH_2)$_4$(BDC-$NH_3^+Cl^-$)$_2$, which was composed of a mixture of –NH_2 and –$NH_3^+Cl^-$ salt functionalities in 2:1 ratio as opposed to complete –NH_2 [87]. The result was substantiated by ^{15}N NMR spectroscopy measurements. The formation of the BDC-$NH_3^+Cl^-$ salt moiety is rationalized by the reaction of BDC-NH_2 with HCl that is generated *in situ* by the hydrolysis of $ZrCl_4$. PSM of the resultant MOF with acetaldehyde (CH_3CHO) was then observed to lead to the MTV MOF, UiO-66-(BDC-$NH_3^+Cl^-$)(BDC-NH-CH(OH)CH_3)(BDC-N-$(CH_2)_2$) that contained hemiaminal and aziridine functionalities in varying ratios (Fig. 30). The composition was dependent on the PSM temperature and ^{15}N and ^{13}C magic angle spinning (MAS) NMR characterizations verified the results.

The post-synthetic Schiff-base condensation between the –NH_2 groups of UiO-66-NH_2 with aldehydes (*e.g.*, salicylaldehyde, 2-pyridinecarboxaldehyde, 4-pyridinecarboxaldehyde, 6-((diisopropylamino)methyl)-picolinaldehyde, and picolinoyl chloride) resulted in imine-functionalized mixed-linker Zr-**fcu**-MOFs, UiO-66-(BDC-NH_2)(BDC-N = CH-R), with varying ratios of the amino and imine functionalized linkers [293–297]. The possibility to post-synthetically immobilize metal ions, such as Ir, Co, Mo, and Fe, on the sal functionalized MOFs allowed for the exploration of their usefulness as heterogeneous catalysts for various types of chemical reactions. Aguilera-Sigalat *et al.* [298] reported UiO-66-(BDC-NH_2)(BDC-N=N-Indole) MOF by post-synthetic diazotization strategy using $NaNO_2$, HCl and 1-methylindole. The robust nature of the framework enabled a diazotization reaction to be accomplished under harsh conditions. The structural integrity of the framework was affected when the reaction time exceeded 3 h as evidenced by PXRD and N_2 adsorption measurements. The amenability of the UiO-66-NH_2 framework for partial PSM in the assembly of mixed-linker Zr-**fcu**-MOFs has been demonstrated by various other reactions of the –NH_2 functional groups [299,300].

Apart from targeting –NH_2 functional groups, PSM of other substituent groups have been successful using the Zr-**fcu**-MOF platform. This is demonstrated by the single-crystal-to-single-crystal PSM of ethylene functionalized UiO-66 via ozonolysis along with further reactions using the appropriate reagents [301]. In these reactions, the olefin groups of a UiO-66-type MOF were transformed into 1,2,4-trioxolane rings using ozone providing access to MOFs that are otherwise difficult to be prepared using the pre-synthesized linker. The resultant MOF was then further treated either with Me_2S or H_2O_2 to selectively transform the metastable 1,2,4-trioxolane group into aldehyde (CHO) or carboxylic acid (COOH) groups, respectively, leading to mixed-linker UiO-66-(BDC-1,2,4-trioxolane)(BDC-CHO) and UiO-66-(BDC-1,2,4-trioxolane)(BDC-COOH). In a separate work, Barkhordarian *et al.* [99] trans-

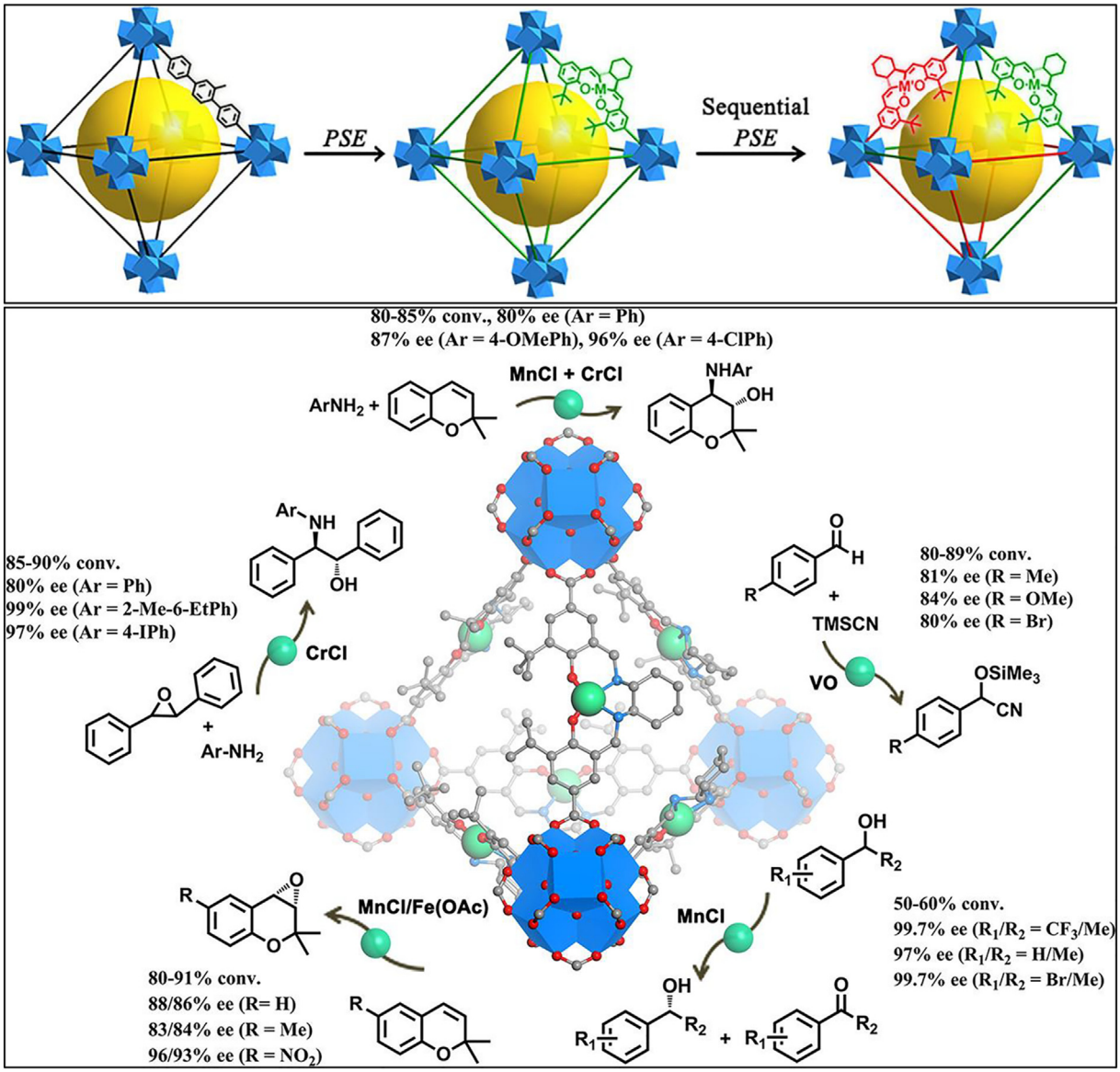

Fig. 28. Schematic representation for the assembly of mixed-linker isostructural UiO-68-[M], and UiO-68-[M]-[M'] MOFs by one or two step post-synthetic linker exchange (Top) and the summarized asymmetric organic transformations catalysed by the synthesized **fcu**-MOFs (Bottom). . Reproduced with permission from [131]

formed two isostructural Zr-PyDC and Zr-PzDC **fcu**-MOFs into the mixed-linker methylated analogues, Zr-(PyDC)(PyDC-MeI) and Zr-(PzDC)(PzDC-MeI), by PSM reaction using methyl iodide to partially methylate the freely available *N*-donor Lewis bases. ^{1}H NMR analyses of the digested methylated MOFs confirmed mixed-linker frameworks with degrees of conversion of 77 and 42% for Zr-PyDC and Zr-PzDC, respectively.

Mixed-linker pore-expanded Zr-**fcu**-MOFs assembled by post-synthetic reactions/metalations of functional groups are also known. The MTV BPV-MOF-Ir and BPV-MOF-$CoCl_2$ MOFs were prepared by post-synthetic metalation of the bipyridyl units in BPV-MOF using either $[Ir(COD)(OMe)]_2$ or $CoCl_2$ in THF, respectively (Fig. 31). Ir-functionalization was reported to afford active and stable single-site solid catalysts for three important organic transformations involving directed C—H activation: tandem hydrosilylation/*ortho*-silylation of aryl ketones/aldehydes, tandem dehydrocoupling/orthosilylation of *N*-methylbenzyl amines, and borylation of aromatic C—H bonds [127].

PSM of functional groups in Zr-**fcu**-MOFs is not limited to single-linker based pre-synthesized MOFs. Various mixed-linker MOFs that were synthesized by either one-pot synthesis or linker exchange processes have also been subjected to further PSM of their functional groups. In 2011, Kim *et al.* [275] prepared mixed-linker Zr-**fcu**-MOFs through independent and orthogonal post-synthetic acylation of the $-NH_2$ functional group and cyanation of the –Br functional groups in pre-synthesized mixed-linker UiO-66-(NH_2)(Br) MOF (Fig. 32). The construction of MTV MOFs was evidenced by ^{1}H NMR spectroscopy analyses.

In an additional example, a one-pot mixed-linker copolymerization of BDC and sodium 2-sulfoterephthalate with $ZrCl_4$ was employed to prepare UiO-66-(BDC)(BDC-SO_3Na) with different amounts of sulfate groups [89,302]. PSM steps were then applied to the mixed-linker MOF to introduce other alkali metal cations (Li(I), K(I), and Rb(I)) leading to MTV UiO-66-(BDC)(BDC-SO_3Na)(BDC-SO_3M). The post-combustion CO_2 capture performances of these materials were superior to pristine UiO-66 in terms of both adsorption capacity and CO_2/N_2 or CO_2/CH_4 selectivity.

The presence of metal-chelating catechol groups on catBDC in the pre-synthesized mixed-linker UiO-66-(BDC)(catBDC) reported by Fei *et al.* [287] enabled the implementation of further PSM to

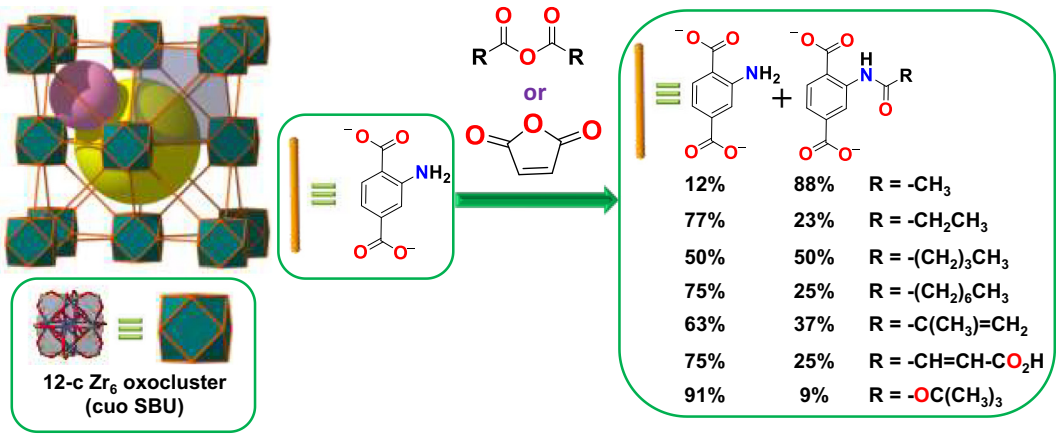

Fig. 29. Schematic showing the construction of mixed-linker UiO-66-(BDC-NH_2)$_x$(BDC-NH-COR)$_{6-x}$ MOFs by post-synthetic covalent modification of UiO-66–NH_2 with various alkyl anhydrides.[90,292].

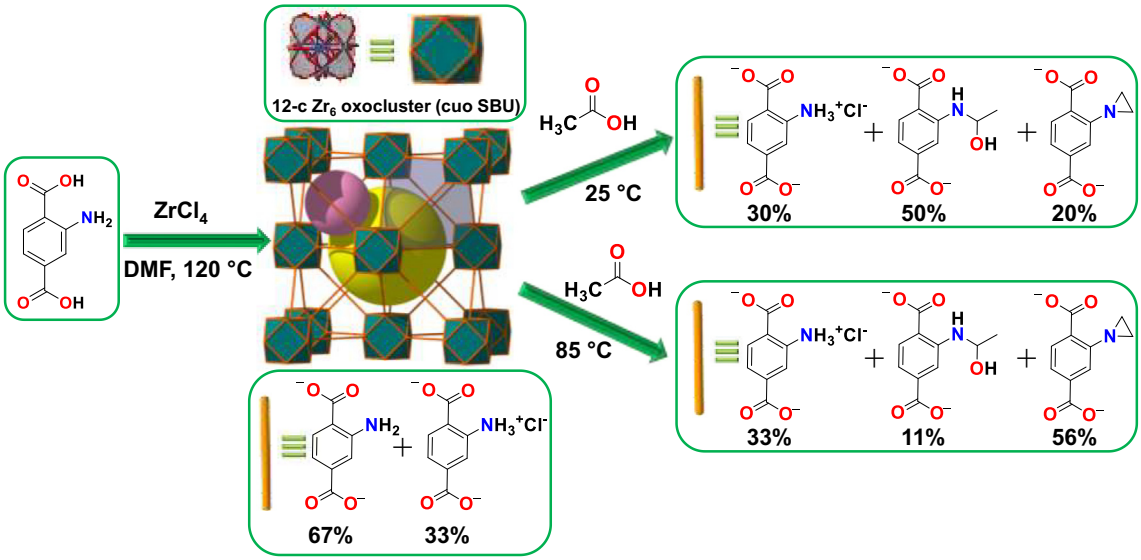

Fig. 30. PSM scheme to transform –NH_2 groups through a reaction with acetaldehyde.

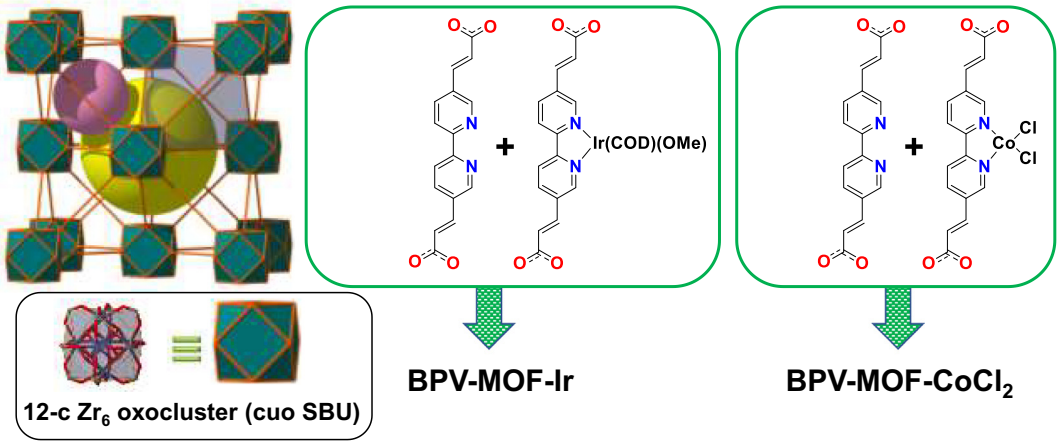

Fig. 31. Representations for the mixed-linker BPV-MOF-Ir, BPV-MOF-$CoCl_2$, mBPV-MOF, and mBPV-MOF-Ir.

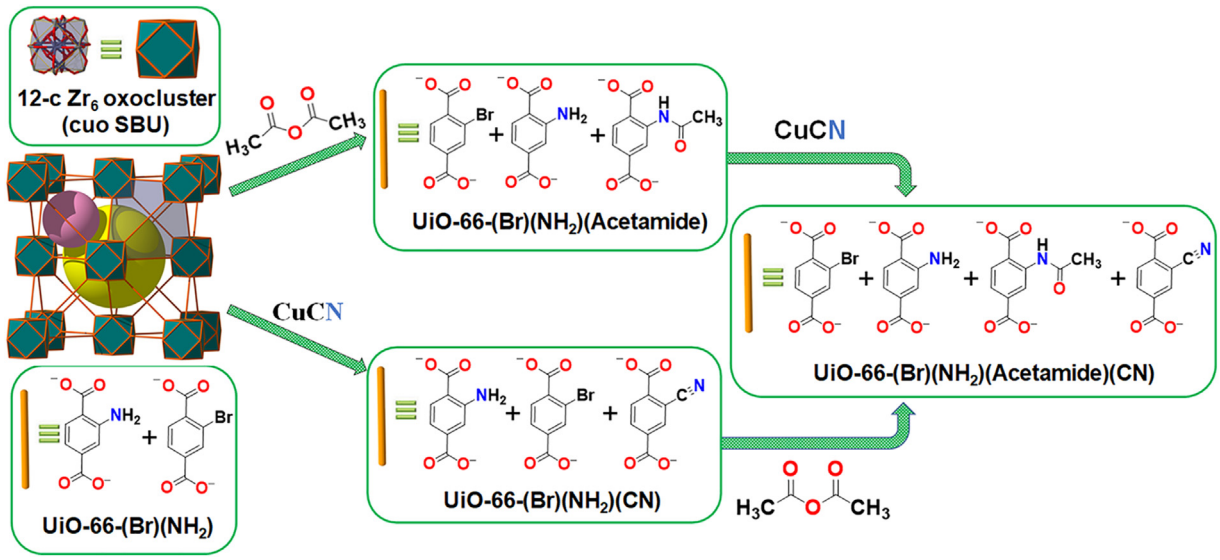

Fig. 32. Schematic showing the sequential construction of mixed-linker MOFs by PSM starting from pre-synthesized UiO-66-(Br)(NH_2).

realize the metalated MTV UiO-66-(BDC)(catBDC)(Fe(III)catBDC) and UiO-66-(BDC)(catBDC)(Cr(III)catBDC) using aqueous solutions of $Fe(ClO_4)_3$ and K_2CrO_4, respectively [287,303]. The introduction of metal ions within the frameworks allowed for these materials as efficient heterogeneous catalysts to oxidize primary and secondary alcohols [287]. In related work, the presence of a soft metal binding functionality (*i.e.*, thiocatecholate) in UiO-66-(BDC)(tcatBDC) MOF paved the way to prepare a Pd-metalated MTV MOF, UiO-66-(BDC)(tcatBDC)(PdtcatBDC), by exposing UiO-66-(BDC)(tcatBDC) to $Pd(OAc)_2$ in dichloromethane at 55 °C. The installation of Pd-mono(thiocatecholato) groups permitted the deployment of the MTV MOF as an efficient, heterogeneous, recyclable catalyst for regioselective functionalization of sp^2 C—H bonds to install alkoxy (C–OR) and C–X (X = halogens) substituents [288]. The successful formation was substantiated by different characterizations such as PXRD, BET surface area values, ^{1}H NMR spectroscopy, ESI–MS, ICP–OES, FT–IR, and X-ray absorption near-edge structure (XANES).

PSM was used in mixed linker UiO-67-(BPDC)(BPyDC) MOFs that were synthesized by either a one-pot system or by partial BPDC to BPyDC linker exchange (Fig. 25). According to Fei *et al.* [283], incubation of the mixed-linker Zr-**fcu**-MOF in an acetonitrile solution containing $PdCl_2$ at 65 °C led to nearly quantitative metalation of the N sites of the linker to afford a metalated MTV MOF with immobilized $Pd(BPy)Cl_2$ species. The metalated MOF exhibited heterogeneous and recyclable catalytic activity for the Suzuki-Miyaura cross-coupling reaction. As a further example of PSM on mixed-linker UiO-67 type MOFs, An *et al.* [284] transformed the MTV UiO-67-(BPDC)(BPyDC-R) (R = H or OH) MOFs, denoted mbpy-UiO and mbpyOH-UiO, into the metalated MTV MOFs, mbpyOH-$IrCl_3$-UiO and mbpy-$IrCl_3$-UiO, by post-synthetic metalation of the N donor atoms of BPyDC linkers of the MOFs with $IrCl_3{\cdot}3H_2O$. The metalated MOFs were explored as catalysts for CO_2 hydrogenation and displayed efficient catalytic performance resulting in selective formic acid/formate formation. The presence of two linkers within a framework was critical for immobilizing appropriate concentrations of catalytic Ir complexes without having steric crowding effects. This was further evidenced in the work of Yaghi and co-workers [304] who reported the mixed-linker UiO-67-(BPDC)(BPyDC-Re(I)$(CO)_3$) that possessed spatially localized Re groups covalently attached to the BPyDC N atoms. The possibility for introducing an optimal number of photoactive Re complexes per unit cell while simultaneously balancing the proximity between the photoactive centers afforded enhanced plasmon-enhanced photocatalytic CO_2-to-CO conversion under visible light. The production of MTV **fcu**-MOFs by PSM of pre-synthesized biphenyl and bipyridyl containing mixed-linker MOFs was also demonstrated by the longer mBPV-MOF-Ir (Fig. 33) [127,272]. The MTV mBPV-MOF-Ir was prepared by post-synthetic metalation of the bipyridyl units of the pre-synthesized mBPV-MOF (Fig. 25) using $[Ir(COD)(OMe)]_2$. Due to increased pore space to facilitate the diffusion of reactants, the mBPV-MOF-Ir had superior catalytic activity than BPV-MOF-Ir, which had no BPDC linker (Fig. 31) [127].

Post-synthetic metalation with either $CoCl_2$ or iridium complex of mixed-linker UiO-69 at the chelating N donors of bipyridyl- and phenanthryl- resulted in the isoreticular MTV MOFs, denoted mBPP-MOF-$CoCl_2$, mPT-MOF-$CoCl_2$, and mPT-MOF-Ir (Fig. 33) [127,272]. The mixed-linker strategy allowed for the transformation of catalytically inactive TPHN-MOF into useful catalysts deployed for different organic transformations. The Ir-functionalized MOFs were active, robust, and reusable solid catalysts in organic reactions, such as C—H borylation of arenes, tandem hydrosilylation of aryl ketones and aldehydes followed by *ortho*-silylation of benzyl silyl ethers. Similarly, mPT-MOF-Ir was reported to have enhanced catalytic activities as compared to the isoreticular BPV-MOF-Ir [127]. The presence of the TPHN linker offered more open space to facilitate both substrate and product diffusion. The Co-bipyridine and Co-phenanthroline based mixed-linker UiO-69 were ultimately proven as robust, active, and reusable catalysts for alkene hydrogenation and hydroboration, aldehyde/ketone hydroboration, and arene C—H borylation [272].

Preparation of mixed-linker MOFs by PSM was extended to the family of PIZOFs. This was illustrated by reactions of 1,3-dipolar cycloaddition between the ethyne moieties of PIZOF-(OMe, $OCH_2C{\equiv}CH$) and 4-methylbenzylazide and the reactions of furan moieties of PIZOF(OMe,$O(CH_2)_3$furan) with maleimide, *N*-methylmaleimide, and *N*-phenylmaleimide transforming the ethyne and furan functional groups into the corresponding Diels-Alder adducts (Fig. 34) [305]. ^{1}H NMR analysis of the digested samples showed the presence of modified linkers along with small

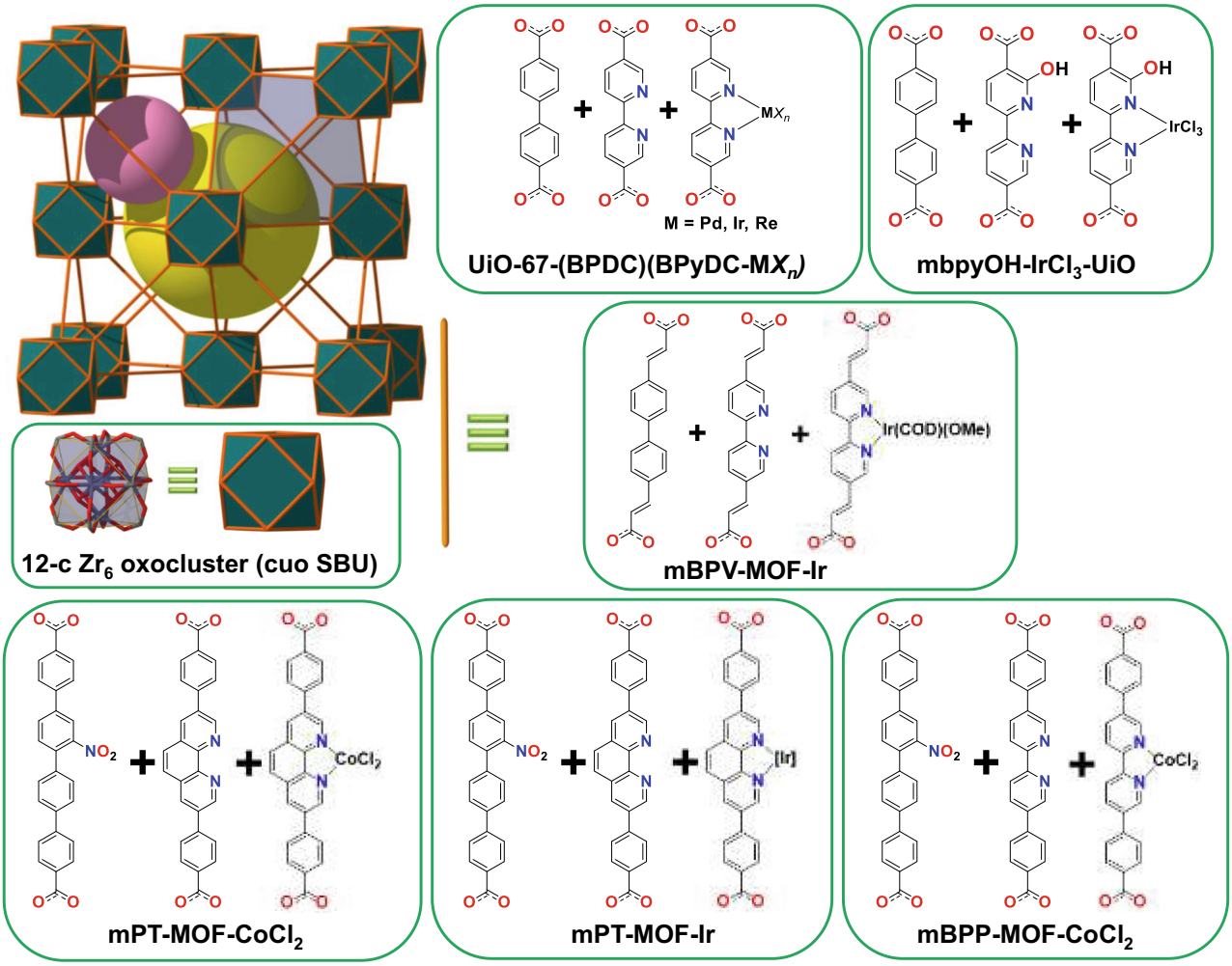

Fig. 33. Isoreticular pore-expanded MTV MOFs obtained by post-synthetic metalation of pre-synthesized biphenyl and bipyridine containing mixed-linker MOFs.

amounts of the unmodified linkers, confirming the assembly of mixed-linker PIZOFs.

In general, the mixed-linker strategy permits the fine-tuning of Zr-**fcu**-MOFs creating opportunities to deploy them in different applications. The examples discussed so far demonstrate the versatility of this MOF platform for fine-tuning their properties. Further imagination in terms of the number of linkers that can be introduced and the type of applications for the MTV MOFs to be prepared are possible, yet thus far unrealized. Even though there have been a considerable number of achievements in the synthesis of mixed-linker Zr-**fcu**-MOFs from two linkers of equal length, MOFs synthesized from two linkers of differing length rarely exist in the published literature. However, a closer look at the 3D arrangement of the MBBs in **fcu**-MOFs show possibilities for introducing multiple linkers of varying size within the structure (Fig. 35). In general, a Zr-**fcu**-MOF can be considered as 2D layers that resemble a **hxl** net with linkers that serve as pillars between each layer – 3 linkers from the top and 3 linkers from the bottom. This structural feature provides an opportunity to design mixed-linker Zr-**fcu**-MOFs using the supermolecular building layer (SBL) strategy, in which either an one-pot synthesis or post-synthetic linker exchange with linkers of shorter/longer length can be employed. Recently, the SBL concept was proven successful in a one-pot solvothermal synthesis of a Zr-**fcu**-MOF, $Zr_6O_4(OH)_4$-$(BDC)_3(fum)_3$, which possesses close-packed hexagonal layers of fumarate-connected clusters that are pillared by BDC linkers [306]. The well-defined arrangement of the linkers preserves the octahedral and tetrahedral pores of the Zr-**fcu**-MOF family, albeit with slight distortion, while generating two distinct triangular window apertures defined by the two different linkers. Alternatively, sequential post-synthetic linker installation on pre-assembled metal oxocluster based 8-c **bcu**- or 10-c **bct**-MOFs was viewed as a viable route in the synthesis of mixed-linker **fcu**-MOFs that possess two or more linear linkers of varying length [307].

2.7.3. Mixed-metal $Zr_{6-x}M_x$ or Zr_6M_x oxocluster-based fcu-MOFs

In addition to the organic linker, there is an extraordinary degree of variability associated with the inorganic MBB of UiO-6*x* structures. The ease with which these inorganic MBBs can be modified has allowed for the proliferation of Zr-**fcu**-MOF structures containing $Zr_{6-x}M_x$ or Zr_6M_x oxoclusters. The *in situ* generation of MBBs has been mainly achieved by either insertion of extra metal ions on μ_3–O or μ_3–OH groups of the $Zr_6(\mu_3\text{–}O)(\mu_3\text{–}OH)_4(\text{–}COO)_6$ cluster or by partial replacement of Zr(IV) by other metal cations [27]. Introduced metal ions can then induce properties to the MOFs that are not otherwise observed for the pristine, parent MOFs. For example, owing to a large band gap with no overlap (4 eV) and inefficient charge transfer between the BDC linker and Zr_6 node, pristine UiO-66 is not suitable for photocatalysis [274]. Introducing other metal cations to the inorganic MBB (*e.g.*, Ti(IV) that has lower *d* states and lanthanide ions with 4*f* levels) improves linker-to-

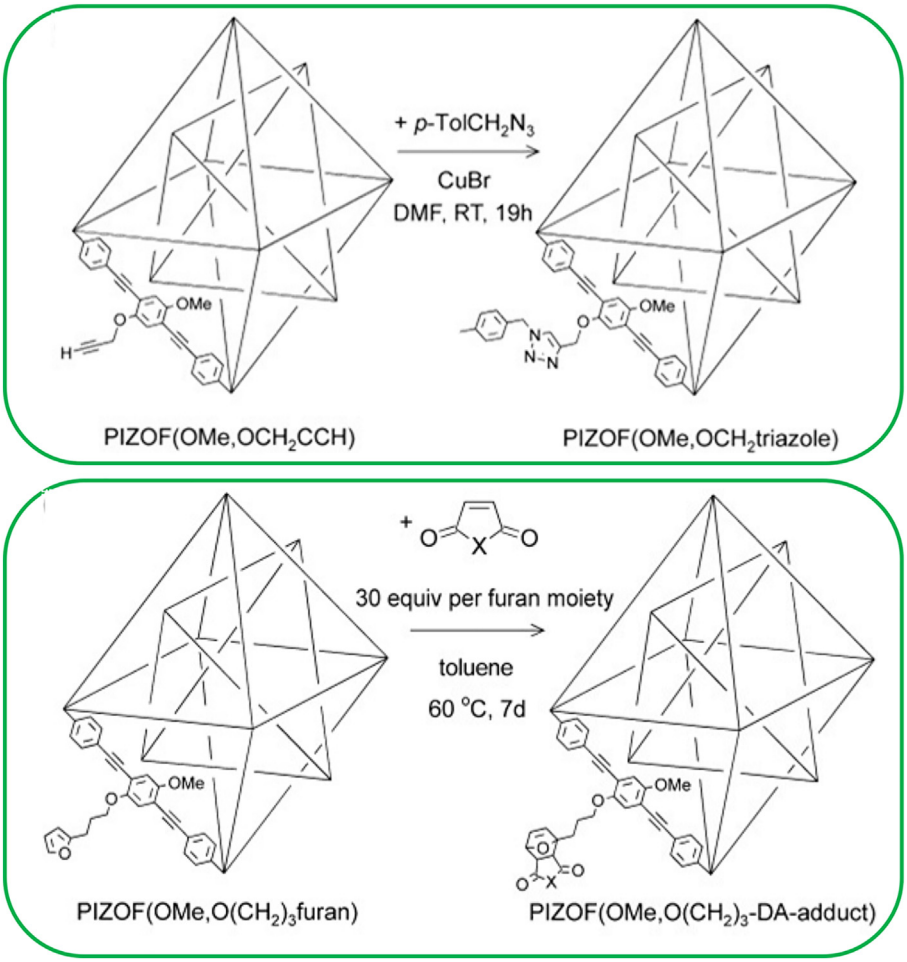

Fig. 34. 1,3-Dipolar cycloaddition reactions on PIZOFs leading to mixed-linker **fcu**-MOFs. Reproduced with permission from ref. [305].

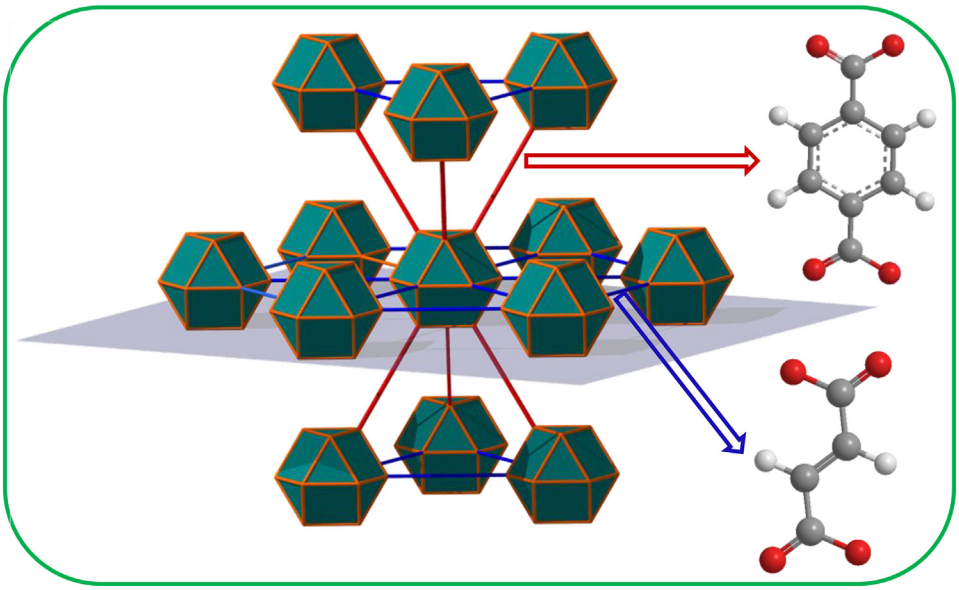

Fig. 35. **fcu**-MOF structure representation as pillared **hxl** layers. The structure shows the possibility to assemble such MOFs using two linear dicarboxylate linkers of different length (represented by blue and red colors) along with the reported examples of linkers that have been used to achieve this structure. (For interpretation of the references to color in this figure legend, the reader is referred to the web version of this article.)

metal-charge-transfer and, therefore, the photocatalytic activity, by modifying the HOCO-LUCO states (HOCO: highest occupied crystal orbital, LUCO: lowest unoccupied crystalline orbital). Another example that illustrates the importance of the mixed-metal approach is the synthesis of ion conductive UiO-6*x* MOFs by modifying the inorganic MBB with an alkoxide base (*e.g.*, lithium *tert*-butoxide) [308]. In this section, the progress made towards realizing such Zr-**fcu**-MOFs will be assessed with implications of their importance to the field of MOF chemistry being highlighted. We do note the following distinction that must be clarified: incorporation of metal ions within Zr-**fcu**-MOFs either by one-pot synthesis or by PSM can occur through either the linker functional groups or on the inorganic MBB. Since the former is treated as a mixed-linker MOF containing both unfunctionalized and metal-functionalized linkers, we will only focus on the latter case in the following section. Furthermore, the introduction of metal ions within the inorganic MBB can also be achieved either by partial substitution of the Zr(IV) ions leading to MOFs that contain $Zr_{6-x}M_x$ in their clusters or by grafting additional metal ions by exploiting linker vacancies that produce MOFs possessing Zr_6M_x clusters. Mixed-metal **fcu**-MOFs of both types will be highlighted in this section.

One-pot synthesis of mixed-metal Zr-**fcu**-MOFs was demonstrated by the cerium-doped UiO-66 and UiO-67 MOFs formed solvothermally by reacting $ZrCl_4$, $CeCl_3$ with H_2BDC or H_2BPDC, respectively [309]. As confirmed by multiple analytical techniques such as EDX mapping, FT–IR spectroscopy, PXRD and N_2 adsorption, the generated MOFs were comprised of both Zr and Ce ions with the Ce composition reaching 13.3 and 7.1% in Ce-UiO-66 and Ce-UiO-67, respectively. Cerium is known for its variable oxidation states, with Ce(III) and C(IV) being the most common. With potential to realize redox-active materials, the partial substitution of Zr by Ce yielded enhanced catalytic activities in various oxidation reactions when compared to the pristine, parent Zr-**fcu**-MOFs.

Due to its versatile electronic properties, selective adsorption, and photocatalytic characteristics, the incorporation of Ti(IV) ions with in Zr-**fcu**-MOFs has been widely pursued. Consequently, several reports have demonstrated the synthesis of mixed-metal Zr/Ti ion-based **fcu**-MOFs and their usefulness for different applications [276,310–317]. One of the seminal works in this regard was reported by Kim *et al.* [310] who prepared Ti(IV)-incorporated UiO-66(Zr/Ti) by solid-solution PSE of Zr in pre-synthesized UiO-66 using DMF solutions of the Ti(IV) salts, $TiCp_2Cl_2$, $TiCl_4(THF)_2$, or $TiBr_4$ (Cp = η^5–cyclopentadienyl, THF = tetrahydrofuran). Positive-ion ATOFMS, ICP–MS, and PXRD techniques were used to characterize the UiO-66 framework post-Ti(IV) incorporation. The change in color of the MOF particles from colorless to pale yellow and the obtained BET surface area of ~1200 m^2/g were used to support arguments that Ti(IV) was incorporated into the inorganic MBBs without these ions or their corresponding metal oxide nanoparticles blocking the pores. The same solid-solution PSE strategy was used by the researchers to prepare Hf(IV) incorporated UiO-66(Zr/Hf), with up to ~20% Hf(IV) at elevated temperatures.

Lau *et al.* [311] reported the enhancement in gravimetric CO_2 uptake by UiO-66 when Zr(IV) was post-synthetically partially replaced with Ti(IV). MOFs with different Ti(IV) loading levels were obtained by exposing UiO-66(Zr) to a DMF solution of $TiCl_4(THF)_2$ at 368 K for incubation periods of 1, 5, and 15 days. The realized MTV UiO-66 MOF, which contains ~50% Ti loading, was found to exhibit almost twice the CO_2 adsorption capacity of the pristine, parent UiO-66(Zr) MOF (2.3 *vs* 4.0 mmol/g CO_2 uptake at room temperature and 1 bar) with higher heats of adsorption that increase with an increase in the Ti content. It was proposed that a better confinement of CO_2 molecules within the resulting smaller pore of the MTV UiO-66(Zr/Ti) MOFs (due to the shorter Ti–O compared to Zr–O bonds) and the lower framework density of MTV UiO-66(Zr/Ti) were the primary contributors toward the enhanced CO_2 uptake properties. The impact of loading lighter Ti(IV) ions on the surface areas and pore volumes, with concomitant shrinkage of the octahedral cages by ~1 Å because of the shorter Ti–O bonds, was evidenced in the N_2 adsorption measurements at 77 K with the corresponding pore size distributions deduced from these N_2 isotherms [311].

Apart from the enhancement in CO_2 capture performance, Ti-functionalized UiO-66 has also been evaluated for their catalytic activity and selectivity in the oxidation of cyclohexene to different oxidation products [313]. There have been several different Ti(IV)-based UiO-66 MOFs investigated: (i) Ti(IV) supported as part of the node in place of Zr(IV) forming $Zr_{6-x}Ti_x$ node (UiO-66-Tiex); (ii) Ti(IV) attached to the node to μ_3-O forming Zr_6Ti_x node (Ti-UiO-66); and (iii) Ti(IV) bound to a catecholate organic linker (mixed linker UiO-66-(cat)(cat-Ti)). Among these, Ti-UiO-66 exhibited the highest catalytic turnover numbers indicating the importance of active site location in the design of MOF-based catalysts.

The possibility to assemble MTV Zr/Ti-**fcu**-MOFs has opened many opportunities in photocatalytic CO_2 capture and conversion to value-added chemicals. A prime example is illustrated in the work of Sun *et al.* [312] who reported the enhanced photocatalytic performance of Ti-substituted NH_2-UiO-66(Zr/Ti) for both CO_2 reduction to formate and H_2 evolution under visible light. The electron accepting potential of the inorganic MBB was enhanced by incorporating Ti(IV) ions, facilitating the transfer of those electrons generated via light absorption by the organic linkers. The partial substitution of Zr(IV) with Ti(IV) was then hypothesized to enhance the electron transfer from the excited BDC-NH_2 linker to either Zr(IV) or Ti(IV), with higher probability of electron transfer to Ti(IV). This then led an excited $(Ti(III)/Zr(IV))_6O_4(OH)_4$ system formation, thereby enhancing the photocatalytic reduction of CO_2 to formate (Fig. 36).

Lee *et al.* [276] prepared mixed-linker Zr-**fcu**-MOF that possessed 86% BDC-NH_2 and 14% 2,5-BDC-$(NH_2)_2$. PSE on the mixed-linker MOF using a DMF solution of $TiCl_4(THF)_2$ resulted in the mixed-linker, mixed-metal UiO-66-derivative, $Zr_{4.3}Ti_{1.7}O_4(OH)_4(C_8H_7O_4N)_{5.17}(C_8H_8O_4N_2)_{0.83}$. This synthesized MTV MOF displayed enhanced photocatalytic activity for reduction of CO_2 to formic acid under visible light irradiation with high durability and turnover number. In addition to the improved electron accepting potential of the Ti-containing inorganic MBB, the introduction of small amounts of the co-linker, 2,5-diaminobenzene-1,4-dicarboxylic acid, was hypothesized to play a critical role in providing new energy levels in the band structure of the MOF, thereby introducing broader light absorption coverage for the MOF [276]. Though UiO-66(Ti/Zr) MOFs have attracted intense research interest in photocatalytic applications [315,317], the type of Ti(IV) binding in most of the reported MOFs has not been obvious or experimentally determined. As previously mentioned, there is a possibility for Ti to be incorporated in the MBBs through either appendage of Ti to a linker vacancy or replacement of Zr.

Manna *et al.* [318] were able to synthesize UiO-6*x* MOFs containing Zr_6Co_4 and Zr_6Fe_4 oxoclusters by metalation of the inorganic MBBs with cobalt and iron salts. In the reported procedure, deprotonation of $Zr_3(\mu_3\text{–}OH)$ sites in MBBs of pre-synthesized UiO-66(Zr), UiO-67(Zr), and UiO-68(Zr) with *n*-BuLi was first carried out and followed by reaction with $CoCl_2$ or $FeBr_2{\cdot}2THF$ in THF. This afforded the Co– or Fe-functionalized mixed-metal MOFs (termed, UiO-CoCl and UiO-FeBr, respectively). A combination of SXRD, X-ray absorption, ICP–MS, and FT–IR spectroscopic characterization showed the disappearance of all μ_3–OH groups and provided evidenced for the existence of 4 Fe or Co cations per Zr_6 node that corresponded to the metalation of all μ_3–OH sites in the inorganic MBBs (Fig. 37). The obtained mixed-metal MOFs were demonstrated to be active and recyclable single-site solid catalysts

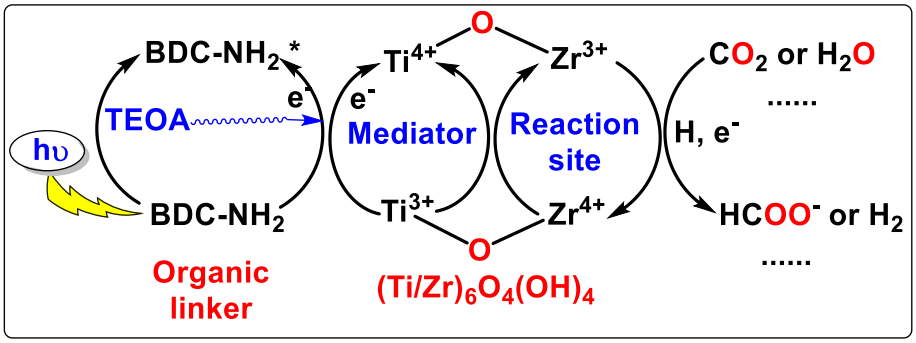

Fig. 36. Proposed mechanism for the photocatalytic reactions over NH_2-UiO-66(Zr/Ti).[312].

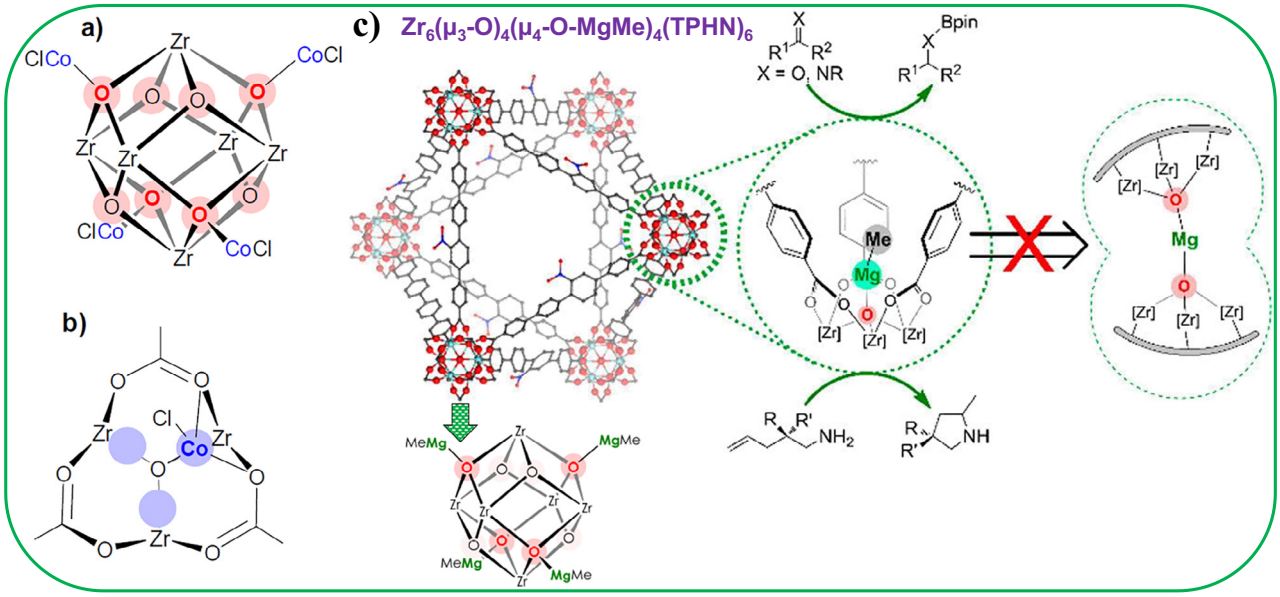

Fig. 37. (a) Random site distribution of 4 CoCl on 8 equivalent μ_3–O; (b) Random orientation of 1 CoCl toward 3 equivalent directions and (c) Crystal structure representation of TPHN-MOF-MgMe and its role as catalyst for organic transformations. Reproduced with permission from references [139,318].

for various organic reactions, including chemoselective borylation, silylation and amination of benzylic C—H bonds, as well as hydrogenation and hydroboration of alkenes and ketones. The preparation of a Zr-**fcu**-MOF containing a Zr_6M_4 oxocluster via deprotonation of $Zr_3(\mu_3$–OH) sites was also demonstrated by the isoreticular UiO-69-NO_2 MOF, termed TPHN-MOF-MgMe [139]. The Mg-functionalized mixed-metal MOF (Fig. 37), $Zr_6(\mu_3$–O$)_4(\mu_4$–O–MgMe$)_4$(TPHN$)_6$, was prepared by post-synthetic metalation of $Zr_3(\mu_3$–OH) sites of the TPHN-MOF using Me_2Mg in THF at room temperature. The occurrence of metalation exclusively at all 4 μ_3–OH sites of $Zr_6(\mu_3$–O$)_4(\mu_3$–OH$)_4$(TPHN$)_6$, but with random distribution of 4-MgMe on 8 crystallographically equivalent μ_3–O and μ_3–OH positions was verified by a detailed XRD study. Furthermore, gas chromatography (GC) analysis showed the generation of equivalent amounts of methane and FT–IR spectroscopy provided evidence for the disappearance of the $\nu_{\mu3\text{–OH}}$ band (~3629 cm^{-1}). The result was further substantiated by ICP–MS analysis of the digested MOF-MgMe, which gave 4 Mg centers per Zr_6 node. The incorporation of –MgMe led to the MOF being used as an active and recyclable single-site solid catalyst for hydroboration of carbonyls and imines and for hydroamination of aminopentene.

In general, both mixed-linker and mixed-metal strategies are effective in modulating the physical–chemical properties of Zr-**fcu**-MOFs without affecting the overall structures. The mixed-metal (Zr/M) **fcu**-MOFs have opened new paths to realize applications that require other metal cations as inorganic MBBs. Even though the underlying **fcu** topology remains intact in MTV MOFs, the random distribution of linkers and metal ions typically pose synthetic and characterization challenges, retarding their development and large-scale practical deployment. The solid solution hypothesis in MTV MOFs is usually supported by high resolution PXRD measurements and DFT calculations [282]. Therefore, the advancement of synthetic strategies that lead to homogeneously distributed components in MTV **fcu**-MOFs are an ideal target. Taken together, Zr-**fcu**-MOFs have already demonstrated a high degree of versatility in terms of both structure and applications. The versatility of these MOFs is reflected in many aspects including the ease with which a researcher can modify the structures through linker design with appropriate length and functional groups and the possibility to incorporate substituent groups that facilitate encapsulation of metals and/or metal clusters. The possibility to engineer defects provides additional alternative pathways

to tune the electronic/proton conductivity, adsorption, catalytic, hydrophobicity properties of the Zr-**fcu**-MOF platform [319–327].

3. Non-zirconium oxocluster-based fcu-MOFs

One effective strategy employed to modulate the physical–chemical properties without altering the overall structure is to develop synthetic protocols that produce M–**fcu**–MOFs using different metal salt precursors other than Zr salts. Although rare, the practice of reticular chemistry has produced M–**fcu**–MOFs from metal clusters constructed from divalent, trivalent and tetravalent metals. Specifically, the synthesis of M–**fcu**–MOFs synthesized from rare earth and actinide hexanuclear clusters are prominent examples [328,329]. In these cases, the judicious choice of metal salts as precursors and the employment of suitable reaction routes allows for the construction of M–**fcu**–MOFs from non-hexanuclear MBBs, octanuclear hydroxocluster of M(II) transition metals [330] and *in situ* generated metal–organic polyhedral (MOP) building units, all of which manifest in the form of cuboctahedron SBUs that are required to create the **fcu** topology. Brief accounts of these topics will be presented in following section of the review.

3.1. Transition metal cluster-based fcu-MOFs

3.1.1. Group IV (Ti and Hf) hexanuclear and non-hexanuclear oxocluster-based fcu-MOFs

As a result of their similarity with Zr(IV) in terms of physical and chemical properties, other Group IV metal cations (Ti(IV) and Hf(IV)) are expected to form MOFs isostructural to Zr-**fcu**-MOFs. However, Ti-based MOFs are known by their non-hexanuclear (M_x, $x \neq 6$) oxocluster MBBs due to differences in coordination number and M–O bond strength of Ti(IV) and Zr(IV). Though the strong M–O bond contributes to the stability of the resulting framework, it also poses some synthetic and characterization challenges. One main challenge is the difficulty to form large, high-quality crystals due to fast linker association and lower metal-linker lability. Polycrystalline products tend to form due to the fast crystal growth and the presence of many nucleation sites, which, consequentially, prevents appropriate characterization by SXRD. This is especially true for Ti-based MOFs as the very strong Ti–O bonds and lack of sufficient linker association/dissociation equilibria prevents the assembly of highly crystalline Ti oxocluster-based MOFs. Thus far, there are no reports of a **fcu**-MOF constructed from a Ti_6 oxocluster MBB that is equivalent to the MBB observed for Zr (IV). Most of the MBBs generated from Ti precursors are characterized by randomly formed oxoclusters with different symmetry and connectivity [331]. Although constructed from a different MBB, the only example of Ti-MOF family that can be deconstructed to a 12-c **fcu** net is MIL-125 (Fig. 38). The structure of MIL-125 is constructed from cubic close packing of *in situ* generated Ti_8O_8 rings that are connected through 12 BDC or BDC-X linkers to produce the $Ti_8(\mu_2\text{–}O)_8(\mu_2\text{–}OH)_4(\text{–}CO_2)_{12}$ structure. As expected, the structure is endowed with two types of cages, a distorted octahedra and another of tetrahedral shape, making the structure very similar to that found for the Zr-**fcu**-MOFs.

MIL-125-X has high stability and permanent porosity with interesting adsorption and catalytic properties, all of which make the framework a suitable candidate for applications ranging from removal of toxic chemicals and gas/liquid separations to water splitting, CO_2 reduction, simultaneous removal of CO_2 and H_2S from biogas and natural gas, photocatalytic reduction of CO_2, and as potential carriers for drugs including aspirin, chloroquine, ibuprofen, and diclofenac sodium [332–343]. In particular, MIL-125-X is a viable photocatalyst due to the photochromic behavior that originates from the generation of T(III)/Ti(IV) states in the Ti_8O_8 rings upon UV irradiation. To overcome the large band gap issue that limits the photocatalytic activity of MIL-125, several isoreticular analogues were synthesized by employing functionalized BDC-X linkers (X = OH, CH_3, Cl, NH_2, –NHMethyl, –NHEthyl, –NH-*i*-Propyl, –NH-*n*-Butyl, –NHCyclopentyl, –NHCyclohexyl, –NH-*n*-heptyl). As was the case with UiO-66, the BDC-NH_2 linker is the most studied linker for the MIL-125 system due to its ability to raise the valence-band edge by donating its N 2*p* electrons to the aromatic ring [115,333–335,339,344–346]. In MIL-125-NH_2, the $Ti_8(\mu_2\text{–}O)_8(\mu_2\text{–}OH)_4$ MBB is useful in loading multiple Cu(I) centers via deprotonation and ion exchange of the μ_2–OH groups, thereby transforming the MOF into a tandem catalyst for CO_2 to ethylene (C_2H_4) [347]. The Cu(I) centers were catalytic centers for CO_2 to ethanol (C_2H_5OH) hydrogenation with the $Ti_2\text{–}\mu_2\text{–}O^-M^+$ (M = H, Li) unit serving to further transform C_2H_5OH to C_2H_4 by dehydration.

In contrast to Ti(IV), Hf(IV) is known to exhibit nearly identical chemical properties to those observed for Zr(IV). In addition to the

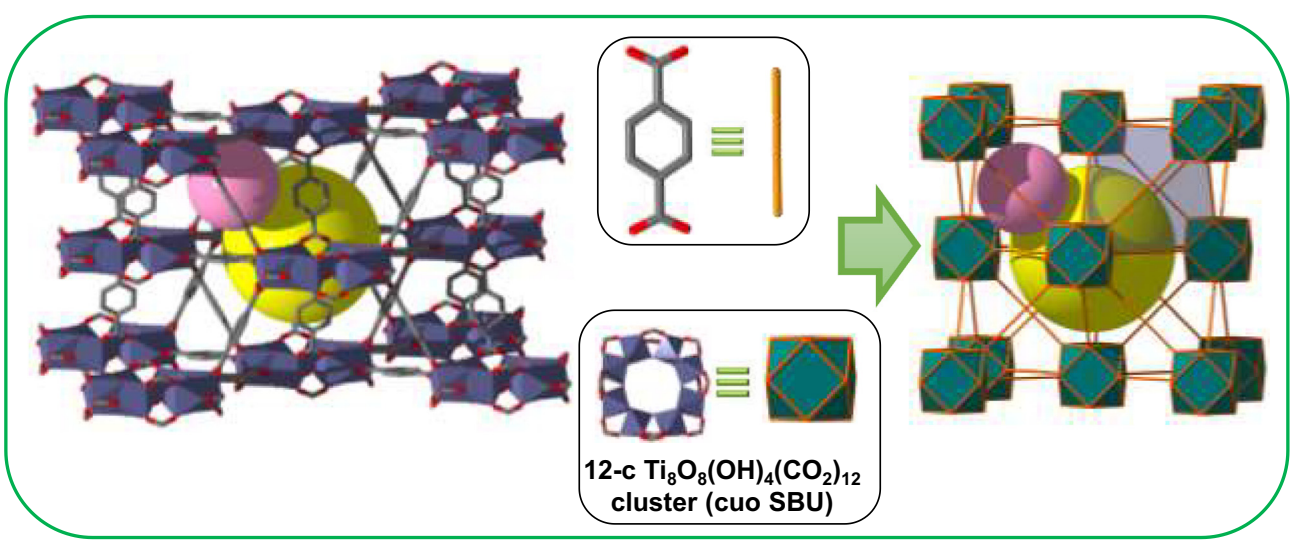

Fig. 38. The crystal structure of MIL-125 based on *in situ* generated $Ti_8O_8(OH)_4(\text{–}CO_2)_{12}$ MBBs and the underlying **fcu** topology representations for the MOF.

similarity in their d^0 electronic configuration, both Hf(IV) and Zr (IV) have similar ionic radii (0.85–0.86 Å), and are larger than Ti (IV) (0.75 Å). The lanthanide contraction effect is the reason for this despite Hf(IV) being in a lower period than Zr(IV). These similarities in the physicochemical properties of the two metal ions are reflected in their reactivity towards organic linkers and the metal-carboxylate bond strengths that arise as a result. The synthesis of numerous non-interpenetrated as well as interpenetrated UiO-6*x*(Hf) structures have been reported from *in situ* generated Hf_6 oxoclusters and linear dicarboxylate organic linkers of various lengths and functionalities [28,249,348–352]. Apart from the increased weight in addition to lower porosity values (*i.e.*, surface areas and pore volumes), **fcu**-MOFs produced from *in situ* generated Zr_6 and Hf_6 oxoclusters are usually indistinguishable in their chemical and physical properties. In most cases, the synthetic conditions (both solvothermal and non-solvothermal routes) employed to synthesize Zr-**fcu**-MOFs can be emulated to generate the Hf analogues [46,59,64]. Due to the tailorability of the MBBs to form isostructural MOFs for almost all Zr analogues, there will be no comprehensive review of Hf-**fcu**-MOFs made in this article. We will only shed light on the differences between the properties of the two MBBs and their corresponding impact on the applications that could be envisaged. For example, the difference in oxophilicity between the two metal cations was reported to have an impact on the Brønsted acidity and on the catalytic activities of the respective MOFs. The acidity advantage of Hf- and Ce-based **fcu**-MOFs over the Zr analogues was concluded in the work of Bakuru *et al.* [28] who reported enhanced catalytic activity of UiO-66(Hf or Ce) for solketal synthesis from glycerol acetalization with 90 times higher turnover frequency than that of the isostructural UiO-66(Zr). They concluded that the catalytic activity was correlated with the varying degree of acidity in their SBUs (acidity order: UiO-66(Hf) > UiO-66(Ce) > UiO-66(Zr)). Recently, UiO-66-X (Hf) (X = H or NH_2) MOFs were also demonstrated to be superior to UiO-66(Zr) in their catalytic efficiency for oxidative denitrification reactions [353].

3.1.2. Divalent transition metal-based fcu-MOFs

The M−**fcu**−MOF series has been reported for various divalent, trivalent and tetravalent transition metal (TM) ions. The TM-**fcu**-MOFs are constructed from 12-c non-hexanuclear oxoclusters or metal–organic polyhedra (MOP) that adopt cuboctahedron-shaped SBUs. Herein, we provide a brief discussion on the chemistry of divalent TM-based **fcu**-MOFs.

3.1.2.1. Non-hexanuclear transition metal oxocluster-based fcu-MOFs. Due to differences between the Group IV metal ions in terms of coordination geometry and oxidation state, other TMs do not form the M_6 oxocluster MBB of **fcu**-MOFs. However, there is a possibility to generate other oxoclusters from divalent TM ions such as Co(II) and Ni(II) whose connectivity of 12 mimics the 12-c cuboctahedron SBU. This was demonstrated a decade ago by the isoreticular Ni-based **fcu**-MOFs, $[Ni_8(OH)_4(OH_2)_2(PBP)_6]\cdot x$solv and $[Ni_8(OH)_4(OH_2)_2(TET)_6]\cdot x$Solv, that were synthesized from the *in situ* generated octanuclear Ni(II) hydroxocluster, $[Ni_8(\mu_4\text{–}OH)_4(\mu_4\text{–}OH_2)_2]^{12+}$, and one of the bis-pyrazolyl linkers, 4,4′-bis(1*H*-pyrazol-4-yl)biphenyl (H_2PBP) or 2,6-bis(1*H*-pyrazol-4-yl)pyrrolo[3,4-*f*]isoindole-1,3,5,7(2*H*,6*H*)-tetrone (H_2TET) (Fig. 39) [354]. From a topological point of view, the structures can be distilled down to a **fcu**-a net since the octametallic node forms highly symmetrical 12-c cuboctahedron SBUs. Unlike the Zr-based hexanuclear oxocluster, the Ni hydroxocluster is octanuclear and each Ni(II) is octahedrally coordinated. The formation of pure phases, the coordination environment surrounding Ni(II), the absence of the Ni(III) ion and other structural details of the synthesized MOFs were confirmed by XRD, UV–Vis, FT–IR, XANES, and EXAFS [354]. Later on, Navaro and co-workers [355] reported contracted isoreticular analogues in their preparation of a series of $[Ni_8(\mu_4\text{–}OH)_4(\mu_4\text{–}OH_2)_2(BDP\text{–}X)_6]$ using the shorter linker, 1,4-bis(pyrazol-4-yl)benzene (H_2BDP) and its functionalized derivatives, H_2BDP-X with X = H, OH, NH_2.

Co(II) precursors are suitable for *in situ* generation of the octanuclear hydroxocluster MBB with subsequent formation of the corresponding **fcu**-MOFs in the presence of linear linkers [330,356]. One of the earlier examples of a **fcu**-MOF based on Co (II) octanuclear MBBs was reported by Holmberg *et al.* [330] who solvothermally isolated $[Co(II)_8(\mu_4\text{–}OH)_6(CPT)_6][CoCl_4]_2\cdot 2H_2O$, denoted Co-MOF3, from $Co(NO_3)_2\cdot 6H_2O$ and an asymmetric linker, 4-(4′-carboxyphenyl)-1,2,4-triazole (HCPT). The addition of small amounts of concentrated HCl was found to be very important in achieving the required low pH conditions for crystallization. The chloride ions from HCl participated in the formation of $[CoCl_4]^{2-}$ counter ions. The metal core, composed of 8 octahedrally coordinated Co(II) ions at each vertex, 6 μ_4–OH groups at each face, and 12 CPT^- linkers, produced the 12-c cuboctahedron SBU that is a prerequisite for realizing a **fcu**-MOF. The possibility of accessing the **fcu**-MOF via a Co(II) core enabled the preparation of magnetic **fcu**-MOFs that could not otherwise be obtained for the parent UiO-6*x*(Zr) series. Recently, Huang *et al.* [356] reported another Co-**fcu**-MOF, denoted as MAF-48 or **Co_4-bdt**, that is isoreticular to Co-MOF3. The framework, formulated as $[Co_8(\mu_4\text{–}OH)_6(BDT)_4(HBDT)_2]$, was synthesized solvothermally through a reaction of $Co(OAc)_2$ with the bis-triazolyl linker, 1,4-benzenedi(1H-1,2,3-triazole) (H_2BDT). The MOF displayed high catalytic activity in water oxidation reactions. As supported by isotope tracing and simulation experiments, the presence of μ_4–OH groups in the $[Co_8(\mu_4\text{–}OH)_6]$ cluster offered an oxygen vacancy site with near-optimal OH^- adsorption energy.

Inspired by the base resistance of the frameworks, López-Maya *et al.* [355] performed PSM on $[Ni_8(\mu_4\text{–}OH)_4(\mu_4\text{–}OH_2)_2(BDP\text{-}X)_6]$ through cation-exchange reactions using ethanolic solution of KOH. Through this approach, modified $[Ni_8(\mu_4\text{–}OH)_4(\mu_4\text{–}OH_2)_2(BDP\text{-}X)_6]$ MOFs were synthesized with missing-linker defects and extra-framework K^+ ions without disrupting the original **fcu** topology. For the structures with X = H, NH_2, post-synthetic treatment resulted in the incorporation of additional framework K^+ ions producing materials whose formula was $K[Ni_8(OH)_5(EtO)(H_2O)_2(BDP\text{-}X)_{5.5}]$ with X = H or NH_2. The transformation involved partial removal of the organic linkers and deprotonation of coordinated water molecules. The same KOH treatment of $[Ni_8(OH)_4(H_2O)_2(BDP\text{-}OH)_6]$ formed the **fcu**-MOF with a higher percentage of missing linker defects, extra-framework cations and phenolate residues yielding $K_3[Ni_8(OH)_3(EtO)(H_2O)_6(BDP\text{-}O)_5]$. The difference of this structure with the other two isoreticular MOFs was the presence of more acidic phenol groups that could be deprotonated with ease. The introduced missing linker defects provided an opportunity to create a more accessible porosity with enhanced adsorption capacity. When compared to the parent, pristine frameworks, the structures with missing linkers displayed increased post-combustion CO_2 capture properties and adsorption heat capacity. The coordinatively unsaturated metal centers, charge gradients, and phenolate nucleophilic sites established by the post-synthetic treatment were the structural features that led to the superior CO_2-MOF interactions in the KOH treated samples. In later work by the same research group, the post-synthetic KOH treated **fcu**-MOFs led to high hydroxide ion-conductivity [357]. As verified by variable temperature alternating current impedance spectroscopy measurements, the KOH treated materials showed higher conductivity values than their non-defective counterparts, $[Ni_8(\mu_4\text{-}OH)_4(\mu_4\text{-}OH_2)_2(BDP\text{-}X)_6]$ (X = H, OH, NH_2), by up to four orders of magnitude in hydroxide ion mobility. This was ascribed to the

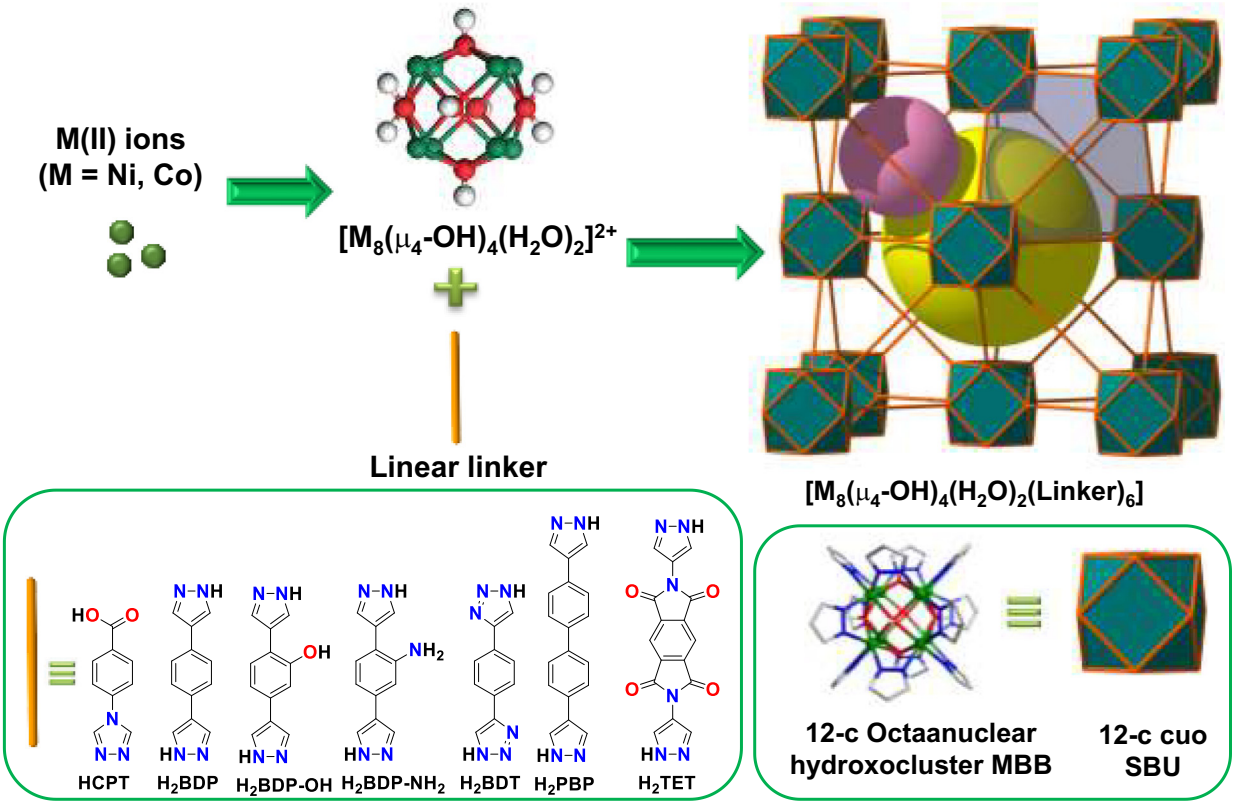

Fig. 39. Schematic for the assembly of the reported octanuclear cluster-based isoreticular **fcu**-MOFs.

evolving higher porosity, framework basicity and hydrophilicity after treatment with KOH.

The presence of extra framework cations in defective **fcu** frameworks permits further ion exchange with aqueous solutions of Ba $(NO_3)_2$ resulting in Ba(II)-exchanged defective structures whose formula are $Ba_{0.5}[Ni_8(OH)_5(EtO)\text{-}(H_2O)_2(BDP\text{-}X)_{5.5}]$, X = H or NH_2 and $Ba_{1.5}[Ni_8(OH)_3(EtO)(H_2O)_6(BDP\text{-}O)_5]$ [212]. Due to enhanced pore accessibility imposed by the missing linker defects, specific interactions with the extra framework Ba(II) ions and exposed –OH functional groups located at the defect sites, the materials showed selective adsorptive properties for SO_2 gas. In a separate work, post-synthetic Cu(II) exchange of the KOH treated sample, $K[Ni_8(OH)_6(BDP\text{-}X)_{5.5}]$, transformed the materials to the Cu(II) exchanged form, $Cu_{0.5}[Ni_5Cu_3(OH)_6(BDP\text{-}X)_{5.5}$ [358]. The ion exchange process involved not only the extra framework cations but also the octanuclear metal MBB. Due to the presence of defects and the milder basicity of the Cu(II)-exchanged forms, the resulting MOFs facilitated the selective direct tandem C—C bond formation process for targeting a pharmaceutical intermediate in a one-pot two-step (*i.e.*, Henry reaction and Michael type addition) synthesis of neuroactive pharmaceutical intermediates from nitromethane and benzaldehyde.

3.1.2.2. fcu-MOFs built from Metal-Organic polyhedra (MOP) building units. The unique structural features of this MOF platform and the possibility for exploring a wide variety of applications has led researchers to push beyond the MBB approach to assemble **fcu**-MOFs. Specifically, researchers developed a supermolecular building block (SBB) approach to construct **fcu**-MOFs by using *in situ* generated metal–organic polyhedra (MOPs) as building units [359,360]. The inspiration for employing MOPs as a building unit came from the discovery of the first copper paddlewheel based cuboctahedron (**cuo**) MOP (MOP-1) formulated as $Cu_{24}(m\text{-}BDC)_{24}(DMF)_{14}(H_2O)_{10}\cdot(H_2O)_{50}(DMF)_6(C_2H_5OH)_6$ or $[(L)(S)Cu_2(1,3\text{-}BDC)_2]_{12}$, L = pyridine, S = methanol (Fig. 40) [361,362]. By taking the apical positions of the 12 paddlewheels as vertices, MOP-1 can be described as a cuboctahedron SBU making it a suitable building unit for the design and construction of **fcu**-MOFs.

The synthesis of the first MOP-based **fcu**-MOF was reported in 2007 [363]. Their strategy exploited the highly symmetrical **cuo** SBU in addition to the ability to functionalize the paddle wheel MBB at the apical positions with ditopic linear linkers that can be coordinated in monodentate fashion from each end. In the first example of a MOP based **fcu**-MOF built from 5-c $Zn_2(-CO_2)_4$ paddlewheel MBBs, formulated as $[Zn_4(mip)_4(dabco)(OH_2)_2]$ (mip = 5-methylisophthalate and dabco = 1,4-diazabicyclo[2.2.2]-octane), dabco served as a linear link to connect the neighboring **cuo** MOPs through the apical positions of the $Zn_2(-CO_2)_4$ paddlewheels (Fig. 40). The versatility of the 12-c MOP for enlargement (using 2,7-naphthalenedicarboxylate in place of mip), decorating the 5-position of the isophthalate unit by different functional groups (*e.g.*, $-CH_3$, –H, $-NH_2$, –OH) and metal substitution (*e.g.*, Co(II), Cu(II)), along with the possibility to expand the cavities of the MOF by using longer linkers (*e.g.*, pyrazine, bipyridine, 1,2-di(pyridin-4-yl)ethene) permitted the assembly of the isoreticular M(II) paddlewheel MOP based **fcu**-MOFs [364–366] (Fig. 40). The inherent porosity of the MOP and the amenability of the MOF platform for isoreticulation afforded promising results for controlled drug release [365] and adsorptive separation of organic dyes [366].

MOPs, as is the case in MOP-1, can also be treated as highly symmetrical **cuo** SBB when the 5-positions of the isophthalate moieties are used as vertices. Therefore, connecting neighboring **cuo** SBBs via the isophthalate moieties is an alternative approach for constructing MOP-based **fcu**-MOFs. The first example of this was realized in 2008 by Cairns *et al.* [367] who reported $[Ni_{12}(3,5\text{-}ATC)_6]$ and $[Co_{12}(BIPA\text{-}TC)_6]$ (3,5-H_4ATC = 3,5-dicarboxyl-(3′,5′-dicarboxylazophenyl)benzene; H_4BIPA-TC = benzoimidephenanthroline tetracarboxylic acid) (Fig. 41), formulated as

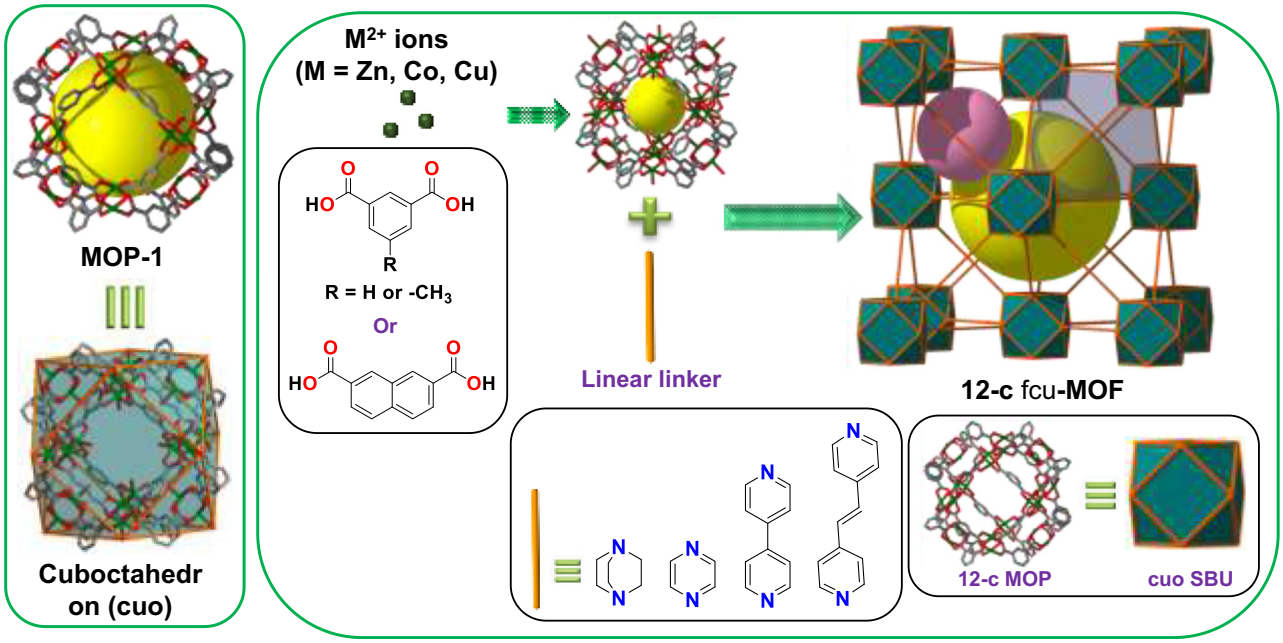

Fig. 40. Crystal structure representation of MOP-1 and its description as a 12-vertex cuboctahedron (Left) and Schematic showing the assembly of the $M_2(-CO_2)_4$ paddlewheel based isoreticular **fcu**-MOFs using different linear linkers with N donors (Right).

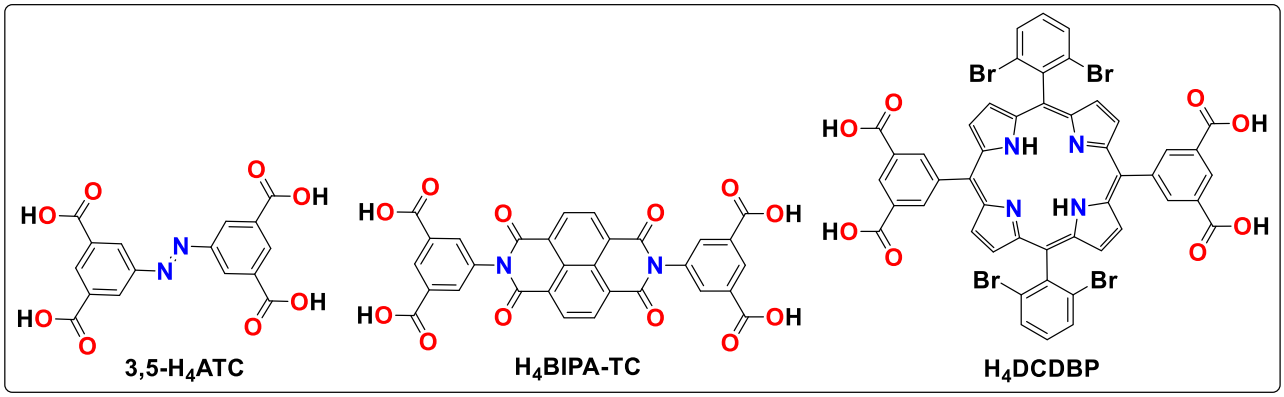

Fig. 41. Tetratopic linkers that serve as linkers in the assembly of **cuo** SBB-based **fcu**-MOFs.

$Ni_2(ABTC)(H_2O)_3$ and $Co_2(BIPA\text{-}TC)(\mu_2\text{–}H_2O)(H_2O)_4$, respectively. Unlike the 5-c paddlewheel found in MOP-1, each Ni cation assumes octahedral geometry with the 4 equatorial positions occupied by 4 monodentate carboxylate-O atoms from the linker and the 2 axial positions are filled by aqua ligands. The isoreticular analogue of the Co-BIPA-TC MOF, MMPF-3 (MMPF denotes metal–metalloporphyrin framework), was also synthesized using the porphyrin linker, 5,15-bis(3,5-dicarboxyphenyl)-10,20-bis(2,6-dibromophenyl)porphyrin (H_4DCDBP) (Fig. 41) [359]. Owing to the presence of catalytically active Co(II) centers within the metalloporphyrin linker, MMPF-3 displayed selectivity and high overall conversion for catalytic epoxidation of *trans*-stilbene. The **fcu** topology of the realized isoreticular MOFs was rationalized by considering the centroids of the isophthalate benzene rings as vertices.

The construction of **fcu**-MOFs via the SBB strategy was extended to a 9H-carbazole-3,6-dicarboxylate (CDC) decorated **cuo** MOP upon using organic linkers functionalized at the bent position of the CDC moieties [368]. By designing a tetracarboxylate CDC-based organic linker with bridging between two CDC units, 9,9′-([1,1′-biphenyl]-4,4′-diyl)bis(9H-carbazole-3,6-dicarboxylate (H_4BBCDC), and employing appropriate solvothermal reactions, the *in situ* generated MOP-based MOF, $Cu_2(BBCDC)$, denoted DUT-49 (DUT = Dresden University of Technology) was isolated. The **fcu**-topology was concluded when considering the carbazole N as the extension points of the MOP and bridging the 12 linkers around each MOP in a linear fashion at their bent positions (Fig. 42). The high specific surface area (5476 m^2/g) and pore volume (2.91 cm^3/g) of the MOF was exploited for methane storage.

These examples generally illustrate the amenability of the **fcu**-MOF platform for design using appropriate pre-selected building units. Besides providing diverse possibilities to assemble MOFs with the favorable **fcu** topology that have interesting porosity attributes, expanding the **fcu**-MOFs across other transition metals provides the opportunity to assemble functional materials from cheaper and lighter metal salt precursors. Accessible catalytic and adsorption sites that cannot be achieved by the Zr_6 oxocluster MBBs can now be custom-built by selecting a suitable transition metal ion. This, in turn, facilitates the deployment of the MOF platform in large-scale industrial settings.

3.2. Rare earth (RE) oxocluster-based fcu-MOFs

Despite the usefulness of RE-based MOFs for various applications such as luminescence, magnetism, and catalysis [369–371],

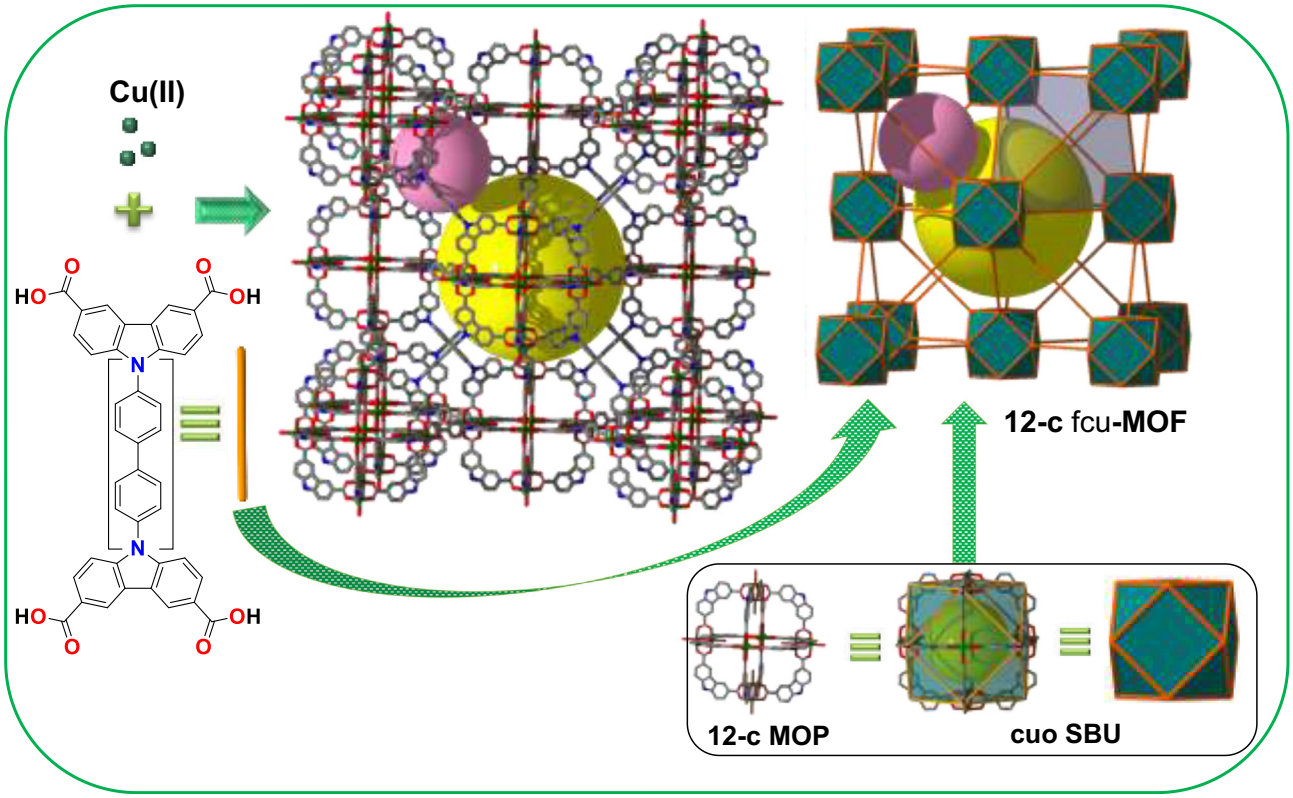

Fig. 42. Topological description of DUT-49 as linear bridging of the CDC-based 12-c **cuo** MOP resulting in **fcu**-a network.

synthesizing well-defined RE cluster-based MOFs has been a challenge to achieve for many years. The inorganic SBUs of most Ln-MOFs are based on randomly discovered lanthanide infinite rods or chains. The challenge in rationally designing RE-MOFs is due to the larger and more flexible coordination sphere of the lanthanide elements with *f* electrons. The discovered 2-fluorobenzoic acid (2-FBA) modulated synthesis approach, however, broke the synthetic roadblock allowing for the *in situ* formation of rationally targeted multi-nuclear RE MBB precursors to assemble MOFs with anticipated structural characteristics [372].

It is proposed that the presence of 2-FBA, with its hydrophobic fluorine in the *ortho* position to the carboxylate, plays a major role in repelling water molecules and stabilizing the *in situ* formation of the 12-c RE hexanuclear oxocluster, $[RE_6(OH)_8(-CO_2)_{12}]^{2-}$, through H–bonding interactions (Fig. 43). This explains the formation of discrete oxoclusters rather than the infinite RE chains or rods commonly observed in RE-MOFs. Consequently, the 2-FBA modulated synthesis enabled researchers to assemble several RE_6 oxocluster based **fcu**-MOFs with a series of linear dicarboxylate linkers that possess a similar topology to that of the UiO-6*x* MOFs (Fig. 43). 2,6-Difluorobenzoic acid (2,6-DFBA) is another modulating agent that has been recently reported effective for the assembly of various isostructural UiO-66(RE) MOFs [373]. This finding further corroborates the importance of fluorine atoms on the α-positions to the carboxylate group in the monocarboxylic acid modulated synthesis of these MOFs. The implementation of the 2-FBA and 2,6-DFBA modulated solvothermal synthesis and the isoreticular chemistry of MOFs have played a crucial role to isolate RE-**fcu**-MOFs with fine-tuned properties that are useful for specific end functions including CO_2 capture, gas and vapor separations, and NO_x adsorption [18,372–375]. This section of the review highlights the progress made regarding the assembly of isostructural and isoreticular RE-**fcu**-MOFs.

The **fcu**-MOFs isolated from RE(III) cations are generally like other M_6 oxocluster-based **fcu**-MOFs in terms of topology and the presence of octahedral as well as tetrahedral cages accessed by triangular apertures. However, a closer look at the RE_6 oxoclusters reveals slight differences. RE(III) cations form $[RE_6((\mu_3-OH)_8]^{10+}$ while the other metal cations (Zr(IV), Hf(IV), and Ce(IV)) generate $[M_6(\mu_3-O)_4(\mu_3-OH)_4]^{12+}$ clusters [372]. In contrast to other classes of M_6 oxoclusters that have 4 μ_3–O (2^- charge) and 4 μ_3–OH (1^- charge) moieties, the RE analogues are hypothesized to exclusively possess 8 μ_3–OH (1^- charge) moieties. The differences in the generated metal oxoclusters is then reflected in the overall charge of the resulting fully coordinated frameworks, with the RE cations forming anionic $[RE_6(OH)_8(-CO_2)_{12}]^{2-}$ versus the traditional structures' neutral $[M_6(\mu_3-O)_4(\mu_3-OH)_4(-CO_2)_{12}]$ [372]. In order to maintain the neutrality of the overall the framework, RE-**fcu**-MOFs have two *N*,*N*'-dimethylammonium cations (DMA) that are hypothesized to form *in situ* due to the decomposition of the DMF solvent [372,376]. The presence of 2 DMA^+ that balance the overall charge of the anionic frameworks is substantiated by ^1H NMR spectroscopy on the acid digested samples, which showed the presence of distinct methyl proton peaks that are clearly separated from the methyl protons of DMF [18]. Furthermore, the methyl proton peaks correlated to the DMA cations were preserved in the case of the fully evacuated RE-**fcu**-MOFs unlike the DMF peaks that disappeared in the fully activated samples. The presence of DMA counterions was also evidenced in the TGA traces of the fully evacuated RE-**fcu**-MOF samples, which showed distinct weight losses around 250 °C that were linked to the decomposition of the dimethylamine molecules [18]. Due to the requirements to have DMA or related cations to balance the overall framework charge, the synthesis of RE-**fcu**-MOFs require solvents that have the potential to generate the targeted species during the solvothermal assembly. DMF and *N*,*N*'-dimethyl acetamide (DMA) are typical examples. In fact, all the RE-UiO-6*x* MOFs reported so far were synthesized by using DMF or DMA, either as pure solvent or as a mixture with other solvents [18,372,373,376]. It is emphasized that these solvents play an important structure directing role

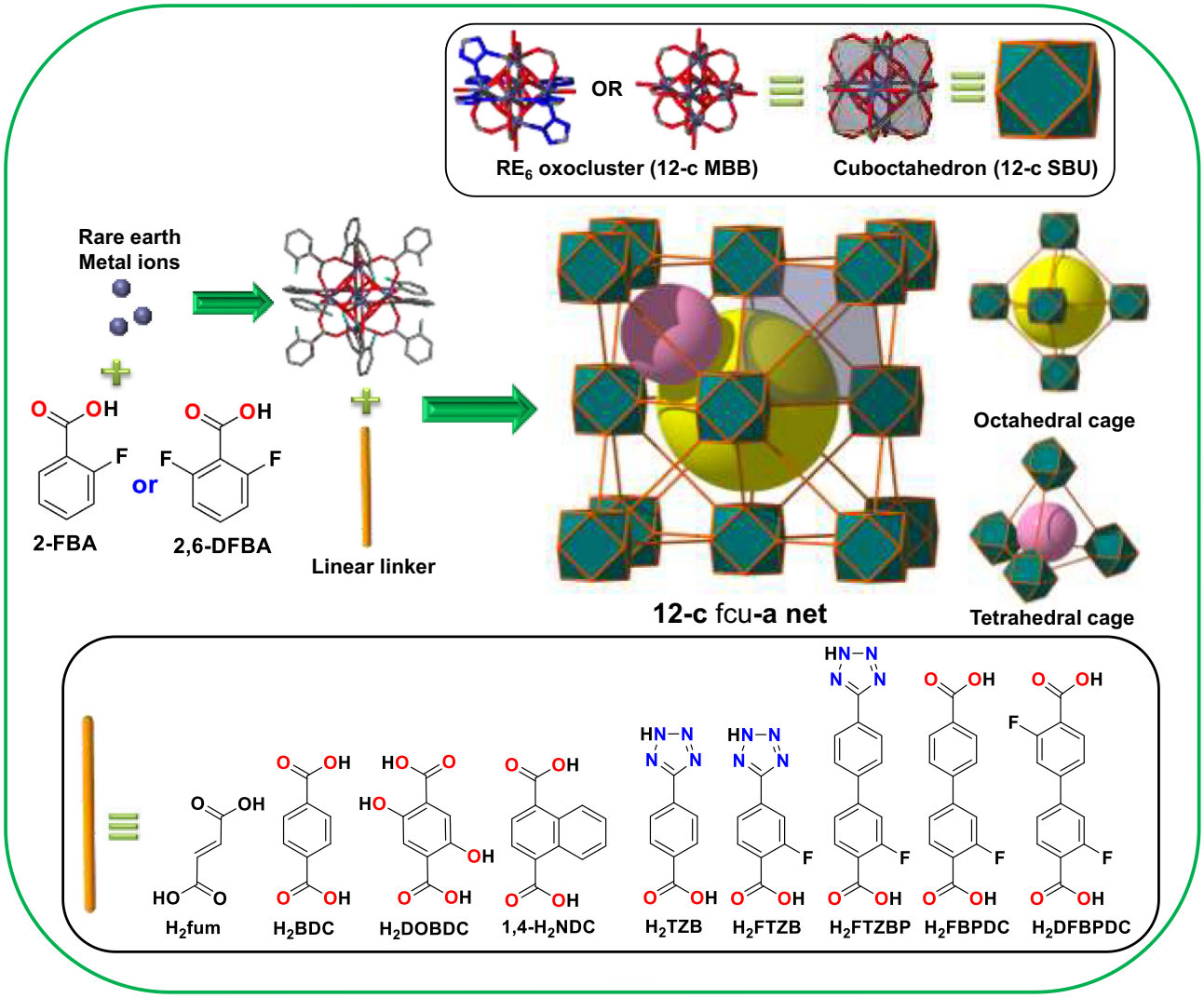

Fig. 43. Scheme showing the 2-FBA/2,6-DFBA modulated synthesis approach employed to assemble various isoreticular RE-**fcu**-MOFs via *in situ* generation of RE_6 oxoclusters.

for the solvothermal assembly of the RE-**fcu**-MOFs. Owing to the similar chemical properties amongst the REs (with the exception of cerium), the synthetic conditions employed to produce a **fcu**-MOF for one lanthanide can easily be emulated for the others leading to a series of isostructural RE-**fcu**-MOFs (RE = Y(III), Eu(III), Gd (III), Tb(III), Ho(III), Er(III), Tm(III), Yb(III), Dy(III), Lu(III)) [18,373,374].

The implementation of isoreticular chemistry in RE-**fcu**-MOFs has produced MOFs with cut-off apertures for molecular size and shape selective separation (Fig. 44) [18,377]. The use of relatively shorter organic linkers to bridge the 12-c RE_6 oxoclusters creates a contracted triangular window aperture, which is the sole access point to the interconnected octahedral and tetrahedral cages. These analogues displayed steric adsorptive separations of molecules with similar physical–chemical properties (paraffin and isoparaffin separation and C_4 olefin splitting, ethene and acetylene separation, selective adsorption of benzene), with several being unique to MOFs as molecular exclusion-based separations of molecules, such as linear and branched paraffins, not being achieved with other classes of porous materials [18,377,378]. The stability of the RE-**fcu**-MOF platform together with the possibility for adjustment of the pore size and functionality has led to demonstrated potential for achieving efficient removal of H_2S from natural gas streams prior to the upgrading process [379], post-combustion CO_2 capture [380], and mitigation of polysulfide diffusion in Li-S batteries [381].

Aside from RE-**fcu**-MOF crystals or powders, researchers have sought to grow RE-**fcu**-MOF thin films on capacitive interdigitated electrodes (IDEs) and mixed-matrix membranes that can be deployed for sensing (Fig. 45) and separation applications [152,382–385]. As confirmed by PXRD measurements and SEM characterizations, the RE-**fcu**-MOF thin films displayed preferential orientation growth along the [111] direction. The growth of the MOF thin films on the IDE substrate in preferential orientation afforded sought after exposure of the triangular windows of the **fcu**-MOF structure (Fig. 45) for monitoring and measuring the change in sensing film permittivity upon gas/vapor adsorption [382,383].

In general, the use of 2-FBA or 2,6-DFBA modulated synthesis, with judicious choice of the organic linker, has enabled the construction of various isoreticular RE-**fcu**-MOFs with controlled aperture size to address complex gas/vapor separations. However, the assembly of the RE analogues of UiO-66*x* MOFs is still in its infancy with many research opportunities ahead. The possible assembly of the MOFs using solvents that can generate other cations to balance the overall framework charge, DEF as an example, is yet to be confirmed. Uncovering the detailed mechanism for the assembly of the MOFs also requires further study to assess whether the

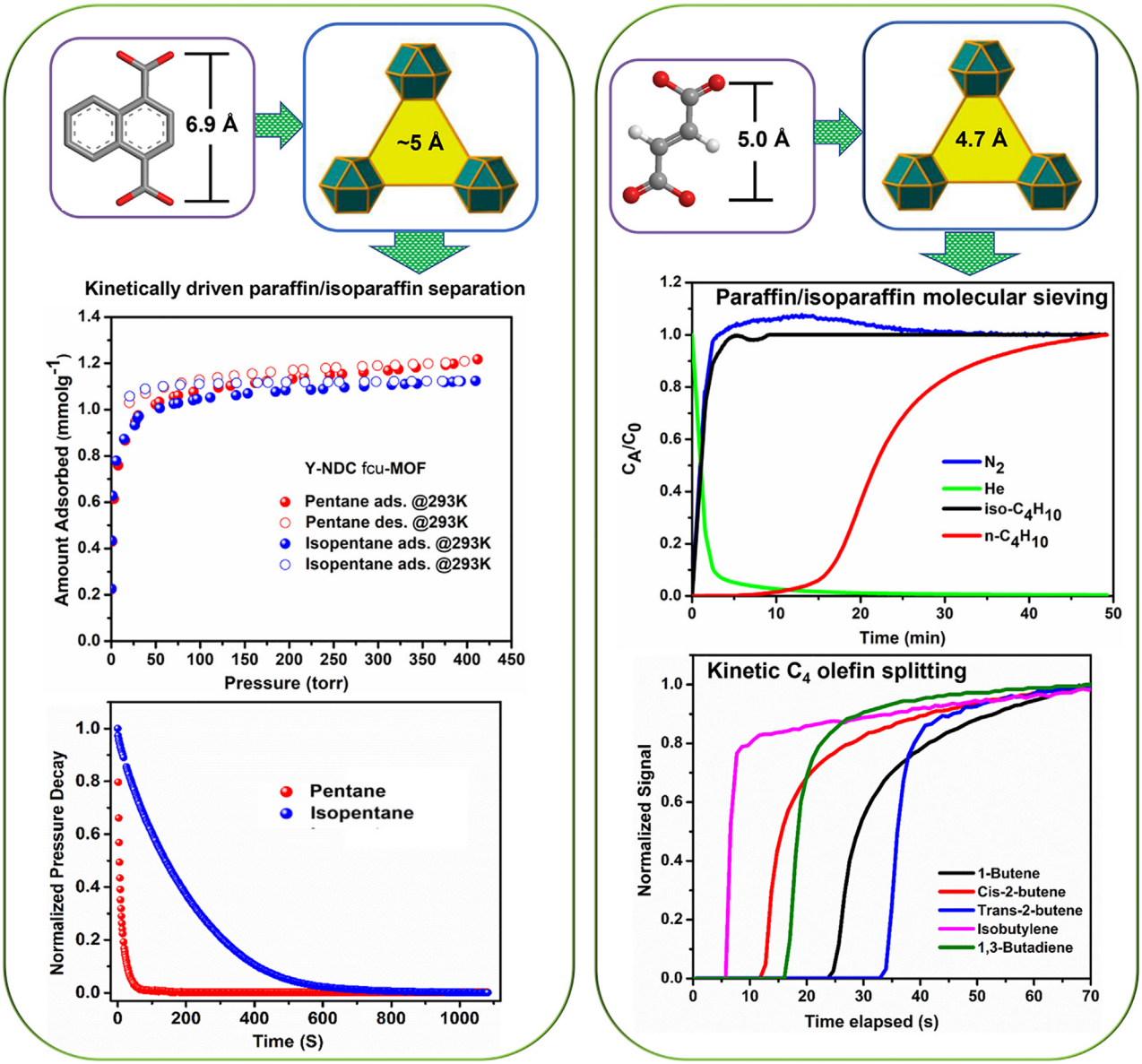

Fig. 44. Schematic showing the impact of triangular aperture size in the isoreticular RE-**fcu**-MOFs for size/shape selective separation of hydrocarbons. Reproduced with permission from [18,377]

RE-**fcu**-MOFs can be synthesized in the presence of other types of added cationic sources. There is also further room to explore other monocarboxylic acid modulators with fluorine groups on the α-positions to the carboxylate groups, such as 2-fluoroacetic acid and trifluoroacetic acid.

The other RE cation that has attracted research interest is cerium. Despite its classification as a RE element, its similarity with the group IV metal ions (Zr(IV) and Hf(IV)) in terms of its physical–chemical properties and the possibility to generate Ce_6 oxoclusters with benzoate linker [386] makes it a candidate for constructing **fcu**-MOFs that are isostructural to the UiO-6*x* MOFs. Consequently, the reaction of cerium salt precursors with linear dicarboxylic acids of various length and functional groups under appropriate synthetic conditions yielded Ce-**fcu**-MOFs [387]. The seminal work in this regard was performed by Lammert *et al.* [387] who reported isoreticular Ce-**fcu**-MOFs by the solvothermal reaction of cerium(IV) ammonium nitrate ($(NH_4)_2Ce(NO_3)_6$) with the linear dicarboxylic acids, fumaric acid, H_2BDC, H_2BDC-X (X = F, CH_3, Cl, COOH, NO_2), 2,6-H_2NDC and H_2BPDC. Characterization of the prepared MOFs by PXRD and XANES confirmed the formation of the MOFs based on 12-c Ce_6 oxocluster, $[Ce_6(\mu_3\text{–}O)_4((\mu_3\text{–}OH)_4]^{12+}$, and the existence of exclusive Ce(IV) species in all of the assembled MOFs. Unlike the trivalent RE system, the solvothermal assembly of the Ce-**fcu**-MOFs was independent of monocarboxylic acid modulators that have fluorine atoms α to the carboxylate moiety. The cerium oxocluster was generated in the same way as its Zr(IV) and Hf(IV) counterparts using modulators such as benzoic acid and formic acid. Structures of various other Ce-UiO-6*x* MOFs, $[Ce_6(\mu_3\text{–}O)_4((\mu_3\text{–}OH)_4L_6]$ with L = 2,5-H_2BDC-$(CH_3)_2$, H_2BDC-N_3, H_2BDC-F_4, H_2BPyDC, and acetylenedicarboxylic acid, with different gas or liquid sorption, catalytic and gas/vapor sensing properties were also reported [28,388–395]. The redox behavior of the cerium ions (Ce(III)/Ce(IV)) and the potential of the Ce-**fcu**-MOFs for various types of oxidation reactions have also been explored. Although the conventional solvo(hydro)thermal reaction is the most widely employed route to assemble isoreticular Ce-**fcu**-MOFs, the adaptability of the MOF platform to other synthetic paths such as the sonochemical

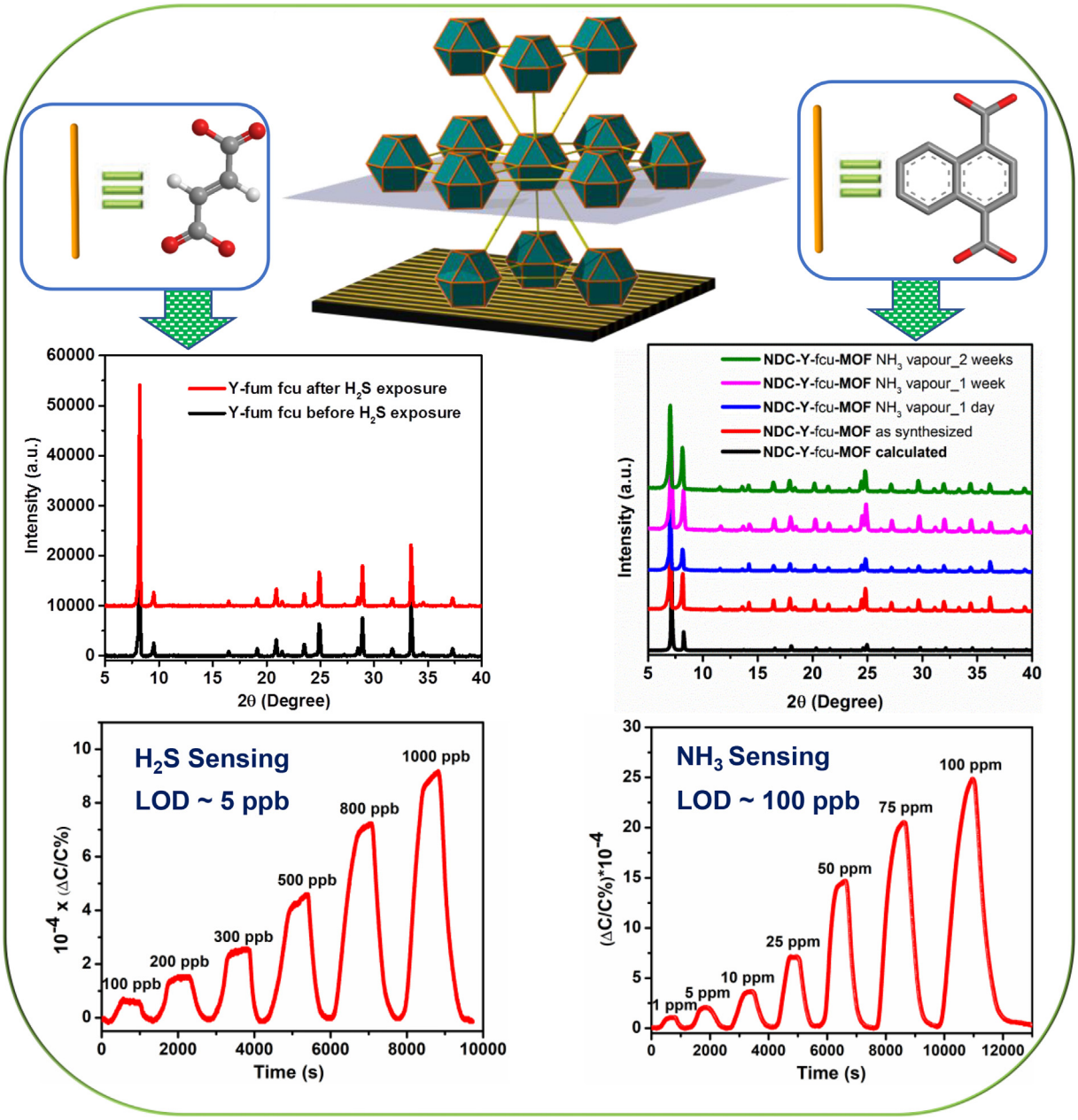

Fig. 45. The growth of isoreticular RE-**fcu**-MOF thin films on IDE device and the sensing performances of the resultant materials towards H_2S and NH_3. Reproduced with permission from [382,383]

and nearly solvent-free mechanochemical routes have been demonstrated [396,397].

3.3. M_6 (M = Actinides or An) oxocluster-based fcu-MOFs

Owing to the high valence nature due to variable oxidation states (*e.g.*, IV, V, and VI) and the complex intersection of the *f*- and *d*-orbitals, actinides (An) can form MOFs with a variety of either single metal ion or metal cluster MBBs of different symmetry and coordination geometry. Therefore, the generation of the 12-c An-based oxoclusters that match the cuboctahedron SBUs of the **fcu**-MOFs and the subsequent generation of An-**fcu**-MOFs, isoreticular to above-discussed transition-metal/rare earth frameworks, are then expected to be dependent on the oxidation state of actinide element. Owing to the possibility to form An(IV) species for the tetravalent metal ions (Th – Pu) with similar ionic charge properties to Zr(IV), the *in situ* generation of An_6 oxoclusters, $[An_6(\mu_3\text{–}O)_4(\mu_3\text{–}OH)_4]$, with isostructural composition to the Zr (IV) analogue, led to the synthesis of various An-**fcu**-MOFs, $[An_6(\mu_3\text{–}O)_4(\mu_3\text{–}OH)_4(Linker)_6]$. In fact similar oxo/hydroxo-bridged hexanuclear clusters were known to form as discrete complexes by the hydrolysis of tetravalent An species such as Th (IV) and U(IV) in aqueous solutions [398]. The existence of the actinides in the IV oxidation state is a prerequisite for the *in situ* generation of $An_6(\mu_3\text{–}O)_4(\mu_3\text{–}OH)_4$. This is evidenced in the work of Zehnder *et al.* [399] who showed the formation of the U(IV)-based structural unit, $U_6O_4(OH)_x$, during the assembly of the U (IV)-based coordination polymer, $U_6(NO_3)_4(Glut)_4(O)_4(OH)_4(H_2O)_6{\cdot}12H_2O$, by the reaction of uranyl nitrate with sodium terephthalate and sodium glutarate. Despite the use of U(VI) precursor, the prepared coordination polymer was observed to possess U (IV) species, which were generated *in situ* by a slow photoreduction

of uranyl ions in an alcohol solution and then stabilized by glutarate linkers.

The assembly of An-**fcu**-MOFs from *in situ* generated U_6 oxocluster MBBs, $[U_6O_4(OH)_4(H_2O)_6]$ with an octahedral configuration of uranium centers and linear dicarboxylate linkers was first demonstrated by the Loiseau research group. In a typical synthesis, the reaction of a tetravalent uranium salt with dicarboxylic acid linkers, H_2BDC, fumaric acid, H_2BPDC, and 2,6-H_2NDC under appropriate formic acid modulated solvothermal conditions led to the assembly of the corresponding 12-c U-**fcu**-MOFs, $[U_6O_4(OH)_4(H_2O)_6(Linker)_6]\cdot x$DMF [328]. The same U(IV) -based hexanuclear core was also used by the same research group to solvothermally synthesize a fum-**fcu**-MOF type architecture but with one missing fumarate linker per cluster, $U_6O_4(OH)_4(fum)_5(form)_2(H_2O)_2\cdot 3$DMF [400]. The missing linker is compensated by 2 formate groups coordinated to each oxocluster of the resulting MOF.

Reaction parameters, such as temperature and addition of water, are important to isolate the hexameric oxocluster. Specifically, the temperature range of 110–120 °C and a water/U molar ratio between 2 and 10 is ideal for forming the targeted cluster [401]. The increased degree of the inorganic condensation at higher temperatures and at high-water concentrations (H_2O/U greater than 15) produced uranium oxide (UO_2). The importance of adding small amounts of water for controlled hydrolysis of An(IV) salts with subsequent formation of An-**fcu**-MOFs were demonstrated during the solvothermal synthesis of the isoreticular Th-**fcu**-MOFs, UiO-66(Th), UiO-67(Th), UiO-67(Th)–NH_2 [402,403,404]. Further expanding the isoreticular chemistry in Th-**fcu**-MOFs, Feng *et al.* recently reported two 12-c Th_6 oxocluster-based MOFs, denoted Th-MOF-67 and Th-MOF-68, using 4-(1H-tetrazol-5-yl) benzoic acid (H_2TZB) or 4-(1,2,4-triazol-4-yl) benzoic acid (HCPT) organic linkers, respectively (Fig. 46) [405]. The two isoreticular Th-**fcu**-MOFs showed high potential for radionuclide sequestration, as evidenced by their high uptake of ReO_4^- (a chemical surrogate of radioactive TcO_4^-), with adsorption of 10, 368, and 560 mg/g for UiO-66(Th), Th-MOF-67, and Th-MOF-68, respectively. As proven by SXRD and theoretical calculation studies, the 36.8- or 56-fold enhancement in the uptake for Th-MOF-67 and Th-MOF-68, respectively, versus UiO-66(Th), is attributed to coordinative interactions of ReO_4^- with the tetrazolate or triazolate moiety and the possibility for anion-exchange for the case of the cationic Th-MOF-68.

Aside from the use of pre-synthesized linear ditopic organic linkers, *in situ* coupling of monovalent linkers coordinated to the $Th_6(\mu_3\text{–}O)_4(\mu_3\text{–}OH)_4(H_2O)_6$ clusters, but with suitable functional groups on the *p*-position, was demonstrated to be a viable route to assemble the isoreticular Th-**fcu**-MOFs. This was illustrated by the assembly of Th-ABDC-**fcu**-MOF via *in situ* homo-coupling and reductive dimerization of nitroso groups from 4-nitrosobenzoate groups on discrete $Th_6(\mu_3\text{–}O)_4(\mu_3\text{–}OH)_4$(4-nitrosobenzoate)$_6$ clusters (Fig. 46) [406].

The trends for An-**fcu**-MOFs were extended to a series of isoreticular UiO-6*x*(Np) MOFs, UiO-66(Np), UiO-67(Np), UiO-67 (Np)–NH_2, and UiO-68(Np)–NH_2, all of which were produced from a $[Np_6O_4(OH)_4(H_2O)_6]^{12+}$ core generated *in situ* by controlled hydrolysis of the tetravalent neptunium salt ($NpCl_4$) and the dicarboxylic acid linkers (H_2BDC, H_2BPDC, H_2BPDC-NH_2, and H_2TPDC-NH_2) in the presence of benzoic acid modulator [404]. To further exemplify the suitability of the An(IV) precursors for the preparation of An_6 oxocluster based **fcu**-MOFs, Hastings *et al.* [329] reported the benzoic acid-modulated solvothermal synthesis and characterization of UiO-66(Pu). The MOF was prepared from Pu (IV) nitrate salt (obtained by washing Pu(IV) stock solution in 2 M HCl with 5 M HNO_3 and subsequent heating to near dryness). TGA evidenced lower thermal stability of the MOF than UiO-66(Zr), with the difference originating from defects in the form of missing linkers or missing clusters. The presence of defects in the prepared UiO-66(Pu) was also claimed from the discrepancy between the

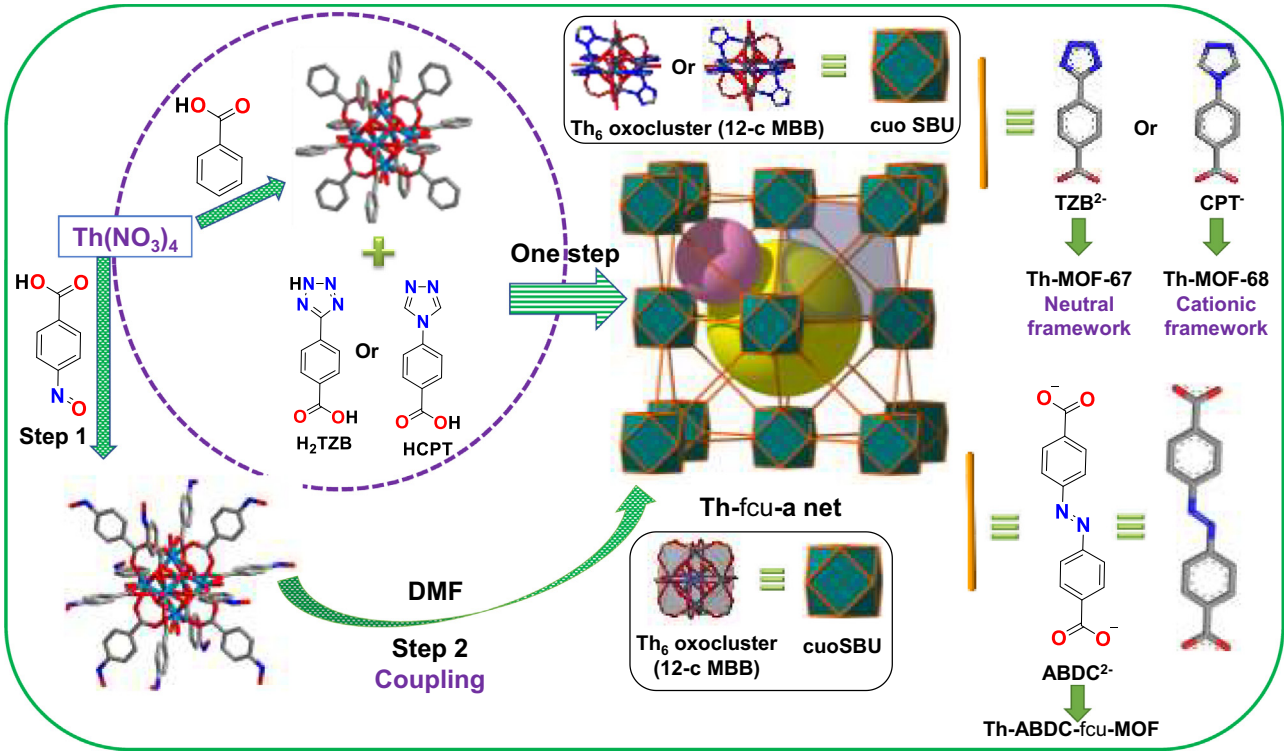

Fig. 46. Schematics showing the assembly of the isoreticular Th-**fcu**-MOFs from pre-synthesized linkers and from *in situ* coupling of nitroso groups on the *p*-position of the monovalent benzoate-based linker decorating the discrete 12-c Th_6 oxo-clusters.

experimental and calculated pore size distributions (PSDs), with broader pore width in the PSD obtained from the N_2 isotherm as compared to the PSDs calculated assuming no defect. The existence of missing cluster defects in the synthesized UiO-66(Pu) was due to the high probability of protonated linkers with passive carboxylic acid functional groups caused by excess protons in the solution from the Pu(IV) precursor [407].

Owing to the multiplicity of their oxidation states and coordination geometries, the number of An_6 oxocluster-based **fcu**-MOFs is relatively scarce. However, the already demonstrated possibility to transcribe the architecturally robust Zr-**fcu**-MOF platform to the An counterparts could be of interest to the nuclear fuel cycle process. Even though the radiation stability of the α-emitter actinides, after being incorporated into MOFs as MBBs, is yet to be studied, the assembly of such MOFs is expected to provide a plausible way to sequestrate the radioactive An fission products into a stable form. Hence, further investigation on the radiation stability of An_6 oxoclusters should be assessed to deploy An-**fcu**-MOFs as an alternative or complementary nuclear waste management approach.

4. Conclusions and perspective

This review details the significant progress made on MOFs whose structure is based on an underlying **fcu** topology from the perspectives of designed synthesis, crystal structure, chemistry, and applications. The reported MBB and SBB approaches that have been employed to form a large number of functional M−**fcu**−MOFs, from the assembly of the 12-c polyatomic oxocluster MBBs as well as MOPs with a series of ditopic homo-/heterofunctional linkers of various lengths, have been discussed. Simply put, the utility, versatility, and fidelity of the **fcu**-MOF platform was demonstrated in this comprehensive review. The article highlighted four key developments that were particularly important in advancing the **fcu**-MOF platform to what it is today. These include: (i) the geometric principles for linking twelve-connected inorganic clusters with linear organic linkers to form the **fcu** topology; (ii) synthetic parameters governing the assembly of **fcu**-MOFs, including the discovery of modulating agents; (iii) exploitation of the isoreticular principle in the design of new **fcu**-MOFs with functionalized internal pore environments, varying window and internal pore metrics, and defected architectures; and (iv) application of the multivariate approach to realize **fcu**-MOFs that are endowed with a high degree of complexity and heterogeneity for unlocking new properties. Furthermore, these developments were supplemented with a survey of various salient **fcu**-MOFs that have achieved important results in applications ranging from gas adsorption to heterogeneous catalysis to even sequestering radioactive fission products for nuclear waste management.

The state-of-the-art developments in the modulated synthesis, isoreticular expansion/decoration, and post-synthetic modifications, that have been successfully employed to rationally construct various **fcu**-MOFs with enhanced properties, are also summarized with holistic generalizations. However, most of the synthetic routes that have been employed to build **fcu**-MOFs have been discovered by trial-and-error. Hence, a detailed understanding of the mechanism for constructing these MOFs is still at a stage of relative infancy. Further investigation is then needed to produce clear insights about the different routes, which, in turn, helps to create new avenues that facilitate the emergence of new members of the MOF family with advanced structural and functional characteristics.

The established versatility of the multinuclear metal cluster MBBs with respect to the nuclear size and metal cation type, diversity of ditopic linkers with respect to length and functionality, and adaptability of the synthetic routes to several conditions, demonstrate that there is still plenty of room to rationally design and discover various other **fcu**-MOFs. The richness in coordination geometry and the range of potential organic linkers that could be designed might lead to the deployment of this MOF platform in various applications that were not foreseen. The reported M−**fcu**−MOFs have already demonstrated promising potential to be deployed in various applications pertinent to energy and environmental issues, with their synthetic flexibility, structural diversity, and ease of tunability still placing the **fcu**-MOFs in active research in various application areas.

Even though M_6 oxocluster-based **fcu**-MOFs are promising for different applications, there remain ample challenges that need to be overcome before pursuing the large-scale syntheses and applications of this class of MOFs. One main obstacle is the impracticability of the conventional solvothermal route for practical continuous processes. Alternative approaches such as mechanochemical synthesis, microwave-assisted preparation, and continuous flow reactor synthesis are still at early and theoretical stages and need to be developed further. The large-scale syntheses and wide accessibility of the MOFs are also hampered by the high temperature requirements. The recently developed mechanochemical and electrochemical syntheses approaches that enable the assembly of MOFs at room temperature either with simple solvent-free milling or in the presence of solvents need to also be developed further to facilitate the large-scale preparation and practical deployment of the **fcu**-MOFs. The possibility to pre-synthesize the discrete oxo-clusters of zirconium, rare earths, or actinides could facilitate the further development of the synthesis methods.

One of the structural attributes that makes **fcu**-MOF platform exciting is that it encloses only equilateral triangular window apertures as the sole access point to the interconnected octahedral and tetrahedral cage pore system. Further development of the mixed-linker strategy could open more opportunities to fine-tune the triangular apertures for a given application. Indeed, thus far, the majority of the mixed-linker Zr-**fcu**-MOFs were assembled from two linkers. The assembly of MTV MOFs with 3 or more linkers introduced within one framework structure in appropriate distributions for specific applications should be targeted. Mixed-metal and mixed-linker **fcu**-MOFs are generally synthesized as solid solutions (*i.e.*, they possess random distribution of linkers and metal cations). There is also a lack of appropriate characterization tools to precisely locate the metal ions or linkers in MTV MOFs. Therefore, the advancement of synthetic strategies that could lead to homogeneously distributed components in MTV **fcu**-MOFs could be an ideal target for effective deployment of those MOFs in real world applications. This, in turn, requires the development of suitable characterization tools that could show the distribution of the components with no ambiguity. As demonstrated by Yaghi and colleagues [44], the development of a large single crystal that could suffice for characterization by XRD, NMR and other techniques could be of great help in this regard. PXRD is the most commonly used method to characterize the structure, phase purity and stability of **fcu**-MOFs. The technique, however, lacks the required accuracy to detect defective structures within the frameworks and partial loss of stability upon exposure to external stimuli. As a result, techniques such as high-resolution neutron diffraction and high-resolution TEM should be pursued to gain precise information regarding the microstructures of the MOFs and the resulting structure–property relationships. In general, we hope the comprehensive analysis of the 12-coordinated **fcu**-MOF platform carried out in this review inspires the MOF community to create and pursue new concepts and ideas that foster the further development of new and existing **fcu**-MOF materials with unique properties.

Declaration of competing interest

The authors declare that they have no known competing financial interests or personal relationships that could have appeared to influence the work reported in this paper.

Acknowledgement

Y.B. and A.H.A. acknowledge Mohammed VI Polytechnic University (UM6P) for the financial support to undertake the work. Y.B., K. E.C., and K.A. acknowledge the Alliance of International Science Organization (ANSO-CR-PP-2020-06) for support in furthering this collaboration. K.E.C. is grateful to the Jordan Ministry of Higher Education and Scientific Research (Project No. BAS/1/6/2020).

References

[1] H. Furukawa, K.E. Cordova, M. O'Keeffe, O.M. Yaghi, The chemistry and applications of metal-organic frameworks, Science 341 (2013) 1230444.
[2] The Cambridge Structural Database (CSD), UK. Available from: https://www.ccdc.cam.ac.uk/Community/csd-community/csd-mof-collection, 2021 (accessed 15 September 2021)..
[3] D.J. Tranchemontagne, J.L. Mendoza-Cortés, M. O'Keeffe, O.M. Yaghi, Secondary building units, nets and bonding in the chemistry of metal–organic frameworks, Chem. Soc. Rev. 38 (2009) 1257–1283.
[4] V. Guillerm, M. Eddaoudi, The importance of highly connected building units in reticular chemistry: thoughtful design of metal-organic frameworks, Acc. Chem. Res. 54 (2021) 3298–3312.
[5] U. Schubert, Cluster-based inorganic–organic hybrid materials, Chem. Soc. Rev. 40 (2011) 575–582.
[6] O. Delgado-Friedrichs, M. O'Keeffe, O.M. Yaghi, Taxonomy of periodic nets and the design of materials, PCCP 9 (2007) 1035–1043.
[7] O.M. Yaghi, M. O'Keeffe, N.W. Ockwig, H.K. Chae, M. Eddaoudi, J. Kim, Reticular synthesis and the design of new materials, Nature 423 (2003) 705–714.
[8] N.W. Ockwig, O. Delgado-Friedrichs, M. O'Keeffe, O.M. Yaghi, Reticular chemistry: Occurrence and taxonomy of nets and grammar for the design of frameworks, Acc. Chem. Res. 38 (2005) 176–182.
[9] O. Delgado-Friedrichs, M.D. Foster, M. O'Keeffe, D.M. Proserpio, M.M.J. Treacy, O.M. Yaghi, What do we know about three-periodic nets?, J. Solid State Chem. 178 (2005) 2533–2554.
[10] J.H. Cavka, S. Jakobsen, U. Olsbye, N. Guillou, C. Lamberti, S. Bordiga, K.P. Lillerud, A New zirconium Inorganic building brick forming metal organic frameworks with exceptional stability, J. Am. Chem. Soc. 130 (2008) 13850–13851.
[11] H. Kim, S. Yang, S.R. Rao, S. Narayanan, E.A. Kapustin, H. Furukawa, A.S. Umans, O.M. Yaghi, E.N. Wang, Water harvesting from air with metal-organic frameworks powered by natural sunlight, Science 356 (2017) 430.
[12] Z. Chen, S.L. Hanna, L.R. Redfern, D. Alezi, T. Islamoglu, O.K. Farha, Reticular chemistry in the rational synthesis of functional zirconium cluster-based MOFs, Coord. Chem. Rev. 386 (2019) 32–49.
[13] D.J. Tranchemontagne, Z. Ni, M. O'Keeffe, O.M. Yaghi, Reticular Chemistry of Metal-Organic Polyhedra, Angew. Chem. Int. Ed. 47 (2008) 5136–5147.
[14] N. Chang, X.-P. Yan, Exploring reverse shape selectivity and molecular sieving effect of metal-organic framework UIO-66 coated capillary column for gas chromatographic separation, J. Chromatogr. A 1257 (2012) 116–124.
[15] W.-W. Zhao, C.-Y. Zhang, Z.-G. Yan, L.-P. Bai, X. Wang, H. Huang, Y.-Y. Zhou, Y. Xie, F.-S. Li, J.-R. Li, Separations of substituted benzenes and polycyclic aromatic hydrocarbons using normal- and reverse-phase high performance liquid chromatography with UiO-66 as the stationary phase, J. Chromatogr. A 1370 (2014) 121–128.
[16] W. Zhao, C. Zhang, Z. Yan, Y. Zhou, J. Li, Y. Xie, L. Bai, L. Jiang, F. Li, Preparation, characterization, and performance evaluation of UiO-66 analogues as stationary phase in HPLC for the separation of substituted benzenes and polycyclic aromatic hydrocarbons, PLoS ONE 12 (2017) e0178513.
[17] P.S. Bárcia, D. Guimarães, P.A.P. Mendes, J.A.C. Silva, V. Guillerm, H. Chevreau, C. Serre, A.E. Rodrigues, Reverse shape selectivity in the adsorption of hexane and xylene isomers in MOF UiO-66, Microporous Mesoporous Mater. 139 (2011) 67–73.
[18] A.H. Assen, Y. Belmabkhout, K. Adil, P.M. Bhatt, D.-X. Xue, H. Jiang, M. Eddaoudi, Ultra-Tuning of the Rare-Earth fcu-MOF Aperture Size for Selective Molecular Exclusion of Branched Paraffins, Angew. Chem. Int. Ed. 54 (2015) 14353–14358.
[19] M. Eddaoudi, J. Kim, N. Rosi, D. Vodak, J. Wachter, M. Keeffe, O.M. Yaghi, Systematic Design of Pore Size and Functionality in Isoreticular MOFs and Their Application in Methane Storage, Science 295 (2002) 469.
[20] B. Bueken, H. Reinsch, N. Reimer, I. Stassen, F. Vermoortele, R. Ameloot, N. Stock, C.E.A. Kirschhock, D. De Vos, A zirconium squarate metal–organic framework with modulator-dependent molecular sieving properties, Chem. Commun. 50 (2014) 10055–10058.
[21] H. Furukawa, F. Gándara, Y.-B. Zhang, J. Jiang, W.L. Queen, M.R. Hudson, O.M. Yaghi, Water Adsorption in Porous Metal-Organic Frameworks and Related Materials, J. Am. Chem. Soc. 136 (2014) 4369–4381.
[22] L. Valenzano, B. Civalleri, S. Chavan, S. Bordiga, M.H. Nilsen, S. Jakobsen, K.P. Lillerud, C. Lamberti, Disclosing the complex structure of UiO-66 metal organic framework: A synergic combination of experiment and theory, Chem. Mater. 23 (2011) 1700–1718.
[23] M.J. Katz, Z.J. Brown, Y.J. Colón, P.W. Siu, K.A. Scheidt, R.Q. Snurr, J.T. Hupp, O. K. Farha, A facile synthesis of UiO-66, UiO-67 and their derivatives, Chem. Commun. 49 (2013) 9449–9451.
[24] A. Schaate, P. Roy, A. Godt, J. Lippke, F. Waltz, M. Wiebcke, P. Behrens, Modulated synthesis of Zr-based metal-organic frameworks: From nano to single crystals, Chem. Eur. J. 17 (2011) 6643–6651.
[25] A.D. Wiersum, E. Soubeyrand-Lenoir, Q. Yang, B. Moulin, V. Guillerm, M.B. Yahia, S. Bourrelly, A. Vimont, S. Miller, C. Vagner, M. Daturi, G. Clet, C. Serre, G. Maurin, P.L. Llewellyn, An evaluation of UiO-66 for gas-based applications, Chem. Asian J. 6 (2011) 3270–3280.
[26] G.C. Shearer, S. Forselv, S. Chavan, S. Bordiga, K. Mathisen, M. Bjørgen, S. Svelle, K.P. Lillerud, In situ infrared spectroscopic and gravimetric characterisation of the solvent removal and dehydroxylation of the metal organic frameworks UiO-66 and UiO-67, Top. Catal. 56 (2013) 770–782.
[27] C. Larabi, E.A. Quadrelli, Titration of Zr3(μ-OH) hydroxy groups at the cornerstones of bulk MOF UiO-67, [Zr6O4(OH)4(biphenyldicarboxylate)6], and their reaction with [AuMe(PMe3)], Eur. J. Inorg. Chem. 2012 (2012) 3014–3022.
[28] V.R. Bakuru, S.R. Churipard, S.P. Maradur, S.B. Kalidindi, Exploring the Brønsted acidity of UiO-66 (Zr, Ce, Hf) metal–organic frameworks for efficient solketal synthesis from glycerol acetalization, Dalton Trans. 48 (2019) 843–847.
[29] Q. He, Q. Chen, M. Lü, X. Liu, Adsorption Behavior of Rhodamine B on UiO-66, Chin. J. Chem. Eng. 22 (2014) 1285–1290.
[30] H. Wu, T. Yildirim, W. Zhou, Exceptional Mechanical Stability of Highly Porous Zirconium Metal-Organic Framework UiO-66 and Its Important Implications, J. Phys. Chem. Lett. 4 (2013) 925–930.
[31] D. Bůžek, S. Adamec, K. Lang, J. Demel, Metal–organic frameworks vs. buffers: case study of UiO-66 stability, Inorg. Chem. Front. 8 (2021) 720–734.
[32] X. Zhao, D. Liu, H. Huang, W. Zhang, Q. Yang, C. Zhong, The stability and defluoridation performance of MOFs in fluoride solutions, Microporous Mesoporous Mater. 185 (2014) 72–78.
[33] F. Ragon, P. Horcajada, H. Chevreau, Y.K. Hwang, U.H. Lee, S.R. Miller, T. Devic, J.-S. Chang, C. Serre, In Situ Energy-Dispersive X-ray Diffraction for the Synthesis Optimization and Scale-up of the Porous Zirconium Terephthalate UiO-66, Inorg. Chem. 53 (2014) 2491–2500.
[34] K. Tulig, K.S. Walton, An alternative UiO-66 synthesis for HCl-sensitive nanoparticle encapsulation, RSC Adv. 4 (2014) 51080–51083.
[35] H. Reinsch, S. Waitschat, S.M. Chavan, K.P. Lillerud, N. Stock, A. Facile, "Green" route for scalable batch production and continuous synthesis of zirconium MOFs, Eur. J. Inorg. Chem. 2016 (2016) 4490–4498.
[36] C. Avci-Camur, J. Troyano, J. Pérez-Carvajal, A. Legrand, D. Farrusseng, I. Imaz, D. Maspoch, Aqueous production of spherical Zr-MOF beads via continuous-flow spray-drying, Green Chem. 20 (2018) 873–878.
[37] F. Ragon, B. Campo, Q. Yang, C. Martineau, A.D. Wiersum, A. Lago, V. Guillerm, C. Hemsley, J.F. Eubank, M. Vishnuvarthan, F. Taulelle, P. Horcajada, A. Vimont, P.L. Llewellyn, M. Daturi, S. Devautour-Vinot, G. Maurin, C. Serre, T. Devic, G. Clet, Acid-functionalized UiO-66(Zr) MOFs and their evolution after intra-framework cross-linking: structural features and sorption properties, J. Mater. Chem. A 3 (2015) 3294–3309.
[38] C. Avci-Camur, J. Perez-Carvajal, I. Imaz, D. Maspoch, Metal acetylacetonates as a source of metals for aqueous synthesis of metal-organic frameworks, ACS Sustain. Chem. Eng. 6 (2018) 14554–14560.
[39] Z. Hu, Y. Peng, Z. Kang, Y. Qian, D. Zhao, A modulated hydrothermal (MHT) approach for the facile synthesis of UiO-66-Type MOFs, Inorg. Chem. 54 (2015) 4862–4868.
[40] H. Reinsch, B. Bueken, F. Vermoortele, I. Stassen, A. Lieb, K.-P. Lillerud, D. De Vos, Green synthesis of zirconium-MOFs, CrystEngComm 17 (2015) 4070–4074.
[41] A.M. Fidelli, B. Karadeniz, A.J. Howarth, I. Huskić, L.S. Germann, I. Halasz, M. Etter, S.-Y. Moon, R.E. Dinnebier, V. Stilinović, O.K. Farha, T. Friščić, K. Užarević, Green and rapid mechanosynthesis of high-porosity NU- and UiO-type metal–organic frameworks, Chem. Commun. 54 (2018) 6999–7002.
[42] R. D'Amato, R. Bondi, I. Moghdad, F. Marmottini, M.J. McPherson, H. Naïli, M. Taddei, F. Costantino, "Shake 'n Bake" Route to Functionalized Zr-UiO-66 Metal-Organic Frameworks, Inorg. Chem. 60 (2021) 14294–14301.
[43] V. Guillerm, S. Gross, C. Serre, T. Devic, M. Bauer, G. Férey, A zirconium methacrylate oxocluster as precursor for the low-temperature synthesis of porous zirconium(iv) dicarboxylates, Chem. Commun. 46 (2010) 767–769.
[44] C.A. Trickett, K.J. Gagnon, S. Lee, F. Gándara, H.-B. Bürgi, O.M. Yaghi, Definitive Molecular Level Characterization of Defects in UiO-66 Crystals, Angew. Chem. Int. Ed. 54 (2015) 11162–11167.
[45] S. Biswas, P. Van Der Voort, A general strategy for the synthesis of functionalised UiO-66 frameworks: Characterisation, stability and CO2 adsorption properties, Eur. J. Inorg. Chem. 2013 (2013) 2154–2160.
[46] S. Dai, F. Nouar, S. Zhang, A. Tissot, C. Serre, One-step room-temperature synthesis of metal(IV) carboxylate metal—organic frameworks, Angew. Chem. Int. Ed. 60 (2021) 4282–4288.

[47] Z. Hu, A. Gami, Y. Wang, D. Zhao, A triphasic modulated hydrothermal approach for the synthesis of multivariate metal-organic frameworks with hydrophobic moieties for highly efficient moisture-resistant CO2 capture, Adv. Sustain. Syst. 1 (2017) 1700092.
[48] Q. Zhao, W. Yuan, J. Liang, J. Li, Synthesis and hydrogen storage studies of metal−organic framework UiO-66, Int. J. Hydrog. Energy 38 (2013) 13104–13109.
[49] I. Pakamorė, J. Rousseau, C. Rousseau, E. Monflier, P.Á. Szilágyi, An ambient-temperature aqueous synthesis of zirconium-based metal–organic frameworks, Green Chem. 20 (2018) 5292–5298.
[50] G. Zahn, P. Zerner, J. Lippke, F.L. Kempf, S. Lilienthal, C.A. Schröder, A.M. Schneider, P. Behrens, Insight into the mechanism of modulated syntheses: in situ synchrotron diffraction studies on the formation of Zr-fumarate MOF, CrystEngComm 16 (2014) 9198–9207.
[51] F. Ragon, H. Chevreau, T. Devic, C. Serre, P. Horcajada, Impact of the nature of the organic spacer on the crystallization kinetics of UiO-66(Zr)-Type MOFs, Chem. Eur. J. 21 (2015) 7135–7143.
[52] H. Xu, S. Sommer, N.L.N. Broge, J. Gao, B.B. Iversen, The chemistry of nucleation. in situ pair distribution function analysis of secondary building units during UiO-66 MOF formation, Chem. Eur. J. 25 (2019) 2051–2058.
[53] M. Taddei, N. Casati, D.A. Steitz, K.C. Dümbgen, J.A. van Bokhoven, M. Ranocchiari, In situ high-resolution powder X-ray diffraction study of UiO-66 under synthesis conditions in a continuous-flow microwave reactor, CrystEngComm 19 (2017) 3206–3214.
[54] Z. Chen, X. Wang, H. Noh, G. Ayoub, G.W. Peterson, C.T. Buru, T. Islamoglu, O. K. Farha, Scalable, room temperature, and water-based synthesis of functionalized zirconium-based metal–organic frameworks for toxic chemical removal, CrystEngComm 21 (2019) 2409–2415.
[55] M.R. DeStefano, T. Islamoglu, S.J. Garibay, J.T. Hupp, O.K. Farha, Room-Temperature Synthesis of UiO-66 and Thermal Modulation of Densities of Defect Sites, Chem. Mater. 29 (2017) 1357–1361.
[56] A. Huang, L. Wan, J. Caro, Microwave-assisted synthesis of well-shaped UiO-66-NH2 with high CO2 adsorption capacity, Mater. Res. Bull. 98 (2018) 308–313.
[57] Y.-H. Huang, W.-S. Lo, Y.-W. Kuo, W.-J. Chen, C.-H. Lin, F.-K. Shieh, Green and rapid synthesis of zirconium metal–organic frameworks via mechanochemistry: UiO-66 analog nanocrystals obtained in one hundred seconds, Chem. Commun. 53 (2017) 5818–5821.
[58] M. Taddei, P.V. Dau, S.M. Cohen, M. Ranocchiari, J.A. van Bokhoven, F. Costantino, S. Sabatini, R. Vivani, Efficient microwave assisted synthesis of metal–organic framework UiO-66: optimization and scale up, Dalton Trans. 44 (2015) 14019–14026.
[59] Y. Thi Dang, H.T. Hoang, H.C. Dong, K.-B.-T. Bui, L.H.T. Nguyen, T.B. Phan, Y. Kawazoe, T.L.H. Doan, Microwave-assisted synthesis of nano Hf- and Zr-based metal-organic frameworks for enhancement of curcumin adsorption, Microporous Mesoporous Mater. 298 (2020) 110064.
[60] B. Karadeniz, A.J. Howarth, T. Stolar, T. Islamoglu, I. Dejanović, M. Tireli, M.C. Wasson, S.-Y. Moon, O.K. Farha, T. Friščić, K. Užarević, Benign by Design: Green and Scalable Synthesis of Zirconium UiO-Metal–Organic Frameworks by Water-Assisted Mechanochemistry, ACS Sustain. Chem. Eng. 6 (2018) 15841–15849.
[61] I.K. Shamsudin, I. Idris, A. Abdullah, J. Kim, M.R. Othman, Development of microporous Zr-MOF UiO-66 by sol-gel synthesis for CO2 capture from synthetic gas containing CO2 and H2, AIP Conf. Proc. 2124 (2019) 020057.
[62] K. Užarević, T.C. Wang, S.-Y. Moon, A.M. Fidelli, J.T. Hupp, O.K. Farha, T. Friščić, Mechanochemical and solvent-free assembly of zirconium-based metal–organic frameworks, Chem. Commun. 52 (2016) 2133–2136.
[63] H. Liu, Y. Zhao, C. Zhou, B. Mu, L. Chen, Microwave-assisted synthesis of Zr-based metal–organic framework (Zr-fum-fcu-MOF) for gas adsorption separation, Chem. Phys. Lett. 780 (2021) 138906.
[64] F.E. Salvador, V. Miller, K. Shimada, C.-H. Wang, J. Wright, M. Das, Y.-P. Chen, Y.-S. Chen, C. Sheehan, W. Xu, G. Rubasinghege, W.-Y. Gao, Mechanochemistry of Group 4 Element-Based Metal-Organic Frameworks, Inorg. Chem. 60 (2021) 16079–16084.
[65] M. Taddei, D.A. Steitz, J.A. van Bokhoven, M. Ranocchiari, Continuous-flow microwave synthesis of metal-organic frameworks: A highly efficient method for large-scale production, Chem. Eur. J. 22 (2016) 3245–3249.
[66] J. Ge, L. Liu, Y. Shen, Facile synthesis of amine-functionalized UiO-66 by microwave method and application for methylene blue adsorption, J. Porous Mater. 24 (2017) 647–655.
[67] X. Sang, J. Zhang, J. Xiang, J. Cui, L. Zheng, J. Zhang, Z. Wu, Z. Li, G. Mo, Y. Xu, J. Song, C. Liu, X. Tan, T. Luo, B. Zhang, B. Han, Ionic liquid accelerates the crystallization of Zr-based metal–organic frameworks, Nat. Commun. 8 (2017) 175.
[68] T. Tsuruoka, S. Furukawa, Y. Takashima, K. Yoshida, S. Isoda, S. Kitagawa, Nanoporous nanorods fabricated by coordination modulation and oriented attachment growth, Angew. Chem. Int. Ed. 48 (2009) 4739–4743.
[69] A. Schaate, S. Dühnen, G. Platz, S. Lilienthal, A.M. Schneider, P. Behrens, A novel Zr-based porous coordination polymer containing azobenzenedicarboxylate as a linker, Eur. J. Inorg. Chem. 2012 (2012) 790–796.
[70] V.V. Butova, A.P. Budnyk, A.A. Guda, K.A. Lomachenko, A.L. Bugaev, A.V. Soldatov, S.M. Chavan, S. Øien-Ødegaard, U. Olsbye, K.P. Lillerud, C. Atzori, S. Bordiga, C. Lamberti, Modulator effect in UiO-66-NDC (1,4-naphthalenedicarboxylic acid) synthesis and comparison with UiO-67-NDC isoreticular metal-organic frameworks, Cryst. Growth Des. 17 (2017) 5422–5431.
[71] O.V. Gutov, S. Molina, E.C. Escudero-Adán, A. Shafir, Modulation by amino acids: toward superior control in the synthesis of zirconium metal-organic frameworks, Chem. Eur. J. 22 (2016) 13582–13587.
[72] R.J. Marshall, C.L. Hobday, C.F. Murphie, S.L. Griffin, C.A. Morrison, S.A. Moggach, R.S. Forgan, Amino acids as highly efficient modulators for single crystals of zirconium and hafnium metal–organic frameworks, J. Mater. Chem. A 4 (2016) 6955–6963.
[73] V.V. Butova, A.P. Budnyk, K.M. Charykov, K.S. Vetlitsyna-Novikova, C. Lamberti, A.V. Soldatov, Water as a structure-driving agent between the UiO-66 and MIL-140A metal–organic frameworks, Chem. Commun. 55 (2019) 901–904.
[74] H.R. Abid, H.M. Ang, S. Wang, Effects of ammonium hydroxide on the structure and gas adsorption of nanosized Zr-MOFs, UiO-66, Nanoscale 4 (2012) 3089–3094.
[75] Y. Han, M. Liu, K. Li, Y. Zuo, Y. Wei, S. Xu, G. Zhang, C. Song, Z. Zhang, X. Guo, Facile synthesis of morphology and size-controlled zirconium metal–organic framework UiO-66: the role of hydrofluoric acid in crystallization, CrystEngComm 17 (2015) 6434–6440.
[76] M. Perfecto-Irigaray, G. Beobide, O. Castillo, I. da Silva, D. García-Lojo, A. Luque, A. Mendia, S. Pérez-Yáñez, [Zr6O4(OH)4(benzene-1,4-dicarboxylato)6]n: a hexagonal polymorph of UiO-66, Chem. Commun. 55 (2019) 5954–5957.
[77] M. Perfecto-Irigaray, G. Beobide, S. Calero, O. Castillo, I. da Silva, J.J. Gutierrez Sevillano, A. Luque, S. Pérez-Yáñez, L.F. Velasco, Metastable Zr/Hf-MOFs: the hexagonal family of EHU-30 and their water-sorption induced structural transformation, Inorg. Chem. Front. 8 (2021) 4767–4779.
[78] M. Rubio-Martinez, M.P. Batten, A. Polyzos, K.-C. Carey, J.I. Mardel, K.-S. Lim, M.R. Hill, Versatile, High Quality and Scalable Continuous Flow Production of Metal-Organic Frameworks, Sci. Rep. 4 (2014) 5443.
[79] P.M. Schoenecker, G.A. Belancik, B.E. Grabicka, K.S. Walton, Kinetics study and crystallization process design for scale-up of UiO-66-NH2 synthesis, AIChE J. 59 (2013) 1255–1262.
[80] S. Waitschat, M.T. Wharmby, N. Stock, Flow-synthesis of carboxylate and phosphonate based metal–organic frameworks under non-solvothermal reaction conditions, Dalton Trans. 44 (2015) 11235–11240.
[81] S. Tai, W. Zhang, J. Zhang, G. Luo, Y. Jia, M. Deng, Y. Ling, Facile preparation of UiO-66 nanoparticles with tunable sizes in a continuous flow microreactor and its application in drug delivery, Microporous Mesoporous Mater. 220 (2016) 148–154.
[82] Y. Huang, W. Qin, Z. Li, Y. Li, Enhanced stability and CO2 affinity of a UiO-66 type metal–organic framework decorated with dimethyl groups, Dalton Trans. 41 (2012) 9283–9285.
[83] S. Biswas, J. Zhang, Z. Li, Y.-Y. Liu, M. Grzywa, L. Sun, D. Volkmer, P. Van Der Voort, Enhanced selectivity of CO2 over CH4 in sulphonate-, carboxylate- and iodo-functionalized UiO-66 frameworks, Dalton Trans. 42 (2013) 4730–4737.
[84] Q. Yang, A.D. Wiersum, P.L. Llewellyn, V. Guillerm, C. Serre, G. Maurin, Functionalizing porous zirconium terephthalate UiO-66(Zr) for natural gas upgrading: a computational exploration, Chem. Commun. 47 (2011) 9603–9605.
[85] M. Kim, J.A. Boissonnault, P.V. Dau, S.M. Cohen, Metal-organic framework regioisomers based on bifunctional ligands, Angew. Chem. Int. Ed. 50 (2011) 12193–12196.
[86] M. Kim, S.J. Garibay, S.M. Cohen, Microwave-assisted cyanation of an aryl bromide directly on a metal−organic framework, Inorg. Chem. 50 (2011) 729–731.
[87] W. Morris, C.J. Doonan, O.M. Yaghi, Postsynthetic modification of a metal-organic framework for stabilization of a hemiaminal and ammonia uptake, Inorg. Chem. 50 (2011) 6853–6855.
[88] C. Zlotea, D. Phanon, M. Mazaj, D. Heurtaux, V. Guillerm, C. Serre, P. Horcajada, T. Devic, E. Magnier, F. Cuevas, G. Férey, P.L. Llewellyn, M. Latroche, Effect of NH2 and CF3 functionalization on the hydrogen sorption properties of MOFs, Dalton Trans. 40 (2011) 4879–4881.
[89] M. Lin Foo, S. Horike, T. Fukushima, Y. Hijikata, Y. Kubota, M. Takata, S. Kitagawa, Ligand-based solid solution approach to stabilisation of sulphonic acid groups in porous coordination polymer Zr6O4(OH)4(BDC)6 (UiO-66), Dalton Trans. 41 (2012) 13791–13794.
[90] S.J. Garibay, S.M. Cohen, Isoreticular synthesis and modification of frameworks with the UiO-66 topology, Chem. Commun. 46 (2010) 7700–7702.
[91] F. Vermoortele, R. Ameloot, A. Vimont, C. Serre, D. De Vos, An amino-modified Zr-terephthalate metal–organic framework as an acid–base catalyst for cross-aldol condensation, Chem. Mater. 47 (2011) 1521–1523.
[92] G.E. Cmarik, M. Kim, S.M. Cohen, K.S. Walton, Tuning the Adsorption Properties of UiO-66 via Ligand Functionalization, Langmuir 28 (2012) 15606–15613.
[93] K.-K. Yee, N. Reimer, J. Liu, S.-Y. Cheng, S.-M. Yiu, J. Weber, N. Stock, Z. Xu, Effective mercury sorption by thiol-laced metal-organic frameworks: in strong acid and the vapor phase, J. Am. Chem. Soc. 135 (2013) 7795–7798.
[94] W.J. Phang, H. Jo, W.R. Lee, J.H. Song, K. Yoo, B. Kim, C.S. Hong, Superprotonic conductivity of a UiO-66 Framework functionalized with sulfonic acid groups by facile postsynthetic oxidation, Angew. Chem. Int. Ed. 54 (2015) 5142–5146.

[95] M. Zha, J. Liu, Y.-L. Wong, Z. Xu, Extraction of palladium from nuclear waste-like acidic solutions by a metal–organic framework with sulfur and alkene functions, J. Mater. Chem. A 3 (2015) 3928–3934.
[96] W. Zhang, H. Huang, D. Liu, Q. Yang, Y. Xiao, Q. Ma, C. Zhong, A new metal–organic framework with high stability based on zirconium for sensing small molecules, Microporous Mesoporous Mater. 171 (2013) 118–124.
[97] S. Ghosh, S. Biswas, Ultrafast and nanomolar level detection of H2S in aqueous medium using a functionalized UiO-66 metal-organic framework based fluorescent chemosensor, Dalton Trans. 50 (2021) 11631–11639.
[98] M. Kandiah, M.H. Nilsen, S. Usseglio, S. Jakobsen, U. Olsbye, M. Tilset, C. Larabi, E.A. Quadrelli, F. Bonino, K.P. Lillerud, Synthesis and stability of tagged UiO-66 Zr-MOFs, Chem. Mater. 22 (2010) 6632–6640.
[99] A.A. Barkhordarian, C.J. Kepert, Two new porous UiO-66-type zirconium frameworks; open aromatic N-donor sites and their post-synthetic methylation and metallation, J. Mater. Chem. A 5 (2017) 5612–5618.
[100] L. Zhang, L. Li, E. Hu, L. Yang, K. Shao, L. Yao, K. Jiang, Y. Cui, Y. Yang, B. Li, B. Chen, G. Qian, Boosting Ethylene/ethane separation within Copper(I)-chelated metal-organic frameworks through tailor-made aperture and specific π-complexation, Adv. Sci. 7 (2020) 1901918.
[101] J. Ethiraj, E. Albanese, B. Civalleri, J.G. Vitillo, F. Bonino, S. Chavan, G.C. Shearer, K.P. Lillerud, S. Bordiga, Carbon dioxide adsorption in amine-functionalized mixed-ligand metal-organic frameworks of UiO-66 topology, ChemSusChem 7 (2014) 3382–3388.
[102] G.W. Peterson, S.-Y. Moon, G.W. Wagner, M.G. Hall, J.B. DeCoste, J.T. Hupp, O. K. Farha, Tailoring the pore size and functionality of UiO-type metal-organic frameworks for optimal nerve agent destruction, Inorg. Chem. 54 (2015) 9684–9686.
[103] I. Stassen, B. Bueken, H. Reinsch, J.F.M. Oudenhoven, D. Wouters, J. Hajek, V. Van Speybroeck, N. Stock, P.M. Vereecken, R. Van Schaijk, D. De Vos, R. Ameloot, Towards metal–organic framework based field effect chemical sensors: UiO-66-NH2 for nerve agent detection, Chem. Sci. 7 (2016) 5827–5832.
[104] M.J. Katz, S.-Y. Moon, J.E. Mondloch, M.H. Beyzavi, C.J. Stephenson, J.T. Hupp, O.K. Farha, Exploiting parameter space in MOFs: a 20-fold enhancement of phosphate-ester hydrolysis with UiO-66-NH2, Chem. Sci. 6 (2015) 2286–2291.
[105] G.W. Peterson, J.J. Mahle, J.B. DeCoste, W.O. Gordon, J.A. Rossin, Extraordinary NO2 Removal by the Metal-Organic Framework UiO-66-NH2, Angew. Chem. Int. Ed. 55 (2016) 6235–6238.
[106] H. Jasuja, G.W. Peterson, J.B. Decoste, M.A. Browe, K.S. Walton, Evaluation of MOFs for air purification and air quality control applications: Ammonia removal from air, Chem. Eng. Sci. 124 (2015) 118–124.
[107] A.J. Howarth, M.J. Katz, T.C. Wang, A.E. Platero-Prats, K.W. Chapman, J.T. Hupp, O.K. Farha, High Efficiency Adsorption and Removal of Selenate and Selenite from Water Using Metal-Organic Frameworks, J. Am. Chem. Soc. 137 (2015) 7488–7494.
[108] Y.-A. Li, C.-W. Zhao, N.-X. Zhu, Q.-K. Liu, G.-J. Chen, J.-B. Liu, X.-D. Zhao, J.-P. Ma, S. Zhang, Y.-B. Dong, Nanoscale UiO-MOF-based luminescent sensors for highly selective detection of cysteine and glutathione and their application in bioimaging, Chem. Commun. 51 (2015) 17672–17675.
[109] H. Jasuja, K.S. Walton, Experimental Study of CO2, CH4, and Water Vapor Adsorption on a Dimethyl-Functionalized UiO-66 Framework, J. Phys. Chem. C 117 (2013) 7062–7068.
[110] X. Han, X. Yang, C. Yu, S. Lu, E.S. Pouya, P. Bai, J. Lyu, X. Guo, Fine-tuning the pore structure of metal–organic frameworks by linker substitution for enhanced hydrogen storage and gas separation, CrystEngComm 23 (2021) 3026–3032.
[111] S. Wang, S. Fan, Z. Fang, Y. Hu, M. Dong, X. Peng, NH2-UiO-66 Metal-Organic Framework Nanoparticles for Hydroxide Ion Conductive Photoswitches, ACS Appl, Nano Mater, 2021.
[112] L. Shen, R. Liang, M. Luo, F. Jing, L. Wu, Electronic effects of ligand substitution on metal–organic framework photocatalysts: the case study of UiO-66, PCCP 17 (2015) 117–121.
[113] D. Sun, Y. Fu, W. Liu, L. Ye, D. Wang, L. Yang, X. Fu, Z. Li, Studies on photocatalytic CO2 reduction over NH2-Uio-66(Zr) and its derivatives: towards a better understanding of photocatalysis on metal-organic frameworks, Chem. Eur. J. 19 (2013) 14279–14285.
[114] C. Gomes Silva, I. Luz, F.X. Llabrés i Xamena, A. Corma, H. García, Water stable Zr–benzenedicarboxylate metal-organic frameworks as photocatalysts for hydrogen generation, Chem. Eur. J. 16 (2010) 11133–11138.
[115] T. Toyao, M. Saito, Y. Horiuchi, K. Mochizuki, M. Iwata, H. Higashimura, M. Matsuoka, Efficient hydrogen production and photocatalytic reduction of nitrobenzene over a visible-light-responsive metal–organic framework photocatalyst, Catal, Sci. Technol. 3 (2013) 2092–2097.
[116] F. Vermoortele, M. Vandichel, B. Van de Voorde, R. Ameloot, M. Waroquier, V. Van Speybroeck, D.E. De Vos, Electronic effects of linker substitution on lewis acid catalysis with metal-organic frameworks, Angew. Chem. Int. Ed. 51 (2012) 4887–4890.
[117] J.M. Mayers, R.W. Larsen, The effect of cavity size on ruthenium (II) Tris-(2,2-bipyridine) photophysics encapsulated within zirconium based metal organic frameworks, Inorganica Chim. Acta (2021) 120537.
[118] S.S. Nagarkar, T. Saha, A.V. Desai, P. Talukdar, S.K. Ghosh, Metal-organic framework based highly selective fluorescence turn-on probe for hydrogen sulphide, Sci. Rep. 4 (2014) 7053.
[119] L. Li, S. Tang, C. Wang, X. Lv, M. Jiang, H. Wu, X. Zhao, High gas storage capacities and stepwise adsorption in a UiO type metal–organic framework incorporating Lewis basic bipyridyl sites, Chem. Commun. 50 (2014) 2304–2307.
[120] X.-C. Yi, F.-G. Xi, Y. Qi, E.-Q. Gao, Synthesis and click modification of an azido-functionalized Zr(iv) metal–organic framework and a catalytic study, RSC Adv. 5 (2015) 893–900.
[121] T. Islamoglu, M.A. Ortuño, E. Proussaloglou, A.J. Howarth, N.A. Vermeulen, A. Atilgan, A.M. Asiri, C.J. Cramer, O.K. Farha, Presence versus proximity: the role of pendant amines in the catalytic hydrolysis of a nerve agent simulant, Angew. Chem. Int. Ed. 57 (2018) 1949–1953.
[122] B. Wang, H. Huang, X.-L. Lv, Y. Xie, M. Li, J.-R. Li, Tuning CO2 selective adsorption over N2 and CH4 in UiO-67 analogues through ligand functionalization, Inorg. Chem. 53 (2014) 9254–9259.
[123] X. Wang, L. Li, Y. Wang, J.-R. Li, J. Li, Exploiting the pore size and functionalization effects in UiO topology structures for the separation of light hydrocarbons, CrystEngComm 19 (2017) 1729–1737.
[124] S. Demir, N. Bilgin, H.M. Cepni, H. Furukawa, F. Yilmaz, C. Altintas, S. Keskin, Enhanced water stability and high CO2 storage capacity of a Lewis basic sites-containing zirconium metal–organic framework, Dalton Trans. 50 (2021) 16587–16592.
[125] N.-X. Zhu, Z.-W. Wei, C.-X. Chen, X.-H. Xiong, Y.-Y. Xiong, Z. Zeng, W. Wang, J.-J. Jiang, Y.-N. Fan, C.-Y. Su, High Water Adsorption MOFs with Optimized Pore-Nanospaces for Autonomous Indoor Humidity Control and Pollutants Removal, Angew. Chem. Int. Ed. 61 (2022) e202112097.
[126] V. Bon, I. Senkovska, M.S. Weiss, S. Kaskel, Tailoring of network dimensionality and porosity adjustment in Zr- and Hf-based MOFs, CrystEngComm 15 (2013) 9572–9577.
[127] K. Manna, T. Zhang, F.X. Greene, W. Lin, Bipyridine- and Phenanthroline-Based Metal-Organic Frameworks for Highly Efficient and Tandem Catalytic Organic Transformations via Directed C-H Activation, J. Am. Chem. Soc. 137 (2015) 2665–2673.
[128] Q. Yang, V. Guillerm, F. Ragon, A.D. Wiersum, P.L. Llewellyn, C. Zhong, T. Devic, C. Serre, G. Maurin, CH4 storage and CO2 capture in highly porous zirconium oxide based metal–organic frameworks, Chem. Commun. 48 (2012) 9831–9833.
[129] M. Sarker, S. Shin, S.H. Jhung, Synthesis and Functionalization of Porous Zr-Diaminostilbenedicarboxylate Metal-Organic Framework for Storage and Stable Delivery of Ibuprofen, ACS Omega 4 (2019) 9860–9867.
[130] Y.-A. Li, X.-D. Zhao, H.-P. Yin, G.-J. Chen, S. Yang, Y.-B. Dong, A drug-loaded nanoscale metal–organic framework with a tumor targeting agent for highly effective hepatoma therapy, Chem. Commun. 52 (2016) 14113–14116.
[131] C. Tan, X. Han, Z. Li, Y. Liu, Y. Cui, Controlled Exchange of Achiral Linkers with Chiral Linkers in Zr-Based UiO-68 Metal-Organic Framework, J. Am. Chem. Soc. 140 (2018) 16229–16236.
[132] H.-L. Jiang, D. Feng, T.-F. Liu, J.-R. Li, H.-C. Zhou, Pore Surface Engineering with Controlled Loadings of Functional Groups via Click Chemistry in Highly Stable Metal-Organic Frameworks, J. Am. Chem. Soc. 134 (2012) 14690–14693.
[133] A. Mallick, A.M. El-Zohry, O. Shekhah, J. Yin, J. Jia, H. Aggarwal, A.-H. Emwas, O.F. Mohammed, M. Eddaoudi, Unprecedented Ultralow Detection Limit of Amines using a Thiadiazole-Functionalized Zr(IV)-Based Metal-Organic Framework, J. Am. Chem. Soc. 141 (2019) 7245–7249.
[134] M. Sk, S. Biswas, A thiadiazole-functionalized Zr(iv)-based metal–organic framework as a highly fluorescent probe for the selective detection of picric acid, CrystEngComm 18 (2016) 3104–3113.
[135] J. Jia, L. Gutiérrez-Arzaluz, O. Shekhah, N. Alsadun, J. Czaban-Jóźwiak, S. Zhou, O.M. Bakr, O.F. Mohammed, M. Eddaoudi, Access to Highly Efficient Energy Transfer in Metal-Organic Frameworks via Mixed Linkers Approach, J. Am. Chem. Soc. 142 (2020) 8580–8584.
[136] C. Kutzscher, G. Nickerl, I. Senkovska, V. Bon, S. Kaskel, Proline functionalized UiO-67 and UiO-68 type metal-organic frameworks showing reversed diastereoselectivity in aldol addition reactions, Chem. Mater. 28 (2016) 2573–2580.
[137] J. Perego, I. Villa, A. Pedrini, E.C. Padovani, R. Crapanzano, A. Vedda, C. Dujardin, C.X. Bezuidenhout, S. Bracco, P.E. Sozzani, A. Comotti, L. Gironi, M. Beretta, M. Salomoni, N. Kratochwil, S. Gundacker, E. Auffray, F. Meinardi, A. Monguzzi, Composite fast scintillators based on high-Z fluorescent metal–organic framework nanocrystals, Nat. Photonics 15 (2021) 393–400.
[138] J.-X. Wang, J. Yin, O. Shekhah, O.M. Bakr, M. Eddaoudi, O.F. Mohammed, Energy Transfer in Metal-Organic Frameworks for Fluorescence Sensing, ACS Appl. Mater. Interfaces 14 (2022) 9970–9986.
[139] K. Manna, P. Ji, F.X. Greene, W. Lin, Metal-Organic Framework Nodes Support Single-Site Magnesium-Alkyl Catalysts for Hydroboration and Hydroamination Reactions, J. Am. Chem. Soc. 138 (2016) 7488–7491.
[140] C. Wang, K.E. deKrafft, W. Lin, Pt Nanoparticles@Photoactive Metal-Organic Frameworks: Efficient Hydrogen Evolution via Synergistic Photoexcitation and Electron Injection, J. Am. Chem. Soc. 134 (2012) 7211–7214.
[141] J.B. DeCoste, G.W. Peterson, H. Jasuja, T.G. Glover, Y.-G. Huang, K.S. Walton, Stability and degradation mechanisms of metal–organic frameworks containing the Zr6O4(OH)4 secondary building unit, J. Mater. Chem. A 1 (2013) 5642–5650.
[142] M.C. Lawrence, C. Schneider, M.J. Katz, Determining the structural stability of UiO-67 with respect to time: a solid-state NMR investigation, Chem. Commun. 52 (2016) 4971–4974.
[143] J.E. Mondloch, M.J. Katz, N. Planas, D. Semrouni, L. Gagliardi, J.T. Hupp, O.K. Farha, Are Zr6-based MOFs water stable? Linker hydrolysis vs. capillary-force-driven channel collapse, Chem. Commun. 50 (2014) 8944–8946.

[144] E. Moumen, A.H. Assen, K. Adil, Y. Belmabkhout, Versatility vs stability. Are the assets of metal–organic frameworks deployable in aqueous acidic and basic media?, Coord. Chem. Rev. 443 (2021) 214020.
[145] V. Guillerm, F. Ragon, M. Dan-Hardi, T. Devic, M. Vishnuvarthan, B. Campo, A. Vimont, G. Clet, Q. Yang, G. Maurin, G. Férey, A. Vittadini, S. Gross, C. Serre, A Series of Isoreticular, Highly Stable, Porous Zirconium Oxide Based Metal-Organic Frameworks, Angew. Chem. Int. Ed. 51 (2012) 9267–9271.
[146] S.M.J. Rogge, M. Waroquier, V. Van Speybroeck, Reliably Modeling the Mechanical Stability of Rigid and Flexible Metal-Organic Frameworks, Acc. Chem. Res. 51 (2018) 138–148.
[147] G. Wißmann, A. Schaate, S. Lilienthal, I. Bremer, A.M. Schneider, P. Behrens, Modulated synthesis of Zr-fumarate MOF, Microporous Mesoporous Mater. 152 (2012) 64–70.
[148] G. Zahn, H.A. Schulze, J. Lippke, S. König, U. Sazama, M. Fröba, P. Behrens, A water-born Zr-based porous coordination polymer: Modulated synthesis of Zr-fumarate MOF, Microporous Mesoporous Mater. 203 (2015) 186–194.
[149] M. Ganesh, P. Hemalatha, M.M. Peng, W.S. Cha, H.T. Jang, Zr-Fumarate MOF a Novel CO2-Adsorbing Material: Synthesis and Characterization, Aerosol Air, Qual. Res. 14 (2014) 1605–1612.
[150] J. Zhang, H.-J. Bai, Q. Ren, H.-B. Luo, X.-M. Ren, Z.-F. Tian, S. Lu, Extra Water- and Acid-Stable MOF-801 with High Proton Conductivity and Its Composite Membrane for Proton-Exchange Membrane, ACS Appl. Mater. Interfaces 10 (2018) 28656–28663.
[151] M. Sk, S. Bhowal, S. Biswas, Synthesis, Characterization, Stability, and Gas Adsorption Characteristics of a Highly Stable Zirconium Mesaconate Framework Material, Eur. J. Inorg. Chem. 2015 (2015) 3317–3322.
[152] S. Zhou, O. Shekhah, J. Jia, J. Czaban-Jóźwiak, P.M. Bhatt, A. Ramírez, J. Gascon, M. Eddaoudi, Electrochemical synthesis of continuous metal–organic framework membranes for separation of hydrocarbons, Nat. Energy 6 (2021) 882–891.
[153] H. Liu, B. Li, Y. Zhao, C. Kong, C. Zhou, Y. Lin, Z. Tian, L. Chen, Investigation on Zr-based metal-organic framework (MOF-801) for high-performance separation of light alkanes, Chem. Commun. 57 (2021) 13008–13011.
[154] A. Buragohain, S. Biswas, Improved synthesis of a Zirconium(IV) muconate metal-organic framework: characterization, stability and gas sorption properties, Eur. J. Inorg. Chem. 2015 (2015) 2463–2468.
[155] K.B. Idrees, Z. Chen, X. Zhang, M.R. Mian, R.J. Drout, T. Islamoglu, O.K. Farha, Tailoring pore aperture and structural defects in zirconium-based metal-organic frameworks for krypton/xenon separation, Chem. Mater. 32 (2020) 3776–3782.
[156] G. Han, K. Wang, Y. Peng, Y. Zhang, H. Huang, C. Zhong, Enhancing higher hydrocarbons capture for natural gas upgrading by tuning van der waals interactions in fcu-Type Zr-MOFs, Ind. Eng. Chem. Res. 56 (2017) 14633–14641.
[157] D.-H. Nam, O. Shekhah, G. Lee, A. Mallick, H. Jiang, F. Li, B. Chen, J. Wicks, M. Eddaoudi, E.H. Sargent, Intermediate binding control using metal-organic frameworks enhances electrochemical CO2 reduction, J. Am. Chem. Soc. 142 (2020) 21513–21521.
[158] D. Cunha, C. Gaudin, I. Colinet, P. Horcajada, G. Maurin, C. Serre, Rationalization of the entrapping of bioactive molecules into a series of functionalized porous zirconium terephthalate MOFs, J. Mater. Chem. B 1 (2013) 1101–1108.
[159] Y.-M. Chung, H.-Y. Kim, W.-S. Ahn, Friedel-crafts acylation of p-xylene over sulfonated zirconium terephthalates, Catal. Lett. 144 (2014) 817–824.
[160] J.N. Joshi, E.Y. Garcia-Gutierrez, C.M. Moran, J.I. Deneff, K.S. Walton, Engineering copper carboxylate functionalities on water stable metal-organic frameworks for enhancement of ammonia removal capacities, J. Phys. Chem. C 121 (2017) 3310–3319.
[161] N. Ko, J. Hong, S. Sung, K.E. Cordova, H.J. Park, J.K. Yang, J. Kim, A significant enhancement of water vapour uptake at low pressure by amine-functionalization of UiO-67, Dalton Trans. 44 (2015) 2047–2051.
[162] E.S. Gutterød, S. Øien-Ødegaard, K. Bossers, A.-E. Nieuwelink, M. Manzoli, L. Braglia, A. Lazzarini, E. Borfecchia, S. Ahmadigoltapeh, B. Bouchevreau, B.T. Lønstad-Bleken, R. Henry, C. Lamberti, S. Bordiga, B.M. Weckhuysen, K.P. Lillerud, U. Olsbye, CO2 hydrogenation over pt-containing UiO-67 Zr-MOFs—the base case, Ind. Eng. Chem. Res. 56 (2017) 13206–13218.
[163] K. Manna, T. Zhang, M. Carboni, C.W. Abney, W. Lin, Salicylaldimine-based metal-organic framework enabling highly active olefin hydrogenation with iron and cobalt catalysts, J. Am. Chem. Soc. 136 (2014) 13182–13185.
[164] J. Ren, H.W. Langmi, B.C. North, M. Mathe, D. Bessarabov, Modulated synthesis of zirconium-metal organic framework (Zr-MOF) for hydrogen storage applications, Int. J. Hydrog. Energy 39 (2014) 890–895.
[165] J. Ren, N.M. Musyoka, H.W. Langmi, B.C. North, M. Mathe, X. Kang, Fabrication of core–shell MIL-101(Cr)@UiO-66(Zr) nanocrystals for hydrogen storage, Int. J. Hydrog. Energy 39 (2014) 14912–14917.
[166] H.R. Abid, H. Tian, H.-M. Ang, M.O. Tade, C.E. Buckley, S. Wang, Nanosize Zr-metal organic framework (UiO-66) for hydrogen and carbon dioxide storage, Chem. Eng. J. 187 (2012) 415–420.
[167] K. Dedecker, R.S. Pillai, F. Nouar, J. Pires, N. Steunou, E. Dumas, G. Maurin, C. Serre, M.L. Pinto, Metal-organic frameworks for cultural heritage preservation: the case of acetic acid removal, ACS Appl. Mater. Interfaces 10 (2018) 13886–13894.
[168] Y.S. Seo, N.A. Khan, S.H. Jhung, Adsorptive removal of methylchlorophenoxypropionic acid from water with a metal-organic framework, Chem. Eng. J. 270 (2015) 22–27.
[169] P. Zhao, N. Liu, C. Jin, H. Chen, Z. Zhang, L. Zhao, P. Cheng, Y. Chen, UiO-66: An advanced platform for investigating the influence of functionalization in the adsorption removal of pharmaceutical waste, Inorg. Chem. 58 (2019) 8787–8792.
[170] E. Žunkovič, M. Mazaj, G. Mali, M. Rangus, T. Devic, C. Serre, N.Z. Logar, Structural study of Ni- or Mg-based complexes incorporated within UiO-66-NH2 framework and their impact on hydrogen sorption properties, J. Solid State Chem. 225 (2015) 209–215.
[171] Z. Hu, M. Khurana, Y.H. Seah, M. Zhang, Z. Guo, D. Zhao, Ionized Zr-MOFs for highly efficient post-combustion CO2 capture, Chem. Eng. Sci. 124 (2015) 61–69.
[172] M.A. Moreira, J.C. Santos, A.F.P. Ferreira, J.M. Loureiro, F. Ragon, P. Horcajada, K.-E. Shim, Y.-K. Hwang, U.H. Lee, J.-S. Chang, C. Serre, A.E. Rodrigues, Reverse shape selectivity in the liquid-phase adsorption of xylene isomers in zirconium terephthalate MOF UiO-66, Langmuir 28 (2012) 5715–5723.
[173] L.-J. Li, P.-Q. Liao, C.-T. He, Y.-S. Wei, H.-L. Zhou, J.-M. Lin, X.-Y. Li, J.-P. Zhang, Grafting alkylamine in UiO-66 by charge-assisted coordination bonds for carbon dioxide capture from high-humidity flue gas, J. Mater. Chem. A 3 (2015) 21849–21855.
[174] R.D. Arrua, A. Peristyy, P.N. Nesterenko, A. Das, D.M. D'Alessandro, E.F. Hilder, UiO-66@SiO2 core–shell microparticles as stationary phases for the separation of small organic molecules, Analyst 142 (2017) 517–524.
[175] Y. Liu, Z. Chen, G. Liu, Y. Belmabkhout, K. Adil, M. Eddaoudi, W. Koros, Conformation-controlled molecular sieving effects for membrane-based propylene/propane separation, Adv. Mater. 31 (2019) 1807513.
[176] F. Vermoortele, B. Bueken, G. Le Bars, B. Van de Voorde, M. Vandichel, K. Houthoofd, A. Vimont, M. Daturi, M. Waroquier, V. Van Speybroeck, C. Kirschhock, D.E. De Vos, Synthesis modulation as a tool to increase the catalytic activity of metal-organic frameworks: The unique case of UiO-66 (Zr), J. Am. Chem. Soc. 135 (2013) 11465–11468.
[177] A. Jrad, M. Hmadeh, B.J. Abu Tarboush, G. Awada, M. Ahmad, Structural engineering of Zr-based metal-organic framework catalysts for optimized biofuel additives production, Chem. Eng. J. 382 (2020) 122793.
[178] V.N. Panchenko, M.M. Matrosova, J. Jeon, J.W. Jun, M.N. Timofeeva, S.H. Jhung, Catalytic behavior of metal–organic frameworks in the Knoevenagel condensation reaction, J. Catal. 316 (2014) 251–259.
[179] A.M. Plonka, Q. Wang, W.O. Gordon, A. Balboa, D. Troya, W. Guo, C.H. Sharp, S. D. Senanayake, J.R. Morris, C.L. Hill, A.I. Frenkel, In situ probes of capture and decomposition of chemical warfare agent simulants by Zr-based metal organic frameworks, J. Am. Chem. Soc. 139 (2017) 599–602.
[180] S. Pu, L. Xu, L. Sun, H. Du, Tuning the optical properties of the zirconium–UiO-66 metal–organic framework for photocatalytic degradation of methyl orange, Inorg. Chem. Commun. 52 (2015) 50–52.
[181] V.L. Rechac, F.G. Cirujano, A. Corma, F.x., Llabrés i Xamena, Diastereoselective Synthesis of Pyranoquinolines on Zirconium-Containing UiO-66 Metal-Organic Frameworks, Eur. J. Inorg. Chem. (2016, 2016,) 4512–4516.
[182] L. Shen, S. Liang, W. Wu, R. Liang, L. Wu, Multifunctional NH2-mediated zirconium metal–organic framework as an efficient visible-light-driven photocatalyst for selective oxidation of alcohols and reduction of aqueous Cr(vi), Dalton Trans. 42 (2013) 13649–13657.
[183] D. Yang, M.A. Ortuño, V. Bernales, C.J. Cramer, L. Gagliardi, B.C. Gates, Structure and Dynamics of Zr6O8 Metal-Organic Framework Node Surfaces Probed with Ethanol Dehydration as a Catalytic Test Reaction, J. Am. Chem. Soc. 140 (2018) 3751–3759.
[184] H. Liu, L. Chang, C. Bai, L. Chen, R. Luque, Y. Li, Controllable Encapsulation of "Clean" Metal Clusters within MOFs through Kinetic Modulation: Towards Advanced Heterogeneous Nanocatalysts, Angew. Chem. Int. Ed. 55 (2016) 5019–5023.
[185] E. López-Maya, C. Montoro, L.M. Rodríguez-Albelo, S.D. Aznar Cervantes, A.A. Lozano-Pérez, J.L. Cenís, E. Barea, J.A.R. Navarro, Textile/metal–organic-framework composites as self-detoxifying filters for chemical-warfare agents, Angew. Chem. Int. Ed. 54 (2015) 6790–6794.
[186] C. Orellana-Tavra, E.F. Baxter, T. Tian, T.D. Bennett, N.K.H. Slater, A.K. Cheetham, D. Fairen-Jimenez, Amorphous metal–organic frameworks for drug delivery, Chem. Commun. 51 (2015) 13878–13881.
[187] X. Zhu, J. Gu, Y. Wang, B. Li, Y. Li, W. Zhao, J. Shi, Inherent anchorages in UiO-66 nanoparticles for efficient capture of alendronate and its mediated release, Chem. Commun. 50 (2014) 8779–8782.
[188] M. Nazari, M. Rubio-Martinez, G. Tobias, J.P. Barrio, R. Babarao, F. Nazari, K. Konstas, B.W. Muir, S.F. Collins, A.J. Hill, M.C. Duke, M.R. Hill, Metal-organic-framework-coated optical fibers as light-triggered drug delivery vehicles, Adv. Funct. Mater. 26 (2016) 3244–3249.
[189] X. Feng, L. Zeng, D. Zou, Z. Zhang, G. Zhong, S. Peng, L. Liu, L. Chen, J. Zhang, Trace-doped metal–organic gels with remarkably enhanced luminescence, RSC Adv. 7 (2017) 37194–37199.
[190] C. Li, J. Huang, H. Zhu, L. Liu, Y. Feng, G. Hu, X. Yu, Dual-emitting fluorescence of Eu/Zr-MOF for ratiometric sensing formaldehyde, Sens. Actuators B Chem. 253 (2017) 275–282.
[191] S.S. Nagarkar, A.V. Desai, S.K. Ghosh, A fluorescent metal–organic framework for highly selective detection of nitro explosives in the aqueous phase, Chem. Commun. 50 (2014) 8915–8918.
[192] A. Shahat, H.M.A. Hassan, H.M.E. Azzazy, Optical metal-organic framework sensor for selective discrimination of some toxic metal ions in water, Analyt. Chim. Acta 793 (2013) 90–98.

[193] X.-Y. Xu, B. Yan, Eu(III) functionalized Zr-based metal-organic framework as excellent fluorescent probe for Cd2+ detection in aqueous environment, Sens. Actuators B Chem. 222 (2016) 347–353.
[194] H.-T. Zhang, J.-W. Zhang, G. Huang, Z.-Y. Du, H.-L. Jiang, An amine-functionalized metal–organic framework as a sensing platform for DNA detection, Chem. Commun. 50 (2014) 12069–12072.
[195] X. Zhang, Z. Zhai, J. Wang, X. Hao, Y. Sun, S. Yu, X. Lin, Y. Qin, C. Li, Zr-MOF Combined with Nanofibers as an Efficient and Flexible Capacitive Sensor for Detecting SO2, ChemNanoMat 7 (2021) 1117.
[196] H.-Y. Zheng, X. Lian, S.-J. Qin, B. Yan, Novel "Turn-On" Fluorescent Probe for Highly Selectively Sensing Fluoride in Aqueous Solution Based on Tb3+-Functionalized Metal-Organic Frameworks, ACS Omega 3 (2018) 12513–12519.
[197] H. Wu, Y.S. Chua, V. Krungleviciute, M. Tyagi, P. Chen, T. Yildirim, W. Zhou, Unusual and Highly Tunable Missing-Linker Defects in Zirconium Metal-Organic Framework UiO-66 and Their Important Effects on Gas Adsorption, J. Am. Chem. Soc. 135 (2013) 10525–10532.
[198] M.J. Cliffe, W. Wan, X. Zou, P.A. Chater, A.K. Kleppe, M.G. Tucker, H. Wilhelm, N.P. Funnell, F.-X. Coudert, A.L. Goodwin, Correlated defect nanoregions in a metal–organic framework, Nat. Commun. 5 (2014) 4176.
[199] B. Bueken, N. Van Velthoven, A. Krajnc, S. Smolders, F. Taulelle, C. Mellot-Draznieks, G. Mali, T.D. Bennett, D. De Vos, Tackling the Defect Conundrum in UiO-66: A Mixed-Linker Approach to Engineering Missing Linker Defects, Chem. Mater. 29 (2017) 10478–10486.
[200] S.M.J. Rogge, J. Wieme, L. Vanduyfhuys, S. Vandenbrande, G. Maurin, T. Verstraelen, M. Waroquier, V. Van Speybroeck, Thermodynamic Insight in the High-Pressure Behavior of UiO-66: Effect of Linker Defects and Linker Expansion, Chem. Mater. 28 (2016) 5721–5732.
[201] Y. Jiao, Y. Liu, G. Zhu, J.T. Hungerford, S. Bhattacharyya, R.P. Lively, D.S. Sholl, K.S. Walton, Heat-Treatment of Defective UiO-66 from Modulated Synthesis: Adsorption and Stability Studies, J. Phys. Chem. C 121 (2017) 23471–23479.
[202] Z. Chen, L. Feng, L. Liu, P.M. Bhatt, K. Adil, A.-H. Emwas, A.H. Assen, Y. Belmabkhout, Y. Han, M. Eddaoudi, Enhanced Separation of Butane Isomers via Defect Control in a Fumarate/Zirconium-Based Metal Organic Framework, Langmuir 34 (2018) 14546–14551.
[203] P. Iacomi, F. Formalik, J. Marreiros, J. Shang, J. Rogacka, A. Mohmeyer, P. Behrens, R. Ameloot, B. Kuchta, P.L. Llewellyn, Role of structural defects in the adsorption and separation of C3 hydrocarbons in Zr-fumarate-MOF (MOF-801), Chem. Mater. 31 (2019) 8413–8423.
[204] L. Feng, S. Yuan, L.-L. Zhang, K. Tan, J.-L. Li, A. Kirchon, L.-M. Liu, P. Zhang, Y. Han, Y.J. Chabal, H.-C. Zhou, Creating hierarchical pores by controlled linker thermolysis in multivariate metal-organic frameworks, J. Am. Chem. Soc. 140 (2018) 2363–2372.
[205] V. Guillerm, H. Xu, J. Albalad, I. Imaz, D. Maspoch, Postsynthetic selective ligand cleavage by solid-gas phase ozonolysis fuses micropores into mesopores in metal-organic frameworks, J. Am. Chem. Soc. 140 (2018) 15022–15030.
[206] I. Abánades Lázaro, C.J.R. Wells, R.S. Forgan, Multivariate modulation of the Zr MOF UiO-66 for defect-controlled combination anticancer drug delivery, Angew. Chem. Int. Ed. 59 (2020) 5211–5217.
[207] Y. Wang, L. Li, P. Dai, L. Yan, L. Cao, X. Gu, X. Zhao, Missing-node directed synthesis of hierarchical pores on a zirconium metal–organic framework with tunable porosity and enhanced surface acidity via a microdroplet flow reaction, J. Mater. Chem. A 5 (2017) 22372–22379.
[208] Z. Wang, S. Hu, J. Yang, A. Liang, Y. Li, Q. Zhuang, J. Gu, Nanoscale Zr-based MOFs with tailorable size and introduced mesopore for protein delivery, Adv. Funct. Mater. 28 (2018) 1707356.
[209] P. Yang, F. Mao, Y. Li, Q. Zhuang, J. Gu, Hierarchical porous Zr-based MOFs synthesized by a facile monocarboxylic acid etching strategy, Chem. Eur. J. 24 (2018) 2962–2970.
[210] G.C. Shearer, J.G. Vitillo, S. Bordiga, S. Svelle, U. Olsbye, K.P. Lillerud, Functionalizing the defects: postsynthetic ligand exchange in the metal organic framework UiO-66, Chem. Mater. 28 (2016) 7190–7193.
[211] S. Li, J. Lin, Y. Ding, P. Xu, X. Guo, W. Xiong, D.-Y. Wu, Q. Dong, J. Chen, L. Zhang, Defects engineering of lightweight metal-organic frameworks-based electrocatalytic membrane for high-loading lithium-sulfur batteries, ACS Nano 15 (2021) 13803–13813.
[212] L.M. Rodríguez-Albelo, E. López-Maya, S. Hamad, A.R. Ruiz-Salvador, S. Calero, J.A.R. Navarro, Selective sulfur dioxide adsorption on crystal defect sites on an isoreticular metal organic framework series, Nat. Commun. 8 (2017) 14457.
[213] M. Erkartal, U. Sen, Boronic acid moiety as functional defect in UiO-66 and its effect on hydrogen uptake capacity and selective CO2 adsorption: A comparative study, ACS Appl. Mater. Interfaces 10 (2018) 787–795.
[214] N. Assaad, G. Sabeh, M. Hmadeh, Defect control in Zr-based metal-organic framework nanoparticles for arsenic removal from water, ACS Appl. Nano Mater. 3 (2020) 8997–9008.
[215] S.-X. Lin, W.-L. Pan, R.-J. Niu, Y. Liu, J.-X. Chen, W.-H. Zhang, J.-P. Lang, D.J. Young, Effective loading of cisplatin into a nanoscale UiO-66 metal–organic framework with preformed defects, Dalton Trans. 48 (2019) 5308–5314.
[216] Y. Xu, J. Lv, Y. Song, X. Zhou, C. Tian, X. Hong, Y. Cai, C. Zhao, Z. Lin, Efficient removal of low-concentration organoarsenic by Zr-based metal–organic frameworks: cooperation of defects and hydrogen bonds, Environ. Sci, NANO 6 (2019) 3590–3600.
[217] R. Xu, Q. Ji, P. Zhao, M. Jian, C. Xiang, C. Hu, G. Zhang, C. Tang, R. Liu, X. Zhang, J. Qu, Hierarchically porous UiO-66 with tunable mesopores and oxygen vacancies for enhanced arsenic removal, J. Mater. Chem. A 8 (2020) 7870–7879.
[218] A.M. Abdel-Mageed, B. Rungtaweevoranit, M. Parlinska-Wojtan, X. Pei, O.M. Yaghi, R.J. Behm, Highly active and stable single-atom cu catalysts supported by a metal-organic framework, J. Am. Chem. Soc. 141 (2019) 5201–5210.
[219] X. Chang, X.-F. Yang, Y. Qiao, S. Wang, M.-H. Zhang, J. Xu, D.-H. Wang, X.-H. Bu, Confined heteropoly blues in defected Zr-MOF (bottle around ship) for high-efficiency oxidative desulfurization, Small 16 (2020) 1906432.
[220] F.G. Cirujano, F.x. Llabrés i Xamena, Tuning the catalytic properties of UiO-66 metal-organic frameworks: from lewis to defect-induced brønsted acidity, J. Phys. Chem. Lett. 11 (2020) 4879–4890.
[221] M.-J. Dong, X. Wang, C.-D. Wu, Creation of redox-active pdsx nanoparticles inside the defect pores of MOF UiO-66 with unique semihydrogenation catalytic properties, Adv. Funct. Mater. 30 (2020) 1908519.
[222] E.S. Gutterød, S.H. Pulumati, G. Kaur, A. Lazzarini, B.G. Solemsli, A.E. Gunnæs, C. Ahoba-Sam, M.E. Kalyva, J.A. Sannes, S. Svelle, E. Skúlason, A. Nova, U. Olsbye, Influence of defects and H2O on the hydrogenation of CO2 to methanol over Pt nanoparticles in UiO-67 metal-organic framework, J. Am. Chem. Soc. 142 (2020) 17105–17118.
[223] X. Ma, L. Wang, Q. Zhang, H.-L. Jiang, Switching on the photocatalysis of metal-organic frameworks by engineering structural defects, Angew. Chem. Int. Ed. 58 (2019) 12175–12179.
[224] F. Meng, S. Zhang, L. Ma, W. Zhang, M. Li, T. Wu, H. Li, T. Zhang, X. Lu, F. Huo, J. Lu, Construction of hierarchically porous nanoparticles@metal–organic frameworks composites by inherent defects for the enhancement of catalytic efficiency, Adv. Mater. 30 (2018) 1803263.
[225] J. Wang, L. Liu, C. Chen, X. Dong, Q. Wang, L. Alfilfil, M.R. AlAlouni, K. Yao, J. Huang, D. Zhang, Y. Han, Engineering effective structural defects of metal–organic frameworks to enhance their catalytic performances, J. Mater. Chem. A 8 (2020) 4464–4472.
[226] D. Yang, C.A. Gaggioli, D. Ray, M. Babucci, L. Gagliardi, B.C. Gates, Tuning catalytic sites on Zr6O8 metal-organic framework nodes via ligand and defect chemistry probed with tert-butyl alcohol dehydration to isobutylene, J. Am. Chem. Soc. 142 (2020) 8044–8056.
[227] G. Ye, D. Zhang, X. Li, K. Leng, W. Zhang, J. Ma, Y. Sun, W. Xu, S. Ma, Boosting catalytic performance of metal-organic framework by increasing the defects via a facile and green approach, ACS Appl. Mater. Interfaces 9 (2017) 34937–34943.
[228] G.C. Shearer, S. Chavan, J. Ethiraj, J.G. Vitillo, S. Svelle, U. Olsbye, C. Lamberti, S. Bordiga, K.P. Lillerud, Tuned to perfection: ironing out the defects in metal-organic framework UiO-66, Chem. Mater. 26 (2014) 4068–4071.
[229] G.E. Decker, Z. Stillman, L. Attia, C.A. Fromen, E.D. Bloch, Controlling size, defectiveness, and fluorescence in nanoparticle uio-66 through water and ligand modulation, Chem. Mater. 31 (2019) 4831–4839.
[230] Y. Zhao, Q. Zhang, Y. Li, R. Zhang, G. Lu, Large-scale synthesis of monodisperse UiO-66 crystals with tunable sizes and missing linker defects via acid/base co-modulation, ACS Appl. Mater. Interfaces 9 (2017) 15079–15085.
[231] G.C. Shearer, S. Chavan, S. Bordiga, S. Svelle, U. Olsbye, K.P. Lillerud, Defect engineering: tuning the porosity and composition of the metal-organic framework UiO-66 via modulated synthesis, Chem. Mater. 28 (2016) 3749–3761.
[232] C. Atzori, G.C. Shearer, L. Maschio, B. Civalleri, F. Bonino, C. Lamberti, S. Svelle, K.P. Lillerud, S. Bordiga, Effect of benzoic acid as a modulator in the structure of UiO-66: an experimental and computational study, J. Phys. Chem. C 121 (2017) 9312–9324.
[233] P. St, G.N. Petkov, J. Vayssilov, O. Liu, Y. Shekhah, C. Wang, T.H. Wöll, Defects in MOFs: A thorough characterization, ChemPhysChem 13 (2012) 2025–2029.
[234] J.K. Bristow, K.L. Svane, D. Tiana, J.M. Skelton, J.D. Gale, A. Walsh, Free energy of ligand removal in the metal-organic framework UiO-66, J. Phys. Chem. C 120 (2016) 9276–9281.
[235] S. Øien, D. Wragg, H. Reinsch, S. Svelle, S. Bordiga, C. Lamberti, K.P. Lillerud, Detailed structure analysis of atomic positions and defects in zirconium metal-organic frameworks, Cryst. Growth Des. 14 (2014) 5370–5372.
[236] J. Ren, N.M. Musyoka, H.W. Langmi, J. Walker, M. Mathe, S. Liao, In-situ IR monitoring to probe the formation of structural defects in Zr-fumarate metal–organic framework (MOF), MOF, Polyhedron 153 (2018) 205–212.
[237] D.M. Driscoll, D. Troya, P.M. Usov, A.J. Maynes, A.J. Morris, J.R. Morris, Characterization of undercoordinated Zr defect sites in UiO-66 with vibrational spectroscopy of adsorbed CO, J. Phys. Chem. C 122 (2018) 14582–14589.
[238] V.S.D. Devulapalli, R.P. McDonnell, J.P. Ruffley, P.B. Shukla, T.-Y. Luo, M.L. De Souza, P. Das, N.L. Rosi, J.K. Johnson, E. Borguet, Identifying UiO-67 Metal-Organic Framework Defects and Binding Sites through Ammonia Adsorption, ChemSusChem 15 (2022) e202102217.
[239] Y. Liu, R.C. Klet, J.T. Hupp, O. Farha, Probing the correlations between the defects in metal–organic frameworks and their catalytic activity by an epoxide ring-opening reaction, Chem. Commun. 52 (2016) 7806–7809.
[240] S. Dissegna, P. Vervoorts, C.L. Hobday, T. Düren, D. Daisenberger, A.J. Smith, R. A. Fischer, G. Kieslich, Tuning the mechanical response of metal-organic frameworks by defect engineering, J. Am. Chem. Soc. 140 (2018) 11581–11584.

[241] D.N. Johnstone, F.C.N. Firth, C.P. Grey, P.A. Midgley, M.J. Cliffe, S.M. Collins, Direct imaging of correlated defect nanodomains in a metal-organic framework, J. Am. Chem. Soc. 142 (2020) 13081–13089.
[242] L. Liu, Z. Chen, J. Wang, D. Zhang, Y. Zhu, S. Ling, K.-W. Huang, Y. Belmabkhout, K. Adil, Y. Zhang, B. Slater, M. Eddaoudi, Y. Han, Imaging defects and their evolution in a metal–organic framework at sub-unit-cell resolution, Nat. Chem. 11 (2019) 622–628.
[243] J. Ren, M. Ledwaba, N.M. Musyoka, H.W. Langmi, M. Mathe, S. Liao, W. Pang, Structural defects in metal–organic frameworks (MOFs): Formation, detection and control towards practices of interests, Coord. Chem. Rev. 349 (2017) 169–197.
[244] Y. Feng, Q. Chen, M. Jiang, J. Yao, Tailoring the Properties of UiO-66 through Defect Engineering: A Review, Ind. Eng. Chem. Res. 58 (2019) 17646–17659.
[245] M. Taddei, When defects turn into virtues: The curious case of zirconium-based metal-organic frameworks, Coord. Chem. Rev. 343 (2017) 1–24.
[246] W. Xiang, Y. Zhang, Y. Chen, C.-J. Liu, X. Tu, Synthesis, characterization and application of defective metal–organic frameworks: current status and perspectives, J. Mater. Chem. A 8 (2020) 21526–21546.
[247] A. Schaate, P. Roy, T. Preuße, S.J. Lohmeier, A. Godt, P. Behrens, Porous Interpenetrated Zirconium-Organic Frameworks (PIZOFs): A Chemically Versatile Family of Metal-Organic Frameworks, Chem. Eur. J. 17 (2011) 9320–9325.
[248] R. Babarao, M. Rubio-Martinez, M.R. Hill, A.W. Thornton, Interpenetrated Zirconium-Organic Frameworks: Small Cavities versus Functionalization for CO2 Capture, J. Phys. Chem. C 120 (2016) 13013–13023.
[249] T.L.H. Doan, H.L. Nguyen, H.Q. Pham, N.-N. Pham-Tran, T.N. Le, K.E. Cordova, Tailoring the Optical Absorption of Water-Stable ZrIV- and HfIV-Based Metal-Organic Framework Photocatalysts, Chem. Asian J. 10 (2015) 2660–2668.
[250] R.J. Marshall, S.L. Griffin, C. Wilson, R.S. Forgan, Stereoselective Halogenation of Integral Unsaturated C-C Bonds in Chemically and Mechanically Robust Zr and Hf MOFs, Chem. Eur. J. 22 (2016) 4870–4877.
[251] R.J. Marshall, Y. Kalinovskyy, S.L. Griffin, C. Wilson, B.A. Blight, R.S. Forgan, Functional Versatility of a Series of Zr Metal-Organic Frameworks Probed by Solid-State Photoluminescence Spectroscopy, J. Am. Chem. Soc. 139 (2017) 6253–6260.
[252] J. Lippke, B. Brosent, T. von Zons, E. Virmani, S. Lilienthal, T. Preuße, M. Hülsmann, A.M. Schneider, S. Wuttke, P. Behrens, A. Godt, Expanding the Group of Porous Interpenetrated Zr-Organic Frameworks (PIZOFs) with Linkers of Different Lengths, Inorg. Chem. 56 (2017) 748–761.
[253] D. Chen, H. Xing, C. Wang, Z. Su, Highly efficient visible-light-driven CO2 reduction to formate by a new anthracene-based zirconium MOF via dual catalytic routes, J. Mater. Chem. A 4 (2016) 2657–2662.
[254] A. Torres-Huerta, D. Galicia-Badillo, A. Aguilar-Granda, J.T. Bryant, F.J. Uribe-Romo, B. Rodríguez-Molina, Multiple rotational rates in a guest-loaded, amphidynamic zirconia metal–organic framework, Chem. Sci. 11 (2020) 11579–11583.
[255] T.L.H. Doan, T.Q. Dao, H.N. Tran, P.H. Tran, T.N. Le, An efficient combination of Zr-MOF and microwave irradiation in catalytic Lewis acid Friedel-Crafts benzoylation, Dalton Trans. 45 (2016) 7875–7880.
[256] R.J. Marshall, S.L. Griffin, C. Wilson, R.S. Forgan, Single-Crystal to Single-Crystal Mechanical Contraction of Metal-Organic Frameworks through Stereoselective Postsynthetic Bromination, J. Am. Chem. Soc. 137 (2015) 9527–9530.
[257] S.M. Cohen, The Postsynthetic Renaissance in Porous Solids, J. Am. Chem. Soc. 139 (2017) 2855–2863.
[258] X. Chen, Y. Cai, R. Liang, Y. Tao, W. Wang, J. Zhao, X. Chen, H. Li, D. Zhang, NH2-UiO-66(Zr) with fast electron transfer routes for breaking down nitric oxide via photocatalysis, Appl. Catal. B 267 (2020) 118687.
[259] S. Chen, Y. Zhou, J. Li, Z. Hu, F. Dong, Y. Hu, H. Wang, L. Wang, K.K. Ostrikov, Z. Wu, Single-Atom Ru-Implanted Metal-Organic Framework/MnO2 for the Highly Selective Oxidation of NOx by Plasma Activation, ACS Catal. 10 (2020) 10185–10196.
[260] C.S. Hinde, W.R. Webb, B.K.J. Chew, H.R. Tan, W.-H. Zhang, T.S.A. Hor, R. Raja, Utilisation of gold nanoparticles on amine-functionalised UiO-66 (NH2-UiO-66) nanocrystals for selective tandem catalytic reactions, Chem. Commun. 52 (2016) 6557–6560.
[261] Z. Gu, L. Chen, B. Duan, Q. Luo, J. Liu, C. Duan, Synthesis of Au@UiO-66(NH2) structures by small molecule-assisted nucleation for plasmon-enhanced photocatalytic activity, Chem. Commun. 52 (2016) 116–119.
[262] Y. Luan, Y. Qi, H. Gao, N. Zheng, G. Wang, Synthesis of an amino-functionalized metal–organic framework at a nanoscale level for gold nanoparticle deposition and catalysis, J. Mater. Chem. A 2 (2014) 20588–20596.
[263] X. Zhang, Q. Hu, T. Xia, J. Zhang, Y. Yang, Y. Cui, B. Chen, G. Qian, Turn-on and Ratiometric Luminescent Sensing of Hydrogen Sulfide Based on Metal-Organic Frameworks, ACS Appl. Mater. Interfaces 8 (2016) 32259–32265.
[264] C. Wang, Z. Xie, K.E. deKrafft, W. Lin, Doping Metal-Organic Frameworks for Water Oxidation, Carbon Dioxide Reduction, and Organic Photocatalysis, J. Am. Chem. Soc. 133 (2011) 13445–13454.
[265] J.-L. Wang, C. Wang, W. Lin, Metal-Organic Frameworks for Light Harvesting and Photocatalysis, ACS Catal. 2 (2012) 2630–2640.
[266] M.I. Gonzalez, E.D. Bloch, J.A. Mason, S.J. Teat, J.R. Long, Single-Crystal-to-Single-Crystal Metalation of a Metal-Organic Framework: A Route toward Structurally Well-Defined Catalysts, Inorg. Chem. 54 (2015) 2995–3005.
[267] D. Kim, D.R. Whang, S.Y. Park, Self-Healing of Molecular Catalyst and Photosensitizer on Metal-Organic Framework: Robust Molecular System for Photocatalytic H2 Evolution from Water, J. Am. Chem. Soc. 138 (2016) 8698–8701.
[268] W.A. Maza, A.J. Haring, S.R. Ahrenholtz, C.C. Epley, S.Y. Lin, A.J. Morris, Ruthenium(ii)-polypyridyl zirconium(iv) metal–organic frameworks as a new class of sensitized solar cells, Chem. Sci. 7 (2016) 719–727.
[269] W.A. Maza, R. Padilla, A.J. Morris, Concentration Dependent Dimensionality of Resonance Energy Transfer in a Postsynthetically Doped Morphologically Homologous Analogue of UiO-67 MOF with a Ruthenium(II) Polypyridyl Complex, J. Am. Chem. Soc. 137 (2015) 8161–8168.
[270] X. Yu, S.M. Cohen, Photocatalytic metal–organic frameworks for the aerobic oxidation of arylboronic acids, Chem. Commun. 51 (2015) 9880–9883.
[271] K. Manna, T. Zhang, W. Lin, Postsynthetic Metalation of Bipyridyl-Containing Metal-Organic Frameworks for Highly Efficient Catalytic Organic Transformations, J. Am. Chem. Soc. 136 (2014) 6566–6569.
[272] T. Zhang, K. Manna, W. Lin, Metal-Organic Frameworks Stabilize Solution-Inaccessible Cobalt Catalysts for Highly Efficient Broad-Scope Organic Transformations, J. Am. Chem. Soc. 138 (2016) 3241–3249.
[273] Y.-A. Li, S. Yang, Q.-K. Liu, G.-J. Chen, J.-P. Ma, Y.-B. Dong, Pd(0)@UiO-68-AP: chelation-directed bifunctional heterogeneous catalyst for stepwise organic transformations, Chem. Commun. 52 (2016) 6517–6520.
[274] K. Hendrickx, J.J. Joos, A. De Vos, D. Poelman, P.F. Smet, V. Van Speybroeck, P. Van Der Voort, K. Lejaeghere, Exploring Lanthanide Doping in UiO-66: A Combined Experimental and Computational Study of the Electronic Structure, Inorg. Chem. 57 (2018) 5463–5474.
[275] M. Kim, J.F. Cahill, K.A. Prather, S.M. Cohen, Postsynthetic modification at orthogonal reactive sites on mixed, bifunctional metal–organic frameworks, Chem. Commun. 47 (2011) 7629–7631.
[276] Y. Lee, S. Kim, J.K. Kang, S.M. Cohen, Photocatalytic CO2 reduction by a mixed metal (Zr/Ti), mixed ligand metal–organic framework under visible light irradiation, Chem. Commun. 51 (2015) 5735–5738.
[277] T.W. Goh, C. Xiao, R.V. Maligal-Ganesh, X. Li, W. Huang, Utilizing mixed-linker zirconium based metal-organic frameworks to enhance the visible light photocatalytic oxidation of alcohol, Chem. Eng. Sci. 124 (2015) 45–51.
[278] Z.H. Rada, H.R. Abid, H. Sun, S. Wang, Bifunctionalized Metal Organic Frameworks, UiO-66-NO2-N (N = -NH2, -(OH)2, -(COOH)2), for Enhanced Adsorption and Selectivity of CO2 and N2, J. Chem. Eng. Data 60 (2015) 2152–2161.
[279] V.V. Butova, A.P. Budnyk, K.M. Charykov, K.S. Vetlitsyna-Novikova, A.L. Bugaev, A.A. Guda, A. Damin, S.M. Chavan, S. Øien-Ødegaard, K.P. Lillerud, A. V. Soldatov, C. Lamberti, Partial and Complete substitution of the 1,4-benzenedicarboxylate linker in UiO-66 with 1,4-naphthalenedicarboxylate: synthesis, characterization, and H2-adsorption properties, Inorg. Chem. 58 (2019) 1607–1620.
[280] V.V. Butova, O.A. Burachevskaya, I.V. Ozhogin, G.S. Borodkin, A.G. Starikov, S. Bordiga, A. Damin, K.P. Lillerud, A.V. Soldatov, UiO-66 type MOFs with mixed-linkers - 1,4-Benzenedicarboxylate and 1,4-naphthalenedicarboxylate: Effect of the modulator and post-synthetic exchange, Microporous Mesoporous Mater. 305 (2020) 110324.
[281] S. Marx, W. Kleist, J. Huang, M. Maciejewski, A. Baiker, Tuning functional sites and thermal stability of mixed-linker MOFs based on MIL-53(Al), Dalton Trans. 39 (2010) 3795–3798.
[282] M. Taddei, D. Tiana, N. Casati, J.A. van Bokhoven, B. Smit, M. Ranocchiari, Mixed-linker UiO-66: structure–property relationships revealed by a combination of high-resolution powder X-ray diffraction and density functional theory calculations, PCCP 19 (2017) 1551–1559.
[283] H. Fei, S.M. Cohen, A robust, catalytic metal–organic framework with open 2,2′-bipyridine sites, Chem. Commun. 50 (2014) 4810–4812.
[284] B. An, L. Zeng, M. Jia, Z. Li, Z. Lin, Y. Song, Y. Zhou, J. Cheng, C. Wang, W. Lin, Molecular Iridium Complexes in Metal-Organic Frameworks Catalyze CO2 Hydrogenation via Concerted Proton and Hydride Transfer, J. Am. Chem. Soc. 139 (2017) 17747–17750.
[285] J.A. Boissonnault, A.G. Wong-Foy, A.J. Matzger, Core-Shell Structures Arise Naturally During Ligand Exchange in Metal-Organic Frameworks, J. Am. Chem. Soc. 139 (2017) 14841–14844.
[286] M. Kim, J.F. Cahill, Y. Su, K.A. Prather, S.M. Cohen, Postsynthetic ligand exchange as a route to functionalization of 'inert' metal–organic frameworks, Chem. Sci. 3 (2012) 126–130.
[287] H. Fei, J. Shin, Y.S. Meng, M. Adelhardt, J. Sutter, K. Meyer, S.M. Cohen, Reusable Oxidation Catalysis Using Metal-Monocatecholato Species in a Robust Metal-Organic Framework, J. Am. Chem. Soc. 136 (2014) 4965–4973.
[288] H. Fei, S.M. Cohen, Metalation of a Thiocatechol-Functionalized Zr(IV)-Based Metal-Organic Framework for Selective C-H Functionalization, J. Am. Chem. Soc. 137 (2015) 2191–2194.
[289] S. Pullen, H. Fei, A. Orthaber, S.M. Cohen, S. Ott, Enhanced Photochemical Hydrogen Production by a Molecular Diiron Catalyst Incorporated into a Metal-Organic Framework, J. Am. Chem. Soc. 135 (2013) 16997–17003.
[290] Z. Hu, S. Faucher, Y. Zhuo, Y. Sun, S. Wang, D. Zhao, Combination of Optimization and Metalated-Ligand Exchange: An Effective Approach to Functionalize UiO-66(Zr) MOFs for CO2 Separation, Chem. Eur. J. 21 (2015) 17246–17255.
[291] G. Nickerl, I. Senkovska, S. Kaskel, Tetrazine functionalized zirconium MOF as an optical sensor for oxidizing gases, Chem. Commun. 51 (2015) 2280–2282.
[292] M. Kandiah, S. Usseglio, S. Svelle, U. Olsbye, K.P. Lillerud, M. Tilset, Post-synthetic modification of the metal–organic framework compound UiO-66, J. Mater. Chem. 20 (2010) 9848–9851.

[293] L. Garzón-Tovar, S. Rodríguez-Hermida, I. Imaz, D. Maspoch, Spray Drying for Making Covalent Chemistry: Postsynthetic Modification of Metal-Organic Frameworks, J. Am. Chem. Soc. 139 (2017) 897–903.
[294] A.M. Rasero-Almansa, A. Corma, M. Iglesias, F. Sánchez, Post-functionalized iridium–Zr-MOF as a promising recyclable catalyst for the hydrogenation of aromatics, Green Chem 16 (2014) 3522–3527.
[295] J. Tang, W. Dong, G. Wang, Y. Yao, L. Cai, Y. Liu, X. Zhao, J. Xu, L. Tan, Efficient molybdenum(vi) modified Zr-MOF catalysts for epoxidation of olefins, RSC Adv. 4 (2014) 42977–42982.
[296] M. Pintado-Sierra, A.M. Rasero-Almansa, A. Corma, M. Iglesias, F. Sánchez, Bifunctional iridium-(2-aminoterephthalate)–Zr-MOF chemoselective catalyst for the synthesis of secondary amines by one-pot three-step cascade reaction, J. Catal. 299 (2013) 137–145.
[297] X. Du, Y. Luan, F. Yang, D. Ramella, X. Shu, Picolinoyl functionalized MOF ligands for an air-promoted secondary alcohol oxidation with CuBr, New J. Chem. 41 (2017) 4400–4405.
[298] J. Aguilera-Sigalat, D. Bradshaw, A colloidal water-stable MOF as a broad-range fluorescent pH sensor via post-synthetic modification, Chem. Commun. 50 (2014) 4711–4713.
[299] H. Saleem, U. Rafique, R.P. Davies, Investigations on post-synthetically modified UiO-66-NH2 for the adsorptive removal of heavy metal ions from aqueous solution, Microporous Mesoporous Mater. 221 (2016) 238–244.
[300] H. Molavi, A. Eskandari, A. Shojaei, S.A. Mousavi, Enhancing CO2/N2 adsorption selectivity via post-synthetic modification of NH2-UiO-66(Zr), Microporous Mesoporous Mater. 257 (2018) 193–201.
[301] J. Albalad, H. Xu, F. Gándara, M. Haouas, C. Martineau-Corcos, R. Mas-Ballesté, S.A. Barnett, J. Juanhuix, I. Imaz, D. Maspoch, Single-crystal-to-single-crystal postsynthetic modification of a metal-organic framework via ozonolysis, J. Am. Chem. Soc. 140 (2018) 2028–2031.
[302] Z. Hu, K. Zhang, M. Zhang, Z. Guo, J. Jiang, D. Zhao, A combinatorial approach towards water-stable metal-organic frameworks for highly efficient carbon dioxide separation, ChemSusChem 7 (2014) 2791–2795.
[303] H. Fei, S. Pullen, A. Wagner, S. Ott, S.M. Cohen, Functionalization of robust Zr (iv)-based metal–organic framework films via a postsynthetic ligand exchange, Chem. Commun. 51 (2015) 66–69.
[304] K.M. Choi, D. Kim, B. Rungtaweevoranit, C.A. Trickett, J.T.D. Barmanbek, A.S. Alshammari, P. Yang, O.M. Yaghi, Plasmon-Enhanced Photocatalytic CO2 Conversion within Metal-Organic Frameworks under Visible Light, J. Am. Chem. Soc. 139 (2017) 356–362.
[305] P. Roy, A. Schaate, P. Behrens, A. Godt, Post-synthetic modification of Zr-metal–organic frameworks through cycloaddition reactions, Chem. Eur. J. 18 (2012) 6979–6985.
[306] A.M. Tollitt, R. Vismara, L.M. Daniels, D. Antypov, M.W. Gaultois, A.P. Katsoulidis, M.J. Rosseinsky, High-throughput discovery of a rhombohedral twelve-connected zirconium-based metal-organic framework with ordered terephthalate and fumarate linkers, Angew. Chem. Int. Ed. 60 (2021) 26939.
[307] S. Yuan, Y.-P. Chen, J.-S. Qin, W. Lu, L. Zou, Q. Zhang, X. Wang, X. Sun, H.-C. Zhou, Linker installation: engineering pore environment with precisely placed functionalities in zirconium MOFs, J. Am. Chem. Soc. 138 (2016) 8912–8919.
[308] R. Ameloot, M. Aubrey, B.M. Wiers, A.P. Gómora-Figueroa, S.N. Patel, N.P. Balsara, J.R. Long, Ionic conductivity in the metal-organic framework UiO-66 by dehydration and insertion of lithium tert-butoxide, Chem. Eur. J. 19 (2013) 5533–5536.
[309] A.M. Ebrahim, T.J. Bandosz, Ce(III) doped Zr-based MOFs as excellent NO2 adsorbents at ambient conditions, ACS Appl. Mater. Interfaces 5 (2013) 10565–10573.
[310] M. Kim, J.F. Cahill, H. Fei, K.A. Prather, S.M. Cohen, Postsynthetic ligand and cation exchange in robust metal-organic frameworks, J. Am. Chem. Soc. 134 (2012) 18082–18088.
[311] C. Hon Lau, R. Babarao, M.R. Hill, A route to drastic increase of CO2 uptake in Zr metal organic framework UiO-66, Chem. Commun. 49 (2013) 3634–3636.
[312] D. Sun, W. Liu, M. Qiu, Y. Zhang, Z. Li, Introduction of a mediator for enhancing photocatalytic performance via post-synthetic metal exchange in metal–organic frameworks (MOFs), Chem. Commun. 51 (2015) 2056–2059.
[313] H.G.T. Nguyen, L. Mao, A.W. Peters, C.O. Audu, Z.J. Brown, O.K. Farha, J.T. Hupp, S.T. Nguyen, Comparative study of titanium-functionalized UiO-66: support effect on the oxidation of cyclohexene using hydrogen peroxide, Catal. Sci. Technol. 5 (2015) 4444–4451.
[314] S.J.D. Smith, B.P. Ladewig, A.J. Hill, C.H. Lau, M.R. Hill, Post-synthetic Ti exchanged UiO-66 metal-organic frameworks that deliver exceptional gas permeability in mixed matrix membranes, Sci. Rep. 5 (2015) 7823.
[315] A. Wang, Y. Zhou, Z. Wang, M. Chen, L. Sun, X. Liu, Titanium incorporated with UiO-66(Zr)-type Metal-Organic Framework (MOF) for photocatalytic application, RSC Adv. 6 (2016) 3671–3679.
[316] Y. Han, M. Liu, K. Li, Q. Sun, W. Zhang, C. Song, G. Zhang, Z. Conrad Zhang, X. Guo, In situ synthesis of titanium doped hybrid metal–organic framework UiO-66 with enhanced adsorption capacity for organic dyes, Inorg. Chem. Front. 4 (2017) 1870–1880.
[317] J.G. Santaclara, A.I. Olivos-Suarez, A. Gonzalez-Nelson, D. Osadchii, M.A. Nasalevich, M.A. van der Veen, F. Kapteijn, A.M. Sheveleva, S.L. Veber, M.V. Fedin, A.T. Murray, C.H. Hendon, A. Walsh, J. Gascon, Revisiting the incorporation of Ti(IV) in UiO-type metal-organic frameworks: metal exchange versus grafting and their implications on photocatalysis, Chem. Mater. 29 (2017) 8963–8967.
[318] K. Manna, P. Ji, Z. Lin, F.X. Greene, A. Urban, N.C. Thacker, W. Lin, Chemoselective single-site Earth-abundant metal catalysts at metal–organic framework nodes, Nat. Commun. 7 (2016) 12610.
[319] J.M. Taylor, T. Komatsu, S. Dekura, K. Otsubo, M. Takata, H. Kitagawa, The role of a three dimensionally ordered defect sublattice on the acidity of a sulfonated metal-organic framework, J. Am. Chem. Soc. 137 (2015) 11498–11506.
[320] J.B. DeCoste, T.J. Demasky, M.J. Katz, O.K. Farha, J.T. Hupp, A UiO-66 analogue with uncoordinated carboxylic acids for the broad-spectrum removal of toxic chemicals, New J. Chem. 39 (2015) 2396–2399.
[321] A. De Vos, K. Hendrickx, P. Van Der Voort, V. Van Speybroeck, K. Lejaeghere, Missing Linkers: An Alternative Pathway to UiO-66 Electronic Structure Engineering, Chem. Mater. 29 (2017) 3006–3019.
[322] S. Dissegna, K. Epp, W.R. Heinz, G. Kieslich, R.A. Fischer, Defective Metal-Organic Frameworks, Adv. Mater. 30 (2018) 1704501.
[323] Y. Feng, Q. Chen, M. Cao, N. Ling, J. Yao, Defect-Tailoring and Titanium Substitution in Metal-Organic Framework UiO-66-NH2 for the Photocatalytic Degradation of Cr(VI) to Cr(III), ACS Appl. Mater. Interfaces 2 (2019) 5973–5980.
[324] D.A. Giannakoudakis, T.J. Bandosz, Defectous UiO-66 MOF Nanocomposites as Reactive Media of Superior Protection against Toxic Vapors, ACS Appl. Mater. Interfaces 12 (2020) 14678–14689.
[325] X. Feng, J. Hajek, H.S. Jena, G. Wang, S.K.P. Veerapandian, R. Morent, N. De Geyter, K. Leyssens, A.E.J. Hoffman, V. Meynen, C. Marquez, D.E. De Vos, V. Van Speybroeck, K. Leus, P. Van Der Voort, Engineering a Highly Defective Stable UiO-66 with Tunable Lewis- Brønsted Acidity: The Role of the Hemilabile Linker, J. Am. Chem. Soc. 142 (2020) 3174–3183.
[326] Y. Huang, Y. Jiao, T. Chen, Y. Gong, S. Wang, Y. Liu, D.S. Sholl, K.S. Walton, Tuning the Wettability of Metal-Organic Frameworks via Defect Engineering for Efficient Oil/Water Separation, ACS Appl. Mater. Interfaces 12 (2020) 34413–34422.
[327] L. Ni, Z. Liao, K. Chen, J. Xie, Q. Li, J. Qi, X. Sun, L. Wang, J. Li, Defect-engineered UiO-66-NH2 modified thin film nanocomposite membrane with enhanced nanofiltration performance, Chem. Commun. 56 (2020) 8372–8375.
[328] C. Falaise, C. Volkringer, J.-F. Vigier, N. Henry, A. Beaurain, T. Loiseau, Three-dimensional MOF-type architectures with tetravalent uranium hexanuclear motifs (U6O8), Chem. Eur. J. 19 (2013) 5324–5331.
[329] A.M. Hastings, D. Ray, W. Jeong, L. Gagliardi, O.K. Farha, A.E. Hixon, Advancement of Actinide Metal-Organic Framework Chemistry via Synthesis of Pu-UiO-66, J. Am. Chem. Soc. 142 (2020) 9363–9371.
[330] R.J. Holmberg, M. Kay, I. Korobkov, E. Kadantsev, P.G. Boyd, T. Aharen, S. Desgreniers, T.K. Woo, M. Murugesu, An unprecedented CoII cuboctahedron as the secondary building unit in a Co-based metal–organic framework, Chem. Commun. 50 (2014) 5333–5335.
[331] L. Rozes, C. Sanchez, Titanium oxo-clusters: precursors for a Lego-like construction of nanostructured hybrid materials, Chem. Soc. Rev. 40 (2011) 1006–1030.
[332] M. Dan-Hardi, C. Serre, T. Frot, L. Rozes, G. Maurin, C. Sanchez, G. Férey, A New Photoactive Crystalline Highly Porous Titanium(IV) Dicarboxylate, J. Am. Chem. Soc. 131 (2009) 10857–10859.
[333] C.H. Hendon, D. Tiana, M. Fontecave, C. Sanchez, L. D'arras, C. Sassoye, L. Rozes, C. Mellot-Draznieks, A. Walsh, Engineering the Optical Response of the Titanium-MIL-125 Metal-Organic Framework through Ligand Functionalization, J. Am. Chem. Soc. 135 (2013) 10942–10945.
[334] Y. Horiuchi, T. Toyao, M. Saito, K. Mochizuki, M. Iwata, H. Higashimura, M. Anpo, M. Matsuoka, Visible-Light-Promoted Photocatalytic Hydrogen Production by Using an Amino-Functionalized Ti(IV) Metal-Organic Framework, J. Phys. Chem. C 116 (2012) 20848–20853.
[335] Y. Fu, D. Sun, Y. Chen, R. Huang, Z. Ding, X. Fu, Z. Li, An Amine-Functionalized Titanium Metal-Organic Framework Photocatalyst with Visible-Light-Induced Activity for CO2 Reduction, Angew. Chem. Int. Ed. 51 (2012) 3364–3367.
[336] H. Guo, F. Lin, J. Chen, F. Li, W. Weng, Metal–organic framework MIL-125(Ti) for efficient adsorptive removal of Rhodamine B from aqueous solution, Appl. Organomet. Chem. 29 (2015) 12–19.
[337] S.-N. Kim, J. Kim, H.-Y. Kim, H.-Y. Cho, W.-S. Ahn, Adsorption/catalytic properties of MIL-125 and NH2-MIL-125, Catal. Today 204 (2013) 85–93.
[338] X. Qiao, Y. Liu, Y. Yang, H. Wang, J. Ma, D. Wang, N. Gao, L. Li, W. Liu, H. Wang, Synthesis optimization of metal-organic frameworks MIL-125 and its adsorption separation on C8 aromatics measured by pulse test and simulation calculation, J. Solid State Chem. 296 (2021) 121956.
[339] M.W. Logan, S. Ayad, J.D. Adamson, T. Dilbeck, K. Hanson, F.J. Uribe-Romo, Systematic variation of the optical bandgap in titanium based isoreticular metal–organic frameworks for photocatalytic reduction of CO2 under blue light, J. Mater. Chem. A 5 (2017) 11854–11863.
[340] Y. Xie, X. Liu, X. Ma, Y. Duan, Y. Yao, Q. Cai, Small Titanium-Based MOFs Prepared with the Introduction of Tetraethyl Orthosilicate and Their Potential for Use in Drug Delivery, ACS Appl. Mater. Interfaces 10 (2018) 13325–13332.
[341] S. Rojas, N. Guillou, P. Horcajada, Ti-Based nanoMOF as an Efficient Oral Therapeutic Agent, ACS Appl. Mater. Interfaces 11 (2019) 22188–22193.
[342] K. Jiang, L. Zhang, Q. Hu, Y. Yang, W. Lin, Y. Cui, Y. Yang, G. Qian, A Biocompatible Ti-based metal-organic framework for pH responsive drug delivery, Mater. Lett. 225 (2018) 142–144.
[343] L. Zhang, J. Tian, F. Cao, Z.-Y. Zhu, F. Hong, J. Wu, F. Wang, Titanium-based metal-organic frameworks as potential chloroquine drug carriers, Inorg. Chem. Commun. 133 (2021) 108870.

[344] I.D. Ivanchikova, J.S. Lee, N.V. Maksimchuk, A.N. Shmakov, Y.A. Chesalov, A.B. Ayupov, Y.K. Hwang, C.-H. Jun, J.-S. Chang, O.A. Kholdeeva, Highly selective H2O2-based oxidation of alkylphenols to p-benzoquinones over MIL-125 metal-organic frameworks, Eur. J. Inorg. Chem. 2014 (2014) 132–139.
[345] M.A. Nasalevich, M.G. Goesten, T.J. Savenije, F. Kapteijn, J. Gascon, Enhancing optical absorption of metal–organic frameworks for improved visible light photocatalysis, Chem. Commun. 49 (2013) 10575–10577.
[346] Y. Zhao, W. Cai, J. Chen, Y. Miao, Y. Bu, A Highly Efficient Composite Catalyst Constructed From NH2-MIL-125(Ti) and Reduced Graphene Oxide for CO2 Photoreduction, Front. Chem. 7 (2019) 789.
[347] L. Zeng, Y. Cao, Z. Li, Y. Dai, Y. Wang, B. An, J. Zhang, H. Li, Y. Zhou, W. Lin, C. Wang, Multiple Cuprous Centers Supported on a Titanium-Based Metal-Organic Framework Catalyze CO2 Hydrogenation to Ethylene, ACS Catal. (2021) 11696–11705.
[348] S. Jakobsen, D. Gianolio, D.S. Wragg, M.H. Nilsen, H. Emerich, S. Bordiga, C. Lamberti, U. Olsbye, M. Tilset, K.P. Lillerud, Structural determination of a highly stable metal-organic framework with possible application to interim radioactive waste scavenging: Hf-UiO-66, Phys. Rev. B 86 (2012) 125429.
[349] W.K. Li Liangsha, H.U.A.N.G. Hongliang, Y.A.N.G. Qingyuan, Z.H.A.N.G. Yi, W.A.N.G. Shaohua, W.U. Pingyi, L.A.N. Ling, L.I.U. Dahuan, Z.H.O.N.G. Chongli, Synthesis of exceptional stable Hf-based metal-organic frameworks: characterization, stability and CO₂ adsorption performance, CIESC J. 65 (2014) 1706–1715.
[350] Z. Hu, A. Nalaparaju, Y. Peng, J. Jiang, D. Zhao, Modulated Hydrothermal Synthesis of UiO-66(Hf)-Type Metal-Organic Frameworks for Optimal Carbon Dioxide Separation, Inorg. Chem. 55 (2016) 1134–1141.
[351] P. Xydias, I. Spanopoulos, E. Klontzas, G.E. Froudakis, P.N. Trikalitis, Drastic Enhancement of the CO2 Adsorption Properties in Sulfone-Functionalized Zr- and Hf-UiO-67 MOFs with Hierarchical Mesopores, Inorg. Chem. 53 (2014) 679–681.
[352] A. Das, N. Anbu, C. Gogoi, A. Dhakshinamoorthy, S. Biswas, Amino Group Functionalized Hf-Based Metal-Organic Framework for Knoevenagel-Doebner Condensation, Eur. J. Inorg. Chem. 2021 (2021) 3396..
[353] R.G. Faria, D. Julião, S.S. Balula, L. Cunha-Silva, Hf-Based UiO-66 as Adsorptive Compound and Oxidative Catalyst for Denitrogenation Processes, Compounds 1 (2021) 3–14.
[354] N. Masciocchi, S. Galli, V. Colombo, A. Maspero, G. Palmisano, B. Seyyedi, C. Lamberti, S. Bordiga, Cubic octanuclear Ni(II) clusters in highly porous polypyrazolyl-based materials, J. Am. Chem. Soc. 132 (2010) 7902–7904.
[355] E. López-Maya, C. Montoro, V. Colombo, E. Barea, J.A.R. Navarro, Improved CO2 capture from flue gas by basic sites, charge gradients, and missing linker defects on nickel face cubic centered MOFs, Adv. Funct. Mater. 24 (2014) 6130–6135.
[356] N.-Y. Huang, J.-Q. Shen, Z.-M. Ye, W.-X. Zhang, P.-Q. Liao, X.-M. Chen, An exceptionally stable octacobalt-cluster-based metal–organic framework for enhanced water oxidation catalysis, Chem. Sci. 10 (2019) 9859–9864.
[357] C. Montoro, P. Ocón, F. Zamora, J.A.R. Navarro, Metal-organic frameworks containing missing-linker defects leading to high hydroxide-ion conductivity, Chem. Eur. J. 22 (2016) 1646–1651.
[358] F.G. Cirujano, E. López-Maya, M. Rodríguez-Albelo, E. Barea, J.A.R. Navarro, D. E. De Vos, Selective one-pot two-step C−C bond formation using metal-organic frameworks with mild basicity as heterogeneous catalysts, ChemCatChem 9 (2017) 4019–4023.
[359] L. Meng, Q. Cheng, C. Kim, W.-Y. Gao, L. Wojtas, Y.-S. Chen, M.J. Zaworotko, X. P. Zhang, S. Ma, Crystal engineering of a microporous, catalytically active fcu topology MOF using a custom-designed metalloporphyrin linker, Angew. Chem. Int. Ed. 51 (2012) 10082–10085.
[360] V. Guillerm, D. Kim, J.F. Eubank, R. Luebke, X. Liu, K. Adil, M.S. Lah, M. Eddaoudi, A supermolecular building approach for the design and construction of metal–organic frameworks, Chem. Soc. Rev. 43 (2014) 6141–6172.
[361] M. Eddaoudi, J. Kim, J.B. Wachter, H.K. Chae, M. O'Keeffe, O.M. Yaghi, Porous Metal−Organic Polyhedra: 25 Å Cuboctahedron Constructed from 12 Cu2(CO2)4 Paddle-Wheel Building Blocks, J. Am. Chem. Soc. 123 (2001) 4368–4369.
[362] B. Moulton, J. Lu, A. Mondal, M.J. Zaworotko, Nanoballs: nanoscale faceted polyhedra with large windows and cavities, Chem. Commun. (2001) 863–864.
[363] H. Chun, Low-Level Self-Assembly of Open Framework Based on Three Different Polyhedra: Metal-Organic Analogue of Face-Centered Cubic Dodecaboride, J. Am. Chem. Soc. 130 (2008) 800–801.
[364] H. Chun, H. Jung, J. Seo, Isoreticular metal-organic polyhedral networks based on 5-connecting paddlewheel motifs, Inorg. Chem. 48 (2009) 2043–2047.
[365] H.-N. Wang, X. Meng, G.-S. Yang, X.-L. Wang, K.-Z. Shao, Z.-M. Su, C.-G. Wang, Stepwise assembly of metal–organic framework based on a metal–organic polyhedron precursor for drug delivery, Chem. Commun. 47 (2011) 7128–7130.
[366] H.-N. Wang, F.-H. Liu, X.-L. Wang, K.-Z. Shao, Z.-M. Su, Three neutral metal–organic frameworks with micro- and meso-pores for adsorption and separation of dyes, J. Mater. Chem. A 1 (2013) 13060–13063.
[367] A.J. Cairns, J.A. Perman, L. Wojtas, V.C. Kravtsov, M.H. Alkordi, M. Eddaoudi, M.J. Zaworotko, Supermolecular building blocks (SBBs) and crystal design: 12-connected open frameworks based on a molecular cubohemioctahedron, J. Am. Chem. Soc. 130 (2008) 1560–1561.
[368] U. Stoeck, S. Krause, V. Bon, I. Senkovska, S. Kaskel, A highly porous metal–organic framework, constructed from a cuboctahedral super-molecular building block, with exceptionally high methane uptake, Chem. Commun. 48 (2012) 10841–10843.
[369] S. Fordham, X. Wang, M. Bosch, H.-C. Zhou, Lanthanide Metal-Organic Frameworks: Syntheses, Properties, and Potential Applications, in: P. Cheng (Ed.), Lanthanide Metal-Organic Frameworks, Springer, Berlin Heidelberg, Berlin, Heidelberg, 2015, pp. 1–27.
[370] Y. Cui, Y. Yue, G. Qian, B. Chen, Luminescent functional metal-organic frameworks, Chem. Rev. 112 (2012) 1126–1162.
[371] M.D. Allendorf, C.A. Bauer, R.K. Bhakta, R.J. Houk, Luminescent metal-organic frameworks, Chem. Soc. Rev. 38 (2009) 1330–1352.
[372] D.-X. Xue, A.J. Cairns, Y. Belmabkhout, L. Wojtas, Y. Liu, M.H. Alkordi, M. Eddaoudi, Tunable Rare-Earth fcu-MOFs: A Platform for Systematic Enhancement of CO2 Adsorption Energetics and Uptake, J. Am. Chem. Soc. 135 (2013) 7660–7667.
[373] P.R. Donnarumma, S. Frojmovic, P. Marino, H.A. Bicalho, H.M. Titi, A.J. Howarth, Synthetic approaches for accessing rare-earth analogues of UiO-66, Chem. Commun. 57 (2021) 6121–6124.
[374] D.F. Sava Gallis, D.J. Vogel, G.A. Vincent, J.M. Rimsza, T.M. Nenoff, NOx Adsorption and Optical Detection in Rare Earth Metal-Organic Frameworks, ACS Appl. Mater. Interfaces 11 (2019) 43270–43277.
[375] K. Adil, K. Świrk, A. Zaki, A.H. Assen, G. Delahay, Y. Belmabkhout, A. Cadiau, Perspectives in Adsorptive and Catalytic Mitigations of NOx Using Metal-Organic Frameworks, Energy Fuels 36 (2022) 3347–3371.
[376] D.-X. Xue, Y. Belmabkhout, O. Shekhah, H. Jiang, K. Adil, A.J. Cairns, M. Eddaoudi, Tunable Rare Earth fcu-MOF Platform: Access to Adsorption Kinetics Driven Gas/Vapor Separations via Pore Size Contraction, J. Am. Chem. Soc. 137 (2015) 5034–5040.
[377] A.H. Assen, T. Virdis, W. De Moor, A. Moussa, M. Eddaoudi, G. Baron, J. F.M. Denayer, Y. Belmabkhout, Kinetic separation of C4 olefins using Y-fum-fcu-MOF with ultra-fine-tuned aperture size, Chem. Eng. J. 413 (2021) 127388.
[378] Y.-Z. Li, H.-H. Wang, G.-D. Wang, L. Hou, Y.-Y. Wang, Z. Zhu, A Dy6-cluster-based fcu-MOF with efficient separation of C2H2/C2H4 and selective adsorption of benzene, Inorg. Chem. Front. 8 (2021) 376–382.
[379] P.M. Bhatt, Y. Belmabkhout, A.H. Assen, Ł.J. Weseliński, H. Jiang, A. Cadiau, D.-X. Xue, M. Eddaoudi, Isoreticular rare earth fcu-MOFs for the selective removal of H2S from CO2 containing gases, Chem. Eng. J. 324 (2017) 392–396.
[380] K. Adil, P.M. Bhatt, Y. Belmabkhout, S.M.T. Abtab, H. Jiang, A.H. Assen, A. Mallick, A. Cadiau, J. Aqil, M. Eddaoudi, Valuing Metal-Organic Frameworks for Postcombustion Carbon Capture: A Benchmark Study for Evaluating Physical Adsorbents, Adv. Mater. 29 (2017) 1702953.
[381] M. Li, Y. Wan, J.-K. Huang, A.H. Assen, C.-E. Hsiung, H. Jiang, Y. Han, M. Eddaoudi, Z. Lai, J. Ming, L.-J. Li, Metal-Organic Framework-Based Separators for Enhancing Li–S Battery Stability: Mechanism of Mitigating Polysulfide Diffusion, ACS Energy Lett. 2 (2017) 2362–2367.
[382] A.H. Assen, O. Yassine, O. Shekhah, M. Eddaoudi, K.N. Salama, MOFs for the sensitive detection of ammonia: deployment of fcu-MOF thin films as effective chemical capacitive sensors, ACS Sens. 2 (2017) 1294–1301.
[383] O. Yassine, O. Shekhah, A.H. Assen, Y. Belmabkhout, K.N. Salama, M. Eddaoudi, H2S sensors: fumarate-based fcu-MOF thin film grown on a capacitive interdigitated electrode, Angew. Chem. Int. Ed. 55 (2016) 15879–15883.
[384] G. Liu, V. Chernikova, Y. Liu, K. Zhang, Y. Belmabkhout, O. Shekhah, C. Zhang, S. Yi, M. Eddaoudi, W.J. Koros, Mixed matrix formulations with MOF molecular sieving for key energy-intensive separations, Nat. Mater. 17 (2018) 283–289.
[385] Y. Liu, G. Liu, C. Zhang, W. Qiu, S. Yi, V. Chernikova, Z. Chen, Y. Belmabkhout, O. Shekhah, M. Eddaoudi, W. Koros, Enhanced CO2/CH4 separation performance of a mixed matrix membrane based on tailored MOF-polymer formulations, Adv. Sci. 5 (2018) 1800982.
[386] R. Das, R. Sarma, J.B. Baruah, A hexanuclear cerium(IV) cluster with mixed coordination environment, Inorg. Chem. Commun. 13 (2010) 793–795.
[387] M. Lammert, M.T. Wharmby, S. Smolders, B. Bueken, A. Lieb, K.A. Lomachenko, D.D. Vos, N. Stock, Cerium-based metal organic frameworks with UiO-66 architecture: synthesis, properties and redox catalytic activity, Chem. Commun. 51 (2015) 12578–12581.
[388] R. Dalapati, B. Sakthivel, A. Dhakshinamoorthy, A. Buragohain, A. Bhunia, C. Janiak, S. Biswas, A highly stable dimethyl-functionalized Ce(iv)-based UiO-66 metal–organic framework material for gas sorption and redox catalysis, CrystEngComm 18 (2016) 7855–7864.
[389] A. Buragohain, S. Biswas, Cerium-based azide- and nitro-functionalized UiO-66 frameworks as turn-on fluorescent probes for the sensing of hydrogen sulphide, CrystEngComm 18 (2016) 4374–4381.
[390] M. Lammert, C. Glißmann, H. Reinsch, N. Stock, Synthesis and Characterization of New Ce(IV)-MOFs Exhibiting Various Framework Topologies, Cryst. Growth Des. 17 (2017) 1125–1131.
[391] R. D'Amato, A. Donnadio, M. Carta, C. Sangregorio, D. Tiana, R. Vivani, M. Taddei, F. Costantino, Water-Based Synthesis and Enhanced CO2 Capture Performance of Perfluorinated Cerium-Based Metal-Organic Frameworks with UiO-66 and MIL-140 Topology, ACS Sustain. Chem. Eng. 7 (2019) 394–402.
[392] S. Smolders, K.A. Lomachenko, B. Bueken, A. Struyf, A.L. Bugaev, C. Atzori, N. Stock, C. Lamberti, M.B.J. Roeffaers, D.E. De Vos, Unravelling the Redox-catalytic Behavior of Ce4+ Metal-Organic Frameworks by X-ray Absorption Spectroscopy, ChemPhysChem 19 (2018) 373–378.

[393] T.J. Matemb Ma Ntep, H. Reinsch, J. Liang, C. Janiak, Acetylenedicarboxylate-based cerium(iv) metal–organic framework with fcu topology: a potential material for air cleaning from toxic halogen vapors, Dalton Trans. 48 (2019) 15849–15855.
[394] M. Farrag, In situ preparation of palladium nanoclusters in cerium metal-organic frameworks Ce-MOF-808, Ce-UiO-66 and Ce-BTC as nanoreactors for room temperature Suzuki cross-coupling reaction, Microporous Mesoporous Mater. 312 (2021) 110783.
[395] R.M. Rego, G. Sriram, K.V. Ajeya, H.-Y. Jung, M.D. Kurkuri, M. Kigga, Cerium based UiO-66 MOF as a multipollutant adsorbent for universal water purification, J. Hazard. Mater. 416 (2021) 125941.
[396] M. Stawowy, M. Róziewicz, E. Szczepańska, J. Silvestre-Albero, M. Zawadzki, M. Musioł, R. Łuzny, J. Kaczmarczyk, J. Trawczyński, A. Łamacz, The Impact of Synthesis Method on the Properties and CO2 Sorption Capacity of UiO-66 (Ce), Catalysts 9 (2019) 309.
[397] M. Campanelli, T. Del Giacco, F. De Angelis, E. Mosconi, M. Taddei, F. Marmottini, R. D'Amato, F. Costantino, Solvent-Free Synthetic Route for Cerium(IV) Metal-Organic Frameworks with UiO-66 Architecture and Their Photocatalytic Applications, ACS Appl. Mater. Interfaces 11 (2019) 45031–45037.
[398] K.E. Knope, L. Soderholm, Solution and Solid-State Structural Chemistry of Actinide Hydrates and Their Hydrolysis and Condensation Products, Chem. Rev. 113 (2013) 944–994.
[399] R.A. Zehnder, J.M. Boncella, J.N. Cross, S.A. Kozimor, M.J. Monreal, H.S. La Pierre, B.L. Scott, A.M. Tondreau, M. Zeller, Network Dimensionality of Selected Uranyl(VI) Coordination Polymers and Octopus-like Uranium(IV) Clusters, Cryst. Growth Des. 17 (2017) 5568–5582.
[400] C. Falaise, C. Volkringer, T. Loiseau, Mixed Formate-Dicarboxylate Coordination Polymers with Tetravalent Uranium: Occurrence of Tetranuclear U4O4 and Hexanuclear U6O4(OH)4 Motifs, Cryst. Growth Des. 13 (2013) 3225–3231.
[401] C. Falaise, A. Assen, I. Mihalcea, C. Volkringer, A. Mesbah, N. Dacheux, T. Loiseau, Coordination polymers of uranium(iv) terephthalates, Dalton Trans. 44 (2015) 2639–2649.
[402] C. Falaise, J.-S. Charles, C. Volkringer, T. Loiseau, Thorium Terephthalates Coordination Polymers Synthesized in Solvothermal DMF/H2O System, Inorg. Chem. 54 (2015) 2235–2242.
[403] T. Islamoglu, D. Ray, P. Li, M.B. Majewski, I. Akpinar, X. Zhang, C.J. Cramer, L. Gagliardi, O.K. Farha, From Transition Metals to Lanthanides to Actinides: Metal-Mediated Tuning of Electronic Properties of Isostructural Metal-Organic Frameworks, Inorg. Chem. 57 (2018) 13246–13251.
[404] N.P. Martin, J. März, H. Feuchter, S. Duval, P. Roussel, N. Henry, A. Ikeda-Ohno, T. Loiseau, C. Volkringer, Synthesis and structural characterization of the first neptunium based metal–organic frameworks incorporating Np6O8 hexanuclear clusters, Chem. Commun. 54 (2018) 6979–6982.
[405] H. Feng, X. Xiong, L. Gong, H. Zhang, Y. Xu, X. Feng, F. Luo, Rational tuning of thorium-organic frameworks by reticular chemistry for boosting radionuclide sequestration, Nano Res. 15 (2022) 1472–1478.
[406] T. Song, W. Tang, C. Bao, Q. Lai, Z. Zhang, X. Feng, C. Liu, An fcu Th-MOF Constructed from In Situ Coupling of Monovalent Ligands, Symmetry 13 (2021) 1332.
[407] B. Shan, S.M. McIntyre, M.R. Armstrong, Y. Shen, B. Mu, Investigation of missing-cluster defects in UiO-66 and ferrocene deposition into defect-induced cavities, Ind. Eng. Chem. Res. 57 (2018) 14233–14241.